Biomimetic artificial cell plasma membranes-on-a-chip for drug permeability prediction

by

Jaime L. Korner
B.Sc. with Honours., Brandeis University, 2017

A Dissertation Submitted in Partial Fulfillment of the
Requirements for the Degree of

DOCTOR OF PHILOSOPHY

in the Department of Chemistry

University of Victoria

We acknowledge and respect the Lekwungen peoples on whose traditional territory the university stands and the Songhees, Esquimalt and W̱SÁNEĆ peoples whose historical relationships with the land continue to this day

Biomimetic artificial cell plasma membranes-on-a-chip for drug permeability prediction

by

Jaime L. Korner

B.Sc. with Honours., Brandeis University, 2017

Supervisory Committee

Dr. Katherine Elvira, Supervisor

(Department of Chemistry)

Dr. Fraser Hof, Departmental Member

(Department of Chemistry)

Dr. John Burke, Outside Member

(Department of Biochemisty and Microbiology)

ABSTRACT

The drug development process is notoriously long and expensive. During preclinical studies, inaccurate prediction of pharmacokinetic properties such as the ability of a drug candidate to passively permeate cell plasma membranes contributes to the high failure rate of drug candidates during clinical trials. Passive drug permeability is currently predicted using *in vitro* techniques such as parallel artificial membrane permeability assays, or PAMPA. In PAMPA, drug transport is predicted between aqueous compartments via a synthetic filter filled with a phospholipid solution in an organic solvent. The lack of translatability of preclinical predictions to humans can be attributed, in part, to lack of biological similarly between models used for permeability prediction and cell plasma membranes *in vivo*. Here, I demonstrate a new method for pharmacokinetic prediction, built by using droplet interface bilayers (DIBs) as human-mimetic artificial cell membranes. DIBs are bilayer sections created at the interface of two aqueous droplets. In the literature, DIBs have been used as artificial cell plasma membranes to study, for example, electrophysiological properties, protein insertion, water permeability, and molecular transport. DIBs can be formed between droplets of differing composition such that one droplet can be used as a donor compartment and the other as an acceptor compartment for the quantification of molecular transport across the artificial cell membrane. DIBs have previously been used to measure the passive permeability of numerous fluorophores as well as the drugs caffeine and doxorubicin. However, the extent to which DIBs have been tuned to mimic human cell plasma membranes and transport across them is limited. I present here the use of microfluidic platforms for bespoke DIB formation, where variables such as temperature, bilayer composition, and droplet contents are customized to create biomimetic cells-on-a-chip. These artificial cells are then used to measure molecular transport with the aim of predicting permeability.

In Chapter 2, I investigate the effectiveness of literature methods for the modification of polydimethylsiloxane (PDMS) microfluidic device channels for aqueous droplet formation and storage. While numerous techniques have been presented as mitigation strategies for common challenges in droplet microfluidics, it is not clear from the literature if any of these methods would be effective or necessary for the formation and analysis of DIBs. With the aim of facilitating aqueous droplet formation, I tested the effect of PDMS silanization using trichloro(1H,1H,2H,2H-perfluorooctyl)silane (PFOS) on surface hydrophobicity and oleophobicity. To assess their effect on reducing the rate of aqueous droplet evaporation, I tested surface treatment of PDMS with Teflon AF or Aquapel. I also tested modifications to the device fabrication process by bonding a glass coverslip to the surface of the device and soaking the device in water overnight. To quantify changes in PDMS surface chemistry, I performed contact angle measurements, aqueous droplet formation experiments, and measurements of droplet size during on-chip storage. I determined that baking PDMS microfluidic devices at 65°C overnight produced channel surfaces which allowed for aqueous droplet formation and storage. In Chapter 3 I present a systematic study on the role of temperature in DIB formation using naturally derived phospholipids. The use of increased temperature to form DIBs using total lipid extracts has previously been demonstrated, but has never before been investigated systematically using naturally derived phospholipids and bespoke formulations thereof. I hypothesized that, in order to form complete phospholipid monolayers and DIBs, the microfluidic device must be held at the phase transition temperature of the phospholipids. Using a custom-built heating platform, I tested DIB formation over a range of temperatures to determine conditions which allowed DIB formation rather than droplet coalescence. I show that temperature is a key parameter for DIB formation using naturally derived phospholipids in a microfluidic device. In Chapter 4, I demonstrate the use of DIBs as a

new type of pharmacokinetic compartment model for intestinal absorption. Using three-droplet networks, the components of which were designed to mimic the intestinal space, the enterocyte cytosol, and the blood, I measured fluorescein permeability across intestine-mimetic DIBs. The model was able to predict the transport of fluorescein more accurately than the current state-of-the-art technique, PAMPA. Chapter 5 describes the development of complex DIB models for pharmacologically relevant membranes as well as an investigation into novel methods of drug transport detection on-chip. I created a new DIB model for the small intestine, incorporating more components of the enterocyte plasma membrane such as cholesterol. Measurement of calcein permeability served as a control experiment, as calcein does not cross cell plasma membranes. Measurement of fluorescein permeability yielded a significantly shorter permeation half-life than was determined in Chapter 4, indicating an increase in permeability with the more complex, biomimetic phospholipid formulation. I also developed sex-specific models for intestinal absorption to investigate the effect of sex-based membrane differences on permeability. This relationship has never before been explored in the literature. In comparison to the initial intestinal phospholipid formulation, the sex-specific formulations contained acyl chain tail groups which have been found in different ratios in male and female cells. A significantly longer half-life for fluorescein permeability was found in female intestine-mimetic DIBs, mirroring the slower drug absorption observed in female patients. I also used DIBs to model blood-brain barrier permeability. I demonstrate this application using two different brain lipid extracts, polar and total brain lipids. Polar brain lipids have previously been used in PAMPA to predict blood-brain barrier permeability, but have been found to overpredict the permeation of charged molecules in comparison to custom lipid formulations which mimic the composition of human brain endothelial cells. Permeability measurements in DIBs formed using polar brain lipids gave results which agree

with PAMPA, as DIBs formed using polar brain lipids were permeable to fluorescein, but those formed using total brain lipids were not. Blood-brain barrier-mimetic DIBs formed using either lipid extract are impermeable to calcein and FITC-dextrans (both 40 and 500 kDa). I also show the formation of the first DIBs to be created using a total lipid extract from human cells as well as their impermeability to calcein. The extract tested was prepared from testicular Sertoli cells, which exhibit properties similar to the blood-brain barrier, but future work will focus on extracts prepared from human brain endothelial cells. Finally, I explore new options for the on-chip detection of the transport of nonfluorescent molecules. To move away from reliance on fluorescent molecules for permeability measurements, I selected three fluorogenic molecular recognition agents (fluorescamine, Chromeo P540, and DimerDye 4) whose fluorescence signal is activated by amine groups. None of the tested methods proved to be viable in DIBs, potentially due to slow permeation, low quantum yield, and side reactions with phospholipids.

Overall, I demonstrate here the microfluidic formation and application of several novel types of biomimetic DIBs to permeability prediction. My work shows that DIBs can be used to predict permeability and mirror effects observed *in vivo*. Future work will focus on the development of new methods for the detection of drug transport and the application of the pharmacokinetic compartment models presented to predicting drug permeability. Further work using total lipid extracts prepared from human cells will also be vital to enhancing the use of biomimetic DIBs as pharmacokinetic permeability prediction tools. As their biological similarity and capacity to accurately predict transport increase, so will the potential of DIBs to improve the accuracy and translatablity of preclinical drug development.

Contents

List of Figures

ACKNOWLEDGEMENTS

This dissertation could not have been completed without the mentorship and support of many people in my life. First, I would like to thank my supervisor, Dr. Katherine Elvira, who has shown me endless patience, kindness, and tough love. Katherine's guidance throughout the design and execution of this project as well as her feedback on countless CVs, conference abstracts, papers, and, of course, this dissertation itself has been invaluable. I want to thank Katherine for always pushing me to improve but also to give myself for my research accomplishments. I took a leap in first joining the Elvira Group: I decided to attend a university to which I had never been, with a supervisor who I had only met via Skype, in a city I hadn't visited for fifteen years, in a new country, to do my PhD in a field of chemistry which I had only just learned existed. I am so grateful I did, for many reasons, but especially because I cannot imagine a better supervisor than Katherine. I am honoured to have been one of the first graduate students in the Elvira Group. I would also like to acknowledge all members of the Elvira Group, past and present, in particular Elanna Stephenson and Dr. Kaitlyn Ramsay, who have been by my side since we began our graduate studies together in 2017. Joining (or, perhaps, creating) a new research group is not easy, but I could not have chosen a better team for the task. They both exemplify the perfect mix of goofiness and ambition and I look forward to seeing where their careers take them. I also thank the graduate students who have joined along the way, Alejandro Forigua-Coronado, Sean Farley, and Alex McDonald, and our first postdoctoral researcher, Arash Dalili, who honoured me with the title of "droplet god." I also want to thank all of the students who I have had the privilege to teach, mentor, and tutor during my time at the University of Victoria. They pushed me to develop my expertise in fields of math and science which I would have otherwise let myself forget and taught me more about learning than I can express here. I

must also thank my first chemistry teacher, Jamie Yoos, whose teaching skill and witticisms I remember to this day. He supervised my very first research project, even driving my group and I across the state to present our findings, and once told me that I could go in any direction in chemistry and succeed. Nearly five years ago, I vowed to acknowledge my dear friend and then-roommate Jessica Hack-Chabot in my future PhD dissertation. In the midst of chaos in my personal life, I nearly missed the deadline to enroll in my senior honours thesis course, which I knew would be a key step in my research career. To make sure I could get the necessary form signed and submitted without being held back by a ridiculously infrequent bus schedule, Jess drove me to, around, and home from campus, a journey which should have taken 20 minutes but instead lasted multiple hours in the worst South St traffic and late summer heat I have ever experienced. Because of this, and countless other demonstrations of love and support on her part, I am here to present this dissertation today. I also want to thank Naomi Shmueli, my best friend for the last ten years. While I had to leave her in Massachusetts to complete my PhD, her friendship and support across the miles (kilometres) has meant everything to me. Naomi has helped me navigate the worst and the best times in my life, and I cannot put into words my appreciation for her. My partner, Eli Siegel, deserves endless thanks for the support he has given me over the last four years. Before we met, I could not have imagined the level of devotion and love that he has shown me. Eli and I met at the beginning of my final year of university, when I already knew I would be leaving Massachusetts (and intended to leave the U.S.) at the end of my degree. During the beginning of my PhD, Eli and I did long-distance for fourteen months, which ended when he moved here to start his own graduate studies (or really, started his graduate studies to move here). I could not have imagined when he walked into my Halloween party that we would be here, after nearly five years, multiple degrees, a cross-continent move, and

a global pandemic. On that note, I must thank our dog, Franklin, for many hours of snuggly distraction from a difficult degree. Eli's family, Barbara, Steve, and Noah Siegel and Chanelle Diaz, have also been a huge source of support, both during our visits home and virtually. Finally, I want to thank my parents, Lynn and Michael Korner, for creating me, loving me unconditionally, and supporting me to achieve this goal. They have worked incredibly hard to put me through school and university and I am endlessly grateful to them for that opportunity.

DEDICATION

I dedicate this dissertation to my Eli and to my parents, Lynn and Michael Korner. Because you believed in me, I believed in me.

"It's impossible to fall off mountains you fool!" – Jack Kerouac

"You can grow ideas in the garden of your mind." – Mr. Rogers

Chapter 1

Introduction

1.1 The importance of *in vitro* drug permeability prediction for drug discovery

In the pharmaceutical industry, the pathway a drug candidate takes during development is arduous and expensive, spanning 10-15 years and costing an average of $2.6 billion USD.[1,2] Over 90% of drug candidates do not make it to the market, even after significant investment in their development;[3] in fact, it has been claimed that only 0.1% of drug candidates avoid failure over the course of the entire development process.[4] After a new drug candidate has been identified during early drug discovery, the development process begins with preclinical studies. During the preclinical stage, first *in vitro* assays are used to predict pharmacokinetics, the effect the body has on a drug, and pharmacodynamics, the effect the drug will have on the human body.[3] Pharmacokinetic processes which are investigated during preclinical studies include absorption, distribution, metabolism, excretion, and toxicity, or ADME-Tox. Candi-

dates that make it through *in vitro* testing are then tested in animal models before going on to clinical trials in humans. Approximately 30% of drug candidates fail during trials in animal models due to inaccurate prediction of their pharmacokinetic properties.[5,6] Nearly 50% of drug candidates fail during clinical trials in humans.[4] These vast failure rates are attributed to lack of translatability of preclinical research to humans, due in part to low correlation between *in vitro* predictions and drug behavior in humans.[4] The false discovery rate, or the rate at which potential drug candidates are falsely identified during preclinical studies, has been estimated to be 92.6%,[7] indicating that a large percentage of the drugs which fail in the late stages of drug development do so due to poor predictions made preclinically. Therefore, improving the accuracy of pharmacokinetic predictions made early in the preclinical stage is imperative to reduce the rate at which candidates fail in later stages of development. Improving the translatability of data gathered using *in vitro* models to drug behavior in humans has the potential to reduce the high costs and time invested in drug candidates by improving the accuracy with which promising candidates are selected.

While all components of ADME-Tox can be poorly predicted during preclinical studies, significantly toxicity, poor prediction of absorption is common.[8–10] Oral administration is the most frequent route of drug delivery, so predicting oral bioavailability is particularly important.[8] Low oral bioavailability of many drug candidates poses a significant challenge to researchers during the preclinical stage.[9,10] Drug candidate attrition is also particularly high in targeting the central nervous system due to the low permeability of the blood-brain barrier.[10] Thus, accurately predicting permeability in the small intestine and the blood-brain barrier are especially significant in improving translatability of preclinical research to clinical results. Prediction of passive permeability is a key component of preclinical drug development and requires significant

improvement to reduce the number of false positives, or drug candidates which are misidentified as promising future drugs.[11] Passive permeability is specifically important due to the large number of drugs which are transported through the cell plasma membrane passively by diffusion through the lipid bilayer rather than actively by a membrane transporter. It has been claimed that up to 95% of all drugs are absorbed passively.[12–14] The *in vitro* techniques currently used to predict passive drug transport through the plasma membrane are limited by factors including lack of biological similarity, low controllability, and high labor requirements.[15–19]

1.2 Strategies for pharmacokinetic passive permeability prediction

In this section, I describe the major techniques which are used, both historically and in the present, in the literature and in the pharmaceutical industry to predict passive drug permeability.[3,20] Passive permeation refers to the transport of a drug from one aqueous compartment to another across a cell plasma membrane without the involvement of membrane proteins. The cell plasma membrane, which forms a barrier between the aqueous extracellular space and the aqueous cytosol, is mainly composed of lipid molecules.[21] Of these lipids, the most important are phospholipids. Phospholipids are amphiphilic molecules, meaning they contain regions of both hydrophobicity (aversion to an aqueous phase) and hydrophilicity (affinity for an aqueous phase). Phospholipids contain hydrophilic head groups (containing a polar phosphate group) and hydrophobic tail groups (acyl chains) and form nanostructures in aqueous solution to protect their nonpolar tail groups from unfavorable interactions with water molecules. In the cell plasma membrane, phospholipids form a bilayer, which provides the structure of the membrane. Mammalian plasma membranes mainly contain phos-

phatidylcholine (PC), phosphatidylethanolamine (PE), phosphatidylserine (PS), and phosphatidylinositol (PI) (Figure 1.1),[21–23] but also include neutral lipids like cholesterol, sphingophospholipids like sphingomyelin, glycolipids, and membrane proteins.[23] While membrane proteins are not insignificant by any means, they are outnumbered by 50-100 to one by lipid molecules.[21] Because of the predominance of phospholipids and the important role passive permeability through the cell plasma membrane plays in drug development, my focus in this section is on techniques to model passive lipoidal permeability. Each has its own advantages, but all are flawed and contribute to the lack of translatability of preclinical research. While not a comprehensive list of every *in vitro* technique tested during preclinical studies, these methods are the main strategies discussed in the literature on drug development which are used to measure and predict passive permeability.

Traditionally, the ability of a drug to passively cross the cell plasma membrane was predicted (without the incorporation of phospholipids) using the shake-flask method, which gives the partition coefficient, expressed as logP.[24] This technique measures how much of a known concentration of drug crosses from an aqueous phase into an organic, non-polar phase, commonly 1-octanol, during a liquid-liquid extraction (Figure 1.2a). logP is a simplistic measurement of drug hydrophilicity (affinity for an aqueous phase) and lipophilicity (affinity for an organic phase) and does not take into consideration potential interactions of the drug candidate with the phospholipid bilayer. The shake-flask method can also be used to determine the distribution coefficient, expressed as logD, which also takes into account presence of ionized drug in the aqueous phase, otherwise, logP is a flawed quantification of the concentration of a ionizable drug, which most are.[25] Octanol partition measurements do not correlate well with absorption in humans. It has been shown that this is especially true for ionizable drugs, which interact with phospholipid bilayers, and hydrophilic drugs, the

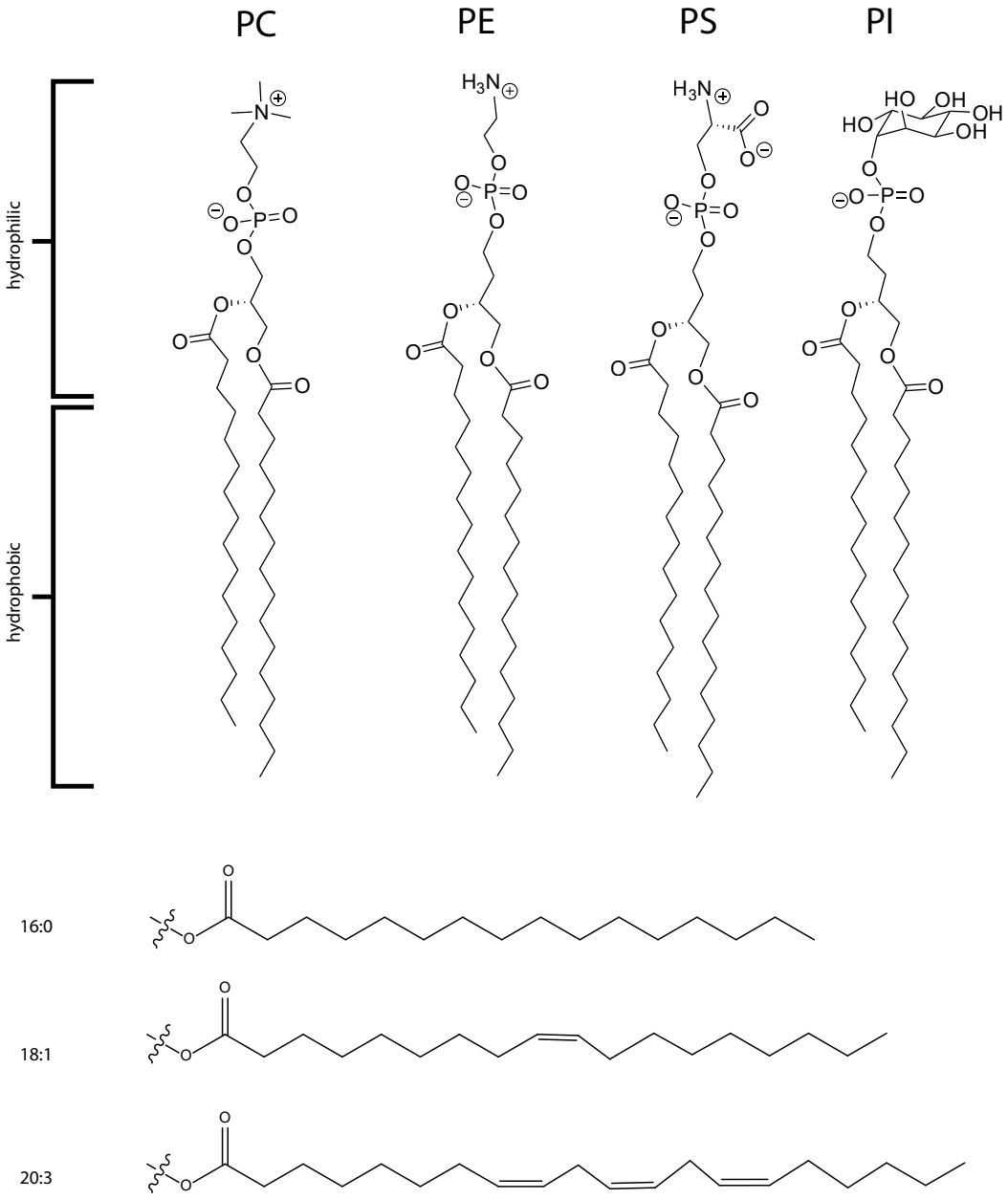

Figure 1.1: **Structures of the major phospholipids in mammalian cell plasma membranes.** PC, PE, PS, and PI are the major phospholipid components of mammalian cell plasma membranes. Each contains a distinct head group, which is hydrophilic, and hydrophilic tail groups. In the membrane, phospholipids form a bilayer to minimize interactions between their hydrophobic tails and water meolcules in both the extracellular space and the cytosol. This bilayer forms the structure of the cell plasma membranes. Passive permeability refers to the diffusion of molecules through the phospholipid bilayer. Representative images of phospholipid acyl chains are shown, with the first number indicating the number of carbon atoms in the chain and the second indicating the number of carbon-carbon double bonds. Phospholipids can contain two of the same or two different acyl chains.

partition of both in underpredicted in the octanol model. Conversely, the partition of lipophilic, neutral drugs is overpredicted by octanol.[26] Partition measurements are biologically dissimilar because they do not take into consideration potential interactions between the drug and the cell plasma membrane, specifically the phospholipid bilayer.

Permeability predictions are also made *in silico* based on Lipinski's famed rule of five, which assesses characteristic features of molecular structure of a drug candidate to predict "drugability," or how similarly to other drugs a molecule is likely to behave.[27] Structural variables including number of hydrogen bond donors and acceptors, lipophilicity, and molecular are used in the literature as a basis for computational prediction of membrane permeability.[27–32] The rule states that for a drug to be orally bioavailable, it must have at least three of the following properties: five or fewer hydrogen bond donors, ten or fewer hydrogen bond acceptors, a logP value of less than five, and a molecular weight of lower than 500 Da. Like partition measurements, these structural predictions provide information on drug lipophilicity and hydrophilicity and are flawed in their reliance on comparison to existing drug molecules. Lipinski's rule was determined in the late 1990s through the study of approved drugs produced by Pfizer. This approach hinders the analysis of novel, creative drug candidate structures, which may have pharmacokinetic properties dissimilar to those of existing drugs. Other sets of rules for oral bioavailability exist, most notably Veber's rule, which sets the requirement for ten or fewer rotatable bonds and a molecular polar surface area of less than $140\,\text{Å}^2$, notably removing the strict molecular weight cutoff at 500 Da. Overall, rather than providing a measurement of the interaction a drug has with a cell plasma membrane, *in silico* predictions are based solely on structure. Because passive drug transport involves permeation across the phospholipid bilayer of the cell plasma membrane, to more accurately predict passive drug transport, a

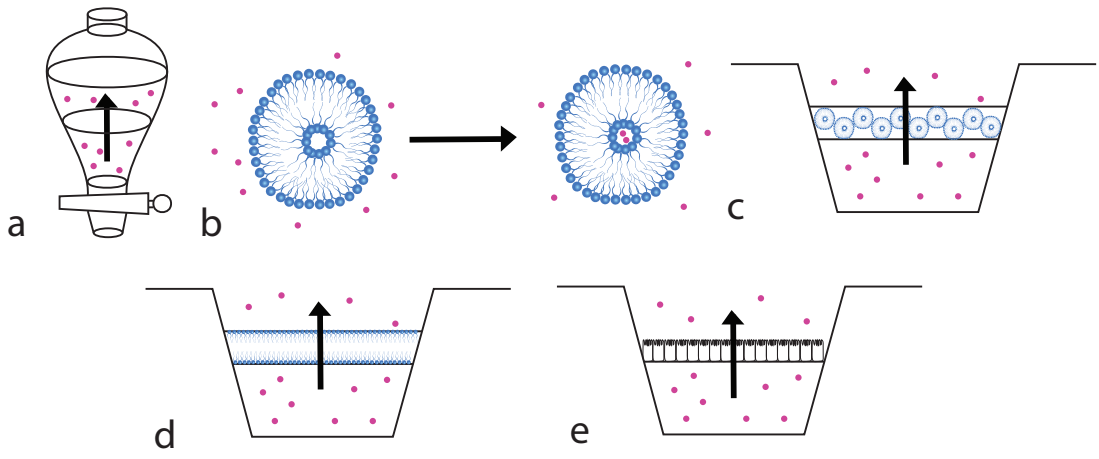

Figure 1.2: ***In vitro* techniques for permeability prediction.** All techniques shown are used to measure passive permeability of drugs with the exception of e), cell monolayer assays. Transport of a drug (pink circles) is shown in *in vitro* assays for permeability prediction. Arrows indicate the direction of drug permeation. a) The traditional shake-flask method uses liquid-liquid extraction in a seperatory funnel to determine the transport of a drug from an organic phase into an aqueous phase. b) In liposome uptake assays in solution, drug concentration inside liposomes is measured following incubation in a solution containing a known concentration of drug. c) Liposomes/vesicles can also be immobilized on a filter support in phospholipid vesicle permeability assays (PVPA). Transport of a known concentration of drug across the vesicle-filled filter is measured. d) Parallel artificial membrane permeability assays (PAMPA) allow for the measurement of drug transport across a synthetic filter filled with a phospholipid solution. Although the exact arrangement of the phospholipids is unknown, here phospholipids are depicted arranged in two monolayers separated by the solvent-filled filter. e) A monolayer of cells grown on an artificial filter support serves as a barrier between two aqueous compartments, between which the transport of a drug is measured. This drawing represents a Caco-2 monolayer, in which cells exhibit properties of enterocytes such as tight junctions and microvilli.

technique should assess interaction with a phospholipid bilayer and allow for prediction of the potential behavior of a drug candidate, not solely its similarity to existing molecules.

Currently, more sophisticated *in vitro* methods are used to predict passive drug transport, including those highlighted here with a focus on relevance in the pharmaceutical industry. These techniques can estimate pharmacokinetic parameters such as drug half-life ($t_{1/2}$), or the time for drug concentration to reduce by one-half, flux (rate of diffusion per unit area) of a drug across a membrane, and most frequently, the apparent permeability coefficient P_{app}. P_{app} is the main pharmacokinetic parameter used to describe permeability[33] and can be compared to *in vivo* measurements of the fraction of drug absorbed (F), the ratio between the concentration of drug in the blood after oral administration and intravenous (IV) administration. P_{app} and F

values correlate well: the boundary between low and high permeability compounds is considered to be an F value of 90% and a P_{app} value of $1.5\,cm\,s^{-1}$.[34]

Liposomes (also called vesicles) are spherical phospholipid bilayers which separate a bulk aqueous solution from an encapsulated aqueous solution. Liposome assays can be used to measure drug uptake into or release from liposomes formed from phospholipids, the predominant component of the cell plasma membrane (Figure 1.2b).[35,36] Liposomes provide a level of biological similarity since the drug under analysis crosses from one aqueous compartment to another through a phospholipid bilayer, much as would occur *in vivo*. Liposomal uptake of drugs has been studied using synthetic phospholipids as well as lipid extracts from plasma membranes.[37–39] Uptake from the bulk solution following incubation is measured through methods such as fluorimetry,[39] high performance liquid chromatography (HPLC),[40] and UV-Vis spectrophotometry.[38] In comparison to the shake-flask method, liposomes provide results which correlate better with human permeability.[26] This improvement in prediction accuracy is particularly pronounced when ionizable drugs are used, which are less lipophilic and less likely to partition into an organic phase,[26,41] indicating that ionizable drugs are more able to cross a localized nonpolar region (within the phospholipid bilayer) than to simply partition into an organic phase and remain soluble there. Use of a more biomimetic technique which incorporates phospholipids, the major component of the cell plasma membrane, improves the accuracy of permeability predictions. In addition to information about drug permeability, liposome uptake assays have also been used to assess interactions of charged drug with charged lipids in the phospholipid bilayer.[42] Because liposomes have structural similarities to the cell plasma membrane (the phospholipid bilayer), the effects of lipid composition on permeability can be isolated. Use of a biomimetic system allows for more accurate permeability predictions as well as investigation of more complex drug-membrane interactions.

Assays in which liposomes are immobilized on a supporting surface are more prevalent than those which rely on a bulk liposome solution, such as those described above. One such example is immobilized liposome chromatography (ILC).[43] In ILC, much as in HPLC, liposomes are immobilized in a chromatography column and an analyte (here, a drug) is allowed to travel through the column. Based on elution time, ILC provides data on drug-membrane interactions which correlate well with results from cell-based assays and human permeability.[43–45] The throughput of ILC is limited by the throughput of HPLC. Throughput can be increased through alternative methods of immobilizing liposomes/vesicles, such as in the phospholipid vesicle permeability assay (PVPA). In PVPA, which can be performed in a 96-well plate, phospholipid vesicles are deposited onto a porous synthetic filter, which forms a barrier between two aqueous compartments (Figure 1.2c). Passive diffusion of a drug across the synthetic filter and through the layer of vesicles can then be measured, giving P_{app} results which correlate well with human intestinal absorption.[46–48] PVPA was originally developed using only PC, but more biomimetic variants which use custom phospholipid formulations to mimic the enterocyte plasma membrane[47] as well as mucosal membranes[49] have been demonstrated as well. The commercially available Permeapad can also be used to predict permeability in high throughput. Permeapad is comprised of two synthetic filter supports filled with PC, which serve as a barrier between two aqueous compartments through which permeability can be assessed.[50] When exposed to aqueous solution, it is assumed that the phospholipids are hydrated and form a tightly packed layer of vesicles.[50] Data gathered using Permeapad correlate well with results from other *in vitro* assays for permeability prediction, both cell-free and cell-based.[50] Despite their biomimetic nature, it is unclear from the literature, which generally focuses on academic research, how frequently liposomal assays are used in the pharmaceutical industry. It seems that liposomes are more frequently used

as vehicles for drug delivery; drug release (rather than uptake) measurements are performed for delivery applications.[51,52] While these measurements also address the passive permeability of a drug of interest, the data gathered is applied toward determining the release profile and kinetics of the liposome-encapsulated drug rather than fundamentally understanding the pharmacokinetics of the drug.

The passive permeability prediction method predominantly used during drug development is the parallel artificial membrane permeability assay, or PAMPA.[3,53] In PAMPA, a porous synthetic filter filled with a solution of phospholipids in an organic solvent separates two aqueous compartments in a 96-well plate (Figure 1.2d). The passive diffusion of a drug candidate through the phospholipid-doped filter occurs during an incubation period and is then quantified, usually through UV-Vis spectrophotometry. PAMPA was designed to perform permeability measurements in high throughput. As in PVPA, a porous synthetic filter is used to support phospholipids while permeation of a compound is assessed, but PAMPA also relies on the presence of an organic solvent, which reduces its biological similarity.

The precise behavior of phospholipids in PAMPA is not clear in the literature. I hypothesize that, due to their amphiphilic nature, phospholipids self-assemble into layers and other nanostructures at solvent-water interfaces within the filter with their polar head groups in the aqueous phase and their nonpolar acyl tail groups in the organic phase within the filter, which is approximately 125 µm thick,[54] I propose that some phospholipids remain in solution, the potential interaction of which with analytes is unknown. Phospholipids are soluble in octanol, whether freely or as micelles, spherical nanostructures in which the hydrophilic head groups are protected from the organic solvent. The discrepancy between the thickness of the filter and the length of phospholipids (2 nm to 3 nm[55]) as well as the porous nature of synthetic filters limits

the extent to which PAMPA enables the formation of a planar, membrane-like phospholipid bilayer. Finally, while PAMPA is generally performed industrially using a single phospholipid, few examples exist incorporating more biomimetic lipid mixtures. These include a blood-brain barrier (BBB) mimic, the results of which correlate well with *in situ* brain perfusion measurements,[56–58] and an intestinal absorption model which uses a lipid composition based on that of human intestine epithelial cells[59] and biologically relevant pH values.[60] Other permutations of PAMPA exist in the literature,[20] including a three-compartment version of PAMPA in which drugs under analysis passively diffuse through two bilayers as they move from a compartment representing the small intestinal lumen through a compartment representing the enterocyte cytosol into a compartment representing the bloodstream.[61] PAMPA is the 'gold standard' technique currently used for the prediction of passive drug permeability.

The final key *in vitro* method used in preclinical trials is the cell monolayer assay (Figure 1.2e). Briefly, a cell monolayer is cultured on a synthetic filter support, which can then be used to separate two aqueous compartments, similar to the structure of PAMPA. A cell monolayer assay accounts for not only transcellular transport, where a drug travels through the cell and through its plasma membrane, but also paracellular transport, where a drug travels through a junction between cells. Here, I will discuss cell monolayer assays for predicting permeability of the small intestinal lining and the blood-brian barrier. The main cell lines used to predict drug absorption in the small intestine are Madin Darby Canine Kidney (MDCK) cells and, more frequently the human epithelial colorectal carcinoma cell line Caco-2.[20] Caco-2 cells exhibit properties native to enterocytes, which line the small intestine and are responsible for absorption, such as tight junctions and microvilli.[62] These physiological features regulate paracellular transport, and increase absorptive cell membrane surface area, re-

spectively. Despite relatively high correlation with F,[15] several variables cannot be precisely controlled, such as the effect of drug partition across the membrane used as a support during monolayer growth, and potential compound metabolism in addition to other competing intracellular processes.[63,64] Additionally, because Caco-2 is a heterogeneous cell line, regional cell differences may interfere with accurate assessment of permeability.[15] Similarly, permeation of the blood-brain barrier can be predicted using monolayer cultures of brain endothelial cells, several types of which have been tested in the literature. Several rat brain cell lines have been used to model the blood-brain barrier, with moderate success.[65] When used in cell monolayer assays, these cell lines generally overestimate paracellular transport as they do not exhibit the tight junctions characteristic of the blood-brain barrier.[65] MDCK cells have also been used to predict blood-brain barrier permeability, but yield results with poor correlation to *in situ* brain perfusion measurements.[57] This has been attributed to differences in cell membrane composition between MDCK and brain endothelial cells. Compared to MDCK cell plasma membranes, brain endothelial cells contain higher ratios of PC to sphingomyelin (SM) as well as high ratios of cholesterol to phospholipid content.[57] Phospholipids in brain endothelial cells also contain higher ratios of saturated to unsaturated acyl chains in their tail groups.[57] These differences in cell plasma membrane composition mean that MDCK cell plasma membranes are more fluid than those of the blood-brain barrier, leading to poor correlation between predicted and measured permeability. Because of the discussed issues associated with using other cell lines, human brain endothelial cell lines have also been used for the prediction of blood-brain barrier permeability with improved correlation to *in situ* brain perfusion data.[66]

It is important to note that *in vitro* techniques which employ cell monolayers provide significantly different information to researchers than the cell-free systems discussed

above. Cell-based systems are also significantly more time- and labour-consuming as well as more expensive than cell-free models, which limits their throughput.[20] Permeation across a cell monolayer takes place not only through passive transcellular diffusion but also carrier-mediated transport involving membrane proteins, as well as paracellular diffusion. Permeability results from a cell monolayer assay may also be confounded by metabolism of the drug candidate of interest. This is important information to determine during the drug development process and marks the key difference between permeability results determined through lipid-only and cell-based *n vitro assays.* Overall, an assay based on living cells cannot isolate the process of passive lipoidal diffusion, as is done in liposome assays and PAMPA.

Overall, the *in vitro* techniques currently used during the preclinical stage of drug development to predict passive drug permeability lack translatability to applications in humans, contributing to the high failure rate of drug candidates during clinical trials. In addition to factors such as high cost, I propose that the major disadvantage of these techniques is lack of biological similarity. A more biomimetic technique to model the passive transport of a drug across the phospholipid bilayer of a cell plasma membrane has the potential to improve the accuracy of predictions made in the early stages of drug development. To ensure that permeability across any cell plasma membrane of interest can be predicted accurately, this technique should have the capacity to isolate transport processes, such as passive permeability, between two discrete and controllable aqueous compartments. The miniaturization of these compartments would also allow for low sample demand and help to increase throughput, which are key parameters for industrial work in particular. A new technique for passive permeability prediction should also be customizable, incorporating biomimetic phospholipids as well as conditions of the aqueous compartments. By incorporating the beneficial features of existing techniques, a new *in vitro* pharmacokinetic prediction tool has the

potential to improve the accuracy and translatability of preclinical research. I aim here to create a new *in vitro* membrane model to complement cell-based assays as well as *in vivo* trials in animal models and humans.

1.3 Microfluidic techniques for droplet interface bilayer (DIB) formation

Microfluidic technology allows for the precise manipulation of fluid flow on the microscale. A microfluidic device contains microscale channels which can be filled with fluid using external syringe pumps or a pressure pump connected to the device with tubing. Since the 1990s, microfluidic devices (or "chips," referencing the original tie the field had to micro-electro-mechanical systems (MEMS)) have been designed for a large variety of applications, including small-scale synthetic chemistry,[67] sample analysis,[68] cell culture,[69] precise sample mixing,[70] optical measurements,[71] and energy applications.[72] Microfluidic devices can also be designed to generate droplets when streams of two immiscible liquids intersect (Figure 1.3. Use of a microfluidic device for droplet generation gives a high level of control over droplet properties and movement, giving aqueous droplets the potential to be used as compartments in a new technique for the prediction of permeability. Fluid flow on the microscale is laminar rather than turbulent, meaning that fluids (and droplets) move linearly and predictably through the channels.[73]

My research employs the formation of aqueous droplets in a bulk oil solution, or "water-in-oil" droplets. Use of a microfluidic platform for the development of an analytical technique has numerous advantages, including low reagent volume requirements, potential for rapid analysis, small lab footprint, low cost, and ease of perform-

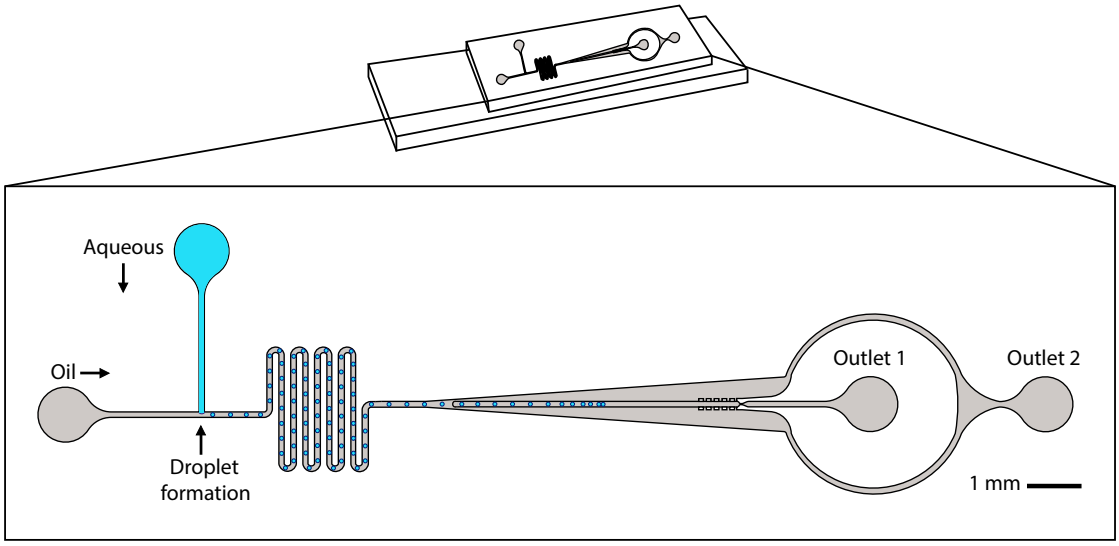

Figure 1.3: **The design of a microfluidic device for droplet formation.** Top: A microfluidic device mounted on a standard microscope slide. Channels are formed when a polymer slab etched with the channel design is bonded to a substrate, sealing off channels so they can only be accessed through inlets and outlets (indicated with labels and arrows). Inset: Droplets form when two immiscible liquid phases intersect at a T-junction and flow through the rest of the device before exiting the chip through outlets. Arrows indicate direction of fluid flow.

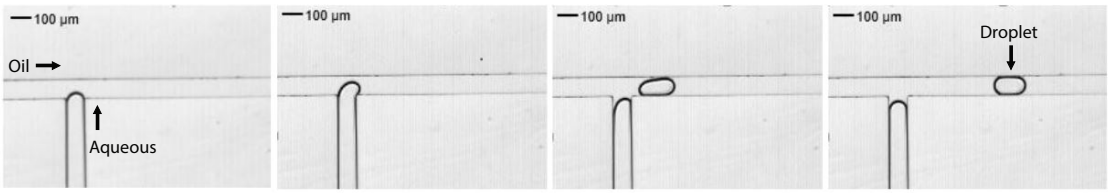

Figure 1.4: **Droplet formation at a T-junction in a microfluidic device.** At a T-junction, where two streams of immiscible fluids intersect perpendicularly, droplets of the discrete phase form and are guided by flow of the mobile phase. Here, the discrete (droplet) phase is an aqueous buffer and the mobile (bulk) phase is squalene. Arrows indicate the direction of fluid flow.

ing experiments in replicate simultaneously.[74] These benefits make a microfluidic platform extremely appealing for pharmacological applications in which a heavy emphasis is placed on efficient measurements. Miniaturization also requires small amounts of analyte, which is preferable in the case of drugs which are expensive or difficult to synthesize. Aqueous droplets can serve as discrete, positionable compartments which allow for the precise and localized measurement of drug concentration.

Droplet interface bilayers are formed when two phospholipid-coated droplets are

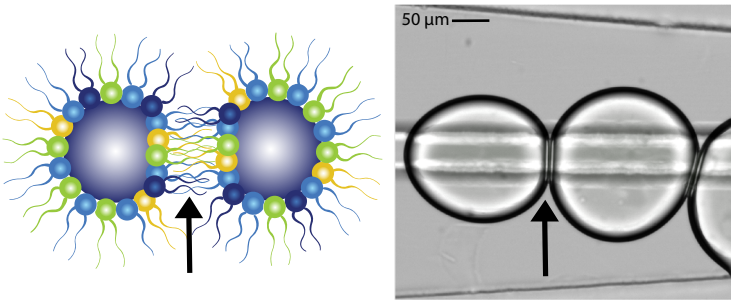

Figure 1.5: **Droplet interface bilayer (DIB) formation.** Left: Phospholipid headgroups are denoted by circles at the water-oil interface. Acyl chain tail groups point out into the oil phase. The arrow indicates the site of DIB formation. Varying colours indicate different phospholipid types present. Right: Image of a DIB formed using DPhPC on a microfluidic device, the design of which is shown in Figure 1.3.

brought into contact (Figure 1.5). When phospholipids are added to a system containing an aqueous droplet in a bulk oil phase, they spontaneously self-assemble into monolayers coating the aqueous droplets with the hydrophilic head groups inside the aqueous droplet and the hydrophobic tail groups in the oil phase. Bringing two monolayer-coated droplets into contact forms a bilayer section at their interface which can be used as a cell membrane model. To facilitate DIB formation, phospholipids can either be dissolved in the oil phase ("lipid-out") or extruded as vesicles in the aqueous phase ("lipid-in"). As opposed to liposomes, which are essentially aqueous droplets separated from a bulk aqueous solution with a phospholipid bilayer, DIBs are aqueous droplet separated from one another with a phospholipid bilayer and separated from a bulk oil solution with a phospholipid monolayer.

In the literature, DIBs have mainly been formed using only single phospholipids, notably 1,2-dioleoyl-sn-glycero-3-phosphocholine (DOPC)[75–77] and DPhPC.[78,79] Both DOPC and DPhPC are synthetic phospholipids not found in mammalian cell membranes[80,81] Reliance on single, synthetic phospholipids to form artificial plasma membranes is not biomimetic, since real cell membranes contain a diverse mixture of lipids. Use of a single phospholipid also ignores the distributions of tail lengths and

degrees of saturation represented in biological cell membranes. Sparse publications exist demonstrating the use of more complex mixtures, including total lipid extracts from soy,[82] *Escherichia coli*,[83] and brain[84] cell membranes. DIBs have also been created using mixtures of synthetic phospholipids,[84,85] mixtures of naturally derived phospholipids,[86,87] monoglycerides,[88–90] and polymers.[91,92] Here, I define synthetic phospholipids to be samples which are synthetically derived and contain only one head and one type of tail group. Naturally derived phospholipids contain a single head group but a diverse distribution of tail groups, which have different acyl chain lengths as well as degrees of unsaturation. Phospholipid formulations are mixtures designed and created by researchers, while lipid extracts are extracted from directly from cell plasma membranes. All of these types of lipids can be used in DIB formation and have the potential to provide researchers with different information.[77,84–87]

The demonstrated applications of DIBs are diverse. DIBs are largely used in the literature to perform electrophysiological measurements, mainly of bilayer capacitance.[75,93–96] Interconnected networks of DIBs can also be formed to create artificial tissues-on-a-chip, while maintaining control over droplet and bilayer size;[76,97–99] DIB networks have also been used for electrical measurements and have been shown to function as diodes.[100] Electrophysiological measurements related to membrane proteins have also been demonstrated, such as measurement of current through pore-forming proteins like α-hemolysin.[93]. Many literature examples exist of the use of DIBs to study proteins and peptides which insert into the cell plasma membrane, including α-haemolysin,[79,101] Pep-1,[102] and ion channels,[103,104] including the human chloride channel CLIC1.[105] One literature example of the insertion of a transporter into a DIB exists: the *E. coli* lactose permease transporter (LacY).[106] In addition to their potential to predict passive transport, prediction of the active transport of drugs may also be possible in DIBs through screening of pharmacologically relevant human

transporters; however, insertion of a human transporter has not yet been achieved. The use of DIBs to screen blockers against a potassium channel has already been shown,[107] illustrating the potential of DIBs in this application.

DIBs can also be used for the analysis of molecular kinetics. When a DIB connects two aqueous droplet compartments, one of which contains a known concentration of a molecule, transport of that molecule across the membrane can be quantified through, for example, fluorescence microscopy. In the literature, DIBs have been used to quantify the passive diffusion of fluorophores[77,82,86,104,108–112] molecules which undergo a fluorogenic reaction,[113] caffeine,[77] and doxorubicin.[87] Recent results demonstrate a relationship between DIB permeability and composition of the membrane, indicating that the choice of phospholipid mixture used for DIB formation for permeability measurements is nontrivial.[85] Quantification of molecular transport mainly relies on the use of fluorescence microscopy for the observation of movement of fluorescent compounds. Only one demonstration of off-chip analysis of molecular transport across a DIB has been reported, wherein transport of rhodamine 6G across DIBs formed on a microfluidic device was measured off-chip using liquid chromatography-mass spectrometry (LC-MS).[112] In addition to the transport of solutes contained within droplets, water permeability across DIBs has been investigated, showing a relationship between membrane composition and permeability.[88–90,114] When DIBs are formed which connect two droplets containing an NaCl concentration gradient, the effect of incorporating cholesterol,[88] cholesterol sulphate,[114] and monoglycerides with varying acyl chain lengths and degrees of unsaturation[88–90] on water permeability could be observed using both microscopy[88–90,114] and Raman microspectroscopy.[115] Water permeability appears to decrease with the addition of cholesterol sulphate[114] as well as when thicker DIBs are formed through the incorporation of longer monoglyceride acyl chains.[89] Permeability of both water and fluorophores like fluorescein increases with

increasing monoglyceride[88–90] and phospholipid[85] unsaturation, due to the formation of less tightly packed bilayers. Water permeability decreases with the incorporation of cholesterol, which appears to create more tightly packed membranes through intercalation with phospholipid tails within the bilayer.[88,90] These applications demonstrate the potential for DIBs to be used to measure molecular permeability across a phospholipid bilayer and to quantify the effects of membrane lipid composition on permeability.

DIBs can be created manually using micropipettes, micromanipulators, and electrodes or on a microfluidic platform. Only around one third of the publications which report the generation and use of DIBs use a microfluidic platform to do so. The majority of these microfluidic papers have been published in the last ten years, indicating a potential shift in the DIBs literature toward microfluidic technology (see Appendix B for a more detailed discussion). Non-microfluidic, manual methods make the use of DIBs for analytical purposes labor-intensive and tedious and limit the droplet size which can be used, often on the scale of 500 µm in diameter, which is quite large compared to the size of human cells.[116] A microfluidic platform allows for miniaturization through the consistent generation of droplets closer to the size scale of cells, which increases the biological similarity of the model.[77,86,108,116] Microfluidic devices also allow for faster formation of DIBs (seconds versus minutes) by incorporating geometries such as meandering channels (Figure 1.3),[117] which decrease the equilibration time required when using manual techniques.[118] Use of a microfluidic platform introduces the possibility of increased throughput, which is limited off-chip.[108] In addition to meanders, microfluidic devices for DIB formation often employ droplet trapping features like pillars[77] and rails[97] to control droplet movement and DIB formation. Although more infrequently used in the field, DIBs can also be formed by solvent evaporation,[119] flow-guiding,[97] "passive" droplet guidance that relies solely on on-chip architectural

features,[86,109,120] and "active" droplet guidance which additionally requires the use of on-chip features such as valves to control droplets.[99] For a detailed review of the history and future potential of DIBs, see Appendix B, a perspective review I co-wrote with Elanna Stephenson.

While they exhibit high potential for the prediction of passive permeability, DIBs have as of yet been underutilized. The membrane created when a DIB is formed as well as the contents of the droplet compartments which the bilayer connects can be customized to mimic pharmacologically relevant tissues. The phospholipids used as well as the composition of the droplets can be tuned to mimic pharmacologically relevant tissues, giving DIBs the potential to model cell plasma membranes. I propose that the use of tailored, biomimetic phospholipid compositions will transform DIBs into true artificial cell plasma membranes which have applications in the early stages of drug discovery as a new method for permeability prediction (Figure 1.2e). The use of DIBs provides an opportunity for a high level of control over assay composition, ease of use, and biological similarity. By creating bespoke lipid formulations as well as customizing the composition of the droplet compartments, researchers can use DIBs to model pharmacologically relevant membranes such as the lining of the small intestine and the blood-brain barrier.

1.4 Presented work

Chapter 2 shows the development the surface modification of microfluidic device channels for DIB formation. Chapter 3 is a systematic study on the effect of temperature on DIB formation using naturally derived phospholipids and formulations thereof. Chapter 4 presents DIBs as a new type of pharmacokinetic compartment model for intestinal absorption and was published in 2020 in *Lab on a Chip*.[86] Elanna

Stephenson and I were joint first authors. Chapter 5 describes the development of complex DIB models for other pharmacologically relevant membranes as well as an investigation into novel methods of drug transport detection on-chip. Appendix B is a perspective review on the history and future potential of DIBs; Elanna Stephenson and I were joint first authors. We also co-authored the first patent in the Elvira Group, entitled "Microfluidics for Drug Discovery" (U.S. patent application No. 17/163,164, filed January 29, 2021).

Chapter 2

Surface treatment of microfluidic devices for droplet interface bilayer (DIB) formation

2.1 Context

Generation of stable water-in-oil droplets is a prerequisite for the creation of DIBs. Microfluidic devices fabricated using polydimethylsiloxane (PDMS) exhibit varying surface chemistry properties as well as permeability to water vapour. These phenomena pose a challenge to the formation of water-in-oil droplets as well as to their long-term (hours) storage in a device. Sufficient channel surface hydrophobicity is required to encourage droplets to form at the intersection of an aqueous and an oil stream. If the channels are hydrophilic, the aqueous phase will adhere to them, discouraging droplet formation. My aim was to determine whether strategies demonstrated in the literature for both increasing channel hydrophobicity and mitigation

of aqueous droplet evaporation are effective and necessary in my own work. Using trichloro(1H,1H,2H,2H-perfluorooctyl)silane (PFOS) to functionalize the interior surfaces of microfluidic devices to increase their hydrophobicity has been shown to encourage water-in-oil droplet formation. To assess the effect of PFOS treatment, I measured the contact angle of fluids which are relevant in DIB experiments on treated and untreated PDMS. I report a comprehensive study of contact angle measurements of commonly used fluids: reverse osmosis (RO) water, DPhPC in buffer, DPhPC in hexadecane, hexadecane, and squalene. I also show preliminary results using Teflon AF (amorphous fluoropolymer) and Aquapel surface treatments as well as bonding a glass coverslip and soaking in RO water, which have all been previously suggested to mitigate droplet evaporation during analysis. Furthermore, I tested baking microfluidic devices for 24 h; this was found to be sufficient to encourage hydrophobic recovery and water-in-oil droplet formation.

I performed all experimental work and dat analysis, with exceptions listed here. DPhPC in hexadecane contact angle measurements were performed by Genie Lee for her CHEM 399 project under my supervision (Figure 2.3). Aquapel and RO water soaking measurements were performed by Nathan Heuver for his CHEM 399 project under my supervision. I performed all other contact angle, droplet formation, and droplet evaporation experiments. I designed the device used for droplet formation and evaporation experiments based on previous generations of designs designed by Elanna Stephenson and Matt Noseworthy (Figure 1.3).

2.2 Introduction

A significant challenge in the field of microfluidics is the creation of device channel surfaces which are consistent and stable over time.[121] Polydimethylsiloxane (PDMS)

is widely used for device fabrication due to the relative ease and low cost associated with its use, but problems with its surface chemistry have been widely documented in the literature.[122–124] The creation of stable microfluidic channels for DIB formation is particularly challenging in that the surfaces must also be compatible with membrane lipids included in the system.[123] Inconsistencies with PDMS surface chemistry have been mainly attributed to uncross-linked mono- and oligomers migrating in the PDMS bulk[125,126] to reduce surface free energy.[127] Changes in overall polymer structure create challenges in the field of droplet microfluidics, as droplet generation fails without proper surface chemistry. Water-in-oil droplet generation requires hydrophobic surfaces.[128] Stable, consistent, hydrophobic microfluidic channels are necessary to facilitate water-in-oil droplet formation, which is necessary for DIB formation, but it is not clear in the literature whether surface modification achieves this. Additionally, PDMS is permeable to gases including water vapour,[129] making the analysis of aqueous droplets on longer timescales (above 1 h) difficult. To facilitate this, it is possible that a surface modification which slows evaporation is necessary. Surface treatments which are claimed to accomplish these objectives have been used in the literature.[121,130–133] My aim was to to determine if these treatments were effective and necessary in my own work.

The structure of PDMS is formed by mixing together a base (dimethylvinyl terminated dimethylsiloxane) and a curing agent (polymethylhydrosiloxane), which permanently cross-link at higher temperatures. After combining at room temperature, the uncured PDMS polymer can be poured into a master mould, baked, and peeled off in a process called soft lithography. This imprints microfluidic channels into the surface of the PDMS slab. In my work, these etched slabs are then bonded to PDMS-coated glass microscope slides using air plasma to create complete channels through the PDMS, open only at inlets and outlets punched prior to bonding (Figure 1.3). Air

plasma activates the surface of PDMS, mainly forming hydrophilic silanol groups (Si-OH)[125] that when brought together condense to extend the siloxane bonding network formed in the cured PDMS (Figure 2.1).[134] However, any unbonded PDMS surfaces will not remain activated: PDMS undergoes a process called hydrophobic recovery in which the activated surface returns to its original hydrophobic state.[125,135–138] This process occurs over several days at room temperature or over 24 h at 65°C.

This phenomenon causes several issues. First, the activated surface created via air plasma is hydrophilic, which is not ideal for the microfluidic generation of water-in-oil droplets. However, the surface also does not remain hydrophilic, making device behavior unpredictable. My research relies on the consistent creation of water-in-oil droplets, so using PDMS immediately following plasma bonding leads to failure (Figure 2.2). Potential strategies for creating a stable hydrophobic PDMS surface which are commonly used in the literature include a days-long waiting period at room temperature,[137] thermal treatment,[135] and chemical or physical derivatization.[121,139] Because chemical derivatization is the most rapid of these techniques, I tested it first.

A common method of chemical derivatization of PDMS surfaces is silanization, in which a silane bonds to silanol groups on the activated PDMS surface. Sui *et al.* developed a protocol for PDMS surface silanization using neat or diluted silane to increase hydrophilicity.[121] Surface treatments for the formation of DIBs have been developed based on this protocol, but with the aim of creating hydrophobic surfaces, for example, Sarles *et al.* reported decreased wetting of the aqueous phase during DIB formation after treatment of activated PDMS channel surfaces with neat (tridecafluoro-1,1,2,2,-tetrahydrooctyl) trichlorosilane.[130] Use of a chlorinated silane facilitates reactivity with surface Si-OH bonds, creating new siloxane bonds (Si-O-Si-R, where R = alkyl or fluoroalkyl chain). Silanization of microfluidic channels

for DIB formation can also be performed using commercial reagents, such as Sigmacote.[109] Use of a silane which contains fluoroalkyl groups rather than alkyl groups has the potential to create more hydrophobic surfaces due to the highly hydrophobic nature of fluorocarbons.[140,141] To create hydrophobic microfluidic channels, I chose to functionalize our air plasma-treated PDMS surfaces through silanization with PFOS (Figure 2.1). Based on previous work in the Elvira Group and manufacturer guidance[142] I decided to use a dilute silane solution (5% (v/v) in isopropyl alcohol).

PDMS is permeable to water vapour, hindering long-term (hours) storage of aqueous droplets on a microfluidic device.[129] Numerous methods have been reported in the literature to slow the evaporation of aqueous droplets through PDMS. Zec *et al.* demonstrated reduced evaporation through PDMS after bonding a glass coverslip to the top surface of the device.[143] Through the treatment of PDMS devices with a Teflon AF solution, Park *et al.* reported reduced aqueous evaporation as well as reduced PDMS uptake of fluorescent dyes.[132] "Water priming," soaking of the microfluidic device in water before use, was also shown to reduce droplet evaporation.[133] The fluorinated water repellent Aquapel has also been used to treat PDMS and was shown to facilitate a ten day droplet incubation without evaporation.[131] I tested each of these evaporation mitigation strategies, observing DIB evaporation over time.

2.3 Results and discussion

2.3.1 Surface treatment for aqueous droplet formation

First, I tested PFOS surface treatment for water-in-oil droplet formation. In comparison to untreated PDMS, PDMS samples treated with PFOS following air plasma activation exhibit an increase in hydro- and oleophobicity up to seven days following

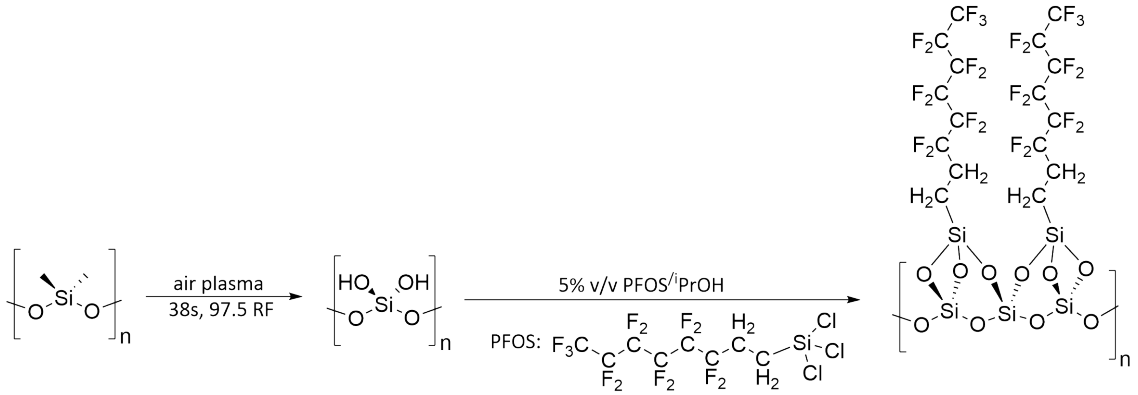

Figure 2.1: **Proposed reaction of air plasma activated PDMS with PFOS.** PDMS slabs are treated with air plasma for 37 s, creating silanol groups on the PDMS surface. The activated surface is then treated with a 5% v/v solution of PFOS in isopropyl alcohol for 1 min, silanizing the PDMS surface through the creation of siloxane bonds. Excess PFOS solution is evaporated with a stream of filtered air.

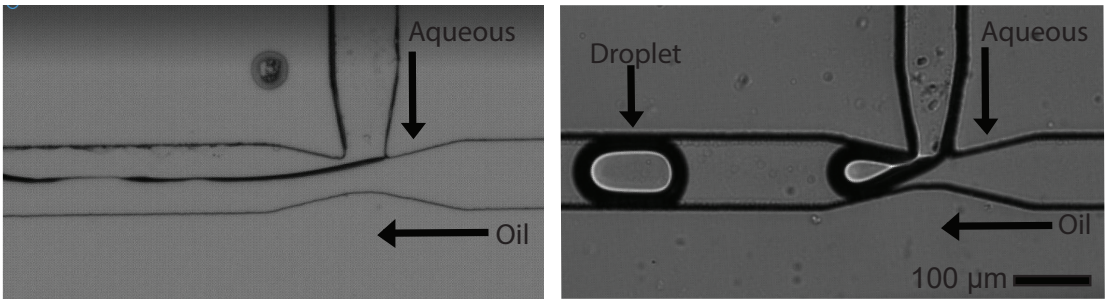

Figure 2.2: **Droplet formation on untreated and treated microfluidic devices.** Left: On PDMS recently treated with air plasma, the aqueous phase wets to the hydrophilic channel surface and co-flows with the oil phase. Right: On PDMS treated with PFOS solution following air plasma, the aqueous phase shears off at the tapered T-junction and droplets form. The aqueous phase is DPhPC (2 mg/mL aqueous buffer and the oil phase is squalene. Both experiments were performed immediately following surface treatment with either air plasma (left) or air plasma followed by PFOS (right). The scale bar applies to both images. Arrows indicate direction of fluid flow on the microfluidic device.

treatment (Figure 2.3). This was observed through measurement of contact angles between a 2 µL droplet and a PDMS surface. Three droplets were placed onto different locations on each PDMS slab and images were taken to allow for contact angle measurement on both sides of each droplet. Because an image is taken of the entire droplet (Figure 2.3), the angle between the droplet and the PDMS surface can be measured on both the left and right. These measurements were repeated in triplicate, yielding 18 data values in total for each time point. An increase in contact angle was observed not only for aqueous solutions (RO water and DPhPC in buffer) but for oils (squalene, hexadecane, and DPhPC in hexadecane) as well, indicating that PFOS functionalization affects not only PDMS hydrophobicity, as has been previously suggested[144] but oleophobicity as well. This indicates that in addition to creating a hydrophobic surface for the creation of water-in-oil droplets, PFOS treatment may also mitigate the permeability of PDMS to solvents and oils.[145] Increased oleophobicity may also have the benefit of stabilizing phospholipid-coated aqueous droplets, such as those necessary for the formation of DIBs.

A contact angle above 90°indicates oleo- or hydrophobicity.[146] While the average con-

tact angle between treated PDMS and oil remained below this threshold, the contact angle was consistently higher than untreated PDMS (Figure 2.3). In Figure 2.3, the leftmost column shows images of droplets of each fluid tested on PDMS surfaces treated with PFOS. The centre column shows droplets on untreated PDMS surfaces, which have only been treated with air plasma. The rightmost column shows quantitative changes in contact angle (n = 18) over 168 h. Contact angle measurements were performed 0 h, 2 h, 24 h, and 168 h (1 week) following treatment.

However, water-in-oil droplet formation was also found to be possible after a minimum 24 h bake at 65°C, rendering PFOS treatment an unnecessary auxiliary step in microfluidic device fabrication. Unless the device must be used immediately following plasma bonding, in which case PFOS treatment would make droplet formation possible, thermal aging is enough to create a useable PDMS device. Baking microfluidic devices for 24 h was found to be sufficient to encourage hydrophobic recovery and water-in-oil droplet formation.

2.3.2 Surface treatments for droplet evaporation mitigation

Droplet evaporation on an untreated PDMS microfluidic device occurs within 4 h, although DIBs remain intact (Figure 2.4). Droplet diameter decreases by an approximate rate of 25% per hour. I first attempted to functionalize the PDMS surface with a Teflon AF solution (1% in FC-40). Although a qualitative increase in contact angle was observed with squalene, hexadecane, and RO water (Figure 2.5), no significant effect on evaporation was apparent. In Figure 2.5, images on the left show droplets of tested fluids on PDMS treated with Teflon AF and images on the right show droplets on untreated PDMS, which was stored at 65°C for over 24 h.

Two of the tested methods yielded modest improvement in droplet evaporation –

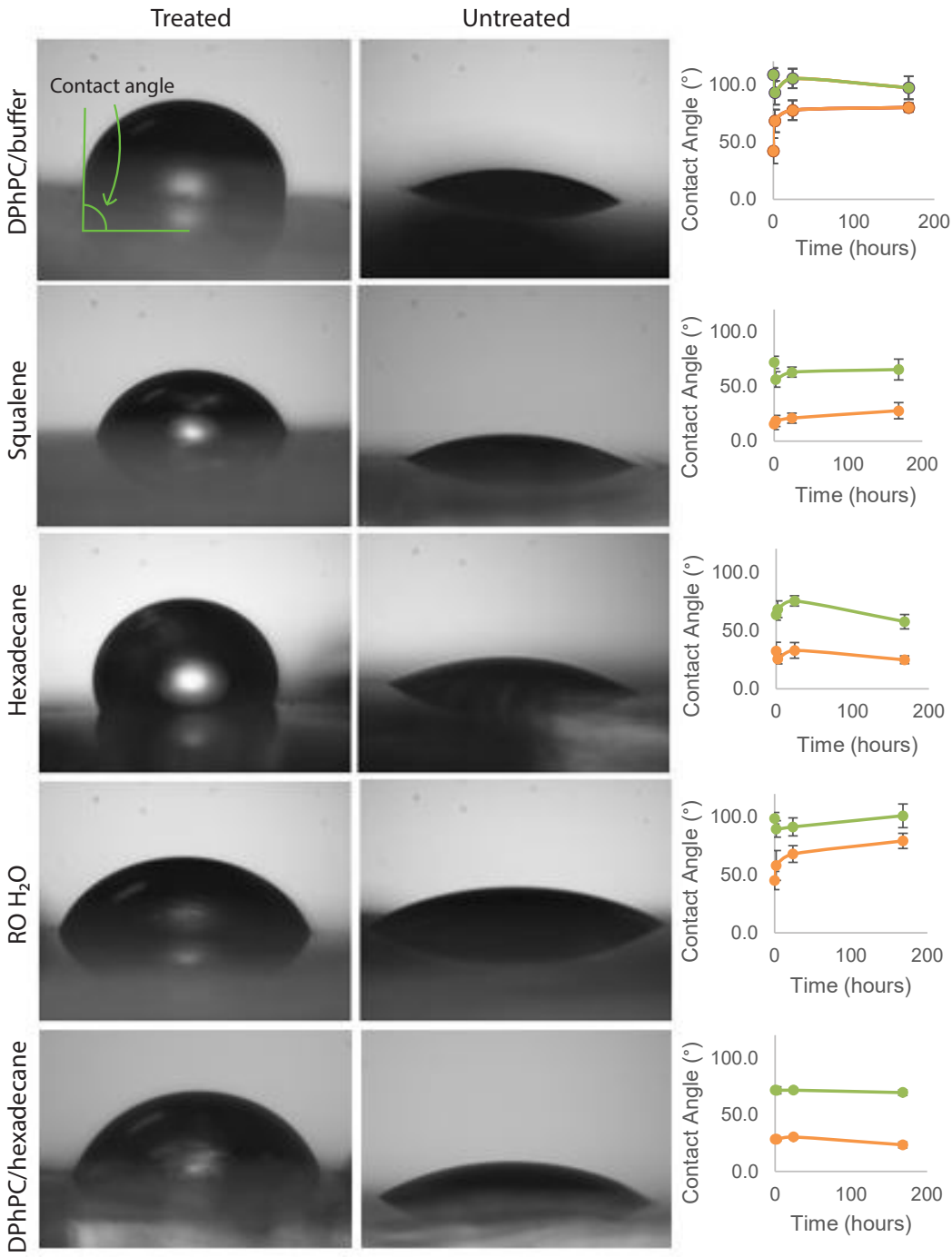

Figure 2.3: **Contact angle measurements on PDMS.** Images of 2 µL droplets of (from top to bottom) DPhPC (2 mg mL^{-1} in aqueous buffer), squalene, hexadecane, RO water, and DPhPC (2 mg mL^{-1} in aqueous buffer) immediately following treatment (t = 0h). Treated PDMS has been exposed to air plasma and treated with a PFOS solution. Untreated PDMS has been exposed to air plasma. PDMS slabs used for contact angle measurements were stored at room temperature until measurement was performed. Contact angle data is shown at 0, 2, 24, and 198 hours for all fluids on PDMS treated with air plasma followed by silanization (green) and PDMS treated with air plasma (orange). Genie Lee collected the DPhPC in hexadecane data for her CHEM 399 project. An example of a contact angle is shown in the first image. Error bars represent standard deviation (n = 18).

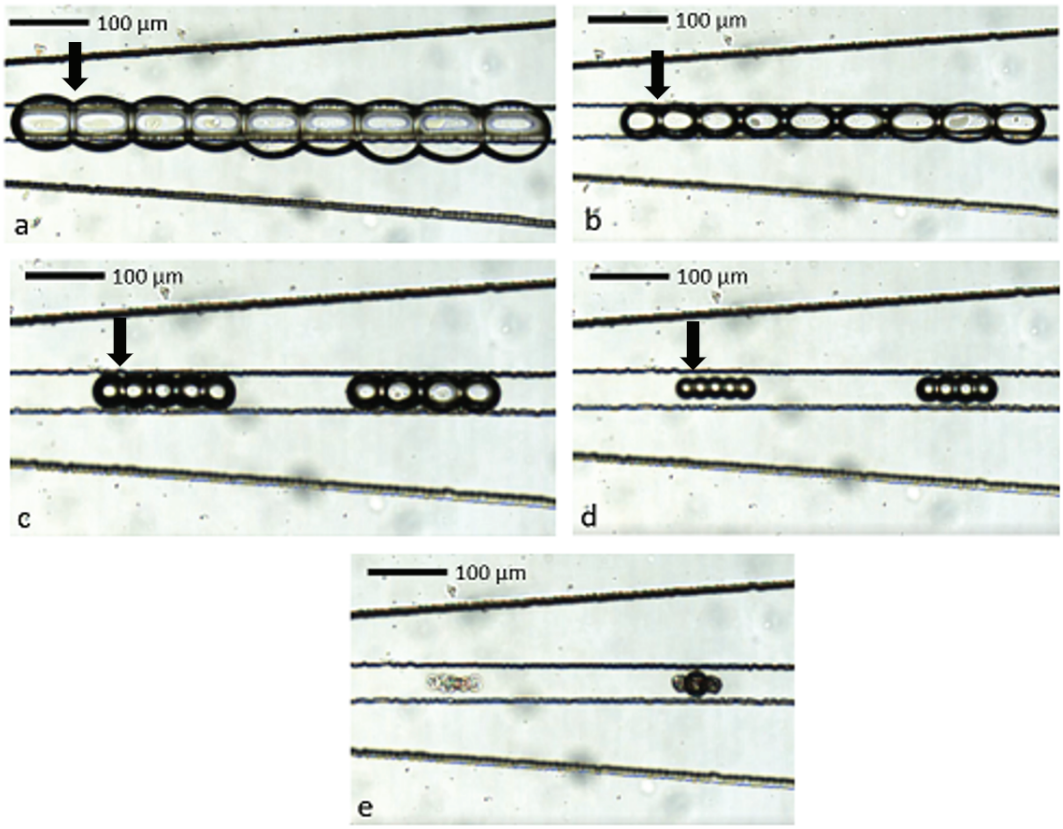

Figure 2.4: **DIB-connected droplet evaporation over time.** DIBs formed using DPhPC at times a) 0 h, b) 1 h, c) 2 h, d) 3 h and e) 3.75 h. Arrows indicate example sites of DIB formation, showing the DIBS are extremely robust over time despite droplet evaporation. The aqueous phase is DPhPC (10 mg mL^{-1} in pH 7.59 HEPES buffer) and the oil phase is squalene. The device used is shown in Figure 1.3.

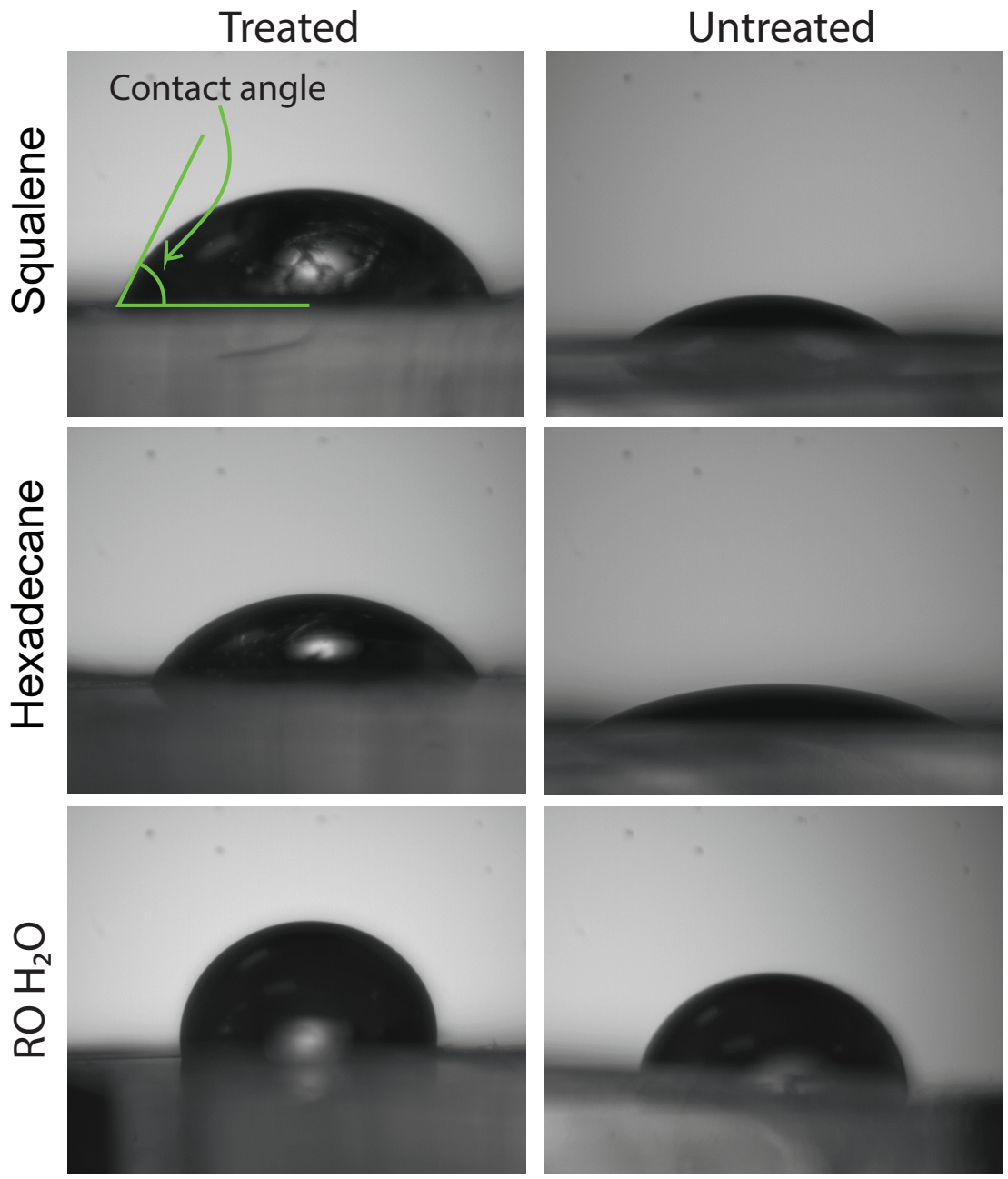

Figure 2.5: **Contact angle measurements on Teflon-coated PDMS.** Images of 2 µL droplets of (from top to bottom) squalene, hexadecane, and RO water immediately following treatment (t = 0h). Untreated PDMS has been exposed to air plasma and stored at 65 °C for over 24 h. Treated PDMS has been exposed to air plasma and a Teflon AF solution. An example of a contact angle is shown in the first image.

Aquapel surface treatment and soaking in RO water. For each of these experiments, evaporation of DIBs formed using DPhPC (5 mg mL^{-1} aqueous buffer) was observed. Under my supervision, Nathan Heuver first tested the effects of an Aquapel surface treatment on droplet evaporation. When microfluidic channels of devices previously stored at 65°C were treated with Aquapel, either once or twice with a 20 min bake at 65°C between, droplet diameter decreased by 24% per hour and 20% per hour, respectively. Repetition of the Aquapel treatment was tested to investigate if creation of a thicker physical coating would affect droplet evaporation. Slightly better results were observed when the device was treated with air plasma immediately prior to Aquapel treatment, with a 13% decrease in droplet diameter per hour. These results are not significant enough to justify the labour required to implement Aquapel surface treatment into our regular device fabrication protocol.

Next, I tested the effects of bonding a glass coverslip to the surface of the device as well as soaking in RO water. I performed initial tests for both techniques and Nathan Heuver gathered all subsequent data. When a glass coverslip was bonded to the top surface of the microfluidic device, droplet diameter decreased by 27.1% per hour. When the microfluidic device was soaked in RO water, no significant change in droplet diameter was observed, with and without a glass coverslip bonded to the chip surface. Simply using a glass coverslip is not enough to slow droplet evaporation, likely due to the thickness of the PDMS device (5 mm). Therefore, pairing the glass coverslip with a RO water soak appears to be the most effective of the tested techniques at reducing the rate of droplet evaporation. However, I do not use this technique throughout the rest of my work, as droplet evaporation was negligible on the timescales used in DIB permeability experiments (30 min). Any evaporation which occurred was easily accounted for by measurement of droplet volume over time and data normalization, as shown in Chapters 3 and 4.

2.4 Conclusions

After testing several methods of surface treatment for droplet formation and reduced droplet evaporation, I determined that baking devices for 24 h at 65°C was found to be sufficient to allow water-in-oil droplet formation. On devices fabricated in this way, droplet evaporation was negligible on the timescales used in DIB permeability experiments. In microfluidic device fabrication, there is always a tradeoff between initial labour and time input and effectiveness of the extra steps included. I decided to simplify the device fabrication as much as possible.

2.5 Materials and Methods

2.5.1 Materials

All reagents were purchased from Millipore Sigma unless otherwise stated. Phospholipids were purchased from Avanti Polar Lipids. Reagents were purchased at the following grades: squalene (>98%), 4-(2-hydroxyethyl)-1-piperazineethanesulfonic acid (HEPES, >99.5%), trimethylchlorosilane (>99%), perfluorooctylsilane (>99%), hydrochloric acid (>36.5-38%), and potassium chloride (>99%). Polydimethylsiloxane (PDMS, Dow Sylgard 184) was purchased from Ellsworth Adhesives. Silicon wafers (100 mm diameter) were purchased from Silicon Materials. SU-8 3050 photoresist and developer were purchased from MicroChem. Polytetrafluoroethylene (PTFE) tubing (1/16" outer diameter, 750 µm inner diameter) was purchased from Chromatographic Specialties. Glass slides and coverslips were purchased from Fisher.

2.5.2 Design and fabrication of the microfluidic platform

Microfluidic devices were fabricated as described in Chapter 4 using traditional photolithography and soft lithography techniques. In brief, features were designed using AutoCAD (Autodesk, 2018) and printed onto two acetate masks at 10 µm resolution by CAD/Art Services. To create the mould using photolithography, a layer of photoresist was spin-coated onto a silicon wafer, and baked prior to exposure to UV light (11.2 s, 19.96 mW/cm^2, OAI Model 800 mask aligner) through the first photomask. Then, a second layer was spin-coated onto the first one, soft-baked, and exposed to UV using the second photomask. Unexposed features from both layers were removed with developer and the mould was subjected to a final hard bake (30 min at 200 °C) and a final UV exposure (90 s, 19.96 mW/cm^2).

To fabricate the microfluidic device using soft lithography, PDMS was prepared as directed by the manufacturer, poured over the mould, degassed to remove air bubbles, and cured overnight at 65°C. To fabricate PDMS slabs for contact angle measurements, the same process was followed using a smooth silicon wafer without a design on its surface. The etched PDMS slab was then removed from the mould, and access holes were punched using a 1 mm biopsy punch to fit the outer diameter of the tubing that connects the microfluidic device to the pressure pump. To create the base of the device, degassed PDMS was spincoated at 1200 rpm for 25 s onto the surface of glass microscope slides to create a thin layer. Both the PDMS devices and the PDMS-coated glass slides were washed, dried with filtered air, and baked at 90 °C for 30 min. The device and the base were then treated with air plasma (Diener Electronic, Zepto ONE, 37 s, 29 W, 1.75 mbar) and permanently bonded to each other. Untreated microfluidic devices were stored at 65 °C for a minimum of 24 h prior to use. For evaporation experiments using the glass coverslip, the device was treated a

second time with air plasma and a glass coverslip was bond to its top surface.

2.5.3 Preparation of phospholipid solutions

All phospholipids were purchased as stock solutions in chloroform. Solutions of vesicles of DPhPC in buffer at a final concentration of $5\,\mathrm{mg\,mL^{-1}}$ were prepared. To do so, chloroform was removed from the stock solutions by placing 400 µL of the $25\,\mathrm{mg\,mL^{-1}}$ chloroform stock solutions in a 10 mL glass roundbottom flask, and subjecting them to a stream of nitrogen gas. To ensure that all chloroform was removed, the phospholipids were then placed under vacuum for 1 h. Each phospholipid or phospholipid formulation was them redissolved in 1 mL of aqueous buffer (pH 7.59, 10mM HEPES, 140mM KCl), vortexing to ensure complete suspension of the phospholipids in the buffer. To create vesicles, these solutions were frozen and thawed 5 times using liquid nitrogen and warm water, before being extruded 21 times through a 0.1 µm polycarbonate membrane (Avanti Polar Lipids) at room temperature.

2.5.4 PFOS surface treatment

5 µL of PFOS was measured into a glass vial using a 10 µL glass syringe (Hamilton). 95 µL of isopropyl alcohol was added to the vial using a micropipette to create a 5% (v/v) solution. Following exposure to air plasma, the surfaces of the PDMS slabs were covered with the PFOS solution for 1 min. Excess solvent was then evaporated using filtered air. When treating microfluidic devices, the PFOS solution was introduced to the interior device channels following air plasma bonding manually using a 1 mL plastic syringe connected to the device with PTFE tubing.

2.5.5 Teflon AF surface treatment

0.0185 g Teflon AF was dissolved in 1 mL FC-40 oil by stirring at 50°C for 1 h to give a 1% (w/w) solution. Following exposure to air plasma, the surfaces of the PDMS slabs were covered with this solution and baked at 80°C for 1 h. When treating microfluidic devices, the microfluidic channels were manually filled with this solution using a plastic syringe and PTFE tubing and baked at 80°C for 1 h.

2.5.6 Aquapel surface treatment

Neat Aquapel was introduced into the microfluidic channels manually using a plastic syringe and PTFE tubing, allowed to sit for 1 min, then expelled using filtered air. This was repeated after a 20 min bake at 65°C for some experiments. The Aquapel treatment process was tested immediately following air plasma treatment as well as after devices were stored for 24 h at 65°C.

2.5.7 Soaking in water

Microfluidic devices were stored in a RO water bath at 65°C for over 24 h prior to use.

2.5.8 Contact angle measurements

A 2 µL droplet was placed on the surface of each PDMS surface. The contact angle of the droplet on the surface was measured using a Holmarc contact angle meter (model H0-CAM-0B1). This process was repeated, placing droplets onto different locations on each PDMS slab, to give three sets of measurements for each sample. These measurements were repeated in triplicate, yielding 18 data values in total for each time point (0 h, 2 h, 24 h, and168 h). Control experiments were performed by

repeating the complete procedure using PDMS treated only with air plasma and stored at room temperature, referred to as untreated. For the investigation of Teflon AF surface treatments, control experiments were performed by repeating the complete procedure using PDMS treated with air plasma and stored at 65°C for over 24 h.

2.5.9 Device operation

Aladdin syringe pumps (World Precision Instruments) and 1000 µL syringes were used to introduce fluid onto the microfluidic devices. The syringes were connected to inlets in the device using PTFE tubing and fluid was introduced into both the oil and aqueous inlets at a flow rate of $1\,\mu L\,min^{-1}$. Droplet formation and behavior was observed using a Genie Nano C1280 camera (Teledyne Dalsa) mounted on a Nikon Eclipse Ti2-U inverted microscope. For PFOS experiments, the aqueous solution was a $2\,mg\,mL^{-1}$ solution of DPhPC in aqueous buffer and the oil phase was squalene. For evaporation experiments, the aqueous solution was a $5\,mg\,mL^{-1}$ solution of DPhPC in aqueous buffer and the oil phase was squalene.

Chapter 3

The role of temperature in the formation of human-mimetic artificial cell membranes using droplet interface bilayers (DIBs)

3.1 Context

In the literature, synthetic phospholipids are overwhelmingly used to create DIBs instead of naturally derived phospholipids, even though the diverse distribution of phospholipids in the latter is more biomimetic. This gap is likely due to difficulties forming complete and stable monolayers using naturally derived phospholipids. To create DIBs using naturally derived phospholipids on a microfluidic device, the device must be heated to or above the phase transition temperature (T_m) of the phospholipids. I present the first systematic study of the role of temperature in DIB formation,

which shows that the temperature at which DIBs are formed is a key parameter for the formation of DIBs using naturally derived phospholipids in a microfluidic platform. I also show a new phenomenon wherein the DIB "melts" without disintegrating for bilayers formed predominantly of phospholipids that occupy cylindrical spaces. Given the difficulties associated with making DIBs using naturally derived phospholipids, I anticipate this work will illuminate the role of phospholipid phase transition in mono- and bilayer formation and lay the foundation for DIBs to be used as human-mimetic artificial cell membranes.

I performed all experimental work and data analysis and designed the chip used for DIB formation (Figure 3.1), based on a previous design by Elanna Stephenson, Matt Noseworthy, and Katherine Elvira. Elanna Stephenson designed the device used for permeability studies (Figure 3.5).

3.2 Abstract

Droplet interface bilayers (DIBs) have recently started to be used as human-mimetic artificial cell membranes. DIBs are bilayer sections created at the interface of two aqueous droplets, such that one droplet can be used as a donor compartment and the other as an acceptor compartment for the quantification of molecular transport across the artificial cell membrane. However, synthetic phospholipids are overwhelmingly used to create DIBs instead of naturally derived phospholipids, even though the diverse distribution of phospholipids in the latter is more biomimetic. We present the first systematic study of the role of temperature in DIB formation, which shows that the temperature at which DIBs are formed is a key parameter for the formation of DIBs using naturally derived phospholipids in a microfluidic platform. The phospholipids that are most abundant in mammalian cell membranes (phosphatidylcholine

(PC), phosphatidylethanolamine (PE), phosphatidylserine (PS), and phosphatidylinositol (PI)) only form DIBs when the temperature is above the phase transition temperature (T_m). Similarly, DIB formation usually only occurs above the highest T_m of a single phospholipid in a bespoke formulation. We show a new phenomenon wherein the DIB "melts" without disintegrating for bilayers formed predominantly of phospholipids that occupy cylindrical spaces. We also demonstrate differences in DIB formation rates as well as permeability of biomimetic membranes. Given the difficulties associated with making DIBs using naturally derived phospholipids, we anticipate this work will illuminate the role of phospholipid phase transition in mono- and bilayer formation and lay the foundation for DIBs to be used as human-mimetic artificial cell membranes.

3.3 Introduction

The use of microfluidic technologies to create artificial lipid bilayers provides advantages over more traditional methods, such as planar lipid bilayers[147] or those formed in bulk emulsions,[148] in terms of reproducibility, throughput, and control over the bilayer composition. In recent years, researchers have developed innovative microfluidic methods for the formation of model membranes, such as liposomes,[149] vesicles,[150] coacervates,[151] proteinosomes,[152] and supported planar bilayers.[153] We have recently shown that droplet interface bilayers (DIBs) are able to model cell membranes for the prediction of molecular transport *in vivo*.[86]

DIBs are formed when phospholipids are added to aqueous droplets in an oil phase (Video S1). A phospholipid monolayer spontaneously self-assembles at the oil-water interface. Then, when these coated droplets are brought into contact, a phospholipid bilayer forms at their interface such that the interfaces between two or more neigh-

bouring droplets become biologically relevant artificial membranes. The first DIBs, made from the synthetic phospholipid 1,2-diphytanoyl-*sn*-glycero-3-phosphocholine (DPhPC), appeared in the literature in 2006.[79] In the years following, research groups around the world have created and used DIBs in a variety of different ways, such as to quantify molecular transport for drug discovery[77,86], redto investigate water permeability,[115,154] to measure electrophysiological bilayer properties,[155–157] and to study the insertion of pore-forming proteins, mainly -haemolysin.[79]

DIBs have been generated using microfluidic methods[108] and manually through the implementation of micromanipulators and electrodes.[155] In both cases, lipids can be added either to the oil phase ("lipid-out"[79]) or the aqueous phase ("lipid-in"[78]). Since the first DIBs were created, they have predominantly been formed using the single synthetic phospholipids 1,2-dioleoyl-*sn*-glycero-3-phosphocholine (DOPC)[75,76,108] and DPhPC.[78,101,107,119,155] This is most likely due to the stability of droplet-coating monolayers formed using these phospholipids, which we attribute to the chemical structure of the phospholipids and their low phase transition temperatures (T_m). Based on robust archaeal phospholipids, DPhPC was designed and synthesized to have completely saturated acyl chains and an extremely low T_m.[80] Sparse publications exist demonstrating the use of single phospholipids that are more relevant to biological systems,[83,85,106,110] or of more complex mixtures, which are currently limited to non-human systems such as total lipid extracts from soy,[82] *E. coli*,[83] and porcine brain.[84]

However, to be fully usable as model artificial cells, DIBs need to mimic the salient features of human cell membranes. Mammalian plasma membranes are mainly comprised of the phospholipids phosphatidylcholine (PC), phosphatidylethanolamine (PE), phosphatidylserine (PS), and phosphatidylinositol (PI).[21–23] Other key components include cholesterol, sphingophospholipids (specifically sphingomyelin), glycolipids, and mem-

brane proteins, including transporters.[23] The phospholipids present in cell membranes contain a distribution of tail lengths and degrees of saturation (Figure 3.2).[23] Thus, naturally derived phospholipids contain a single head group but a wide distribution of acyl chain lengths and saturation levels. Conversely, synthetic phospholipids such as DPhPC and DOPC contain only one head group and identical acyl chains throughout. To date, we have published the only example of DIBs made using naturally derived phospholipids found in human cell membranes (PC and PE),[86] incorporating more than one head group as well as many different acyl chain structures.

One of the main advantages of using DIBs as artificial cell membranes is that there is a donor and an acceptor compartment on either side of the artificial cell membrane. Hence, molecular transport across the membrane can be isolated and quantified. An additional functionality that DIBs provide is the ability to create bespoke lipid formulations to investigate the relationship between membrane composition and transcellular molecular transport. Our focus here is to develop methods for the formation of biomimetic DIBs using phospholipid formulations made from naturally derived phospholipids containing many different acyl tails. In this paper, we define a "lipid formulation" as a customized mixture of naturally derived phospholipids at predetermined concentrations. We aim not to replace but to complement the use of total lipid extracts in the formation of DIBs. Total lipid extracts are perhaps more similar in some ways to the phospholipid composition of cell membranes, but also include many unknown components.[158] Therefore, the use of phospholipid formulations to make DIBs allows us to precisely study the effect of membrane composition on molecular transport and DIB formation rates.

We present here a systematic study of the role of temperature in DIB formation using naturally derived phospholipids and bespoke formulations. The role of tem-

perature in DIB formation and stability has been investigated using total lipid extracts[ringley, 83,84,159,160] as well as single synthetic phospholipids[161]. Yanigasawa et al. found that following DIB formation, increasing the temperature led to droplet coalescence when using saturated phospholipids and no change when using unsaturated phospholipids. They used synthetic lipids. Work from the Sarles group has focused on manipulation of temperature prior to droplet contact, facilitating DIB formation using complex lipid mixtures[83,84]. They found that brain total lipid extract[84,159,160,162] and E.coli total lipid extract[83] both require heating to enable DIB formation rather than droplet coalescence.

We have performed an in-depth investigation of DIB formation for use as artificial cell membranes using a variety of mammalian phospholipids and phospholipid formulations, varying both head groups and acyl chain length and saturation. We designed a microfluidic platform to form these DIBs at biomimetic temperature and pH conditions. By controlling these properties, we can answer biophysical membrane questions more accurately than was previously possible. We are also able to form DIBs using complex phospholipid formulations, moving closer to the creation of truly biomimetic artificial cell membranes. Using the "lipid-in" approach, we made DIBs from the main phospholipids found in mammalian cells (PE, PC, PS and PI) and of different ratios of each of these lipids to create bespoke formulations for DIB formation. The "lipid-in" approach was selected due to previous data demonstrating the role of phase transition temperature in monolayer assembly at a phase interface.[163] All phospholipids used are naturally derived, meaning that only one head group but a distribution of acyl chain lengths and saturation is present in each sample. We also demonstrate DIB formation using formulations of these phospholipids. The main difficulty with making DIBs from phospholipid formulations is the fact that each single phospholipid present may have a different T_m. Our data show that varying and con-

trolling the temperature of the microfluidic device allows for successful DIB formation at or above the phospholipid T_m values, even for complex phospholipid formulations. Using bilayers formed from selected phospholipid formulations, we also demonstrate differences in the fluorescein transport flux as well as rate of bilayer formation.

3.4 Results and discussion

We designed our microfluidic device for DIB formation (Figure 3.1) to enable a high level of control over droplet position on the chip, droplet volume, and droplet speed and hence the speed at which droplets come together to form a DIB. As described previously,[86,109] DIB formation requires that droplets are brought into contact with each other slowly, especially when compared to the speed at which droplets are usually formed in microfluidic devices.[164] There are two reasons for this. Firstly, there must be enough time between droplet and DIB formation on the chip to allow the phospholipids to form a complete (hole-free) monolayer at the droplet surface, otherwise droplets will coalesce when they come into contact with each other (Video S4). Our droplets were brought together at an approximate velocity of $200\,\mu m\,s^{-1}$, which corresponds to a Reynolds number of 0.00143. When forming DIBs on microfluidic devices, the fluid dynamics and channel effects on the microscale yield faster monolayer formation times using the "lipid-out" method than "lipid-in," as opposed to non-microfluidic DIB formation.[128] Off-chip, monolayer formation times are close to 5 minutes for the "lipid-in" method and up to 30 minutes for "lipid-out."[165] Secondly, even when droplets are fully covered with a phospholipid monolayer, the speed at which they are brought into contact with each other must be slow enough to enable a bilayer to form between the droplets. Ideal droplet velocity and lipid concentration for DIB formation have previously been investigated.[109] Once a bilayer is formed

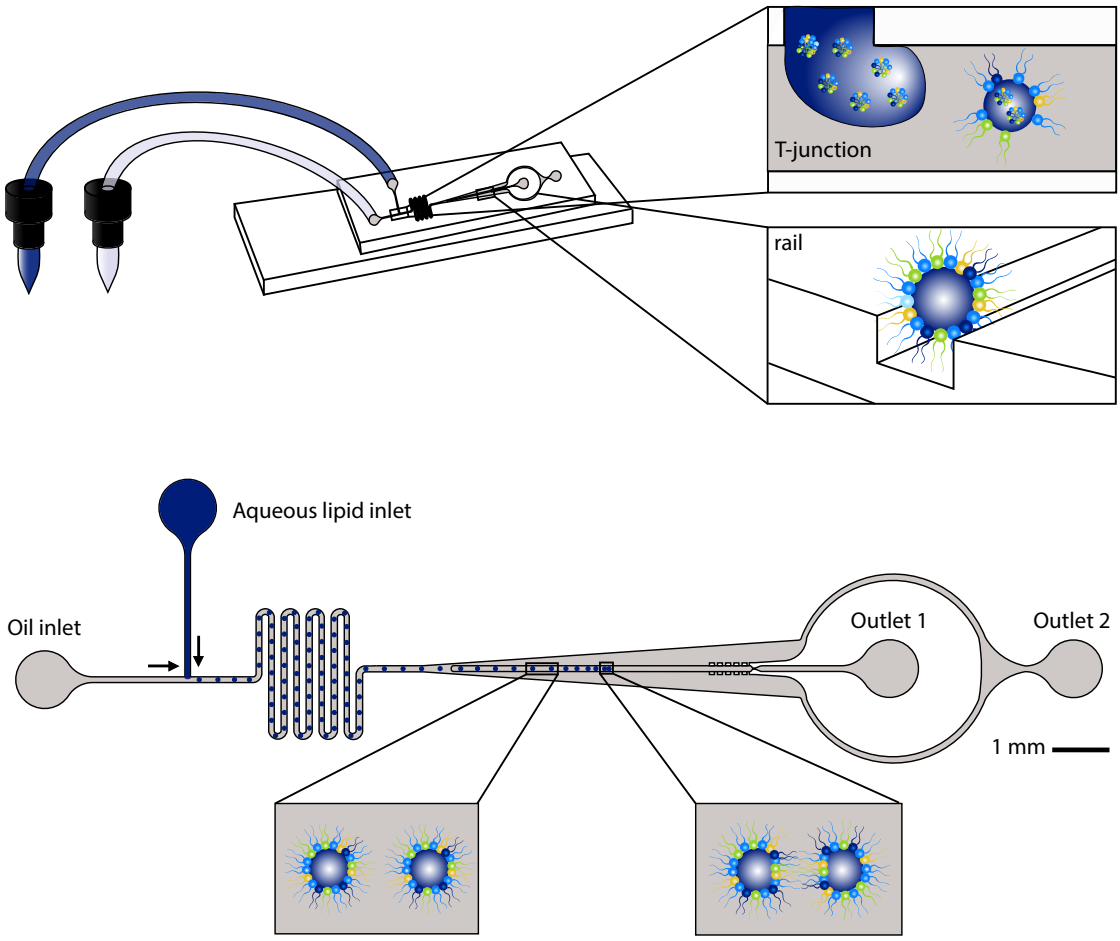

Figure 3.1: **Design of the microfluidic platform for DIB formation.** Top: 3D depiction of the microfluidic device and experimental setup. Droplet formation occurs at the T-junction (see inset), where the squalene (grey) and aqueous (blue) streams meet. The aqueous phase, containing phospholipid vesicles, forms droplets in the bulk oil phase and monolayer self-assembly begins. A widening chamber is used to slow down the droplets so that the aqueous droplet is completely coated by a phospholipid monolayer and is guided down the centre of the chamber by a rail (see inset). Bottom: Top-down view of the design of the microfluidic device. The microfluidic device is drawn to scale. The insets represent phospholipid-coated droplets just before contact and droplets after DIB formation. In our microfluidic device, these droplets have a diameter of around 100 µm. Phospholipids are not drawn to scale to show their arrangement in a DIB.

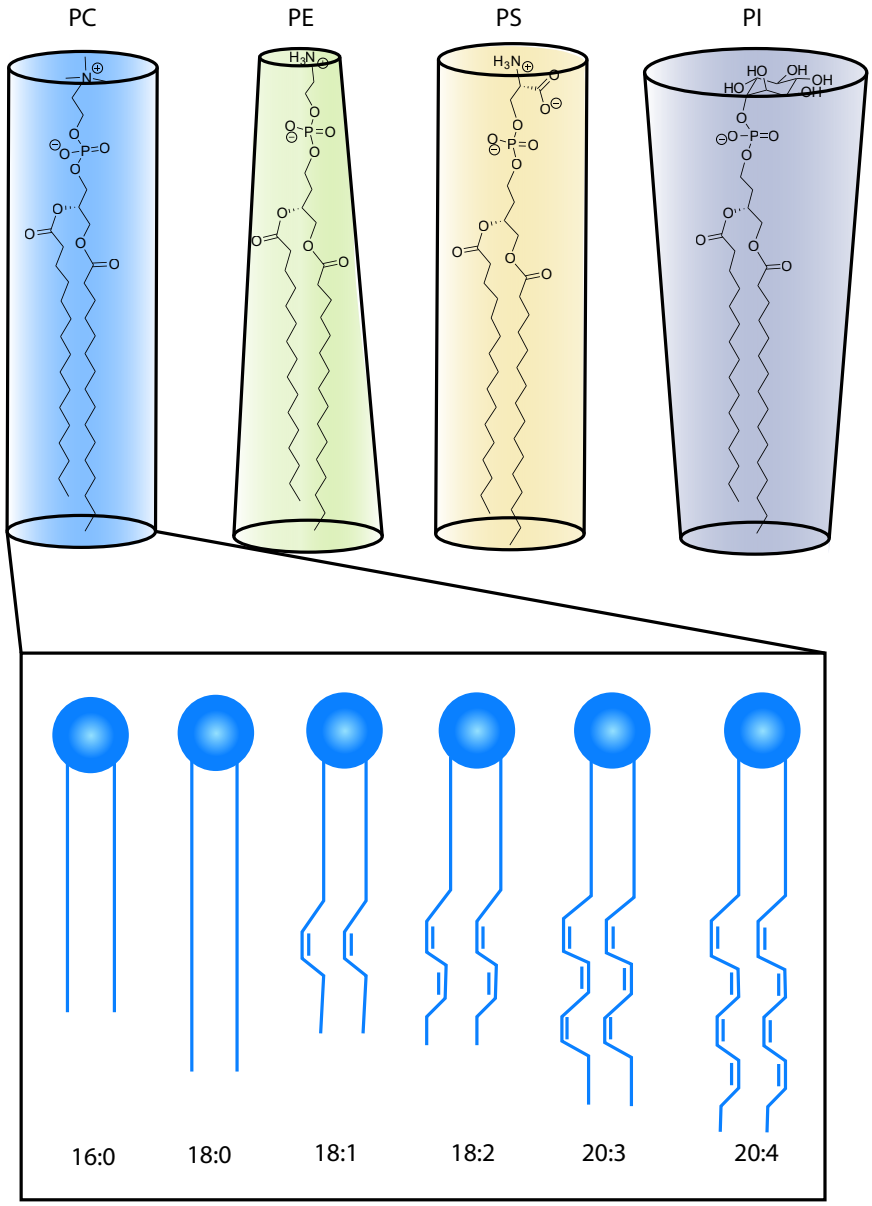

Figure 3.2: **Shapes and compositions of naturally derived phospholipids.** Top: From left to right, the structures of 16:0 PC, PE, PS, and PI are shown in the three-dimensional shapes they occupy. PC and PS are cylindrical, while PE is inverted conical and PI is conical. Bottom: While all the lipids in naturally derived Liver PC have a choline head group, multiple acyl chains are present. These tail groups are illustrated here, highlighting the difference lengths and degrees of unsaturation.

while the pressure pump is off, turning the pressure pump back on does not cause droplet coalescence. If a DIB forms under flow conditions, the oil flow around the DIB pair does not cause the bilayer to rupture. However, prior to full bilayer formation, the interface between the droplets is delicate and hence susceptible to droplet merging since there are no other stabilising molecules in the system. Prior work has shown that droplets must be brought together at low velocities to form a DIB and avoid droplet oalescence.[109] Here, so long as the device was held at the appropriate temperature, droplets can be brought together quickly and under flow conditions, demonstrating the effectiveness of the phospholipids as a surfactant. Droplet velocity at the point of contact appears to be a secondary factor in determining the success of DIB formation: when velocity, phospholipid concentration, and microfluidic device design are constant, change in temperature appears to dictate DIB formation success. Therefore, to be able to determine whether it is possible to form DIBs using phospholipids found in human cell membranes, we designed the microfluidic device such that the forces that the device subjects the droplets to was not an experimental variable.

Aqueous suspensions of each phospholipid or phospholipid formulation are prepared in a buffer and inserted into the microfluidic device using a pressure pump. Simultaneously, squalene is pumped into the device through a perpendicular channel at a similar pressure, so that aqueous droplets form at the T-shaped junction where the two channels (and thus the aqueous and oil streams) meet (Figure 3.1). After budding off at this intersection, the aqueous droplets become coated with a phospholipid monolayer as the vesicles inside the droplets contact the oil-water interface. To allow enough time for this process to occur without significantly increasing device size, a meandering channel section immediately follows the droplet formation junction. After exiting the meander, phospholipid-coated droplets enter a gradually

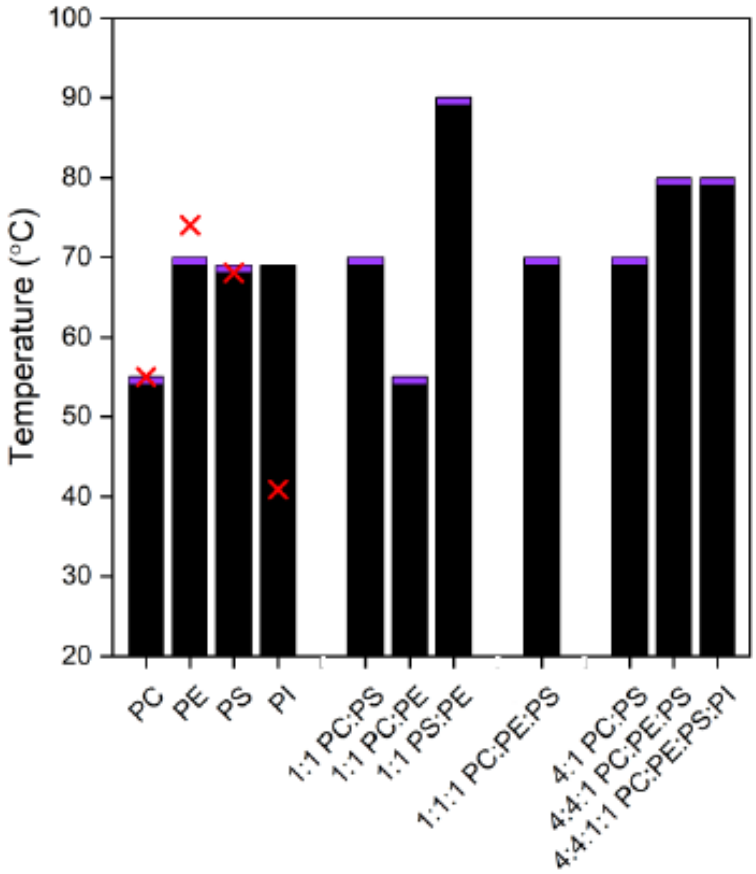

Figure 3.3: **Temperatures at which DIB formation occurs with different phospholipids.** We tested DIB formation of four naturally derived phospholipids and phospholipid formulations over a range of temperatures, beginning at ambient temperature (20°C). Black indicates that DIB formation was not possible (droplets merged upon contact) and purple indicates successful DIB formation. At constant pressures and lipid concentrations, DIB formation consistently failed below the indicated temperature and consistently occurred above the indicated temperature. Red crosses indicate the T_m of the dominant component of each natural phospholipid. In the phospholipid formulations, the biological source of PC, PE and PI is liver, and that of PS is brain.

widening chamber, which causes a decrease in the speed of the droplets since an equal volume of fluid is now present in a larger chamber. This chamber also has a second layer which consists of a "rail" etched into the chamber that guides the droplets on a straight path down its centre.[166] Droplets can be stopped precisely anywhere in the device using the pressure pump, as we did when gathering the data shown here (Video S2). Stopping the pressure pump stops the droplets in place,[86] and DIB formation occurred as they flowed down the rail. The microfluidic device was designed for use in any lab, even without access to expensive pressure pumps. Formation of DIBs on the rail has its own advantages, as the use of pillars in droplet traps, another method for DIB formation, is linked to increased droplet merging.[167] As the fluid flow rate slows in the chamber and the droplets are guided by the central rail, the droplets come into contact and a DIB forms at each point of contact. Successful DIB formation is defined as lack of droplet merging and formation of a distinctive and visible bilayer section at the interface (Figure 3.4a).

Since amphiphilic lipids will spontaneously form large, multilamellar vesicles in aqueous solution,[168] prior to introduction into the microfluidic device, phospholipid suspensions were first extruded through a porous membrane to create small, unilamellar vesicles. In this work, we use the "lipid-in" approach for DIB formation. Using our microfluidic platform, we first tested DIB formation using each of these phospholipids (PC, PS, PE and PI) separately, and then tested various phospholipid formulations over a range of temperatures both above and below the T_m of each phospholipid or phospholipid formulation. We held the pH of the aqueous lipid suspensions constant to account for any potential differences in T_m that can arise with changes in phospholipid protonation state[169]. We designed binary, ternary, and quaternary phospholipid formulations to mimic the ratios in which these phospholipids are found in mammalian cells[59] and have previously been used to model molecular transport in

cell-mimetic systems.[60] We used naturally derived phospholipids to ensure that our DIBs are made from phospholipids that contain the diverse distribution of acyl chains found *in vivo*.

T_m values are rarely determined for naturally derived phospholipids, but can be found for some of their components. In fact, T_m values for naturally derived lipids and lipid extracts are not reported by lipid suppliers or in the literature. To estimate the T_m of a naturally derived lipid, which contains a distribution of acyl chains, suppliers recommend using the T_m of the predominant lipid component. For example, no T_m value is reported for Liver PC as a whole, but the major component of Liver PC (18:0 PC[170]) has a T_m value of 55°C.[171] We approximate T_m values for each of the naturally derived phospholipids from the major component of each. Similarly, since there are no literature T_m values for our bespoke phospholipid formulations, we determined experimentally a range of temperatures at which DIB formation was possible for each phospholipid formulation (Figure 3.3). Droplets were formed in high throughput, at an approximate rate of one droplet per second and DIB formation was observed over the course of a minute for each condition. A custom-made heating platform,[86] was used to accurately control the temperature in the microfluidic device and hence the temperature of DIB formation. The heating platform setpoints were increased from room temperature and droplet behavior (coalescence or DIB formation) was observed (Table C.1). Data was collected during temperature ramp-up as well as at each setpoint, allowing us to test the effects of every temperature point on DIB formation. We tested each naturally derived phospholipid or phospholipid formulation on 2-4 different microfluidic devices.

As mentioned previously, naturally derived phospholipids containing more than one acyl chain type are not usually used to form DIBs. This is likely due to the instability

of the phospholipid monolayer (and hence high occurrence of droplet merging) at room temperature, which is significantly below the T_m of these phospholipids. We know that failure to form a DIB due to droplet merging can happen if droplet velocity at the time of attempted contact is too high[109] or if phospholipid monolayer formation is incomplete.[83] Additionally, a full monolayer will not form if the concentration of phospholipid is too low.[109] Our data show (Figure 3.3) that DIB formation also does not occur if the temperature of the microfluidic channel is below the T_m of the phospholipids for single phospholipids. We observed successful DIB formation using Liver PC, Egg PC, Liver PE, and Brain PS near or above the T_m of the major component of each (Figure 3.3, Table C.1).

Liver PI alone did not form DIBs under any experimental conditions, likely due to its shape and corresponding low packing parameter. PI is an inverted conical phospholipid, meaning that the head group is significantly larger than the tail groups, disallowing the assembly of tightly packed monolayers and bilayers on the curved surfaces of droplets[23,172–175](Figure 3.2). We also tested DIB formation using formulations of the mentioned naturally derived phospholipids (Figure 3.3). The binary formulations of PC and PS (in both 1:1 and 4:1 ratios) formed DIBs at 70°C and above, which aligns with the T_m of PS at 68°C.[171] As expected, we found that a ternary formulation of PC, PE, and PS (4:4:1) successfully formed DIBs at and above 80°C. Surprisingly, adding PI to create a quaternary formulation (4:4:1:1 PC:PE:PS:PI) did not prevent DIB formation, indicating that the mono- and bilayer stabilizing effects of the other three phospholipids were dominant. We propose that the curvature of the droplet and the membrane surface plays a larger role when using PI alone versus as a minor component of a formulation. These data appear to agree with the literature showing phases with the opposite curvature when using inverted conical surfactant molecules.[23,172–175]

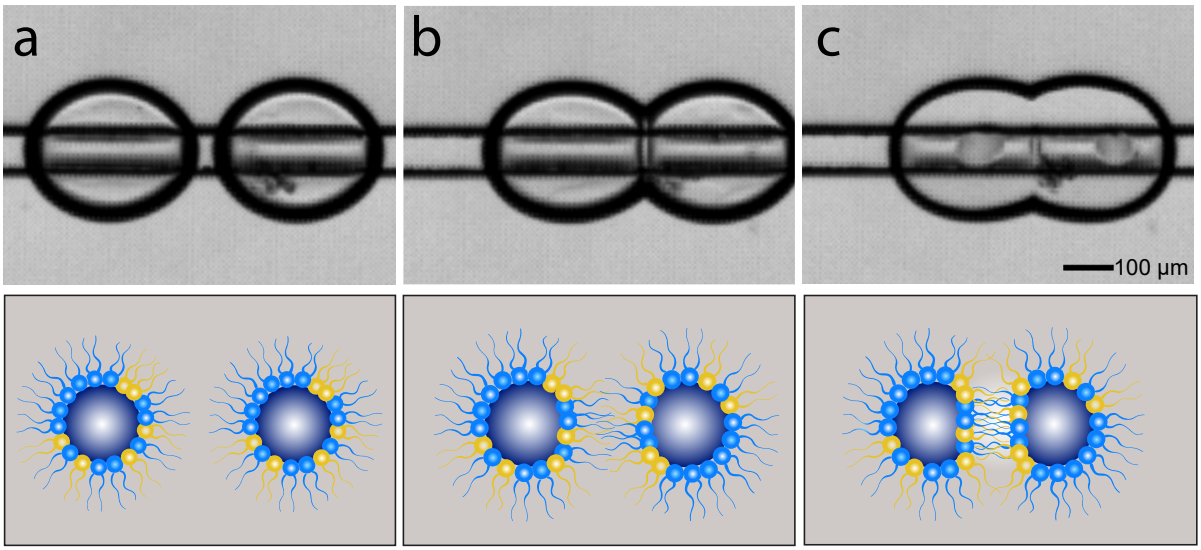

Figure 3.4: **"Melting" of the DIB bilayer.** DIB "melting" was observed when Egg PC, DPhPC, 1:1 PC:PS, and 4:1 PC:PS (cylindrical phospholipids) were used for DIB formation (Table C.1, Figure C.5), Videos S3 and S5). a) Microscopy image showing DIB formation using 4:4:1 PC:PE:PS occurring when the droplets are brought in contact with each other. The schematic shows the bilayer formed between the droplets. b) Microscopy image showing that, at elevated temperatures, the "melty" DIB, here formed using 4:1 PC:PS, is extremely thin and nearly invisible. The schematic represents a more efficient packing of the lipid tails. The scale bar is 50 µm in all microscopy images. Phospholipids are not drawn to scale.

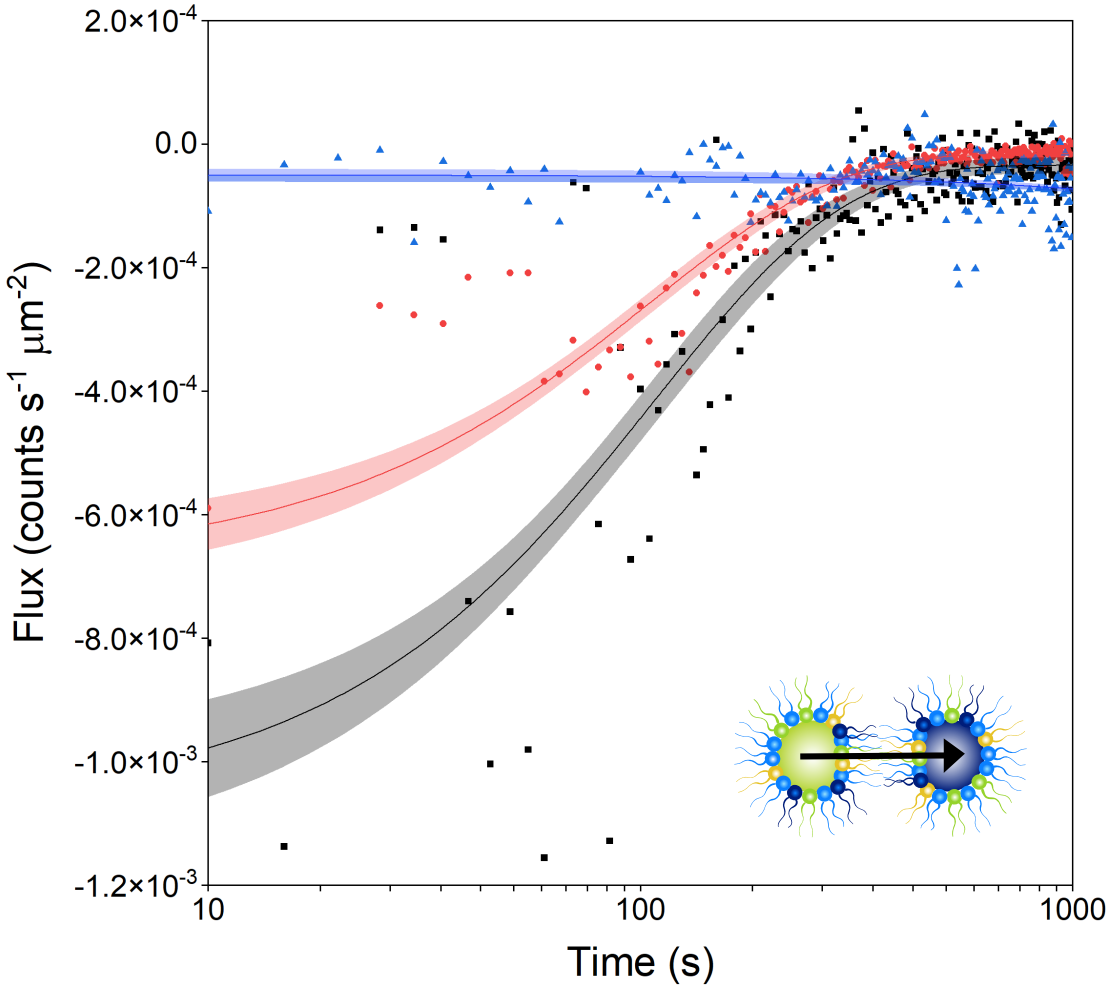

Figure 3.5: **Fluorophore flux over time in three different lipid formulations.** Following DIB formation between a donor (containing fluorophore) and an acceptor (empty) droplet, diffusion of fluorophore through the bilayer was measured, as shown in the diagram in the inset. Data shown for the flux of fluorophore across bilayers formed using 4:1 PC:PS (black), 4:4:1 PC:PE:PS (red), and 4:4:1:1 PC:PE:PS:PI (blue). Maximum flux and fluorophore half-life were determined using the fitted curve and are shown in Table 3.1. The microfluidic device was held at 37°C while fluorescein transport occurred. An exponential curve of the form $y = a * e^{(} - x/b) + c$ was fitted to the 4:1 and 4:4:1 data sets and a linear function of the form $y = a + b * x$ was fitted to the 4:4:1:1 data set in OriginPro. Curve fitting found the parameters $a = -0.00104 \pm 0.0000482$, $b = 107.9 \pm 7.800$, and $c = -0.0000343 \pm 0.00000689$, $a = -0.000660 \pm 0.0000254$, $b = 104.7 \pm 5.79$, and $c = -0.0000155 \pm 0.00000254$, and $a = -0.0000503 \pm 0.00000534$ and $b = -0.0000000226 \pm 0.00000000509$ for 4:1 PC:PS, 4:4:1 PC:PE:PS, and 4:4:1:1 PC:PE:PS:PI, respectively. 95% confidence bands were calculated from the standard deviation at each timepoint.

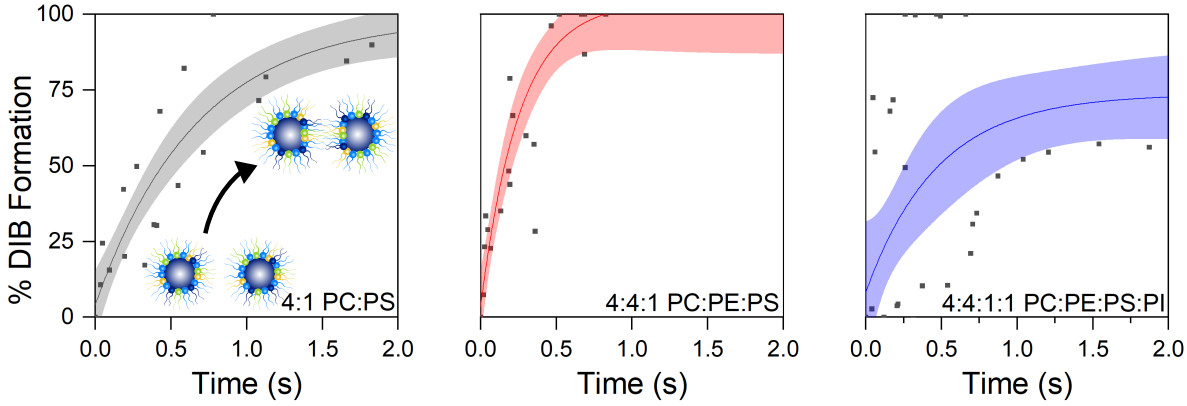

Figure 3.6: **Ratio of DIB diameter to droplet circumference.** To assess differences in the rate of DIB formation, we measured the ratio of DIB diameter to droplet circumference of 4:1 PC:PS (black), 4:4:1 PC:PE:PS (red), and 4:4:1:1 PC:PE:PS:PI (blue) and normalized these data as a percentage. A DIB formation value of 0% indicates complete droplet separation and lack of DIB formation. As a DIB forms, more of the droplet circumference is involved in bilayer formation and the DIB formation approaches 100% (see inset in first graph). An exponential curve of the form $y = a * e^{(} - x/b) + c$ was fitted to these data in OriginPro. Curve fitting found the parameters $a = -0.945 \pm 0.071$, $b = 0.666 \pm 0.130$, and $c = 0.986 \pm 0.055$, $a = -1.01 \pm 0.092$, $b = 0.255 \pm 0.062$, and $c = 1.04 \pm 0.083$, and $a = -0.653 \pm 0.132$, $b = 0.471 \pm 0.236$, and $c = 0.736 \pm 0.078$ for 4:1 PC:PS, 4:4:1 PC:PE:PS, and 4:4:1:1 PC:PE:PS:PI, respectively. 95% confidence bands were calculated from the standard deviation at each timepoint.

Also interesting is the fact that 1:1 PC:PE formed DIBs at 55°C and above, which falls between the T_m values of the two formulation constituents. This behavior is only observed when using the "lipid-in" approach; we have previously demonstrated "lipid-out" DIB formation using 1:1 PC:PE at physiological temperatures (37°C).[86] We propose that the increased energy input needed to facilitate monolayer formation using the "lipid-in" approach is due to the difference in phospholipid structure formation in the aqueous and oil phases. Phospholipids extruded into an aqueous phase form uniformly sized unilamellar vesicles, which exist in a gel phase as long as they are held below the appropriate T_m. Heating the suspension to or above the T_m initiates a gel-to-liquid phase transition, which encourages monolayer formation. On the other hand, phospholipids are soluble in oil and so do not require a higher temperature to self-assemble at the droplet-oil interface of the droplets to form a monolayer or a DIB.

To ensure that DIB formation is not affected by other components of the microfluidic platform, we tested other parameters that can potentially affect lipid distribution in DIBs. As previously discussed, droplet velocity at point of contact is a significant factor in successful DIB formation.[109] We applied pressures as low as 20 mbar to both the aqueous and oil channels, slowing droplets as much as possible while keeping droplet formation consistent. This did not result in successful DIB formation at room temperature for any of the phospholipids or phospholipid formulations shown in Figure 3.3. We also varied the composition of the oil phase, replacing squalene with hexadecane, which is more commonly used for DIB formation,[118] and observed no effect on the success of DIB formation. Finally, Najem et al. also found that extrusion of lipid suspension at elevated temperature encouraged easier extrusion.[159]. However, we extruded the phospholipid suspensions at their T_m value rather than at room temperature, but this again had no effect on the success of DIB formation. Hence, taking into account the relevant T_m values is key to successful DIB formation

when using a "lipid-in" approach as it encourages complete formation of the droplet-coating phospholipid monolayer. This fits with prior work showing a correlation between temperature and completeness of the droplet monolayer covering, and hence successful DIB formation, using a total lipid extract from *E. coli*.[83]

We also observe a new phenomenon where DIBs "melt" (Figure 3.4b). Given sufficient heat, the bilayers in these cases become extremely thin and nearly invisible, but the droplets do not merge. "Meltiness," which we define as the formation of a thin, nearly invisible bilayer, as shown in Figure 3.4b, occurs on the same timescale as "non-melty" DIB formation and does not reverse with a decrease in temperature. Using squalene as the oil mobile phase, we noticed DIB "melting" at 40°C and above for DPhPC (Figure **??**, Video S5), 55°C and above for Egg PC (Table C.1), 69°C for PS, and 70°C and above for both 1:1 and 4:1 PC:PS. Notably, Liver PC on its own did not melt; the presence of PS in a formulation appears to dictate both the T_m of the natural phospholipid formulation and whether melting occurs. DIB melting appears to occur at temperatures above the T_m in bilayers comprised of cylindrical phospholipids, i.e. DPhPC, PC, PS, and formulations thereof (Videos S3 and S5). This is likely a reflection of a more complete gel-to-liquid phase transition and thus higher ability of the phospholipids to pack together tightly. This phenomenon occurs with cylindrical phospholipids due to their ability to pack tightly together in a planar bilayer. The composition of phospholipid formulations appears to be a key factor in DIB thickness as "meltiness" was only observed using cylindrical phospholipids. Oil exclusion is unlikely to contribute to DIB "melting" because squalene is easily excluded from lipid bilayers[159,176] The "meltiness" could potentially be due to lipid exchange between leaflets or between the monolayer and bilayer sections; this will be a focus of future work.

We then selected three phospholipid formulations to investigate whether lipid composition affects the passive molecular transport of fluorescein. We tested 4:1 PC:PS, 4:4:1 PC:PE:PS, and 4:4:1:1 PC:PE:PS:PI. Initial transport rates were highest in the binary phospholipid formulations and decreased as the formulation complexity increased (Figure 3.5). Increasing membrane permeability has previously been found to correlate with a decreasing proportion of PC in the model membrane.[85] Following curve fitting, we determined the y-intercept, j_{max}, as well as the fluorophore half-life for all three formulations (Table 3.1). Although the maximum flux differs by an order of magnitude between each of the three phospholipid formulations, the fluorescein half-life for the binary and ternary phospholipid formulations is essentially identical. This indicates that bilayer phospholipid composition affects initial rates of fluorescein transport, but those rates equilibrate to give similar half-lives.

Bilayer packing depends on membrane lateral pressure and phospholipid type.[85] The relative lateral pressure of a leaflet of the bilayer, π, can be determined using the equation $\pi = \gamma(1 - cos\theta)$, where γ is the interfacial tension of the monolayer and θ is the half contact angle between the droplets comprising the DIB[85]. We measured γ and θ for these bespoke lipid formulations and calculated π for each (Table S2). For 4:1 PC:PS, 4:4:1 PC:PE:PS, and 4:4:1:1 PC:PE:PS:PI, the lateral pressure was found to be, respectively, $(2.35 \pm 0.05)\,\mathrm{mN/m}$, $(3.92 \pm 0.86)\,\mathrm{mN/m}$, and $(4.13 \pm 0.23)\,\mathrm{mN/m}$. This demonstrates the significant effect membrane composition has on lateral pressure and packing. Membranes formed using only cylindrical phospholipids demonstrate the lowest lateral pressure. Addition of the conical lipid PE as well as the inverted conical lipid PI correlate with an increase in lateral pressure. This trend aligns with the observed permeability trend: more tightly packed membranes are less permeable, as observed using DIBs formed using 4:4:1:1 PC:PE:PS:PI. This correlation between lateral pressure and permeability has been previously observed[85] in DIBs formed using

synthetic phospholipids.

In addition to the observed permeability effects, we hypothesized that changing the phospholipid formulation would alter the rate of DIB formation. We propose that the size, shape, and charge of the phospholipids included in the formulation influences DIB formation rate. Bilayer formation depends on factors such as the viscosity of the oil phase, which must be excluded from the bilayer region, and the energy of adhesion between droplets.[177,178] Bilayer formation also requires formation of a stable monolayer, which is encouraged by bringing the system to or above its T_m. We propose that monolayer formation is affected by the phospholipid head groups present and bilayer formation rate is affected by the tail groups. For the same three phospholipid formulations, 4:1 PC:PS, 4:4:1 PC:PE:PS, and 4:4:1:1 PC:PE:PS:PI, we measured the droplet circumference and DIB diameter over time above the T_m value for each phospholipid formulation for consistency, at 70°C, 89°C, and 84°C, respectively. Relative bilayer diameters were measured as a proxy for energy of adhesion. The DIB diameter was then divided by the droplet circumference for each droplet pair to give a ratio of DIB to droplet size. These measurements were performed on 3-5 DIB-connected droplet pairs for each lipid formulation. To account for minor variations in droplet size between replicates, these ratios were then normalized on a 0-100 scale (Equation S1). A value of 0% indicates that the droplets are completely separated and a value of 100% indicates that DIB formation is complete and the ratio of DIB diameter to droplet circumference is no longer changing. Data normalization details are provided in the ESI. The resulting values are plotted over time in Figure 3.6. Similar measurements were performed for videos in which DIBs "melted," but no significant difference was observed between the values or DIB formation rate between "melty" and non-"melty" DIBs. Lipid behavior differs between phospholipid formulations, giving DIB formation rates that depend on formulation when other variables, such

as flow rate and identity of the mobile oil phase, are kept constant. Following curve fitting, we graphically determined $t_{1/2}$ values for DIB formation, which are given in Table 3.1. The highest rate of DIB formation, corresponding to the shortest half-life, was observed using the ternary mixture, followed by the binary and the quaternary mixtures. The complexity of phospholipid behavior means that no simple, linear relationship exists between the number of phospholipids in a mixture and the rate of DIB formation. Addition of the conical lipid PE to the binary mixture of cylindrical phospholipids PC and PS shortens DIB formation time significantly, potentially due to hydrogen bonding between the small, charged amine head group of the PE and the phosphate groups on adjacent phospholipids.[169] However, incorporation of the inverted conical lipid PI in the quaternary mixture reduces the DIB formation rate again, indicating that the steric effect of the large inositol head group significantly influences lipid packing kinetics. It has been suggested that the use of squalene masks some of the effects of phospholipid type on DIB permeability, so it is possible that these effects may appear even more significant with use of a different mobile phase.

Table 3.1: **Quantifying the effect of membrane formulation on molecular permeability.** Maximum fluorophore flux (j_{max}), fluorophore half-life ($t_{1/2}$) and the time taken for bilayer formation (formation $t_{1/2}$) were determined for three bespoke phospholipid formulations. We measured fluorescence intensity over time in both the acceptor and donor droplets and show here the flux of fluorophore out of the donor droplet normalized for droplet volume and DIB surface area. Maximum flux and $t_{1/2}$ were determined graphically. The microfluidic device was held at physiological temperature (37°C) while fluorescein transport was observed and image data collected. To quantify DIB formation time, DIB diameter and droplet circumference were measured and the ratio of the two normalized as a percentage, as shown in Figure 3.6. DIB formation $t_{1/2}$ was determined graphically, indicating the timepoint at which the bilayer is halfway complete. Measurements were performed above the T_m for each phospholipid formulation.

Phospholipid	$\mathbf{j_{max}}$ **(counts µm** $^{-2}$ **s** $^{-1}$**)**	$\mathbf{t_{1/2}}$ **(s)**	**Formation** $\mathbf{t_{1/2}}$ **(s)**
4:1 PC:PS	-1.04×10^{-3} $\pm 4.824 \times 10^{-5}$	107.9±7.8	0.67±0.13
4:4:1 PC:PE:PS	-6.60×10^{-4} $\pm 2.544 \times 10^{-5}$	104.7±5.8	0.26±0.06
4:4:1:1 PC:PE:PS:PI	-5.03×10^{-5} $\pm 5.339 \times 10^{-6}$	N/A	0.47±0.24

3.5 Conclusions

We have developed a microfluidic platform that allows us to quantify the parameters associated with the formation of DIBs using naturally derived phospholipids (PE,

PC, PS and PI) and bespoke formulations thereof for use as artificial cell models. We used phospholipids derived from mammalian biological sources to ensure that each phospholipid contained one type of head group and a distribution of acyl chain lengths and saturation levels, as occurs in cells. This is the first time that DIBs have been made using naturally derived phospholipids using the "lipid-in" approach, where lipids are dosed in the aqueous phase.

Our data show that to form DIBs in this way, droplets must be brought into contact with each other while they are at a temperature above the T_m of the phospholipid. For phospholipid formulations, the temperature must usually be above the highest T_m, though there is an interplay between T_m and the phospholipid shape, and hence packing ability. For example, PI, an inverted conical lipid, does not form DIBs alone at any of the temperatures tested, but does form DIBs when it is a minor component of a phospholipid formulation. We also show a new phenomenon in the field of DIB research. Over time, DIBs made from cylindrical phospholipids "melt" together without merging. We propose that this shows a more complete gel-to-liquid phase transition and formation of a more tightly packed phospholipid monolayer. We also show how molecular transport through the bilayer depends on the lipid formulation using fluorescein. Finally, we quantify how the lipid formulations affect the rate of formation of the DIB.

Since their first use, DIBs have been formed mostly using synthetic phospholipids such as DPhPC, and have predominantly been used to study passive or active (through pores such as -haemolysin) molecular transport. However, as we have previously shown,[86] DIBs have the potential to be used as human-mimetic artificial cell membranes for drug discovery applications. Up until now, it has been experimentally complicated to form DIBs in a microfluidic device using naturally derived phospholipids,

especially using the "lipid-in" approach. Our work shows that careful regulation of temperature allows DIB formation from the major components of mammalian cells. DIB "meltiness", the dependence of DIB formation rates on phospholipid formulation, and other biophysical lipid questions are interesting topics for further investigation. For example, by performing systematic studies correlating temperature, DIB formation rate, and DIB "meltiness" with lipid head and tail groups, employing single synthetic phospholipids to allow for a higher level of control. It would also be interesting to further investigate the potential effects of the oil phase composition on DIB formation and "meltiness". Impactful information on the biomimetic nature of DIBs will be gained if lipid domains can be shown to form in these systems, as well as through the quantification of lipid exchange between monolayers. We look forward to seeing DIBs reach their full potential as artificial cell models by providing methods for DIB formation that allow the use of many more, and much more biologically relevant, types of phospholipids.

3.6 Materials and methods

3.6.1 Materials

All reagents were purchased from Millipore Sigma unless otherwise stated. Phospholipids were purchased from Avanti Polar Lipids. The biological sources of L–phosphatidylcholine (>99%) were egg and bovine liver. The biological source of L–phosphatidylethanolamine (>97%) and L–phosphatidylinositol (>99%) was bovine liver. The biological source of L–phosphatidylserine (>99%) was bovine brain. Reagents were purchased at the following grades: squalene (>98%), 4-(2-hydroxyethyl)-1-piperazineethanesulfonic acid (HEPES, >99.5%), trimethylchlorosilane (>99%), hydrochloric acid (>36.5-38%), potassium chloride (>99%), and sodium fluorescein

(BioReagent, suitable for fluorescence). Polydimethylsiloxane (PDMS, Dow Sylgard 184) was purchased from Ellsworth Adhesives. Silicon wafers (100 mm diameter) were purchased from Silicon Materials. SU-8 3050 photoresist and developer were purchased from MicroChem. Polytetrafluoroethylene (PTFE) tubing (1/16" outer diameter, 250 µm inner diameter) was purchased from Chromatographic Specialties.

3.6.2 Design and fabrication of the microfluidic platform

The microfluidic devices are based on a prior design.[97] They have two layers, one which contains the features required to make droplets (the T-junction) and the other which contains the features required to make DIBs (rail that is used to bring the phospholipid monolayer-covered droplets into contact with each other). Target height for each layer was 50 µm.

Microfluidic devices were fabricated as described previously[86] using traditional photolithography and soft lithography techniques. In brief, features were designed using AutoCAD (Autodesk, 2018) and printed onto two acetate masks at 10 µm resolution by CAD/Art Services. To create the mould using photolithography, a layer of photoresist was spin-coated onto a silicon wafer, and baked prior to exposure to UV light (11.2 s, 19.96 mW/cm^2, OAI Model 800 mask aligner) through the first photomask. Then, a second layer was spin-coated onto the first one, soft-baked, and exposed to UV using the second photomask. Unexposed features from both layers were removed with developer and the mould was subjected to a final hard bake (30 min at 200 °C) and a final UV exposure (90 s, 19.96 mW/cm^2).

To fabricate the microfluidic device using soft lithography, PDMS was prepared as directed by the manufacturer (previously described in detail[86]), poured over the mould, degassed to remove air bubbles, and cured overnight at 65°C. The PDMS microfluidic

device was then removed from the mould, and access holes were punched using a 1 mm biopsy punch to fit the outer diameter of the tubing that connects the microfluidic device to the pressure pump. To create the base of the device, degassed PDMS was spincoated at 1200 rpm for 25 s onto the surface of glass microscope slides to create a thin layer. Both the PDMS devices and the PDMS-coated glass slides were washed, dried with filtered air, and baked at 90 °C for 30 min. The device and the base were then treated with air plasma (Diener Electronic, Zepto ONE, 37 s, 29 W, 1.75 mbar) and permanently bonded to each other. The microfluidic devices were stored at 65 °C for a minimum of 24 h prior to use.

3.6.3 Preparation of phospholipid solutions

All phospholipids were purchased as stock solutions in chloroform. Solutions of vesicles of each phospholipid (or phospholipid formulation) shown in Figure 3.3 in buffer at a final concentration of 10 mg/mL were prepared. To do so, chloroform was removed from the stock solutions by placing 400 µL of the 25 mg mL^{-1} chloroform stock solutions in a 10 mL glass roundbottom flask, and subjecting them to a stream of nitrogen gas. To ensure that all chloroform was removed, the phospholipids were then placed under vacuum for 1 h. Each phospholipid or phospholipid formulation was them redissolved in 1 mL of aqueous buffer (pH 7.59, 10mM HEPES, 140mM KCl), vortexing to ensure complete suspension of the phospholipids in the buffer. To create vesicles, these solutions were frozen and thawed 5 times using liquid nitrogen and warm water, before being extruded 21 times through a 0.1 µm polycarbonate membrane (Avanti Polar Lipids) at room temperature. For fluorescein transport experiments, 100 µM sodium fluorescein was added to the buffer.

3.6.4 Operating parameters of the microfluidic platform

To create droplets and then DIBs on the microfluidic platform, a phospholipid solution and squalene oil were placed in reservoirs (1.5 mL Eppendorf tubes, one each for the phospholipid suspension and the oil, see Figure 3.1) and two equal lengths of PTFE tubing were used to connect the reservoirs to a pressure pump (OB1 MK3, Elveflow). Squalene and aqueous buffers were introduced into the microfluidic device by applying a pressure of 100 mbar to both reservoirs. Once droplet formation began, the pressure on each reservoir was gradually decreased to 20-50 mbar. Following DIB formation, flow was stopped from both reservoirs using the Elveflow control software. To visualise droplet and DIB formation, devices were mounted in a custom-made heating platform[86] on a Nikon Eclipse Ti2-U inverted microscope. Brightfield images were collected using a Genie Nano C1280 camera (Teledyne Dalsa). The specifications of our custom-made heating platform have been previously described in detail.[86] For permeability experiments, we used a microfluidic device containing two parallel droplet and DIB formation geometries (T-junctions, meandering channels, and rails). In a bulk squalene solution, DIBs were formed between pairs of droplets: a donor droplet containing a 100 µM solution of sodium fluorescein in buffer and an acceptor droplet containing only buffer in a similar way to that shown previously.[86]

3.6.5 Fluorescence data collection

Once a DIB pair formed and the flow was stopped, brightfield and fluorescence images were taken every 5 s with a 10 ms exposure time until experiment termination. Fluorescence images were collected using a Hamamatsu ORCA-Flash4.0 V3, with an LED (Thorlabs) and SemrockBrightline large field of viewa GFP filter cube (excitation 466/40 nm, emission 525/50 nm) on a Nikon Eclipse Ti2-E inverted microscope.

DIBs were formed at the required T_m and the platform temperature was then decreased to 37°C for permeability measurements. Quantification of fluorescence intensity was performed via time-based measurement of mean intensity in regions of interest (ROIs) within each droplet in each frame using NIS Elements. Fluorescence intensity data was normalised for phospholipid bilayer surface area and droplet volume as previously described[86]. Briefly, bilayer diameters and droplet semiaxes were measured using, respectively, the "Distance Measurement" and the "Measurements and Annotations" modules in NIS Elements. Subsequent calculations were performed by approximating artificial cell membrane surface areas as ellipses and droplet volumes as ellipsoids. Each data set in this paper represents 2-5 replicates performed on different microfluidic devices. Different microfluidic devices were used to ensure reproducibility and to remove variables associated with the device itself from the measurements.

3.6.6 DIB formation data collection

Bilayer diameters and droplet semiaxes were measured before, during, and after DIB formation using the "Distance Measurement" and the "Measurements and Annotations" modules in NIS Elements. Subsequent calculations were performed by approximating droplet circumferences as ellipses.

3.6.7 Interfacial tension measurements

Interfacial tension measurements were performed through pendant drop tensiometry using a DataPhysics TBU90E goniometer. A 0.9 mm needle tip was used to dispense a 10 µl droplet of each phospholipid suspension into a cuvette filled with squalene. This was repeated in triplicate for each phospholipid formulation. Eight images were collected of each droplet and analysed in OpenDrop. The density of the phospholipid

suspensions was determined to be $0.956\,\mathrm{g\,ml^{-1}}$. Measured interfacial tension values, half DIB contact angles, and calculated membrane lateral pressures are provided in Table C.2.

Chapter 4

A bespoke microfluidic pharmacokinetic compartment model for drug absorption using artificial cell membranes

4.1 Context

When a microfluidic platform is optimized for droplet and DIB formation, DIBs can be used as artificial cells in permeability prediction studies. We created a new type of pharmacokinetic compartment model for the prediction of intestinal absorption by tuning the phospholipid composition, pH, ionic strength, and temperature to mimic the path an orally administered drug takes from the small intestine to the blood-stream. Early prediction of the rate and extent of intestinal absorption is vital for the efficient development of orally-administered drugs. Using this DIB model, we show a

threefold improvement in the prediction of molecular absorption in rat jejunum than the current state-of-the-art *in vitro* technique, parallel artificial membrane permeability assays (PAMPA).

Elanna Stephenson designed and developed the microfluidic device for the formation of ABC droplet triplets. I developed the biomimetic lipid formulations for use in the microfluidic platform. Elanna Stephenson and I conducted the triplet formation experiments for the quantification of device performance and gathered preliminary data for the fluorescence diffusion experiments in duplicate. I collected the fluorescence diffusion data we present in this paper. Elanna Stephenson collected the data for the calibration curves. Elanna Stephenson and I performed half the control experiments each. I performed the volume and surface area measurements, and the measurements of ROI and intensity. Elanna Stephenson performed the data normalisation and data analysis. Albert Escobar Mingo designed, built, and performed initial tests on the heating platform for his CHEM 399 project (Appendix D).

4.2 Abstract

Early prediction of the rate and extent of intestinal absorption is vital for the efficient development of orally-administered drugs. Here we show a new type of pharmacokinetic compartment model that shows a threefold improvement in the prediction of molecular absorption in rat jejunum than the current state-of-the-art *in vitro* technique, parallel artificial membrane permeability assays (PAMPA). Our three-stage pharmacokinetic compartment model uses microfluidic droplets and bespoke, biomimetic artificial cells to model the path of a drug proxy from the intestinal space into the blood via an enterocyte. Each droplet models the buffer and salt composition of each pharmacokinetic compartment. The artificial cell membranes are made from

the major components of human intestinal cell membranes (L-α-phosphatidylcholine, PC and L-α-phosphatidylethanolamine, PE) and sizes are comparable to human cells (˜0.5 nL).We demonstrate the use of the microfluidic platform to quantify common pharmacokinetic parameters such as half-life, flux and the apparent permeability coefficient (P_{app}). Our determined P_{app} more closely resembles that of actual intestinal tissue than PAMPA, which overestimates it by a factor of 20.

4.3 Introduction

In this paper, we present a new method for the *in vitro* quantification of passive drug diffusion. We have developed a microfluidic platform to create a new type of pharmacokinetic compartment model using artificial cell membranes created from a phospholipid mixture designed to mimic human cells. The measurement and prediction of pharmacologically relevant processes such as intestinal absorption are key to successful and efficient drug development.[179,180] New drugs take on average 10-15 years[1] to be developed and cost around 2.6 billion US dollars each.[2] Around 30% of drug candidates fail during testing on animals because we cannot accurately predict their pharmacokinetics.[5,6] Current methods used to predict passive drug transport have limitations including biological dissimilarity, high time and labour input and lack of control over assay composition.[15–19] We have developed a "slow microfluidic" platform that uses droplets covered in bespoke phospholipid mixtures to form artificial cell membranes that mimic the pathway that drugs follow from the intestine into blood via an enterocyte.

At present, oral drug absorption is predicted using a variety of *in vitro* methods that range in complexity from cell-based assays to artificial membrane models.[179,180] Drug absorption can occur through both carrier-mediated uptake and passive lipoidal

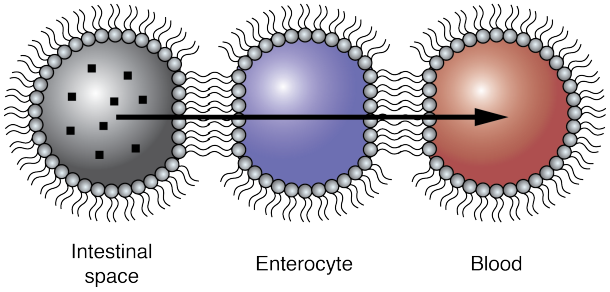

Figure 4.1: **A new type of pharmacokinetic compartment model.** Our *in vitro* droplet-based pharmacokinetic compartment model is designed to mimic the path that an orally administered drug follows from the intestine to the blood. Each compartment is made from a ~0.5 nL microfluidic droplet, where the interior of the droplet represents the compartment itself, and the phospholipid bilayer between the droplets represents an artificial cell membrane. The first droplet (droplet A, grey) mimics the intestinal space, the second droplet (droplet B, purple) mimics an enterocyte and the third droplet (droplet C, red) mimics the blood. Diffusion of a fluorophore (represented in the intestinal space droplet as black squares) occurs in the direction of the arrow.

diffusion.[12] With cell-based techniques, the estimation of drug transport through both passive diffusion and carrier-mediated transport can be simultaneous, using supported monolayers of standard cell lines such as Caco-2 or Madin-Darby canine kidney (MDCK) to model transport out of the small intestine.[181,182] Data gathered from these assays are used to calculate apparent permeability coefficients (P_{app}) which correlate to *in vivo* fractional drug absorption (F). These cell lines are also able to mimic the physiological properties of enterocytes such as microvilli.[62] Conversely, artificial cell membrane models, such as parallel artificial membrane permeability assays (PAMPA) and liposome-based assays, have other advantages: relatively low labour requirements, the ability to isolate the role of lipoidal diffusion, and tunability, which allows the mimicking of different types of membranes.

However, there is no research to show that the membranes formed in PAMPA resemble true phospholipid bilayers as found in cells. In PAMPA, *in situ* drug absorption occurs through phospholipid-doped plastic filters placed in 96-well plates.[53] The lipid composition can be customised, and the pH in the donor and acceptor compartments on either side of the filter can be tuned to mimic physiological conditions in specific

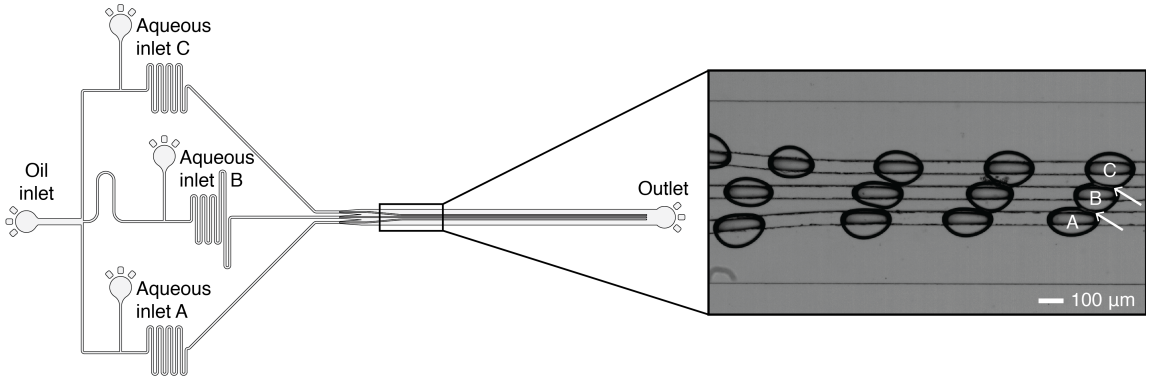

Figure 4.2: **Microfluidic platform.** Design of the "slow microfluidic" platform for the formation of ABC droplet triplets. The device schematic shows the three separately controlled aqueous inlets (A, B and C) used for the formation of three different aqueous droplets at three T-junctions. Each droplet represents a compartment in the pharmacokinetic model. To equilibrate the pressure in the system, a single oil inlet is used and the length of each channel is the same before and after each T-junction. Stabilisation of the lipid monolayer covered aqueous droplets occurs as they travel through the meanders, and bilayer formation occurs when the rails guide the droplets into contact with each other. Each DIB represents an artificial cell membrane between each compartment. The inset is a photograph showing the formation of ABC DIB triplets in parallel using the rails. The continuous phase is squalene and aqueous droplets contain 10 mM HEPES, 140 mM KCl and 10 mg mL^{-1} DPhPC at pH 6.5. Arrows highlight the artificial cell membranes formed between the droplets. A video of the microfluidic platform in use is provided in Appendix D.

tissues, which is a vital parameter in assessing the transport of ionisable compounds.[61] Concerns have been raised regarding the disproportionate thickness of the plastic filter used (˜125 µm)[54] in comparison to the thickness of a cell membrane (˜5 nm)[55] as well as the presence of organic solvent in the interior of the phospholipid "membrane".[54]

Liposomes can be comprised of one[26] or more[183] phospholipids, or even sourced directly from living cell membranes.[38] Results from these assays correlate well with human intestinal absorption in some cases.[26] However, liposome-based predictions of drug absorption rely on the use of bulk solutions, eliminating the potential for the creation of tunable, biomimetic pharmacokinetic compartments. Therefore we focus on the comparison of our model to PAMPA.

Our artificial cell membranes are based on droplet interface bilayers (DIBs), which are lipid bilayers created by bringing two aqueous droplets covered by lipid monolayers into contact (Figure 4.1). Since they were first created,[79,101] DIBs have almost exclusively been made with the archaeal phospholipid 1,2-diphytanoyl-*sn*-glycero-3-

phosphocholine (DPhPC), with a handful of exceptions, including soy[82] and *E. coli*[83] total lipid extracts. Here we show the first example of DIBs with human-mimicking phospholipid compositions.

Many different methods for the formation of DIBs using microfluidic technologies[98,184] have been developed since we published the first high-throughput method in 2010.[108] Lipid bilayers can also be formed in chambers in microfluidic platforms.[185–187] However, these methods cannot form multiple compartments of cell-scale droplets using human-mimetic phospholipid compositions in high-throughput. Therefore we have designed a new channel-based droplet microfluidic technology where a high level of control over fluid flow rates and droplet position are prioritised. To enable the prediction of pharmacologically relevant drug absorption in this *in vitro* platform, there are three design constraints. Firstly, the platform must be capable of forming droplet triplets of three different compositions, ABC, where A, B and C denote the different compartments in the pharmacokinetic model. Secondly, each droplet should be cell-scale and formed in high-throughput with high reproducibility. And finally, the platform design and surrounding equipment should be simple, to enable replication in other laboratories.

In our platform (Figure 4.2), three different types of ˜0.5 nL droplets are created and brought into contact with each other to form DIBs using rails in parallel at a rate of 0.5 Hz. Rails were first used for guiding droplet movement in series in microfluidic devices by Abbyad *et al.*[166] and for DIB formation by Carreras *et al.*, who use the rails to direct droplets for the formation of AB chains of DIBs in series.[97] In comparison, the novel use of three parallel rails allows us to control the flow of droplets into triplet DIB networks and has the potential to allow parallel assays to be performed in the same on-chip structure. Once a triplet is formed, we use a pressure

pump to instantly stop the flow for assay quantification without the need for any other on-chip features such as pillars[77] or electromagnetic valves.[188] For comparison, Czekalska *et al.*[188] were able to form one DIB ABCD network at a time and hold it in place for measurements using droplets that were approximately 500 nL in size at a rate of approximately one per minute. Also noteworthy is the microfluidic platform developed by Schmidt *et al.*[77] using approximately 5 nL AB droplets in series and the synthetic lipid 1,2-dioleoyl-*sn*-glycero-3-phosphocholine (DOPC) to measure the permeability of caffeine. Schmidt *et al.* do not report a formation rate and their platform relies on pillars and manually activated oil-withdrawing channels to form DIBs, which limits the potential for automation and increased throughput. The DIBs themselves are formed using a formulation composed of a single (synthetic) phospholipid, whereas cell membranes are usually formed of a formulation of many different types of phospholipids.[23] Other microfluidic platforms for the formation of DIBs are also flow-based, but only able to form networks of ABAB configuration.[108,109] Our platform allows us to form multiple pharmacokinetic assays simultaneously using only a pressure pump with a fast response time and one pressure channel per droplet type.

We have used our microfluidic platform to create a droplet triplet that mimics the path that an orally administered drug follows from the intestine to the blood (Figure 4.1), with droplet A mimicking the intestinal space, droplet B mimicking an enterocyte and droplet C mimicking the blood. Pharmacokinetic compartment models describe tissues as mathematical compartments, simplifying the prediction of the distribution of drugs in the body. A single-compartment model treats the body as a single space, assuming that the administered drug is uniformly distributed, while a multicompartmental model integrates tissue-specific rates of absorption and distribution into these calculations.[189] Here we present a new type of pharmacokinetic compartment

model, using droplets to model human tissues which are relevant to the absorption of orally administered drugs while maintaining important properties such as pH, ionic strength and phospholipid composition. The interior of each droplet is a buffer (Table 4.1) that mimics the pH and salt composition of each these compartments[190–192] and the artificial cell membrane between each droplet is an equal mixture of the phospholipids L-α-phosphatidylcholine (PC) and L-α-phosphatidylethanolamine (PE), a pared down version of the lipid formulation used in PAMPA assays to mimic the small intestine,[60] since these are the major components of intestinal cell membranes.[59,193–198] The droplet size mimics the volume of human cells[199] and is within two orders of magnitude of the size of human enterocytes[200–202]. Most importantly, the size of droplets formed is ten times smaller than the smallest droplets used in the literature for DIB diffusion quantification.[77] This microfluidic platform allows the quantification of the passive diffusion of fluorescein, which is commonly used as a drug proxy in release studies,[203–206] from the intestinal compartment to the blood compartment. Our new *in vitro* technique for the quantification of drug absorption of orally administered drugs provides an alternative to PAMPA for the determination of fluorescent drug absorption rates. Our method preserves the compartment model seen in PAMPA, but replaces the thick, lipid filled membrane with a biomimetic lipid mixture that mimics that found in human cells. We also preserve the differing rates of diffusion seen with different ionisation states of a drug in the gastrointestinal tract.

4.4 Materials and methods

4.4.1 Materials

1,2-diphytanoyl-*sn*-glycero-3-phosphocholine (DPhPC, $\geq$99% pure) was purchased from Avanti Polar Lipids. Sodium phosphate dibasic and sodium phosphate monoba-

sic were purchased from Fisher Scientific. Sodium chloride and sodium carbonate were purchased from Bio Basic. L-α-phosphatidylcholine (PC, $\geq$99% pure, bovine liver), L-α-phosphatidylethanolamine (PE, $\geq$97% pure, bovine liver), squalene ($\geq$98% pure), 4-(2-hydroxyethyl)-1-piperazineethanesulfonic acid (HEPES, $\geq$99.5% pure), trimethylchlorosilane ($\geq$99% pure), sodium fluorescein (BioReagent, suitable for fluorescence), potassium hydroxide, hydrochloric acid ($\geq$36.5-38%) and potassium chloride ($\geq$99% pure) were purchased from Millipore Sigma. Polydimethylsiloxane (PDMS, Dow Sylgard 184) was purchased from Ellsworth Adhesives. Acetate masks were printed at 10 µm resolution by CAD/Art Services Inc. Silicon wafers (100 mm diameter) were purchased from Silicon Materials. SU-8 3050 and developer were purchased from MicroChem. Polytetrafluoroethylene (PTFE, 1/16" outer diameter, 250 µm inner diameter) tubing was purchased from Chromatographic Specialties Inc.

4.4.2 Design and fabrication of the microfluidic platform

Microfluidic devices (Figure 4.2) have two layers. The first layer contains the channels and geometries used for the formation of the three different types of droplets used to model each pharmacokinetic compartment. The second layer contains the rails, which are 50 µm apart. The three rails encourage the three aqueous droplets covered with a phospholipid monolayer to come into contact to form an artificial cell membrane at the points of interaction. The 5° angle of the rails means that the droplets can be brought into contact at a slow speed of approximately 40 µm s^{-1}. The layers were designed using AutoCAD (Autodesk, 2018, see Appendix D) and printed onto acetate to create positive photomasks. A 50$\pm$2 µm thick layer of the negative photoresist SU-8 3050 was spincoated onto a silicon wafer, and the edgebead was removed with a stream of acetone. The wafer was subjected to a soft bake (5 min at 35 °C, 2 min at 65 °C and 30 min at 95 °C), and subsequently exposed to UV light (11.2 s, 19.96 mW/cm^2,

OAI Model 800 mask aligner) through the first photomask. A second layer was spincoated, softbaked, aligned and exposed to UV using the same parameters and the second layer photomask. Development removed the unexposed, non-crosslinked SU-8, and adhesion of the SU-8 features was accelerated by a final hard bake (30 min at 200 °C) and a third UV exposure (90 s, 19.96 mW/cm^2).

Trimethylchlorosilane (50 µL) and the wafer mould were placed under vacuum for 1 h to ensure the deposition of a thin film of silane on the surface of the wafer. PDMS base and curing agent were mixed together in a 10:1 ratio, poured over the aforementioned mould, degassed for 1 h under vacuum to remove any air bubbles introduced during mixing, and cured overnight at 65°C. The cured PDMS was then peeled from the mould. Inlets and outlets for each device were punched using a 1 mm biopsy punch. To create the base of the device, a 10:1 mixture of PDMS base and curing agent was mixed, degassed and spincoated at 1200 rpm for 25 s onto the surface of glass microscope slides to create a thin layer. Both the PDMS devices and the coated glass slides were washed with soapy reverse osmosis (RO) water, rinsed with RO water, isopropyl alcohol, ethanol and Milli-Q water, blown dry with filtered air, baked at 90 °C for 30 min, treated with air plasma (Diener Electronic, Zepto ONE, 37 s, 29 W, 1.75 mbar) to activate the surfaces and placed into contact with each other to bond the surfaces together. The microfluidic devices were then stored at 65 °C for a minimum of 48 h prior to use.

4.4.3 Preparation of lipid solutions

Chloroform was removed from the lipid stock solutions by placing 10 mg (400 µL of a 25 mg mL^{-1} solution dispensed using a P1000 Gilson pipette) of lipids in a 10 mL glass roundbottom flask, and rotating the flask under a stream of nitrogen gas to create a

thin film. The flask was then placed in a desiccator under vacuum for 1 h to remove residual solvent. For DPhPC solutions, 1 mL aqueous buffer (buffer composition is the same as that of the intestinal space in Table 4.1) was then added and the flask was vortexed to resuspend the lipids. After freezing and thawing 5 times using liquid nitrogen and warm water, the lipids were extruded 21 times through a 0.1 µm polycarbonate membrane (Avanti Polar Lipids) at room temperature. For 1:1 PC:PE solutions, 1 mL of squalene was added to the flask, which was then vortexed for 30 s and stirred at 50 °C until the phospholipids dissolved. The final concentration was 5 mg mL^{-1} PC and 5 mg mL^{-1} PE in squalene. For absorption experiments, 100M fluorescein sodium was added to the buffer.

Table 4.1: **Composition of the buffers used for each pharmacokinetic compartment.**

Droplet designation	Buffer	Salt
Intestinal space[190,207]	10 mM Na_2HPO_4, pH 6.5	140 mM KCl
Enterocyte	10 mM HEPES, pH 7.4	140 mM KCl
Blood[208]	10 mM Na_2CO_3, pH 7.4	140 mM NaCl

4.4.4 Operating parameters of the microfluidic platform

For all experiments, devices were mounted in a custom-made heating platform set to 37 °C (see the Appendix D for further details) on the stage of either a Nikon Eclipse Ti2-E or a Nikon Eclipse Ti2-U inverted microscope for visualisation. Brightfield images for statistical analysis were collected using a Motion Blitz EoSens Cube7 or a Phantom VEO 710L high speed camera. Fluorescence and brightfield images for fluorescence experiments were captured using a Hamamatsu ORCA-Flash4.0 V3, with a Solis 1C cold white LED (Thorlabs) and a GFP SemrockBrightline large field of view filter cube (Nikon).

Reagents were introduced into the microfluidic devices using an Elveflow OB1 MK3 pressure pump, four 1.5 mL Eppendorf tubes as reservoirs and four matched lengths

of PTFE tubing. Squalene and aqueous buffers were introduced to the microfluidic device by applying a pressure of 100 mbar to 140 mbar to the squalene reservoir, and a pressure of 60 mbar to 100 mbar to each of the aqueous reservoirs. Following equilibration, the main chamber was monitored in Motion Blitz Director for quantification of device performance, and NIS Elements Advanced Research (Nikon, version 5.11.01) for fluorescence data collection. Following formation of a triplet for a fluorescence experiment, flow was stopped from all reservoirs from within the Elveflow control software. Typical droplet speeds were approximately 450 µm s^{-1}, allowing this full stop to be done without the use of triggers.

The speed at which droplets are brought into contact with each other is crucial for the formation of stable artificial cell membranes, and this is especially true when using phospholipids below their phase transition temperatures, as we do here. The response time of the pressure pump means that the flow can be stopped within 130 ms of when an ABC droplet triplet forms and the assay starts. We are therefore able to accurately determine the initial time point of the assay and to discard substandard triplets.

4.4.5 Fluorescence data collection

Once ABC droplet triplets formed and the flow was stopped, brightfield and fluorescence images were taken every 10 s with a 300 ms exposure time until experiment termination. Quantification of fluorescence intensity was performed via time-based measurement of mean intensity in regions of interest (ROIs) within each droplet in each frame using NIS Elements. Fluorescence intensity data was normalised for phospholipid bilayer surface area and droplet volume. To do this, bilayer diameters and droplet semiaxes were measured using, respectively, the "Distance Measurement" and

the "Measurements and Annotations" modules in NIS Elements. Subsequent calculations were performed by approximating artificial cell membrane surface area as ellipses and droplet volumes as ellipsoids. Each graph in this paper represents the replicate of 5 experiments conducted on 5 different microfluidic devices. Figures D.2, D.3, and D.4 in Appendix D provide detailed information about the ROI selection, the quantification of fluorescence intensity, volume calculations and data normalisation for the artificial cell membrane surface area and droplet volume.

4.4.6 Quantification of microfluidic device performance

To quantify the performance of the microfluidic devices, squalene was pumped into the oil inlet and DPhPC in buffer was pumped into each of the three aqueous inlets with the pressure pump in constant pressure mode. Assessment of the efficacy of ABC DIB triplet formation on the platform was performed using DPhPC to allow for comparison with other DIB forming methodologies in the literature. After letting the flow equilibrate, the high-speed camera was centered on the main chamber, and 60 s of footage were captured for each replicate. The number of ABC DIB triplets formed in each sequence was counted, as summarised in Table 4.2. The total number of droplets forming triplets was then determined as a percentage of the total number of droplets passing through the field of view. To show the robustness of our method, two sets of two replicates each were carried out, with a different researcher carrying out each set on separate days. For each replicate, a different microfluidic device was used. Statistical analysis indicated that triplets could be formed at a rate of 0.5 ± 0.1 Hz and that 45 ± 8 % of droplets entering the rail section of the platform were able to form triplets. No precedent for reproducibility exists in the literature, so this may serve as a benchmark by which throughput and reproducibility of DIB forming methodologies (both microfluidic and not) may be assessed.

Table 4.2: **Statistical data used to quantify device performance.** All replicates were collected from 60 s of video captured at 30 frames per second. Triplets were counted from the beginning of the captured video and the number of triplets (n) for each experimental repeat are shown in the first column.

n	Formation rate	Oil pressure	Aqueous pressure
34	0.57 Hz	120 mbar	113 mbar to 115 mbar
32	0.53 Hz	120 mbar	113 mbar to 115 mbar
26	0.43 Hz	100 mbar	90 mbar to 95 mbar
18	0.30 Hz	100 mbar	90 mbar to 95 mbar

4.5 Results and discussion

4.5.1 A new *in vitro* model for intestinal absorption

The time-resolved diffusion of fluorophore between pharmacokinetic compartments A, B and C may be seen in Figure 4.3. Timepoints are chosen to show when the fluorophore is concentrated in the intestinal compartment A (t = 0 s), a mid-assay timepoint (t = 420 s) where the fluorophore is concentrated in the enterocyte compartment B, and the endpoint of the assay (t = 1800 s). All data were gathered at physiological temperatures (37°C).

Figure 4.4 shows the change in concentration over time for each compartment in the system. Given the well-known nature of PDMS and how droplet volume varies over time in these platforms,[128] intensity measurements were first scaled based on changes in droplet volume over the course of the experiment, due to either evaporation or osmosis, using Equation 4.1, where I_s is the scaled intensity, I_t is the intensity at time t, and V_t and V_0 are the droplet volumes at times t and 0 respectively.

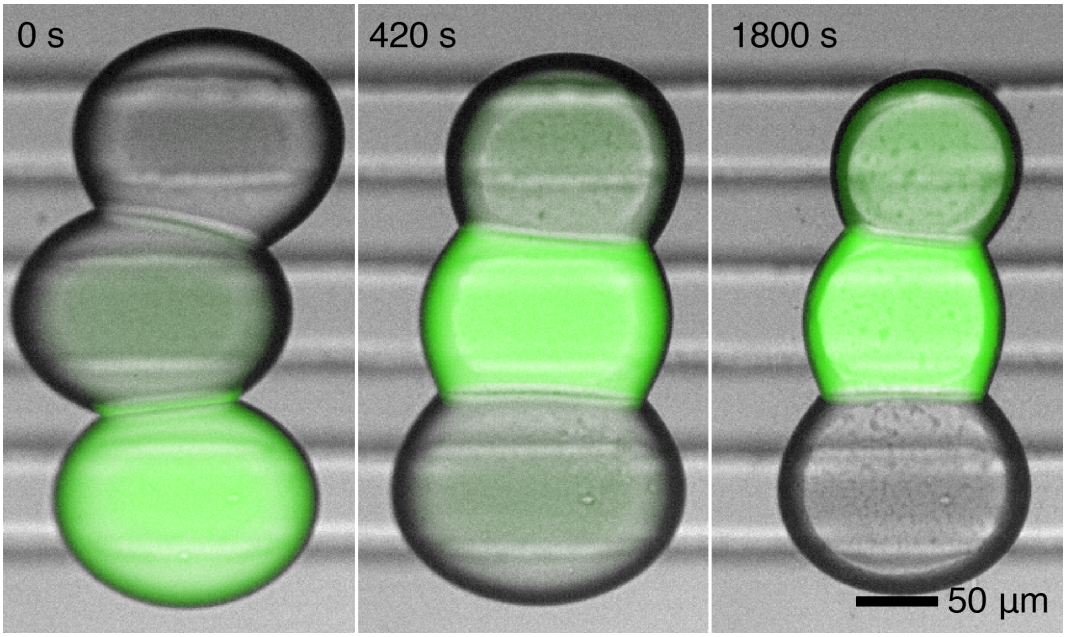

Figure 4.3: **Images of fluorophore diffusion.** Composite brightfield and fluorescence images showing the diffusion of fluorophore from the droplet that represents the intestinal compartment in the pharmacokinetic compartment model (bottom), to the droplet that represents an enterocyte (t = 420 s, middle), after which it continues diffusing into the droplet that represents the blood compartment (t = 1800 s, top). The fluorophore in the fluorescence images has been tinted green to aid visualisation. Brightfield and colour intensity-corrected fluorescent images were exported from NIS Elements and overlaid with a screen blending mode. Brightness was raised to visible levels by applying a lookup table.

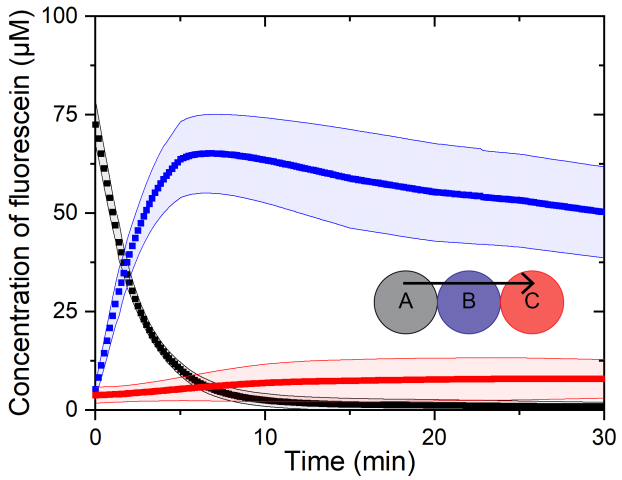

Figure 4.4: **Fluorophore diffusion over time.** Normalised concentration curves for each pharmacokinetic compartment in the droplet triplet model over 30 minutes. The fluorophore is initially concentrated in the droplet representing the intestinal space, A, but rapidly diffuses through the artificial cell membrane into the droplet representing an enterocyte, B, and slowly diffuses through the artificial cell membrane into the droplet representing the blood, C. 95 % confidence bands were calculated from the standard deviation for each timepoint, where n = 5 using 5 different microfluidic devices.

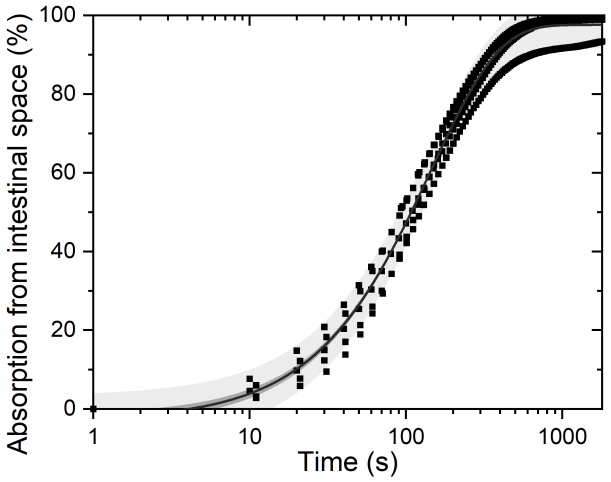

Figure 4.5: **Fluorophore absorption over time.** Absorption of fluorophore from the intestinal space compartment A, into the enterocyte compartment, B, shown as percentage of fluorescence decrease from initial intensity. The fitted curve and narrow confidence band allow the prediction of the half-life of the fluorophore in the intestinal space compartment with a 2 % relative standard deviation.

To determine concentration and account for pH-dependent changes in fluorophore intensity, calibration curves were generated for fluorescein in each buffer and a linear fit was calculated using OriginPro 2019b. Concentration was then calculated from the fitted curve using the scaled intensity measurements. Calibration curves (Figures D.5, D.6 and D.7) and additional experimental information are provided in Appendix D.

$$I_s = I_t \frac{V_t}{V_0} \tag{4.1}$$

Figure 4.5 shows the absorption of the fluorophore from the intestinal space compartment A into the enterocyte and the blood compartments, B and C. The rapid absorption of the fluorophore from the intestinal space into both the enterocyte and the blood can be clearly seen. To find the half-life ($t_{\frac{1}{2}}$) of the fluorophore in the intestinal space, an exponential curve of the form $y = a - bc^x$ was fitted to this data in OriginPro. This curve fitting found the parameters $a = 0.976 \pm 0.001$, $b = 1.004 \pm 0.007$,

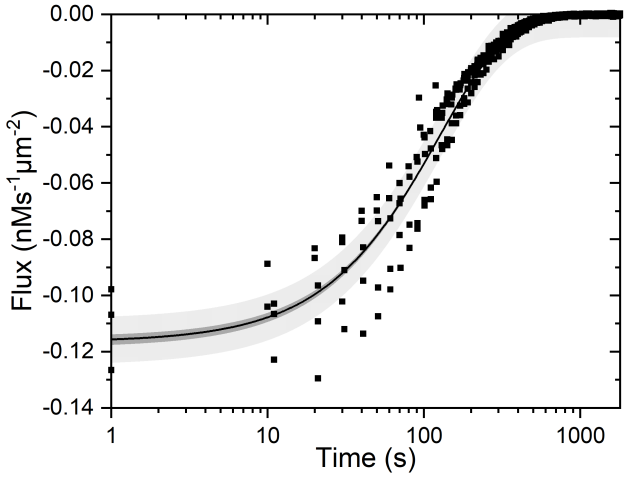

Figure 4.6: **Fluorophore flux over time.** Flux of fluorophore from the intestinal space compartment, A, into the enterocyte, B, calculated using Equation 4.2. Maximum flux may be determined using the fitted curve, providing a measurement of the permeability of the membrane to the fluorophore.

and $c = 0.99311 \pm 0.00005$. The slope of the intensity curve gives the diffusion rate. From this curve a $t_{\frac{1}{2}}$ of 108 ± 2 s was determined.

The accuracy of this technique was improved by accounting for the area dependence of diffusion rates through the artificial cell membrane. This flux was calculated using Equation 4.2, where j_t is the flux at time t, $\Delta C/\Delta t$ is the momentary slope, and $A_{DIB,t}$ is the measured artificial cell membrane area at time t.

$$j_t = \frac{\Delta C}{\Delta t}\frac{1}{A_{DIB,t}} \tag{4.2}$$

The flux of all five runs is plotted in Figure 4.6. Following curve fitting the y-intercept, j_{max}, was calculated to be $-0.117 \pm 0.002\,\mathrm{nMs^{-1}\mu m^{-2}}$.

4.5.2 Correlation to cell-based assays

Our method is three times better at predicting P_{app} of actual intestinal tissue than PAMPA. For direct comparison with literature permeability values for fluorescein, we adapted the equation for the P_{app} used by Berginc *et al.*[209] We treated the system as a two compartment model, allowing us to treat diffusion out of the intestinal space (droplet A) as having the same magnitude as diffusion into the enterocyte (droplet B). This gives Equation 4.3, where $\Delta C/\Delta t$ (µM/s) is the maximum rate of diffusion out of droplet A, V ($\mathrm{cm^3}$) is the initial volume of droplet B, C_0 (µM) is the initial concentration of droplet A, and A ($\mathrm{cm^2}$) is the maximum artificial cell membrane surface area.

$$P_{app} = \frac{-\Delta C_{max}}{\Delta t}\frac{V}{C_0 A} \tag{4.3}$$

We found P_{app} to be $(5.6 \pm 0.7) \times 10^{-5}\,\mathrm{cm\,s^{-1}}$. PAMPA assays carried out previously by Berginc *et al.*[209] found P_{app} for fluorescein to be $(16 \pm 3) \times 10^{-5}\,\mathrm{cm\,s^{-1}}$ with pH 6.5 and 7.5 in the donor and acceptor compartments respectively, a whole order of magnitude higher. However when they performed this absorption assay using rat jejunum under the same pH conditions we used they found P_{app} to be $(0.8 \pm 0.1) \times 10^{-5}\,\mathrm{cm\,s^{-1}}$.

4.5.3 Control experiments

Direct comparison in intensity between the compartments is complicated by matrix differences since the composition of the droplets was customised to mimic specific biological compartments using different buffering agents and salts. Interestingly, there was a very narrow spread of data for the fluorophore leaving the intestinal space compartment (droplet A), but a wider spread of behaviours upon entering the enterocyte and blood droplets. This can be seen as a wider spread in Figure 4.4 for these compartments. Control experiments were performed to assess the matrix effect, which was easily done with this microfluidic platform. In these control experiments, the fluorophore was always dosed in droplet A (the intestinal space), but the composition of the triplet was varied to allow a different diffusion pathway in each case, namely: AAA, BAC, ABB, ACC and ACB, where B represents an enterocyte and C represents the blood (see Figure D.1 in Appendix D for data).

As expected, complete fluorophore equilibration was observed when all three compartments were tuned to mimic the pH and ionic composition of the enterocyte (AAA). Likewise, when triplets of the composition BAC were formed, rapid equivalent diffusion out of droplet A into droplets B and C was observed, and in the case of ABB triplets, rapid diffusion into droplet B_1 was followed by equilibration between both B droplets. The behavior of ACB triplets closely followed that of ABC triplets.

However, when ACC triplets were formed, rapid diffusion into C_1 occurred, and the fluorophore did not continue into the second C droplet, C_2. In all cases where pH 7.4 droplets were tested with pH 6.5 droplets, fluorescein demonstrated a clear preference for pH 7.4 compartments.

The primary driving force for the selective diffusion path seen in our pharmacokinetic compartment model is the different pH environments encapsulated in droplets A and B, and hence the fluorophore rapidly leaves the intestinal space and enters the enterocyte. Fluorescein has a pKa of 6.43,[210] so a smaller fraction of molecules exist in the more lipid-soluble monoanionic form at pH 7.4 and a larger fraction exist in the less lipid-soluble dianionic form at pH 6.5. This effectively allows fluorescein to easily diffuse into the artificial cell membrane from the intestinal space, but to diffuse back into the intestinal space from the cytosol at a far reduced rate. This ties rate of diffusion to lipophilicity in the same way as PAMPA.[53] The fluorescein monoanion and dianion exhibit slight differences in absorption and emission spectra, including in fluorescence intensity and quantum yield.[211,212] The movement of the fluorophore between droplets B and C, which are at the same pH, is explained by the second driving force for the observed transport phenomenon, which is the difference in osmolality between these droplets.

$$Osmolality = 2[Na^+ + K^+] + [urea] + [glucose]^{213} \tag{4.4}$$

Respectively, the calculated osmolalities of droplets A, B, and C are 320 mM, 280 mM, and 320 mM. Diffusion will be driven towards higher osmolality compartments, but because the majority of fluorescein exists as a dianion in droplet B and thus cannot diffuse back into droplet A, the equilibrium lies further towards droplet C.

4.6 Conclusions

Here we show a new type of pharmacokinetic compartment model with higher correlation to cell-based assays than PAMPA, the current state-of-the-art technology. This suggests that a higher degree of *in vitro-in vivo* correlation may also be found using our bespoke pharmacokinetic compartment model. We intend our method to be complementary to cell-based assays by providing a way of creating bespoke artificial cell membranes and pharmacokinetic compartments to quantify the effect that each membrane component has on drug transport.

We have used a new type of microfluidic platform for the formation of DIBs in parallel to build a pharmacokinetic compartment model of the path that an orally administered drug takes from the intestinal space, into enterocytes and finally into the blood. We demonstrate how this compartment model can predict pharmacokinetic properties of a drug including half-life, flux and P_{app}. Our pharmacokinetic compartment model demonstrates a greater degree of similarity of P_{app} to a true biological system (rat jujenum) than is possible with PAMPA.

Our microfluidic platform is simple to use (it only requires a fast response pressure pump) and allows the artificial cells to be formed of sizes (˜0.5 nL) that more closely mimic human cells than preceding work and that use the major phospholipid components (PE and PC) of intestinal cells. We demonstrate and quantify the reproducibility of this platform and show the collection of data with far better time resolution than previously possible. Ongoing and future developments include modelling drug transport in other human tissues and investigating new drug tagging and detection methods.

The limited correlation between *in vitro* and *in vivo* methods for the prediction of

drug behaviour in humans is a severe constraint in the timely and cost-effective development of new drugs. Our new *in vitro* model could allow the early prediction of pharmacokinetic parameters of drug candidates by enabling researchers in academia and the pharmaceutical industry to build bespoke pharmacokinetic compartment models.

Chapter 5

DIBs for drug permeability prediction in the small intestine and blood-brain barrier

5.1 Context

In this chapter, I use complex bespoke phospholipid formulations as well as total lipid extracts to build DIBs to model other pharmacologically relevant tissues. Accurately predicting drug permeability across the lining of the small intestine and the blood-brain barrier is vital in the early stages of drug development. I present here custom-made pharmacokinetic compartment models for the path a drug takes from the small intestinal lumen to the bloodstream as well as the path a drug takes from the bloodstream into the brain interstitial fluid. Here, I used a more complex lipid formulation to create the intestinal model and also show sex-specific intestinal models, which are able to predict the slower absorption observed in female subjects. using two

different lipid extracts, I demonstrate blood-brain barrier DIB models which mimic differences in molecular transport observed in BBB-PAMPA. Finally, I demonstrate preliminary results creating droplet compartment models for testicular Sertoli cells. These are the first DIBs to be created using a total lipid extract made from human cells, as well as the first non-commercial total lipid extract.

I performed all experimental work and data analysis, with exceptions listed here. Meghan Robinson at the Vancouver Prostate Centre cultured the Sertoli cells and extracted the plasma membrane lipids. Allison Selinger from the Hof Group designed, prepared, and donated one of the fluorogenic dyes tested, DimerDye 4. Maria Hangad performed data normalization for fluorescence data presented in Figures 5.3 and 5.6. Elanna Stephenson designed the microfluidic device used for all the permeability experiments (Figure 5.1).

5.2 Introduction

Here, I show the creation of more permutations of the pharmacokinetic model demonstrated in Chapter 4. As discussed in Chapter 4, it is of particular interest to model the small intestine epithelial cell membrane in order to investigate drug transport from the small intestine into the bloodstream and thus quantify oral bioavailability. Towards this aim, in this chapter I implement more complex, biomimetic intestinal lipid formulations. Additionally, demonstrated differences in pharmacokinetics between male and female patients suggest that sex-specific prediction models must also be created.[214] I created male and female intestine-mimetic DIBs to investigate the role of membrane composition on passive permeability. Next, I set out to model the blood-brain barrier, as predicting activity in the central nervous system is vital in the early stages of drug development. Finally, I demonstrate initial findings modelling

Sertoli cells using a total lipid extract.

In Chapter 4 I propose that human small intestine-mimetic DIBs can be used to quickly and accurately predict oral bioavailability and predicted the transport of fluorescein using intestine-mimetic DIBs (Chapter 4). Here, I demonstrate the formation and application of DIBs using a more complex intestinal lipid formulation, which incorporates more components of the enterocyte plasma membrane, specifically PS, PI, and cholesterol. I designed a lipid formulation for use in the creation of DIBs to model the path an orally administered drug takes from the inside of the small intestine into the blood. This formulation was based on lipids used to create biomimetic PAMPA.[60,215,216] These formulations were in turn designed based on analysis of total membrane extracts of mammalian cells.[59] I also demonstrate intestine-mimetic DIB formation incorporating the membrane lipid sphingomyelin (SM).

I also designed and tested intestine-mimetic DIBs which mimic sex-based differences in the cell plasma membrane, specifically, the slower absorption observed in female patients.[217] These are the first human-mimetic DIBs which mimic membrane composition differences that are specific to sex, or, in fact, specific to any population. The effect of these sex-based membrane differences on drug absorption has not previously been studied. Pharmacokinetic processes like absorption differ between populations, including male and female patients. The role of biological sex-based differences in pharmacokinetic processes has been noted in a variety of cases, including the metabolism of ethanol, iron, and calcium.[218] However, very little information exists for healthcare providers in terms of sex-based prescription guidelines, potentially leading to the recommendation of dosages of inappropriate levels, which contribute to the increased number and severity of adverse events female patients experience as compared to male patients.[218–220] This is compounded by the underrepresentation of

female subjects in clinical trials, which existed both historically and continues in the present.[214,218] Factors like body weight, body composition, gastric pH, retention time, fatty acid and phospholipid ratios, and enzyme and transporter expression and activity play roles in mediating drug absorption.[214] Differences in these factors between male and female patients cause observable sex-based differences in pharmacokinetics.[214] Some of the effects have already been quantified in the literature, such as the fact that gastric pH is significantly lower in male patients versus female patients (1.92 versus 2.59),[214] which leads to decreased absorption of weak acids and increased absorption of weak bases, which include many antidepressant drugs,[214,221] and the fact that gastrointestinal retention time is also significantly shorter in male bodies (44.8 hours) than female bodies (91.7 hours) on average.[214,222] The relationship between sex-based differences in membrane composition and correlated differences in drug absorption have not previously been investigated. Here, I focus on modelling differences in the composition of cell plasma membranes and their effects on passive permeability.

Cell plasma membrane composition differs between male and female subjects, specifically in the distribution of phospholipid chain lengths and degrees of saturation.[223,224] In general, the types of acyl chain tail groups present in cell plasma membranes differ: female subjects exhibit higher levels of arachidonic acid (AA), docosahexaenoic acid (DHA), and linoleic acid (LA) than men; conversely, male subjects exhibit higher levels of DPA than women.[224] It has also been found that, compared to male rats, female rat cell plasma membranes exhibit lower levels of LA (18:2n-6) and AA (20:4n-6) PC but higher levels of AA PE and higher levels of both DHA (22:6n-3) PE and PC.[223] These differences could play a role in membrane fluidity and permeability and can be easily modelled using DIBs through the use of bespoke lipid formulations. I developed male and female intestine-mimetic DIBs and performed fluorescein permeability measurements.

Predicting the permeability of ionizable compounds across cell membranes is important in drug discovery due to the variation in physiological pH between different tissues. The small intestinal lumen has a slightly acidic pH of 6.5 versus the blood, which has a pH of 7.4.[225] Many drugs are weak acids and bases, the protonation state of which dictates ionization state and absorption: neutral molecules easily cross cell membranes while ionized molecules are more limited in their transport.[25] I used fluorescein as a drug proxy due to its ionizability and pK_a values which fall near the pH values present in the intestinal model as well as its high intensity fluorescence emission signal. Fluorescein permeability was measured across intestine-mimetic DIBs. Calcein, which is the membrane-impermeable derivative of fluorescein,[226] was used as a control. DIBs formed using DOPC have previously been demonstrated to be impermeable to calcein.[109,112] Based on these existing data, I expected that calcein would not cross any of the biomimetic DIBs formed in this section.

In addition to intestinal absorption, it is vital to predict the interaction a drug will have with the blood-brain barrier early on in the preclinical stage of its development.[3] Whether a drug candidate is intended to cross the blood-brain barrier, as is the case for many drugs intended to treat neurodegenerative diseas, or not, as is the case for drugs which could potentially exhibit central nervous system toxicity, prediction of this process is important to ensuring drug effect and safety.[227] Polar brain lipid extracts have previously been used in more biomimetic versions of PAMPA, which demonstrated good correlation to *in vivo* blood-brain barrier permeability results.[56,57,228–230] DIBs formed using total lipid extracts from brain cells have previously been demonstrated in the literature, but their potential to model permeability of the blood-brain barrier has not been studied.[84,159,160,162] DIBs formed using brain total lipid extracts have been used to mimic human synapses as a scaffold for electrophysiological measurements such as membrane capacitance[84] as well as study of the role of

temperature in DIB formation.[162] Najem *et al.* have also demonstrated insertion of the ion channel alamethicin into DIBs formed using a brain total lipid extract.[159,160] Despite their applications in PAMPA,[231] polar brain lipid extracts have never been used in the literature for DIB formation. Here, I use both total brain lipids (TBL) and polar brain lipids (PBL) to build compartment models for the blood-brain barrier. I chose to test DIB formation and permeability using both available types of brain lipid extracts to investigate the role that lipid composition and lipid extract type play in permeability. Fluorescein and calcein were used to measure permeability in addition to FITC (fluorescein isothiocyanate)-tagged dextrans (40 and 500 kDa). FITC-dextrans are used in the literature to assess permeability, including of the blood-brain barrier,[232] and so were used here as an additional set of control experiments. Due to their large size and molecular weight, FITC-dextrans are not passively membrane-permeable.[232]

While DIB formation using lipid extracts has been shown previously in the literature[83,84,160,162,233] and through my own work using total and polar brain lipid extracts (Section 5.3.3), there are many cell types of interest for which commercial lipid extracts do not exist. There are also population-based differences in membrane composition, such as the sex-based differences discussed here, as well as changes in membrane composition associated with disease states.[234–237] This variability in cell plasma membrane composition and thus, potential variability in passive permeability, is difficult to model using commercial lipid extracts or even bespoke formulations designed from the bottom up to mimic specific membranes. Expanding the future applications of DIBs as a pharmacokinetic model for permeability prediction depends on the use of a large library of lipid mixtures for DIB formation.

My permeability experiments thus far have relied on fluorescence microscopy to quan-

tify the transport of fluorophores across biomimetic DIBs. In the literature, nearly all studies which quantify molecular transport in DIBs on a microfluidic device also rely on fluorescence microscopy to quantify transport,[77,82,86,104,108–112] with the exceptions of water permeability, which can be assessed using brightfield microscopy,[88–90,114] and a recent publication in which droplets are separated following rhodamine 6G diffusion and analyzed using LC-MS. Io be useful as an *in vitro* model for drug transport, a DIB pharmacokinetic prediction model should have the capacity for the detection of nonfluorescent compounds on-chip. Most drugs are not fluorescent, with exceptions including, for example, the chemotherapy drug doxorubicin,[238,239] the transport of which has been studied using DIBs,[87] and tetracycline drugs, which have poor quantum yield in aqueous solution,[240] making them difficult to analyze using DIBs. On-chip quantification of permeability of a nonfluorescent compound has been done once before through reaction of the fluorogenic dye Chromeo P540, localized in the acceptor droplet, with ethanolamine, which diffused across a DIB from the donor droplet.[113] For a pharmacokinetic prediction tool to be useful in preclinical research, it should be able to measure the passive transport of any drug, not only a select few which are fluorescent. Derivatizing these compounds prior to DIB formation is nonideal since addition of a fluorescent tag could change the permeability properties of the molecule. I therefore tested the compatibility of three fluorogenic molecular recognition agents with my biomimetic DIB models.

Initial DIB formation tests were performed on the device depicted in Figure 3.1, which provides a simple platform for the formation of DIBs between droplets of identical composition. All of the permeability measurements presented in this chapter were performed using a two-rail analogue of the device presented in Chapter 4 (Figure 5.1), which was designed by Elanna Stephenson. This device allows for DIB formation between pairs of droplets with different contents. In this device, aqueous droplets of

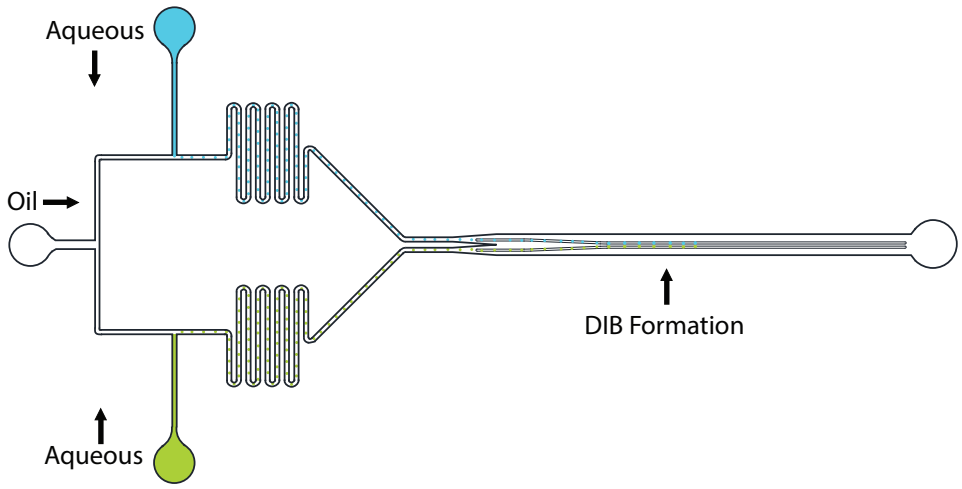

Figure 5.1: **Design of the microfluidic device design used for permeability measurements.** Oil is introduced through the labelled inlet. Two different aqueous solutions, which will comprise the donor and acceptor compartments, are introduced through the labelled inlets and form droplets at the parallel T-junctions. Droplets flow through the device and, guided by two parallel rails, form DIBs. Transport of a compound from the donor to the acceptor compartment can be measured on-chip. Arrows indicate direction of fluid flow. Design by Elanna Stephenson.

differing composition (one of which can contain a drug or fluorophore) are formed at parallel T-junctions in the same oil phase. Droplets flow through meandering channels to allow for complete monolayer formation and are then brought together for DIB formation using two parallel rails to guide their flow.

5.3 Results and Discussion

5.3.1 Modelling intestinal absorption

To create a DIB model for intestinal absorption, I designed a bespoke lipid formulation based on lipids previously used in biomimetic PAMPA measurements.[60,215,216] Sugano *et al.* used a mixture of PC and PE (both 0.8% w/w) as well as PI and PS (both 0.2% w/w) and cholesterol (CHO) (1.0% w/w) in 1,8-octadiene (97% w/w) to

mimic the enterocyte plasma membrane in PAMPA. Excluding the organic solvent and taking into consideration the concentration of phospholipid necessary to easily form DIBs, I adapted these ratios to give a lipid formulation containing PC, PE, PS, PI, and CHO in a 4:4:1:1:5 weight ratio and a final phospholipid concentration of $10\,\mathrm{mg\,mL^{-1}}$ in either buffer or oil. Because $10\,\mathrm{mg\,mL^{-1}}$ has been found to be the optimal concentration for phospholipids extruded into unilamellar vesicles in an aqueous buffer,[109] 1 mL of intestinal lipids (IL) is prepared using 4 mg PC, 4 mg PE, 1 mg PI, 1 mg PS, and 5 mg CHO.

I initially tested DIB formation using this formulation using the lipid-in approach at room temperature, which failed. When droplets were brought into contact, they merged to form one large droplet instead of forming a DIB at their interface which would keep the donor and acceptor droplet compartments separate. However, intestine-mimetic DIB formation using the lipid-in approach is successful at temperatures of 70°C or higher, which I propose is due to a more complete gel-to-liquid phase transition and thus more complete monolayer formation, which enables bilayer formation. When the microfluidic device is held at or above the phase transition temperature of the phospholipids in the system, DIBs are easily formed and remain intact when cooled. For a more complete discussion of the role of temperature in DIB formation using naturally derived phospholipids, see Chapter 3. As in Chapter 4, I was able to form stable intestine-mimetic DIBs at 37°C using the lipid-out method and did so for all permeability experiments presented here.

I measured the permeability of intestine-mimetic DIBs to fluorescein and calcein. The donor droplet contained an initial concentration of 100 µM fluorophore in pH 6.5 buffer. The acceptor droplet initially contained only pH 7.4 buffer. These pH values were chosen to mimic the more acidic conditions of the small intestine.[225] As expected,

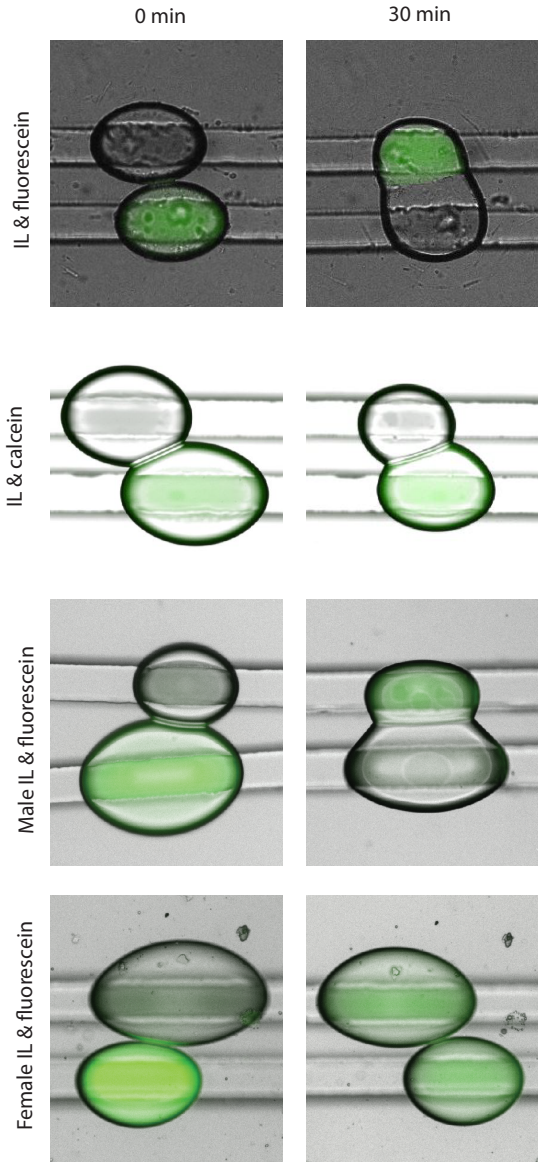

Figure 5.2: **Fluorophore transport in intestine-mimetic DIBs.** In the left column are images at t = 0 min, where the fluorophore is solely located in the donor droplet. In the right column are images at t = 30 min. From top to bottom: fluorescein permeability in IL DIBs, calcein permeability in IL DIBs, fluorescein permeability in male IL DIBs, and fluorescein permeability in female IL DIBs.

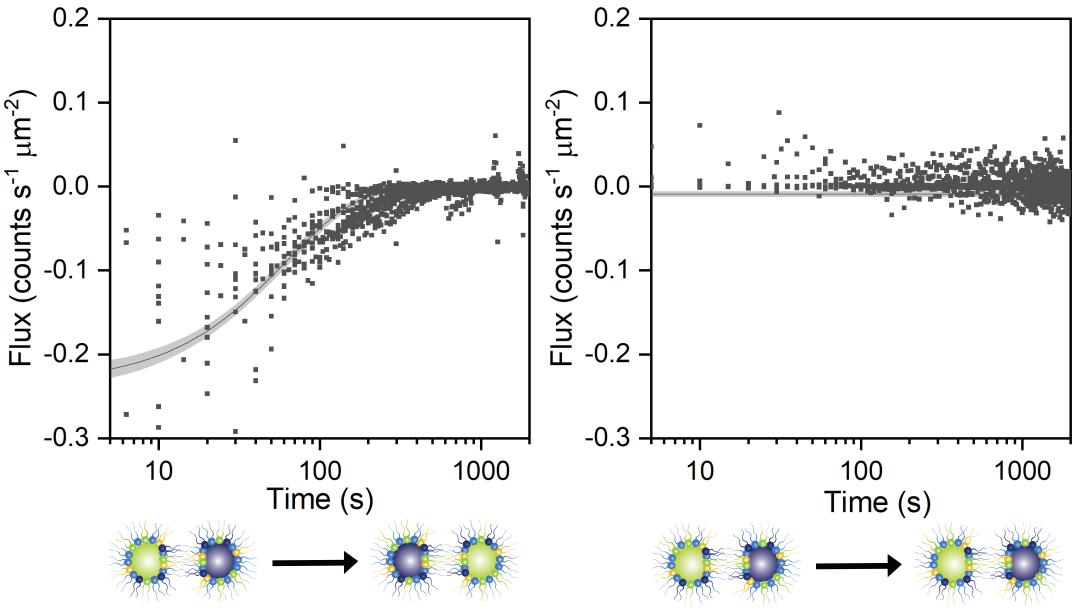

Figure 5.3: **Fluorophore flux in human intestine-mimetic DIBs.** Following DIB formation between a donor (containing fluorophore) and an acceptor (empty) droplet, diffusion of fluorophore through the bilayer was measured, as shown in the diagrams below the graphs. Left: Fluorescein flux across intestine-mimetic DIBs (n = 13). Right: Calcein flux across intestine-mimetic DIBs (n = 7). Maximum flux and fluorophore half-life were determined using the fitted curve and are shown in Table 5.1. The microfluidic device was held at 37°C while fluorescein transport occurred. An exponential curve of the form $y = a * e^{(}-x/b) + c$ was fitted to the fluorescein data in OriginPro. Curve fitting found the parameters $a = -0.226 \pm 0.00606$, $b = 66.5 \pm 3.16$, and $c = -0.00259 \pm 0.000866$. A linear function of the form $y = a + b * x$ was fitted to the calcein data in OriginPro with the parameters $a = 0.0705 \pm 0.0118$ and $b = -0.0265 \pm 0.00388$. 95% confidence bands were calculated from the standard deviation at each timepoint.

membrane-impermeable calcein served as a control measurement against which to observe the transport of fluorescein. Representative images of IL DIB permeability assays can be found in Figure 5.2. Fluorescein passively permeates the intestine-mimetic DIB and preferentially localizes in the acceptor compartment (Figure 5.2). This is primarily due to the difference in pH between the compartments. Fluorescein has a pKa of 6.43,[210] just below the pH of the donor droplet (6.5). In the donor droplet, a larger fraction of fluorescein molecules exist in the membrane-permeable, monoanionic form, but in the acceptor droplet, a larger fraction exist in the dianionic form. The effect of this pH differential is to allow for the diffusion of fluorescein into the acceptor droplet (modelling its diffusion out of the intestinal space) but to reduce the rate at which it diffuses back into the donor droplet significantly. As expected, calcein does not permeate intestine-mimetic DIBs (Figure 5.2). The flux of fluorescein and calcein across intestine-mimetic DIBs is plotted over time in Figure 5.3. By measuring the rate of diffusion out of the donor droplet (yielding a negative value) I determined a value of (-0.23 ± 0.01) counts/μm^2s for the maximum flux of fluorescein and a half-life of (63 ± 3) s. This is significantly shorter than the fluorescein transport half-life determined in Chapter 4 ((108 ± 2) s), indicating that inclusion of PS, PI, and CHO increases intestine-mimetic DIB permeability.

I also report initial findings incorporating SM into intestine-mimetic DIBs. SM is a minor but important component of enterocyte plasma membranes[59] which, along with cholesterol, is thought to localize in membrane regions known as lipid rafts.[241] I excluded SM from intestine-mimetic DIBs used above to measure fluorescein permeability to allow for direct comparison with permeability predictions made using biomimetic PAMPA, which also excluded SM.[60] I demonstrate DIB formation using a modified intestinal lipid formulation which includes $5\,mg\,mL^{-1}$ SM (Figure 5.4). These are the first intestine-mimetic DIBs to incorporate SM. DIB formation using

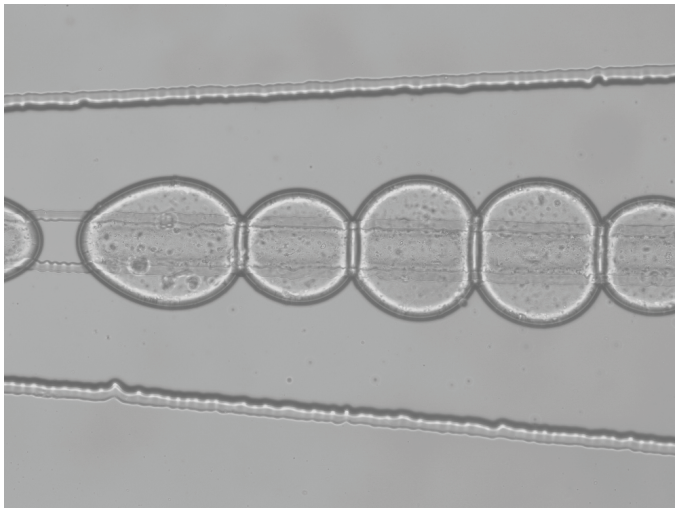

Figure 5.4: **DIB formation using intestinal lipids plus sphingomyelin.** DIBs can be formed using a modified intestinal lipid formulation which includes $5\,\mathrm{mg\,mL^{-1}}$ SM.

SM has been previously demonstrated. SM, which is almost exclusively found in the outer leaflet of cell plasma membranes,[242] was used to model membrane asymmetry and its effect on passive drug transport.[87] Future work in the creation of intestine-mimetic DIBs should incorporate SM as well as other minor components of the enterocyte plasma membrane to create more biomimetic artificial cell plasma membranes and quantify the effects of these membrane components on passive permeability.

5.3.2 Modelling sex-based differences in intestinal absorption

As discussed above, differences in drug permeability as well as in cell plasma membrane composition exist between male and female subjects. The role membrane composition plays in these permeability differences has not previously been investigated. My aim was to create models for the small intestine which incorporate sex-based differences in membrane composition.

I demonstrate here the formation of male and female IL DIBs and their application in fluorescein permeability measurements. Both formulations are based on my original IL formulation, containing a 5:4:4:1:1 ratio by weight of cholesterol, PC, PE, PS, and PI, but with fatty acid tail groups altered to mimic sex-based differences in membrane composition. The female IL formulation contains $4\,\mathrm{mg\,mL^{-1}}$ 22:6 PC, $2\,\mathrm{mg\,mL^{-1}}$ 22:6 PE, $2\,\mathrm{mg\,mL^{-1}}$ 20:4 PE, $1\,\mathrm{mg\,mL^{-1}}$ L-α-PS, $1\,\mathrm{mg\,mL^{-1}}$ L-α-PI, and $5\,\mathrm{mg\,mL^{-1}}$ CHO. The male IL formulation contains $2\,\mathrm{mg\,mL^{-1}}$ 20:4 PC, $2\,\mathrm{mg\,mL^{-1}}$ 18:2 PC, $4\,\mathrm{mg\,mL^{-1}}$ L-α-PE, $1\,\mathrm{mg\,mL^{-1}}$ L-α-PS, $1\,\mathrm{mg\,mL^{-1}}$ L-α-PI, and $5\,\mathrm{mg\,mL^{-1}}$ CHO.

I measured the permeability of fluorescein across both male and female intestine-mimetic DIBs using the microfluidic device depicted in Figure 5.1. The donor droplet contained an initial concentration of 100 µM fluorophore in pH 6.5 buffer. The acceptor droplet initially contained only pH 7.4 buffer. Fluorscein flux is plotted over time in Figure 5.5. Male IL DIBs are more permeable to fluorescein than female IL DIBs (Figure 5.5). Maximum flux (j_{max}) was measured out of the donor droplet (yielding negative values) and determined to be $(-0.51 \pm 0.05)\,\mathrm{counts/\mu m^2 s}$ for female IL DIBs and $(-0.59 \pm 0.07)\,\mathrm{counts/\mu m^2 s}$ for male IL DIBs. Fluorescein half-life was also determined for both IL mixtures: $(131 \pm 24)\,\mathrm{s}$ for female IL DIBs and $(77 \pm 14)\,\mathrm{s}$ for male IL DIBs. Maximum flux did not differ significantly between the two mixtures. However, the half-life of fluorescein transport does appear to be influenced by sex-correlated membrane differences, with slower transport in female IL DIBs. These results appear to correlate with literature claims that drug absorption is slower in female patients.[217] Representative images of fluorescein permeability assays can be found in Figure 5.2.

DIBs formed using both sex-based IL formulations exhibited increased permeability in comparison to the regular IL formulation ($j_{max} = (-0.23 \pm 0.01)\,\mathrm{counts/\mu m^2 s}$). Based

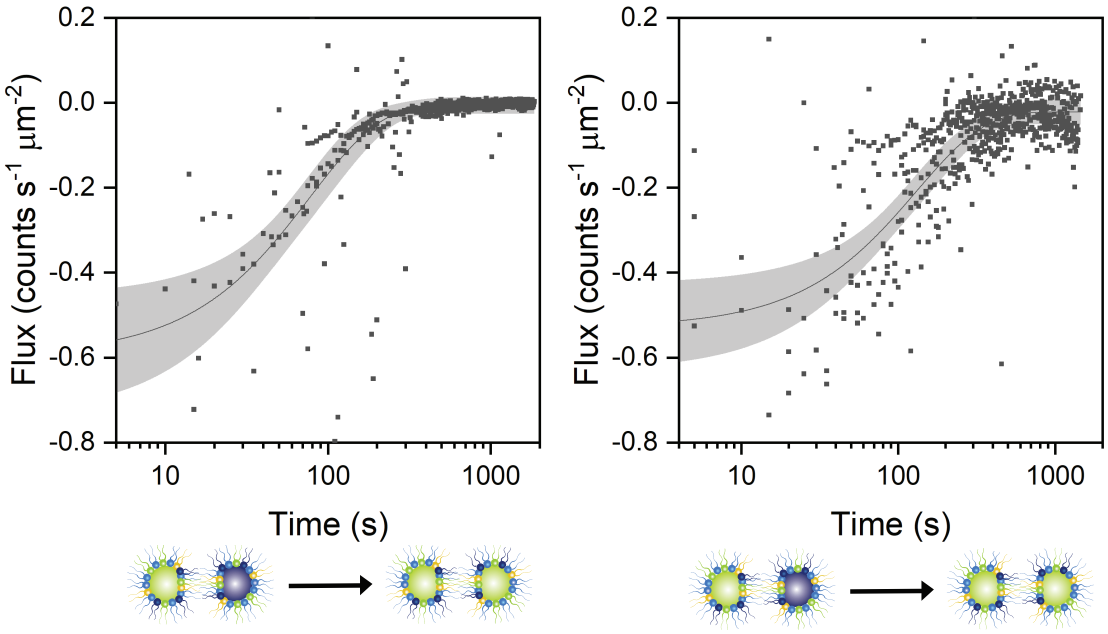

Figure 5.5: **Fluorophore flux in sex-specific intestine-mimetic DIBs.** Following DIB formation between a donor (containing fluorophore) and an acceptor (empty) droplet, diffusion of fluorophore through the bilayer was measured, as shown in the diagrams below the graphs. Left: Fluorescein flux across a male IL DIB (n = 3). Right: Fluorescein flux across a female IL DIB (n = 4). Maximum flux and fluorophore half-life were determined using the fitted curve and are shown in Table 5.1. The microfluidic device was held at 37°C while fluorescein transport occurred. An exponential curve of the form $y = a * e^{(} - x/b) + c$ was fitted to these data in OriginPro. Curve fitting found the parameters $a = 0.0.589 \pm 0.072$, $b = 77.3 \pm 14.4$, and $c = -0.00616 \pm 0.0101$ for male IL and $a = -0.507 \pm 0.051$, $b = 130.7 \pm 23.6$, and $c = -0.02163 \pm 0.0149$ for female IL. 95% confidence bands were calculated from the standard deviation at each timepoint.

on the differences in their composition, this appears to be attributable to differences in the level of saturation of phospholipid acyl chain tails in each mixture. Both sex-based phospholipid formulations contain higher levels of unsaturated lipids, including polyunsaturated acyl chains (22:6 PC, 22:6 PE, and 20:4 PE in the female IL formulation and 20:4 and 18:2 PC in the male IL formulation). Although initial flux was higher in both sex-based IL DIBs, the observed half-life for fluorescein transport was shorter in IL DIBs ((63 ± 3) s). In Chapter 4, the half-life of fluorescein transport was determined to be (108 ± 2) s. These variations indicate the important role that membrane lipid composition plays in determining permeability.

Table 5.1: **Quantifying the effect of membrane formulation on molecular permeability.** Maximum fluorophore flux (j_{max}) and fluorophore half-life ($t_{1/2}$) were determined for all biomimetic DIBs which exhibited transport (IL, female IL, and male IL formulations). I measured fluorescence intensity over time in both the acceptor and donor droplets and show here the flux of fluoroscein out of the donor droplet normalized for droplet volume and DIB surface area. Maximum flux and $t_{1/2}$ were determined graphically. The microfluidic device was held at physiological temperature (37°C) while fluorescein transport was observed and image data collected.

Phospholipid	**j_{max} (counts µm $^{-2}$ s^{-1})**	**$t_{1/2}$ (s)**
IL	-0.23±0.01	63±3
Female IL	-0.51±0.05	131±24
Male IL	-0.59±0.07	77±14

5.3.3 Modelling blood-brain barrier permeability

My aim here was to develop the first DIB pharmacokinetic compartment model for the blood-brain barrier. BIB formation using a PBL extract has not been demonstrated in the literature and TBL DIBs have never before been used to predict permeability. I decided to use a phospholipid mixture which had previously been implemented in biomimetic PAMPA to facilitate comparison. While intestinal lipid extracts are not commercially available, PBL extract is. PBL has been used in BBB-PAMPA, which yields results which correlate well with *in situ* brain perfusion measurements.[56,57] TBL extract is also commercially available. I tested DIB formation and permeability using both lipid extracts. Similarly to my work with intestinal lipid formulations (Section 5.3.1), I determined that PBL and TBL could be used to form lipid-in DIBs at or above 80°C, but could be used to form lipid-out DIBs at physiological temperature (37°C). Information about the phospholipid acyl chains in total lipid extracts is not provided,[158,243] so lipid-in DIB formation was tested at increasing temperature, as was done with naturally derived phospholipids in Chapter 3. All permeability experiments in this section were performed using the lipid-out method at 37°C. I demonstrate here the first DIBs formed using PBL as well as DIB formation using TBL. I also performed permeability measurements in both lipid systems of fluorescein, calcein, and FITC-dextrans (40 and 500 kDa), which has never been done in brain-mimetic DIBs. In these permeability assays, both the donor and acceptor droplets had a pH of 7.4 to

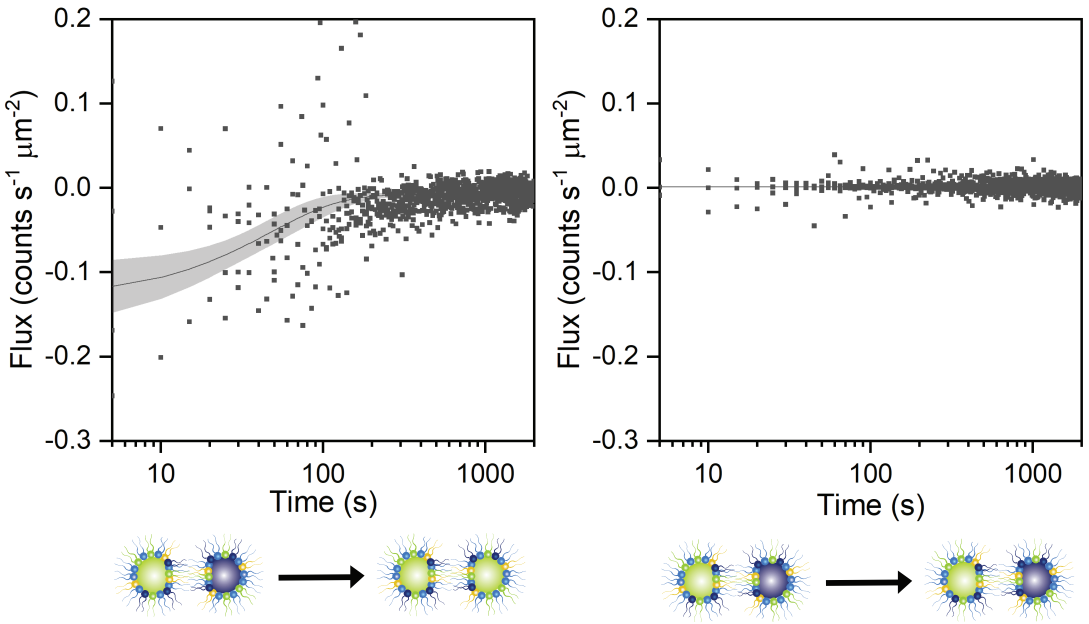

Figure 5.6: **Fluorophore flux in human blood-brain barrier-mimetic DIBs.** Following DIB formation between a donor (containing fluorophore) and an acceptor (empty) droplet, diffusion of fluorophore through the bilayer was measured, as shown in the diagrams below the graphs. Left: Fluorescein flux across a PBL DIB (n = 5). Right: Calcein flux across a PBL DIB (n = 4). Maximum flux and fluorophore half-life were determined using the fitted curve. The microfluidic device was held at 37°C while transport occurred. An exponential curve of the form $y = a * e^{(} - x/b) + c$ was fitted to the fluorescein data in OriginPro. Curve fitting found the parameters $a = -0.0424 \pm 0.00451$, $b = 265 \pm 47$, and $c = -0.00466 \pm 0.000928$. A linear function of the form $y = a + b * x$ was fitted to the calcein data in OriginPro with the parameters $a = 0.00588 \pm 0.00291$ and $b = -0.002 \pm 0.0009$. 95% confidence bands were calculated from the standard deviation at each timepoint.

mimic conditions in the blood and the interstitial fluid.[244]

I expected both PBL and TBL DIBs to have low permeability to fluorescein and to be impermeable to calcein. *In vivo*, fluorescein can only cross the blood-brain barrier paracellularly when tight junctions are not formed, such as in disease states such as diabetes.[245,246] In the literature, fluorescein is used as a marker for lack of tight junction formation. Thus, fluorescein was not expected to permeate blood-brain barrier-mimetic DIBs, which model transcellular transport. Unexpectedly, PBL DIBs were permeable to fluorescein (Figure 5.6). Representative images of fluorescein and calcein permeability assays can be found in Figure 5.7. Fluorophore flux across both blood-brain barrier-mimetic DIBs is plotted over time in Figures 5.6 and 5.8.

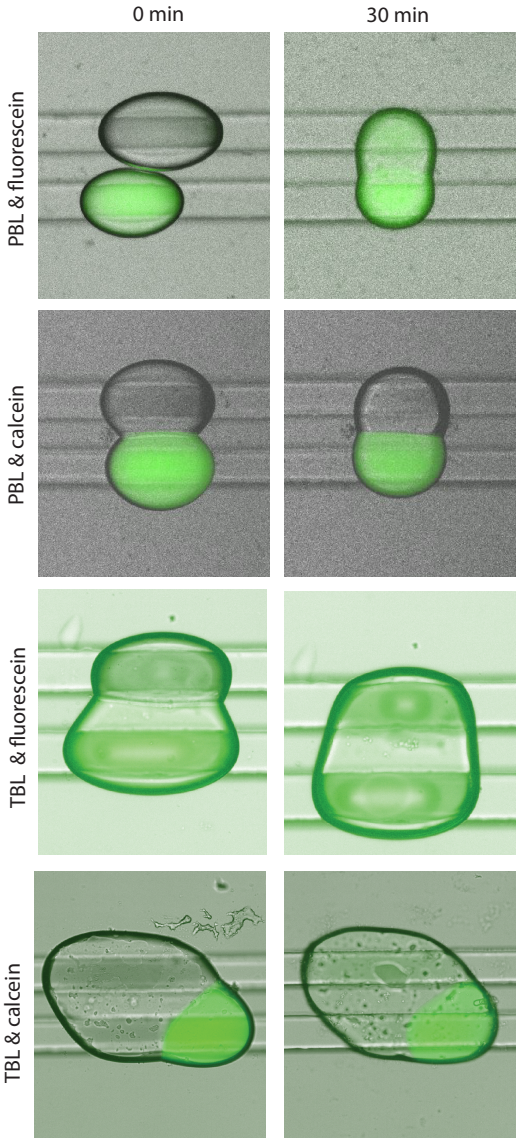

Figure 5.7: **Fluorophore transport in blood-brain barrier-mimetic DIBs.** In the left column are images at t = 0 min, where the fluorophore is solely located in the donor droplet. In the right column are images at t = 30 min. From top to bottom: fluorescein permeability in PBL DIBs, calcein permeability in PBL DIBs, fluorescein permeability TBL DIBs, and calcein permeability in TBL DIBs.

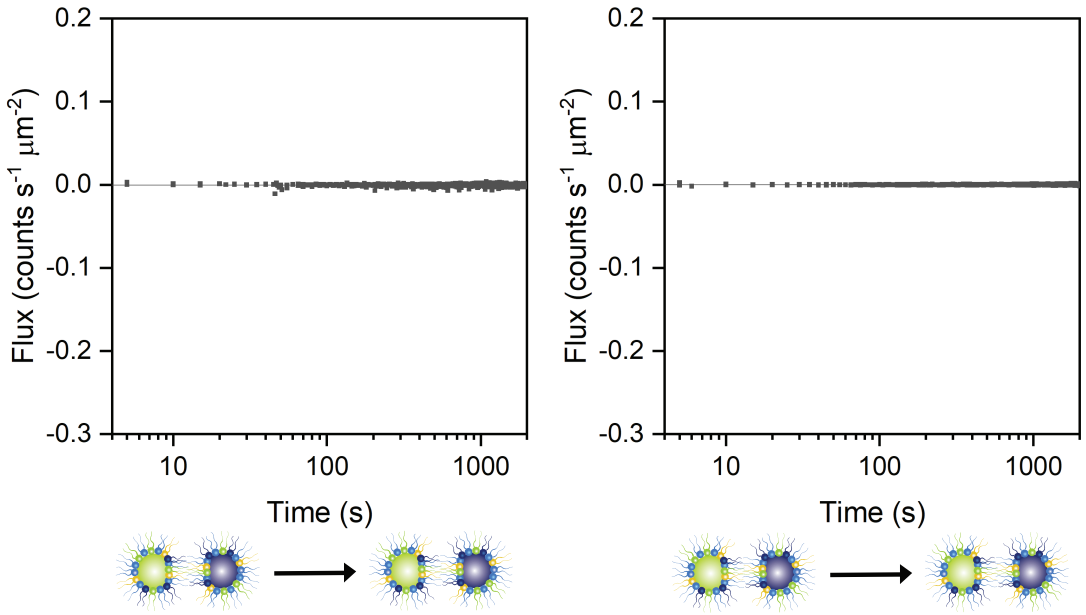

Figure 5.8: **Fluorophore flux in human blood-brain barrier-mimetic DIBs.** Following DIB formation between a donor (containing fluorophore) and an acceptor (empty) droplet, diffusion of fluorophore through the bilayer was measured, as shown in the diagrams below the graphs. Left: Fluorescein flux across a TBL DIB (n = 3). Right: Calcein flux across a TBL DIB (n = 3). The microfluidic device was held at 37°C while transport occurred. A linear function of the form $y = a + b * x$ was fitted to these data. Fitting found the parameters $a = -0.000406 \pm 0.000056$ and $b = 0.000000204 \pm 0.000000035$ for fluorescein and $a = -0.000203 \pm 0.000076$ and $b = 0.00012 \pm 0.000026$ for calcein. and 95% confidence bands were calculated from the standard deviation at each timepoint in OriginPro.

PBL DIBs are permeable to fluorescein, but not to calcein (Figure 5.6). However, TBL DIBs are impermeable to both fluorescein and calcein. The significant difference in permeability between PBL and TBL DIBs highlights the important role that membrane composition plays in regulating permeability. Both brain lipid extracts contain similar ratios of PC, PE, PS, and PI, but TBL contains a significantly higher percentage of unknown compounds.[158,243] The permeability of PBL DIBs to fluorescein, which does not cross the blood-brain barrier paracellularly *in vivo*,[245,246] suggests a discrepancy in phospholipid composition. TBL DIBs appear to more accurately model the transport (or lack thereof) of fluorescein in the blood-brain barrier.

Although permeation of fluorescein across PBL DIBs was observed, it occurred at a lower rate than in any variation of intestine-mimetic DIBs. Maximum flux of fluorescein out of the donor droplet (yielding a negative value) was determined to be (-0.12 ± 0.02) counts/μm^2s, which is significantly lower than the flux measured in intestine-mimetic DIBs (Table 5.1). However, the half-life of fluorescein transport across a PBL DIB was determined to be (47 ± 12) s, much shorter than the half-lives determined for fluorescein across intestine-mimetic DIBs. The difference in pH between the two systems plays an important role in this difference. In the intestinal model, the rate of fluorescein transport into the acceptor droplet, which has a pH of 7.4, is high, but the rate of fluorescein transport back into the donor droplet, which has a pH of 6.5, is low, effectively negligible. In the blood-brain barrier-mimetic system, both droplets have a pH of 7.4, so fluorescein exists in the same form (mostly dianionic) in both droplet compartments, reducing its ability to cross the phospholipid bilayer. Both pH and lipid composition of the artificial cell plasma membrane are key determinants of permeability, particularly for charged molecules.

Both types of brain-mimetic DIBs were impermeable to FITC-dextrans (molecular

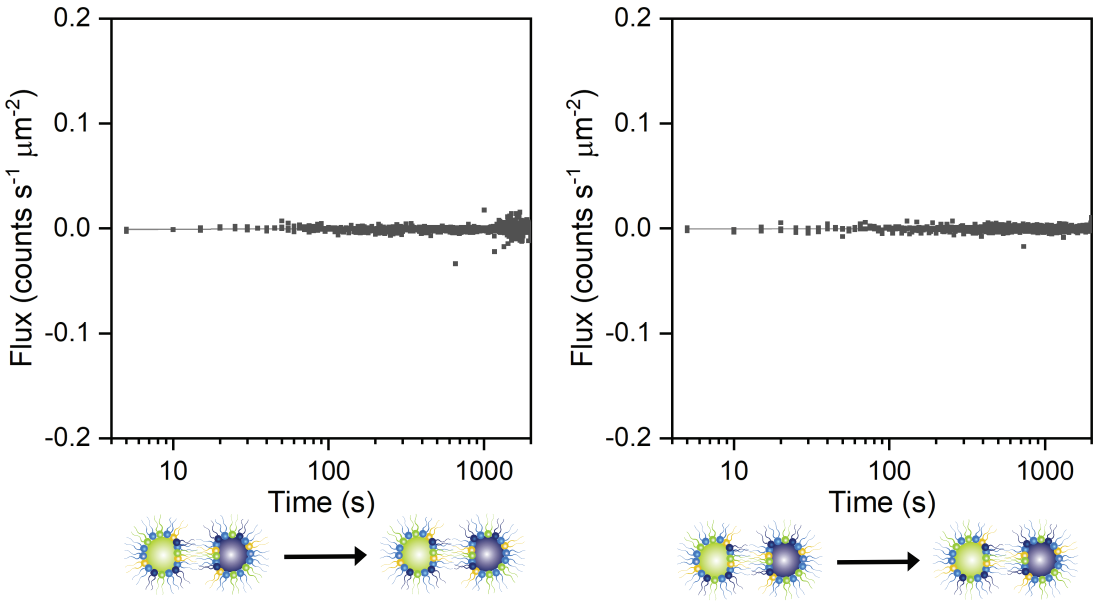

Figure 5.9: **FITC dextran flux in human blood-brain barrier-mimetic DIBs.** Following DIB formation between a donor (containing fluorophore) and an acceptor (empty) droplet, diffusion of fluorophore through the bilayer was measured, as shown in the diagrams below the graphs. Left: 40 kDa FITC dextran flux across a PBL DIB (n = 3). Right: 500 kDa FITC dextran flux across a PBL DIB (n = 3). The microfluidic device was held at 37°C while transport occurred. A linear function of the form $y = a + b * x$ was fitted to these data. Fitting found the parameters $a = -0.001 \pm 0.00057$ and $b = 0.00020 \pm 0.00019$ and $a = -0.00052 \pm 0.00038$ and $b = 0.00024 \pm 0.0.00013$, for 40 kDa and 500 kDa FITC dextrans, respectively. 95% confidence bands were calculated from the standard deviation at each timepoint in OriginPro.

weights of 40 and 500 kDa), which serve as control experiments to confirm the formation of a robust bilayer section. The flux of 40 and 500 FITC-dextran across PBL and TBL DIBs is plotted over time in Figures 5.9 and 5.10, respectively. Representative images of FITC-dextran permeability assays can be found in Figure 5.11. Permeation of either size of FITC-dextran was not observed in either type of blood-brain barrier-mimetic DIB, which indicates formation of a robust, brain-mimetic artificial cell plasma membrane.

While both PBL and TBL DIBs exhibit near-planar bilayer sections upon formation, TBL bilayers exposed to 500 FITC-dextran in the donor droplet become significantly more curved over time. This can be seen in the bottom row of Figure 5.11. Curvature

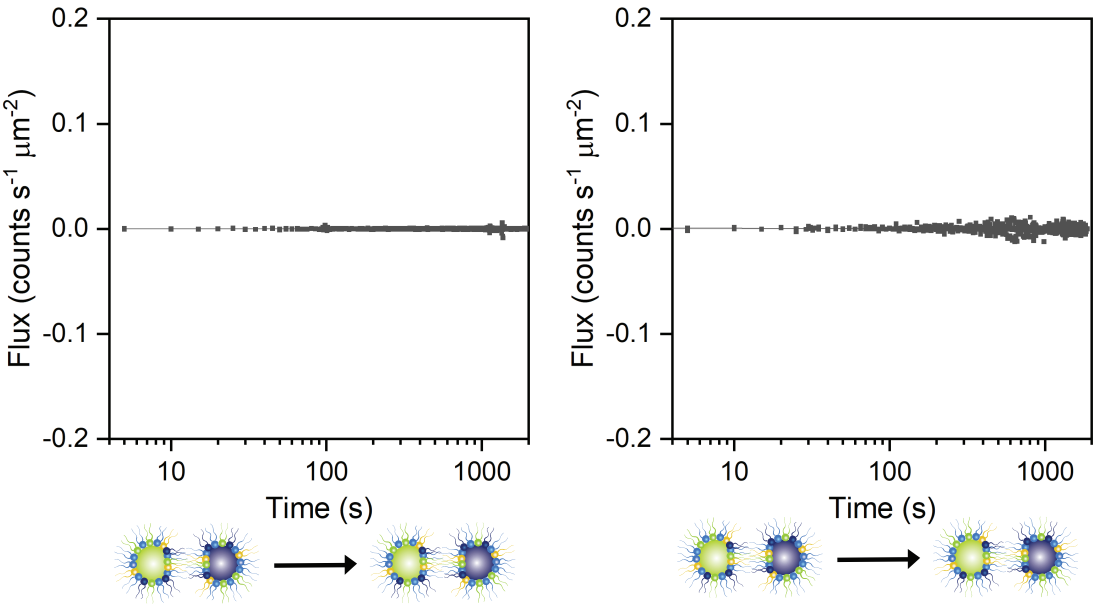

Figure 5.10: **FITC dextran flux in human blood-brain barrier-mimetic DIBs.** Following DIB formation between a donor (containing fluorophore) and an acceptor (empty) droplet, diffusion of fluorophore through the bilayer was measured, as shown in the diagrams below the graphs. Left: 40 kDa FITC dextran flux across a TBL DIB (n = 4). Right: 500 kDa FITC dextran flux across a TBL DIB (n = 3). The microfluidic device was held at 37°C while transport occurred. A linear function of the form $y = a + b * x$ was fitted to these data. Fitting found the parameters $a = 0.000066 \pm 0.0001$ and $b = 0.00020 \pm 0.00019$ and $a = 0.00069 \pm 0.00045$ and $b = -0.00025 \pm 0.0.00016$, for 40 kDa and 500 kDa FITC dextrans, respectively. 95% confidence bands were calculated from the standard deviation at each timepoint in OriginPro.

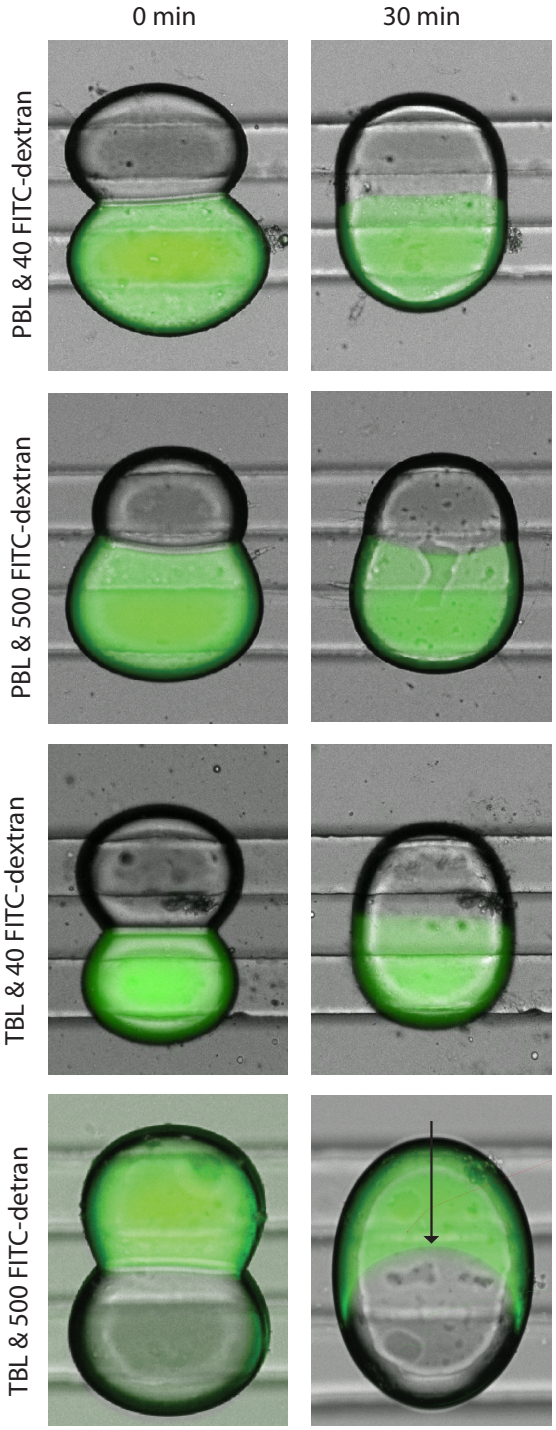

Figure 5.11: **FITC-dextran transport in human blood-brain barrier-mimetic DIBs.** The left column shows images at t = 0 min of a permeability experiment, where the fluorophore is solely located in the donor droplet (100 µM). The right column shows images at t = 30 min of a permeability experiment. From top to bottom is shown 40 FITC-dextran permeability in PBL DIBs, 500 FITC-dextran permeability in PBL DIBs, 40 FITC-dextran permeability in TBL DIBs, and 500 FITC-dextran permeability in TBL DIBs. Arrow highlights change in TBL DIB curvature observed over time using 500 FITC-dextran.

of artificial cell plasma membranes has previously been linked to asymmetry between the two phospholipid leaflets.[87,247] This suggests the possibility of the formation of an asymmetric bilayer. In the literature, asymmetric DIBs have been formed using both synthetic[78,82,112,114,248] and naturally derived[87] phospholipids. Different phospholipids, which will form separate leaflets of the bilayer, can either be extruded into vesicles in separate aqueous solutions[78,114,247,248] or dissolved in separate oil solutions.[87,112] When droplets coated in monolayers with differing lipid compositions are brought into contact, either manually or on a microfluidic platform, an asymmetric bilayer is formed. However, in my work, the TBL extract was dissolved in a single oil solution, indicating that any potential membrane asymmetry arises following DIB formation. This phenomenon is unprecedented in the literature. Because this pronounced curvature was only observed in TBL DIBs containing 500 FITC-dextran, and not in PBL DIBs containing FITC-dextran nor TBL DIBs containing other fluorophores, there appears to be a unique interaction between the artificial cell plasma membrane and the dye. Because TBL DIBs are not usually permeable to fluorescein (Figure 5.8), I hypothesize that the interaction is between the large dextran and unknown components of the TBL extract. More analysis is necessary to determine if the observed curvature can be attributed to bilayer asymmetry and, if so, how this asymmetry arises.

In future work, I propose that TBL DIBs will more accurately mimic the blood-brain barrier than PBL DIBs. Additionally, use of a bespoke lipid formulation designed to mimic the human brain endothelial cell plasma membrane may allow for the formation of DIBs which are even more biomimetic. A comparative study of permeability measurements performed through PAMPA using PBL and two different bespoke lipid formulations found no difference in the prediction of the permeability of small, neutral molecules, but discovered that the PBL method overestimated the transport of

some charged, bulky molecules.[228] This aligns with fluorescein permeability results presented here, since PBL DIBs were much more highly permeable to charged fluorescein than TBL DIBs. Measuring transport between aqueous compartments of biomimetic pH (here, both pH 7.4) is key to accurate prediction. Although PBL and TBL contain similar ratios of the major membrane phospholipids,[158,243] differences in their composition regulate membrane permeability, allowing for fluorescein permeability through DIBs formed using PBL but not TBL.

5.3.4 DIB formation using non-commercial, human total lipid extracts

My aim here was to model cell plasma membranes for which commercial lipid extracts are not available and to move the use of DIBs as a pharmacokinetic tool toward personalized medicine. I therefore collaborated with Meghan Robinson (Vancouver Prostate Centre) who grew cells and isolated their plasma membrane lipids for DIB formation experiments. I performed initial DIB formation as well as calcein permeability tests using a lipid extract prepared from Sertoli cells. Sertoli cells are present in the testes and play an essential role in regulating spermatogenesis. Like brain endothelial cells, Sertoli cells form tight junctions and form a blood-testis barrier analogous to the blood-brain barrier. Due to ease of access and relatively low cost, a Sertoli cell plasma membrane total lipid extract provided the ideal initial experiment for the creation of human-mimetic DIBs using a made-to-order lipid extract from human cells. These are the first DIBs to be formed using a non-commercial lipid extract as well as the first DIBs to be formed using phospholipids derived from human cells. At a concentration of $10\,\mathrm{mg\,mL^{-1}}$ in squalene, Sertoli cell plasma membrane lipid extract was used to form DIBs at 37°C, 50°C, and 70°C. Qualitative permeability tests were conducted at 37°C; calcein appeared not to permeate through the

membrane after 30 min of observation. As discussed earlier in this chapter, calcein is not expected to cross DIBs and serves as a control experiment to confirm formation of a robust phospholipid bilayer.

In the future, I plan to perform quantitative measurements of fluorophore permeability through Sertoli DIBs, beginning with fluorescein and calcein to allow for comparison with my previously gathered data from the intestinal and blood-brain barrier models. Future work will also include DIB formation and permeability experiments using lipids extracted from human brain endothelial cells, which are now in preparation by my collaborator. As discussed above, use of PBL to form blood-brain barrier-mimetic DIBs appears to overpredict the transport of fluorescein and, hypothetically, other charged molecules. Additionally, replacing PBL with a bespoke human-mimetic lipid formulation in BBB-PAMPA yielded permeability results which correlated better with *in vivo* permeability, suggesting that the source species of a lipid extract is nontrivial in permeability prediction.[57] Therefore, implementation of a total lipid extract prepared from human brain endothelial cells has high potential for the creation of biomimetic artificial cell plasma membranes to mimic the blood-brain barrier. Future work on this project should also include an analysis of the lipid composition of any total extracts prepared by my collaborator and used for DIB permeability assays. Quantification of membrane composition will allow for analysis of their role in membrane permeability and comparison between cell type and source. The use of a total lipid extract made from human cell plasma membranes opens the door to a new world in the DIBs field by achieving an unprecedented level of biological similarity. I propose that the prediction of permeability through these types of biomimetic DIBs will yield more accurate predictions for human pharmacokinetics than the use of lipid extracts from other species or even bespoke lipid formulations.

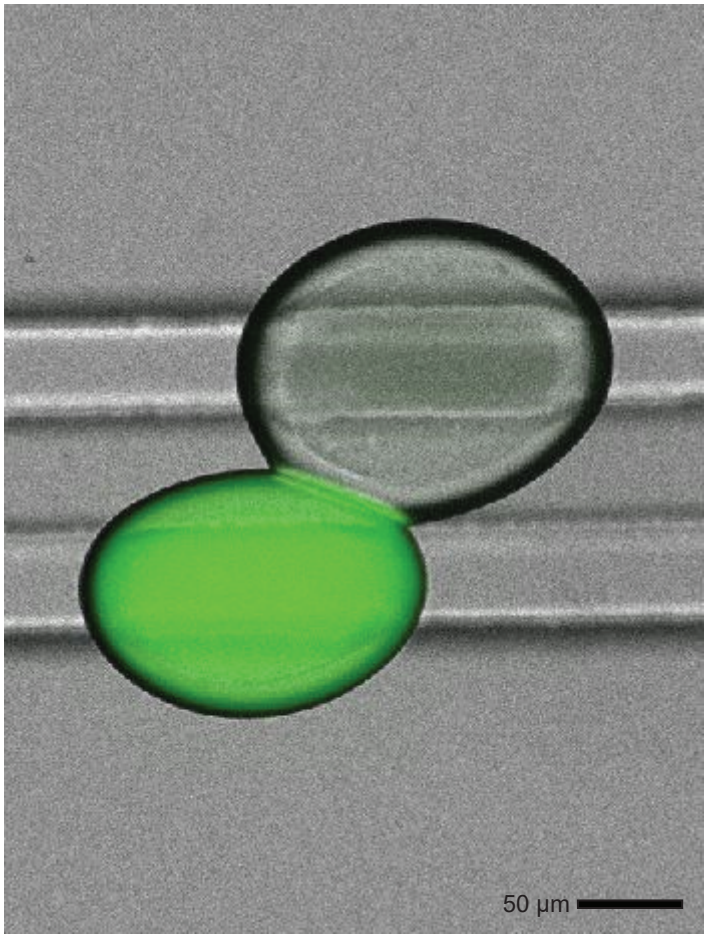

Figure 5.12: **DIB formation using a lipid extract from Sertoli cells.** The donor droplet (bottom) contains calcein (100 µM in pH 7.4 HEPES buffer) and the acceptor droplet (top) is pH 7.4 HEPES buffer.

5.3.5 Detection of drug permeability of non-fluorescent drugs

My aim here was to determine the effectiveness of using fluorogenic molecules to detect the permeation of drugs across DIBs in real time. I tested fluorogenic molecular recognition agents to assess their viability in DIBs. In these systems, the donor droplet compartment contained a known concentration of drug and the acceptor droplet compartment contained a known concentration of fluorogenic molecule. Ideally, as the drug permeates the DIB, it would quickly react with the fluorogenic tag and "turn on" its fluorescence, thus providing a real-time measurement of drug transport without needing to remove droplets from the microfluidic device. I chose three different fluorogenic molecules: Chromeo P540, which has previously been used to measure molecular transport in DIBs,[113] fluorescamine,[249] and DimerDye 4 (Figure 5.13).[250] I chose these fluorogenic molecules due to their demonstrated ability to detect small amount of analyte, the accessibility of their fluorescence excitation and emission wavelengths, and the fact that they react with amine functional groups.[113,249,250]

I selected amine-containing drugs to test the use of these fluorogenic dyes: tranexamic acid, lisinopril, memantine, dopamine, levodopa, and carbidopa. Tranexamic acid and lisinopril are orally administered drugs, the intestinal permeability of which has previously been predicted using biomimetic PAMPA.[60,215,216,251] The rest are drugs whose interaction with the blood-brain barrier is important to predict and have previously been studied using BBB-PAMPA.[56,57] Reaction of fluorogenic dyes with orally administered drugs was tested in intestine-mimetic DIBs and with brain-relevant drugs was tested in PBL DIBs. Reaction of fluorogenic dyes with all six drugs was also tested in DPhPC DIBs to ensure that the complexity of the biomimetic lipid formulations did not affect observed results.

None of the fluorogenic molecular recognition agents tested yield a visible fluores-

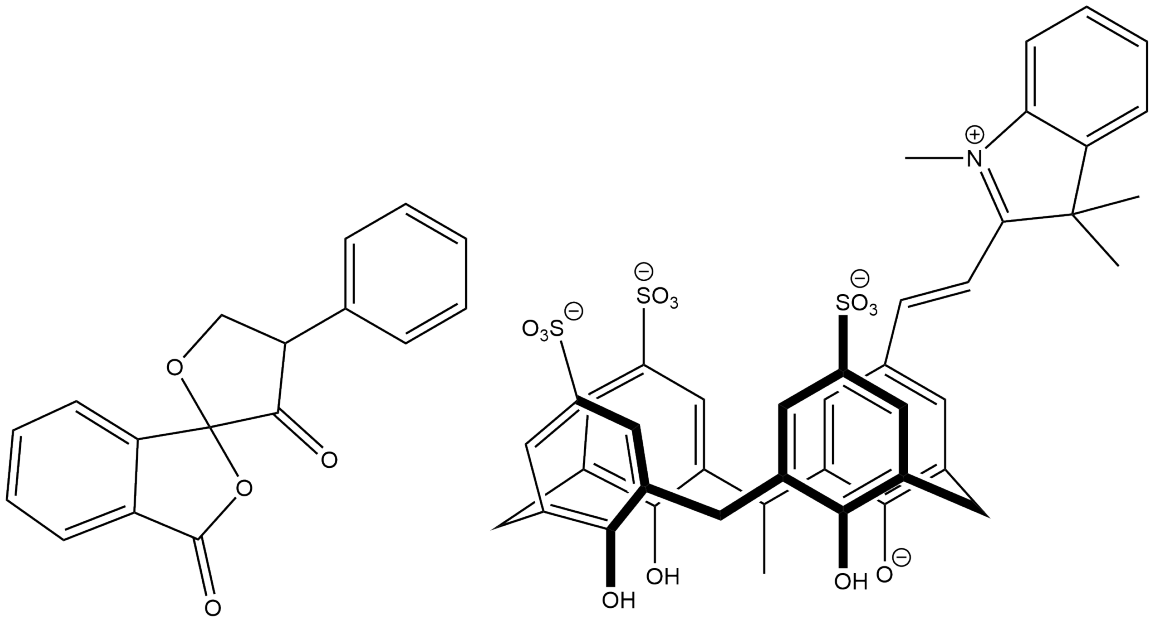

Figure 5.13: **Structures of fluorogenic molecules tested in DIBs.** The structures of fluorescamine (left) and DimerDye 4[250] (right) are shown. The structure of Chromeo P540 is proprietary.

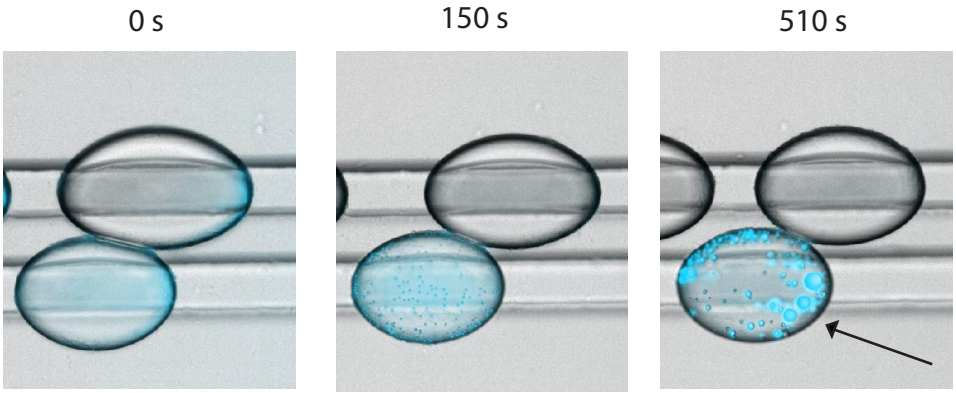

Figure 5.14: **Fluorescamine-tagged tranexamic acid in DPhPC DIBs.** Fluorescamine (50 mg mL^{-1} in DMF) was mixed off-chip with tranexamic acid (50 mg mL^{-1} in pH 7.4 aqueous buffer) in a 1:1 (v/v) ratio. The resulting solution was used as the donor droplet compartment (bottoms droplets) in DPhPC DIB pairs. The acceptor droplet (top droplets) contained a 1:1 (v/v) solution of DMF and pH 7.4 aqueous buffer. As shown over time (0 s to 510 s), fluorescamine-tagged tranexamic acid does not cross the DIB but appears instead to interact with the phospholipid monolayer which coats the droplets (indicated by arrow).

cence signal with any drug or type of DIBs, even after upwards of 60 min of observation. However, when mixed with analyte off-chip, both fluorescamine and Chromeo P540 yield a visible fluorescence signal on-chip (representative images in Figure 5.14). When a solution containing fluorescamine-tagged tranexamic acid is used for the donor droplet in DPhPC DIBs, the drug-dye complex exhibits a surprising interaction with the phospholipid monolayer. Over the course of less than 5 min, new droplets, which are intensely fluorescent, appear at the droplet-oil interface of the donor droplet. This phenomenon is potentially a process known as Ostwald ripening wherein smaller droplets "bud" off of a larger one.[252,253] Because the aim of this project was to develop a fluorogenic method for detecting drug permeation, not to tag drugs off-chip, use of fluorescamine was not investigated further. Fluorescamine is also hydrolyzable, although this reaction occurs on a longer timescale than reaction with amines and does ot produce a fluorescent product, and thus nonideal for use in an aqueous solution.[249] My ability to observe a fluorescence signal using fluorescamine and Chromeo P540 to tag drugs off-chip indicates that their application for real-time permeation detection is possible, but may not occur at the concentrations or on the timescales used in my experiments. It is also possible that the dyes react with amines present in phospholipids coating the droplet and dissolved in the bulk oil solution, which would inhibit their ability to react with any drug present.

5.4 Conclusions

I developed pharmacokinetic DIB models for passive permeability in the small intestine, incorporating more membrane phospholipids than in Chapter 4, and the blood-brain barrier, comparing the effects of two different lipid extracts. I also created sex-specific intestinal models which mimic the slower drug absorption observed

in vivo in female subjects. In each of these models I measured the transport of fluorescein, the flux and half-life of which was quantified, as well as of calcein and FITC-dextrans of different molecular weights, which served to confirm the presence of a biomimetic artificial cell plasma membrane. I also demonstrate the first DIBs which mimic the plasma membrane of Sertoli cells. These are also the first DIBs to be formed using a made-to-order, non-commercial phospholipid extract and the first DIBs to be formed using a lipid extract from human cells. Calcein permeation across Sertoli DIBs was qualitatively measured and confirms the formation of a robust, biomimetic artificial cell plasma membrane. Finally, I tested the effectiveness of fluorogenic molecular recognition agents to detect the permeation of amine-containing drugs. Future work on this project will focus on permeability tests in Sertoli DIBs as well as DIBs formed from lipid extracts from cultured human cells. Future research will also focus on the development of a system for the detection of the transport of nonfluorescent molecules, through either the development of a new fluorogenic agent more compatible with a system containing phospholipids, or the pairing of the microfluidic device with off-chip analysis.

5.5 Materials and Methods

5.5.1 Materials

All materials were purchased from Millipore Sigma unless otherwise indicated. Chromeo P540 was purchased from Active Motif. DimerDye was donated by the Hof Group at the University of Victoria.

5.5.2 Operating parameters of the microfluidic platform

To create droplets and then DIBs on the microfluidic platform (Figure 5.1), aqueous buffer and a lipid solution (10 mg mL^{-1} squalene) (prepared as described in Chapter 4) were placed in reservoirs (1.5 mL Eppendorf tubes) and equal lengths of PTFE tubing were used to connect the reservoirs to a pressure pump (OB1 MK3, Elveflow). Squalene and aqueous buffers were introduced into the microfluidic device by applying a pressure of 100 mbar to both reservoirs. Following DIB formation, flow was stopped from both reservoirs using the Elveflow control software. To visualise droplet and DIB formation, devices were mounted in a custom-made heating platform[86] on a Nikon Eclipse Ti2-E inverted microscope. Brightfield and fluorescence images were captured using a Hamamatsu ORCA-Flash4.0 V3, with an LED (Thorlabs) and SemrockBrightline large field of view filter cubes (Nikon). A GFP filter cube (excitation 466/40 nm, emission 525/50 nm) was used for fluorescein, calcein, FITC-dextran, and DimerDye 4 experiments alongside a Solis 1C cold white LED. A DAPI filter cube (excitation 356/30 nm, emission 447/60 nm) was used for all fluorescamine experiments alongside a Solis 365C UV LED. A TRITC filter cube (excitation 554/23 nm, emission 609/54 nm) was used for Chromeo P540 experiments alongside a Solis 1C cold white LED. The specifications of the custom-made heating platform are described in detail in Appendix D).

5.5.3 Preparation of solutions

Lipid solutions were prepared as described in Chapter 4 to give a final phospholipid concentration of 10 mg mL^{-1}. IL formulations also contained 5 mg mL^{-1} cholesterol. The aqueous phase was a buffer which contained 10 mM HEPES and 140 mM KCl and had a pH of 7.4, with the exception of the donor compartment in intestine-mimetic

DIBs, which had a pH of 6.5. Donor droplets contained 100 µM fluorescein, calcein, or FITC-dextran (40 or 500 kDa).

5.5.4 Fluorescence data collection

Once a DIB pair was formed and the flow was stopped, brightfield and fluorescence images were taken every 5 s with a 33.33 ms exposure time until experiment termination. Quantification of fluorescence intensity was performed via time-based measurement of mean intensity in regions of interest (ROIs) within each droplet in each frame using NIS Elements. Fluorescence intensity data was normalised for phospholipid bilayer surface area and droplet volume as previously described (Appendices D and C). Briefly, bilayer diameters and droplet semiaxes were measured using, respectively, the "Distance Measurement" and the "Measurements and Annotations" modules in NIS Elements. Subsequent calculations were performed by approximating artificial cell membrane surface areas as ellipses and droplet volumes as ellipsoids. Each data set represents 3-13 replicates performed on different microfluidic devices for reproducibility.

Chapter 6

Conclusions and Future Work

6.1 Conclusions

The aim of this work was to develop a new type of pharmacokinetic compartment model using artificial cells-on-a-chip for the prediction of drug permeability, with potential applications in the pharmaceutical industry. My goal was to develop a variety of permutations of this model and to investigate the biophysics of lipid membranes using DIBs. These aims were met, making accessible many possibilities for future work on the pharmacological applications of DIBs.

There are four conclusions from this dissertation. First, as detailed in Chapter 2, I explored the potential for several surface treatments as shown in the literature to optimize the performance of PDMS microfluidic devices in the formation and analysis of DIBs. These studies quantified the effects of PFOS functionalization of PDMS and explored strategies for the mitigation of water evaporation through PDMS. I drew the conclusion that baking microfluidic devices for over 24 h at 65°C is a key step in the fabrication of PDMS microfluidic devices for the formation and application

of DIBs. Quantification of the effectiveness of literature methods for microfluidic device surface treatment allowed me to optimize my device fabrication protocol for the rest of the work presented. This work was a key step in the development of DIB pharmacokinetic compartment models.

In Chapter 3, I investigated the role that temperature plays in DIB formation and was able to create the first DIBs made using naturally derived phospholipids, whose variety of acyl chains and degrees of unsaturation make them difficult to work with at room temperature. I performed a systematic study of naturally derived phospholipids and formulations thereof, testing wide temperature ranges to determine the ideal conditions for DIB formation. I also measured DIB formation rates and fluorescein permeability through selected phospholipid formulations. Chapter 3 represents the first study of the relationship between phospholipid formulation and temperature used for DIB formation. Elucidation of this key relationship was vital to the creation of DIB permeability prediction models in that it enabled the work presented in Chapters 4 and 5. This detailed study made possible the formation of DIBs using bespoke phospholipid formulations and lipid extracts.

Next, I used my knowledge on phospholipid formulation development to collaborate with Elanna Stephenson to develop a pharmacokinetic compartment model for passive intestinal absorption. Our platform, which paired my initial intestinal lipid formulation with Elanna's device design, was able to predict the absorption of fluorescein three times better than the current gold standard technique, PAMPA. This work, presented in Chapter 4, was published in *Lab on a Chip*.[86] Development of this platform set an important benchmark in the field and in my own work in that it supports my hypothesis that biomimetic DIBs have the potential to accurately model passive molecular transport.

Finally, I created several more complex pharmacokinetic compartment models for drug transport. I modelled passive intestinal absorption using a full intestinal lipid formulation as well as sex-specific formulations. These are the first DIBs to be used to model population-based differences in membrane composition and to predict correlated differences in passive absorption. I was also able to model transport across the blood-brain barrier using two types of brain lipid extracts. This work represents the first DIBs formed using a polar brain lipid extract, the permeability of which mimics results determned using PAMPA, and the first total brain lipid DIBs to be used for permeability measurements. I present preliminary results modelling Sertoli cells using the first DIBs made using a lipid extract prepared from human cells. These are also the first DIBs to be formed using a made-to-order, non-commercial lipid extract. These results open up a route towards personalized medicine; if cells from a patient are cultured and their plasma membrane lipids extracted, DIBs formed from them could be used to predict drug transport in that particular patient. Finally, I tested fluorogenic molecular recognition agents for the detection of nonfluorescent molecules on-chip. Detection of molecular transport across DIBs is mainly limited to inherently fluorescent molecules. I determined that the fluorogenic agents I tested are not suitable for on-chip detection of molecular transport in DIBs, potentially due to low quantum yield, side reactions with phospholipids, or slow reaction times in DIBs.

6.2 Future work

There are several directions this work could go in the future. Because DIBs can be linked together in networks, they have the potential to model tissues rather than individual or small networks of plasma membranes, as I demonstrated in Chapters 4 and 5. Studies involving the formation of complex DIB networks have the potential

to elucidate processes like cell signaling and molecular permeation of tissues. DIB technology may also be used as a scaffold to further explore biophysical questions, such as formation of lipid domains, lipid flip-flop, and processes involving membrane proteins, in ways that previous, less biologically similar model membranes cannot. DIBs which incorporate membrane proteins could be leveraged to create a transporter or receptor assay with applications in drug development.

Because the detection methods I tested were not found to be effective in measuring passive transport through DIBs, more research on potential methods for the real-time detection of molecular transport is needed, whether through the detection of a turn-on fluorescence signal, as I investigated, or by pairing a microfluidic device with an off-chip detection method. In the literature, there are already early results showing the analysis of DIBs formed on a microfluidic device using off-chip LC-MS.[112] This technology has the potential to expand the library of molecules whose transport is predictable using microfluidic DIBs. Bringing the field away from a reliance on fluorescent molecules will expand the pharmacokinetic application of DIBs. A detection method which has (near) universal applications paired with biomimetic DIBs will allow for the prediction of the passive permeability of any drug across any type of cell plasma membrane. Future work in this area should focus on the development and synthesis of fluorogenic receptor molecules which detect common functional groups and are compatible with an aqueous system as well as the presence of phospholipids. In parallel, microfluidic technology to enable post-permeation droplet separation and off-chip analysis should be tested and optimized to allow for streamlined, reliable detection.

The potential of DIBs to facilitate personalized pharmacokinetic predictions has significant implications for the medical field. The use of total lipid extracts from human

cells, perhaps even patient samples, will allow for the analysis of membrane permeability in cell types or phenotypes associated with disease states which were previously difficult to model. DIBs have the potential to be used to model numerous types of human cells which are pharmacologically relevant through the use of phospholipid formulations and extracts. In the immediate future, a total lipid extract made from human brain endothelial cells will be tested in DIB formation and permeability experiments to assess its potential to model the human blood-brain barrier.

Appendix A

Overview

The following appendices contain supplementary information for the previous chapters. Appendix B is a perspective review on the history and future potential of DIBs, for which I was joint first author with Elanna Stephenson. Appendix C contains supplementary information for Chapter 3. Appendix D contains supplementary information for Chapter 4.

Appendix B

Droplet Interface Bilayers: How can they achieve their full potential?

B.1 Abstract

Model membranes can be used to elucidate the intricacies of the chemical processes that occur in cell membranes. But the perfectly biomimetic, yet bespoke, model membrane has yet to be built. Droplet interface bilayers (DIBs) are a new type of model membrane that are able to mimic some features of real cell membranes better than traditional models such as liposomes and black lipid membranes. In this perspective we discuss recent work in the field that is starting to showcase the potential of these model membranes to enable the quantification of membrane processes, such as the behaviour of protein transporters and the prediction of *in vivo* drug movement. We will also highlight the challenges remaining to enable DIBs to achieve their full

potential as artificial cells, and as a biological analytical platforms for quantifying molecular transport.

Unanswered questions about the chemistry of fundamental biological mechanisms often drive the development of new analytical techniques. One such example is the use of Droplet Interface Bilayers (DIBs) as tools for the analysis and quantification of membrane processes. DIBs are a type of artificial bilayer created by amphiphilic molecules at the interface between two aqueous droplets in a surrounding immiscible (usually oil) phase (Figure B.1A). Each droplet in a DIB is effectively a compartment on either side of the artificial bilayer, which can hence be used to quantify molecular transport across it.

From a classical perspective, DIBs can be said to provide answers to many of the shortcomings of other model membrane systems, such as liposomes (Figure B.1B) and black lipid membranes (BLMs) (Figure B.1C). DIBs are easier to make, their formation can be automated using microfluidic technologies, they can be arranged to create complex networks that exhibit emergent properties similar to those found in cells and tissues[155] and can be made with volumes similar to those of human cells[86,116]. They also have the potential to mimic features of real cell membranes such as asymmetry[78] and curvature[247]. However, to the detriment of the field, DIBs have generally been made from one type of synthetic phospholipid (1,2-diphytanoyl-sn-glycero-3-phosphocholine, DPhPC)[119] and used mostly to study the transport of fluorescent dyes passively or through one type of membrane pore (α-hemolysin)[119].

A quantitative analysis of all DIB publications shows that research into the formation and use of DIBs has been growing steadily over the last 15 years. Early work focused on the formation of DIBs using almost exclusively DPhPC and the use of electronic measurements to study the insertion of the pore forming proteins and pep-

tides alamethicin and α-hemolysin. This emphasis on electronic studies continued through the late 2000s and early 2010s with the insertion of the first ion channels and pore forming antibiotics. Another trend that arises from this analysis is that the type of analytical techniques available for use with DIBs guides the field. For example, the use of fluorescence or spectroscopic detection methods has an inverse relationship with electronic studies during this period: a drop-off in the insertion of new pores and channels following 2011 seems to align with a relative explosion in publications using fluorescence for quantification, primarily to studying molecular diffusion across these model membranes. Later in the 2010s, more exotic compounds such as membrane transport proteins and mechanoselective ion channels were inserted into DIBs, with both electrical and fluorescent methods used for quantification of molecular transport. Another trend seen since 2008 is the use different lipids for DIB formation. In fact, between 2019 and 2020, the publications using cholesterol comprised nearly half of all publications. We believe interest in this area will continue to grow as a result of a greater focus on biomimeticity, which shows an increasing interest in these model membranes as artificial cells. It is notable that the proportion of publications using microfluidic techniques for DIB formation has remained constant. We think that this is primarily due to difficulties associated with developing and using microfluidic technologies in laboratories that lack the facilities and equipment for doing so, an issue often referred to as the "chip-in-a-lab" problem.

In the first review of the field[118], the authors predicted that DIBs would be used to facilitate precise membrane measurements to answer fundamental biophysical questions about membrane proteins, lipid diffusion and lipid flip-flop, and that asymmetric DIBs had not reached their full potential. In this perspective, we will discuss the progress that has taken place since then and highlight the major challenges facing the field, including the limitations associated with microfluidic methods for the forma-

Figure B.1: **A)** Schematic showing the formation of DIBs. Lipids self-assemble at the interface of aqueous droplets to form monolayers. Droplets are then brought into contact with each other manually or using microfluidic technologies to encourage bilayer formation between the droplets. DIBs can then be formed into networks in both two and three dimensions. **B)** Schematic showing the arrangement of lipids to form a liposome and **C)** a black lipid membrane. Triangles denote the solid support used to build the bilayer. Phospholipid size is exaggerated to show assembly. Microfluidic methods for the formation of DIBs usually rely on on-chip features such as **D)** rails[86] or **E)** pillars[109] to align the droplets and slowly bring them into contact with each other. **F)** Cylindrical and conical shapes used to describe the packing characteristics of different types of lipids.

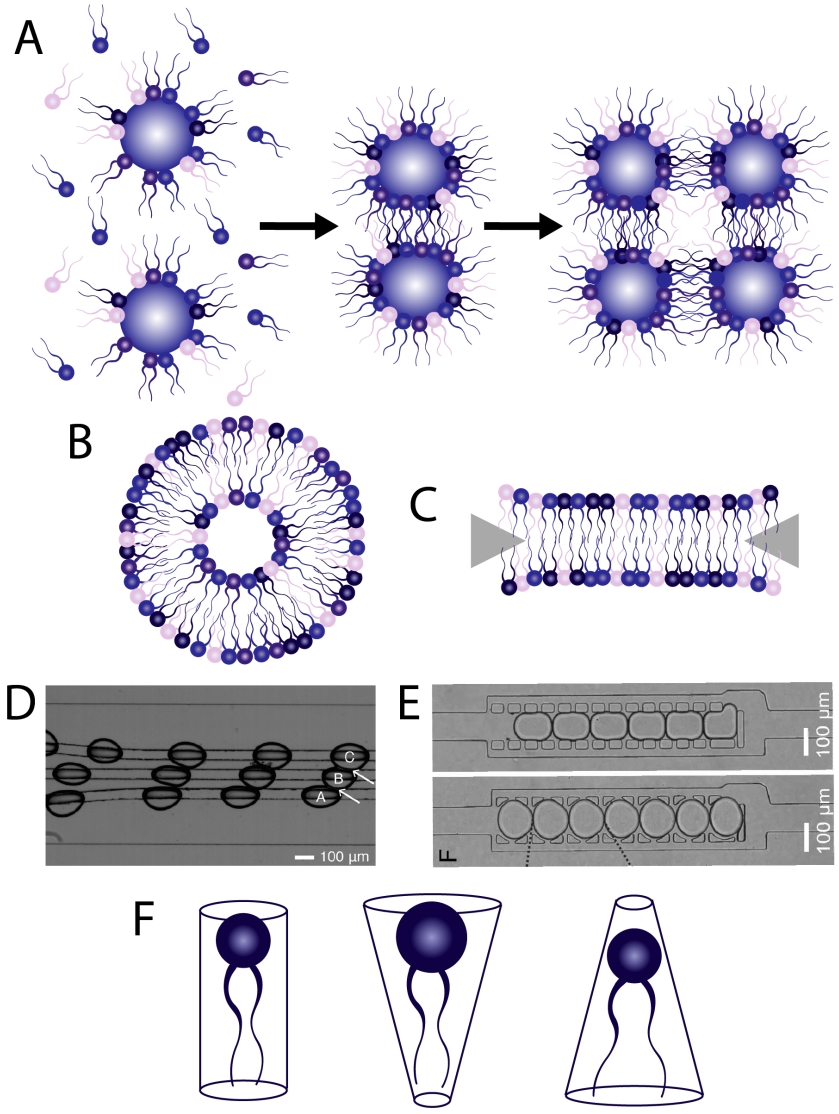

tion of DIBs, how the lack of suitable detection techniques for quantifying molecular transport within DIBs is limiting their application in more diverse fields, and how to increase the biomimetic nature of DIBs. We will also explore what the future holds for DIBs.

B.2 Designing and building DIBs as biomimetic model membranes

The ultimate goal when developing model membranes is to build a fully biomimetic bilayer from the bottom up. Each component of the membrane, from the molecular composition to the membrane proteins, should mimic those found in nature, while also enabling bespoke model membranes to be created for a wide range of applications. Traditional model membrane systems can be broadly categorised into planar or curved. BLMs are the earliest example of planar model membranes[147], but some of their inherent characteristics have limited widespread adoption of these systems. BLMs are short lived and unstable, which means that they are mostly used to study fast processes carried out by ion channels and pores[254]. Forming BLMs is also a particularly delicate process, requiring a high degree of skill that is not compatible with high throughput experimentation[255]. Because they are planar bilayers formed between aqueous wells, BLMs fail to capture features of cellular membranes such as membrane curvature, and the vastly different ratio of cellular volume to bilayer surface area. Liposomes are the most commonly used curved model membranes and are relatively straightforward to make compared to BLMs, leading to their widespread adoption as model membranes for studying lipid interactions[256]. However, achieving consistency in terms of size and lipid distribution can be difficult, as can be modelling features of cellular membranes such as the asymmetric molecular composition

of each of the monolayers that form the bilayer in cell membranes. DIBs represent a third category of model membranes, which have advantages associated with planar membranes, such as the ease of compartmentalisation of the fluid on each side of the membrane, and advantages associated with curved model membranes, such as control over membrane curvature and the formation of asymmetric bilayers.

Microfluidic technologies allow unprecedented control over how DIB systems are built and interrogated. Microfluidic technologies are designed to enable accurate control of fluids on the micron scale, for example to create aqueous droplets of volumes similar to the size of cells, which can then be used to build biomimetic DIBs. Over the last decade, around a third of publications have used microfluidic methods for DIB formation, highlighting a significant shift in the field since the first high-throughput method was published in 2010[108]. Microfluidic technologies have enabled the creation of artificial tissues-on-a-chip, where multiple DIBs are arranged into interconnected networks, by refining control over droplet and bilayer size and their precise arrangement in the network[76,97–99] and can hence be used for the measurement of passive molecular movement across the membranes[77,109]. These applications require the isolation of distinct chemical environments in separate droplets which is enabled by the highly tunable nature of microfluidic platforms, and showcase properties of DIBs that are not possible with other types of model membranes.

There are several key designs of on-chip features that allow this level of control and are consistently used in the field. The introduction of meanders[257] allows time for lipids to self-assemble as monolayers on the droplet surface before DIB formation, bypassing the long equilibration times (minutes) required when using manual micromanipulators[118]. This means that whereas manual methods for DIB formation are usually limited to tens of DIBs, microfluidic methods can generate hundreds or even

thousands of DIBs per minute[108]. Droplet trapping geometries such as pillars[77] and rails[97] are commonly used to guide droplets to exact locations and hence provide control over the exact composition of DIB networks (Figure B.1D and E). However, DIB formation techniques are far from homogeneous and more esoteric microfluidic DIB formation strategies include bilayers formed by solvent evaporation[119], flow-guiding[97], "passive" droplet guidance that relies solely on on-chip architectural features[86,109,120], and "active" droplet guidance which additionally requires the use of on-chip features such as valves to control droplets[99].

From a molecular perspective, the design of the membrane fundamentally limits the type of assays that can be performed in the DIB, both from the perspective of the molecules used to form the bilayer and the oil phase used to support the amphiphilic molecules prior to DIB formation. So far, DIBs have largely been built using single synthetic phospholipids, mainly DPhPC and DOPC (1,2-dioleoyl-sn-glycero-3-phosphocholine) and are hence not very biomimetic. The few exceptions include polymers[91,92], and more biomimetic bespoke lipid formulations[84,86] and total lipid extracts[82–84,160]. Other components of cell membranes, including neutral lipids such as cholesterol and monoglycerides, have also been used along with phospholipids for DIB formation[84,88–90]. The chemical structure of phospholipids is a factor in membrane permeability, with both acyl chain and polar head group type influencing bilayer packing and permeability[85]. In biological systems, lipid packing depends partially on the relative space occupied by the head group and acyl chains[23,172] (Figure B.1F). Lipids with similarly sized head groups and acyl chains have an overall cylindrical shape and pack together as flat bilayers. Lipids with head groups that are much larger than the space occupied by the acyl chains form a cone shape that creates curvature when packing. Finally, lipids with small head groups are the opposite, where the cone is inverted because the head groups are much smaller than the splayed tails. These

structural complexities create differences in molecular packing which are only recently beginning to be understood[85]. It is also important to note that bilayer formation in cells in not just dependent on self-assembly, but is also reliant on cellular machinery that is not currently present in these types of artificial cells.

From an energetic perspective, DIBs present a non-biomimetic system where the tail groups of the lipids are in a supportive oil phase, rather than in fully aqueous biological systems. This means that there needs to be an energetic advantage to forming a bilayer in a DIB[165] and this is dependent on the molecular composition used to form them. Lipids available for use in building model membranes are either synthesised directly or extracted from natural sources, which leads to differences in the molecular composition of the reagents. Synthetic lipids are formed from molecules with the same head groups and acyl chains, and usually have high degrees of purity. Naturally derived lipids have been extracted from a natural source (mostly egg or animal tissues) and purified to ensure that all molecules present in the sample have the same head group. However, the sample contains a range of acyl chains lengths and degrees and location of unsaturation. The most biomimetic lipid source are total lipid extracts, where all head groups (and hence acyl chains) from a natural source are extracted. Both of the naturally derived lipids may also include other molecules present in cell membranes, such as polyunsaturated fatty acids. Hence, the choice of lipids used to form DIBs has a direct effect on the degree of biomimicry of the model membrane.

However, being able to make DIBs from either bespoke naturally derived lipid formulations or biomimetic total lipid extracts is a key step for DIBs to fulfil their potential as an elegant model for complex cell membranes. Controlled heating of the aqueous droplets has been shown to facilitate complete monolayer self-assembly and encourage

DIB formation[83,84,86]. We have also recently shown that the lipid-out method, where lipids are dosed in the oil phase, allows DIB formation at physiological temperatures with naturally derived lipids[86], whereas when the same lipids are dosed in the aqueous phase (lipid-in) higher temperatures are required to enable DIB formation. Hence, temperature is another factor that can affect packing dynamics in DIBs by allowing the molecules to rearrange themselves to accommodate their neighbours[85]. Generally, the lipid-out method is slower to form a monolayer because of the high energy required for inverse micelles to form a monolayer due to tail-tail interactions. Repulsive interactions between micelles in the water phase favours monolayer formation when using the lipid-in method. However, this does not hold for naturally derived lipids, where heating is required to overcome this energetic barrier.

DIBs allow the interplay between the molecular components of membranes and their biological behaviour to be elucidated. Fundamental research into water permeability across DIBs provides insight into the role that key lipid types play in membrane permeability. DIBs built between two droplets containing a NaCl concentration gradient allowed the observation of osmotic transport of water across the membrane using microscopy[88–90,114] and Raman microspectroscopy[115]. By designing lipid formulations containing precise amounts of membrane components such as cholesterol[88], cholesterol sulphate[114], monoglycerides with varying acyl chain lengths and saturation levels[88–90] and asymmetric DIBs[114], it is possible to isolate the effects these wide-ranging membrane properties have on water permeability. For example, increasing monoglyceride unsaturation is correlated with increasing water permeability across the DIB[88–90] and addition of cholesterol is correlated with decreasing permeability[88,90]. This is because unsaturated lipids have a cis bond which allows for looser packing. Cholesterol itself actually sits inside the bilayer causing the lipid tails to agglomerate around it and hence packing becomes tighter making the membrane less permeable. Increasing

monoglyceride acyl chain length, which leads to creation of thicker bilayers, is also correlated with decreasing water permeability[89]. Addition of cholesterol sulphate to a DPhPC bilayer correlates with decreasing permeability, while addition of this molecule to only one leaflet of the DIB creates an intermediate condition[114]. It is exciting to see that the ease with which both symmetric and asymmetric DIBs can be formed from bespoke lipid formulations means that they are used to precisely quantify how molecular transport across membranes is affected by changes in lipid composition.

B.3 DIBs to quantify molecular kinetics

DIBs represent a simple method to quantify molecular transport across an artificial bilayer because the droplets on either side of the bilayer serve as donor and acceptor compartments, with volumes small enough to enable detection at low concentrations and the potential to perform parallelised assays. This is one of the major advantages of DIBs when compared to other model membranes for chemical analysis. However, this has not been exploited to its full advantage and most research has been performed using dyes such as fluorescein[77,86,108,109], carboxyfluorescein[111], calcein[104,109] and resorufin[82,110]. In fact, diffusion of fluorescein is regularly used in place of capacitance measurements[79] to verify that contacted droplets have formed a DIB, especially within microfluidic devices.

An interesting example shows the translocation of large molecules across a DIB with the horseradish peroxidase enzyme as a detector using the cell penetrating peptide Pep-1[102]. Translocation across the bilayer was verified by merging the acceptor droplet with a droplet of fluorogenic substrate, demonstrating the possible utility of this technique for droplet sized fluorescence assays. Furthermore, by treating multiple

encapsulated DIBs as a reactor unit, it is possible to use these "multisomes" as self-contained chemical reactors for the synthesis of a fluorescent pyridinium reporter (Figure B.2)[113]. This *in-situ* synthesis opens the door to performing multi-step synthetic chemistry in biologically relevant environments, for example for the synthesis of drugs close to their membrane-bound targets and the study of membrane-bound signalling pathways.

From a pharmacological perspective, early work showing the diffusion of caffeine in DIBs showed their potential to become an alternative to parallel artificial membrane permeability assays (PAMPA)[77], which are a commercial *in vitro* platform used in drug discovery to predict the ability of drugs to cross cell membranes *in vivo*. There is no true model membrane in PAMPA, instead, a plastic filter placed in a well and infused with lipids is used to quantify molecular transport. This work is also interesting because it addresses another current limitation of DIB research, namely the over reliance on fluorescence microscopy for detection, and instead uses UV microspectroscopy to monitor molecular movement. We have recently demonstrated that DIBs more accurately predict apparent permeability than PAMPA for fluorescein absorption in rat intestinal cells[86]. Our DIBs were made using naturally derived lipids that mimicked the lipid composition of intestinal cells. This means that DIBs are potentially a more reliable indicator of passive drug permeability than the current state of the art commercial technique.

B.4 DIBs to study integral membrane proteins

Being structurally analogous to a cell membrane, DIBs provide a useful scaffold to study membrane proteins[258]. Since DIBs are more stable than other artificial membrane systems they provide an attractive platform for this kind of analysis. The

first protein to be inserted into a DIB was α-haemolysin[79,101], a pore forming toxin from *Staphylococcus aureus*. Due to its relative ease of use, and ability to self insert in a membrane, α-hemolysin has dominated the field perhaps to the detriment of more exciting biological entities. In the past decade many more proteins and peptides have been successfully reconstituted and inserted into DIBs using three main methods: self-insertion, reconstitution in liposomes before DIB formation, and *in vitro* transcription/translation (IVTT). Proteins can sometimes be self-inserted into membranes without any external influence through self-assembly under favourable conditions. Usually, however, proteins need to be reconstituted using detergents to solubilise them, which are then exchanged for lipids using dialysis. In IVTT, cellular machinery (ribosomes, DNA, amino acids etc.) is inserted into a droplet of the DIB to express the protein *in situ* directly into the bilayer.

Notable examples of protein insertion into DIBs include the incorporation of the eukaryotic hERG potassium channel and NMDA receptor in DIBs after expression in mammalian cells[103]. Electrical measurements of these, as well as endogenously expressed mammalian potassium channels, and prokaryotic KcsA were carried out with no purification. Since purification of membrane proteins is notoriously difficult[260], bypassing this step greatly increases the accessibility of methods to study them. The incorporation of ion channels into DIBs suggests that DIBs may also be used as an alternative to patch clamp experiments. The patch clamp technique is used to compartmentalise sections of live cells such that transport across ion channels can be measured while in their natural environment. The compartmentalisation inherent in DIBs means that these experiments can happen in model membranes that mimic the natural environment much easier. The mechanoselective MscL channel, a stretch activated ion channel found in *E. coli*, has been incorporated into DIBs and activated using the compound 2-(trimethylammonium)ethyl methane thiosulphonate

Figure B.2: **A)** Use of IVTT to insert a variant of α-hemolysin into a multisome, allowing the precursor compound 3-carboxyumbelliferyl-β-D-galactopyranoside (CUG) to diffuse through to the droplet containing β-galactosidase. This enzymatic reactor creates a fluorescent reporter[259]. **B)** Multisomes have been made in large quantities using microfluidic methods, creating several self-contained reaction vessels, also used in this work to create a fluorescent reporter[113]. **C)** IVTT has also been used for the expression of an ATP powered transporter protein from the major facilitator superfamily, shown here pumping the fluorescent sugar 4-methylumbelliferyl-β-galactopyranoside[106].

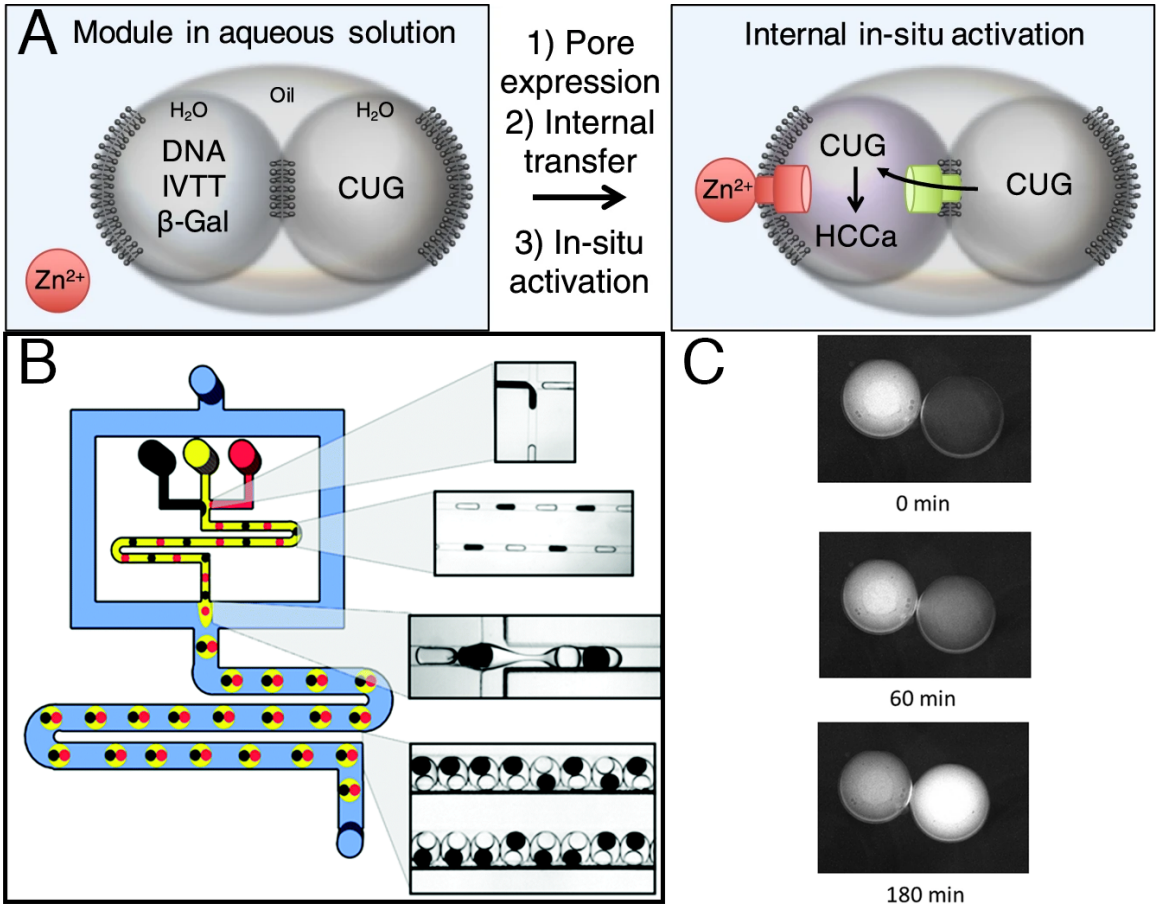

bromide[104]. Further work has confirmed that MscL proteins incorporated into DIBs retain their stretch responsive properties by taking electrical measurements while mechanically stimulating the DIB in which MscL was incorporated[233]. More recently, the spontaneous insertion of the human chloride channel CLIC1 has been shown in a DIB, and quantification of chloride flux using the quenching of a chloride responsive fluorescent dye[105]. This work is particularly interesting due to their unique approach to forming DIB pairs using a microfluidic device that created a multiplexed array of several replicates.

While most proteins successfully inserted into DIBs are pores or ion channels, so far only one example of active transport across a DIB has been demonstrated through the insertion of the *E. coli* lactose permease transporter (LacY) (Figure B.2)[106]. The uphill transport of a fluorescent sugar using this transporter was shown and through manipulation of the lipid composition, the authors were able to vary the activity level of LacY. In this case, exchanging DOPC with DOPE (1,2-dioleoyl-sn-glycero-3-phosphoethanolamine) increased the membrane curvature, which led to a change in the rate of molecular transport by causing a change in the energy of the conformational change in the protein. LacY was successfully incorporated in a DIB using both reconstitution in liposomes after expression in *E. coli*, and with IVTT. However no human proteins have so far been inserted into DIBs. With screening of drugs against transporter libraries forming an important and costly part of early drug discovery[261], successfully inserting pharmacologically relevant transporters into DIBs will mark a turning point in the use of DIBs as biomimetic model membranes and we predict that interest in their use as a tool to enable cheaper and faster early drug discovery by supplementing or replacing cell cultures will be high.

B.5 DIBs as scaffolds for electrophysiological measurements

Electrochemical gradients provide the driving force for cellular processes such as nerve conduction and respiration. Studying the electrophysiological characteristics of lipid membranes is essential to fully understand this aspect of cellular physiology. The electrical properties of DIBs have been measured extensively, with capacitance measurements and measurement of current through α-hemolysin forming the bulk of these measurements. Fundamental research into the voltage-current relationship of DPhPC membranes and the effect of α-hemolysin and of alamethicin on this relationship has shown that α-hemolysin decreases membrane resistance through formation of pores, and alamethicin causes a voltage dependant increase in conductance[93]. The dependence of bilayer capacitance on bilayer area has been exploited to accurately measure the specific capacitance of DPhPC based DIBs in hexadecane[94]. While electrodes used for these types of measurements are frequently Ag/AgCl electrodes inserted into the droplets themselves, it has also been shown that electrodes external to the droplets may be used to induce or measure flow of ions between DIBs[156]. The advantage of external electrodes is that they can be easily integrated into microfluidic devices for analysis of molecular transport across DIBs, potentially expanding the types of analyses that can be performed in DIBs, which is one of the current main limitations in the field.

Engineered networks of DIBs had already been shown to exhibit interesting emergent properties prior to the first review of the field, such as functioning as batteries or light sensors[101]. Since then, networks of DIBs have been shown to be capable of functioning as diodes when treated with modified, heptameric α-hemolysin[100]. Droplets

containing these modified α-hemolysin heptamers were arranged to create a half wave rectifier, a current limiter, and even a full wave bridge rectifier. Because DIBs can easily be built into networks, more complex signal processing may be carried out with systems like this, for example to perform computing, or to serve as an interface between electronics and tissue. A recent review of the field further expands these ideas by elegantly describing the potential of DIBs from an engineering and materials science perspective[262].

From a more biomimetic perspective, bilayer capacitance and air flow-induced current measurements have been used to model the mechanotransduction properties of animal sensory hairs via DIBs made from DPhPC as model hair cells[91,263,264]. In this work, an artificial hair was inserted into one of the droplets forming the DIB, allowing the effect of hair movement on the membrane to be investigated. This integration of macro and micro biological entities serves as a new kind of electromechanical sensor for small air movements and sound. DIBs made from DPhPC and DOPC have also been used as models for biophysical kinetic measurements by monitoring changes in transmembrane potential of asymmetric DIBs before and after insertion of alamethicin. It is not easy to form asymmetric bilayers using other types of model membranes, and few systems even exist that enable these types of studies. Being able to easily model this asymmetry using DIBs revealed new insights into how this pore interacts with the membrane by inducing lipid "flip-flop". Hence, DIBs allowed the elucidation of the behaviour of the antibiotic in the membrane[248]. Prior work shows the use of a combination of interfacial tension (IFT) measurements and computational analysis to investigate the effects of lipid adsorption kinetics on phospholipid monolayer self-assembly at an oil-water interface[165]. The quantification of the success rate of DIB formation as well as resistance and rupture potential of the DIBs successfully formed using each of the aforementioned techniques showed a significant difference

between DPhPC and the unsaturated lipid DOPC. Even when the IFT value determined to be optimal for DIB formation was attained, DOPC monolayers required a longer incubation time than DPhPC to form DIBs. Studying the factors affecting the kinetics of monolayer formation not only provides explanations for success rates of DIB formation in future work, but also provides useful information for processes involving lipid emulsion formation. The authors apply these findings to optimise DIB formation using unsaturated phospholipids[265], showing that the mechanics of membrane formation in DIBs requires further investigation. This is especially true since DIBs made from more biomimetic lipids and more complex lipid mixtures are needed to enable them to become the go-to model membrane system.

B.5.1 The future and potential of DIBs

The last decade has shown that DIBs are versatile and biomimetic model bilayers for applications ranging from the study of protein transport to artificial cells. The ease of formation of DIBs using manual or microfluidic methods means that they have the potential to become a widely used model membrane system. However, it is clear that they have yet to achieve their full potential. We believe that advances in the following research areas will be key drivers in terms of the development and application of these systems in coming years.

Fundamental bilayer behaviour. There is a lack of fundamental chemical insight into the kinetics and mechanics of monolayer and DIB formation. For example, why the method of lipid delivery (lipid-in or lipid-out) affects the kinetics of DIB formation, the kinetics of lipid domain formation, lipid flip-flop and lateral diffusion within the bilayer, and small molecule diffusion through bilayers of differing composition. The incorporation of fluorescently tagged lipids into DIBs may be a key component of this

research. Understanding these fundamental biophysical processes will enable more complex DIBs to be formed, and will enable comparison of the model membrane with their biological comparators.

Biomimetic artificial cells. Cells are complex entities. DIBs can function as bespoke artificial cells that can be built from the bottom up to enable the quantification of the behaviour of each component of the cell membrane. To function as artificial cells for the understanding of chemical interactions in the cell membrane, we must expand the library of lipids and biomimetic lipid mixtures that can be used for DIB formation. Making DIBs more biomimetic also necessitates the development of strategies to reproducibly generate asymmetric DIBs and to insert a range of human membrane proteins into DIBs. Creating more complex DIB-linked droplet networks will enable the investigation of larger scale cell communication and molecular transport. Progress on these fronts will allow DIBs to be developed specifically as a screening tool for early-stage drug candidate permeability and activity.

Technological advances. Microfluidic technologies have enabled a host of new advances in the field. However, most microfluidic platforms are made using polydimethylsiloxane (PDMS), a choice of material that both limits assay length as the droplets evaporate over short time-frames and limits the commercialisation of microfluidic methods for DIB formation because other materials are used for the mass manufacture of microfluidic devices. More high-throughput methods for DIB formation would enable rapid screening of drugs in DIBs for potentially dangerous interactions with channels and pore proteins. To increase the biomimetic nature of DIBs, microfluidic technologies that enable even smaller DIBs to be formed would allow more cell types to be modelled. Most fundamentally, the field would benefit from a streamlined strategy for the design of microfluidic platforms for DIB formation both

Figure B.3: **A)** An automated microfluidic platform that uses electronic control of valves to assemble and disassemble networks of DIBs on demand[188]. Complex experiments involving DIBs may potentially be done using such a system to increase throughput. **B)** A machined polycarbonate device for assembly of many DIB pairs on demand[266]. With multiplexed arrays of DIBs, single bilayer experiments may be carried out in replicate much like traditional macroscopic experiments in well plates.

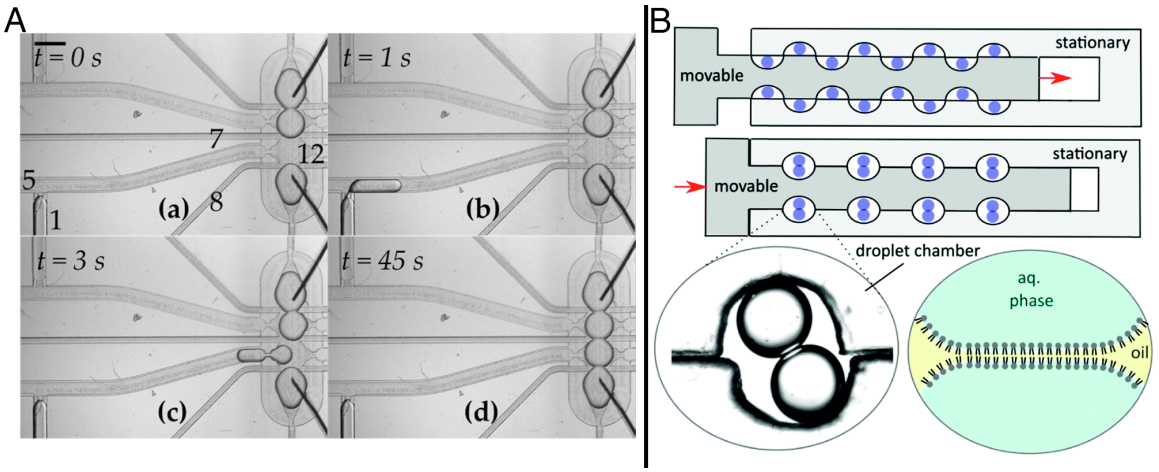

in specialist and non-specialist laboratories, and from better integration of a variety of detection methods into these microfluidic platforms. This would enable these technologies to be used in laboratories with no microfluidic expertise.

Detection methods. One of the greatest barriers to the widespread adoption of DIBs as model membranes for the quantification of molecular behaviour is the reliance on fluorescence microscopy. This is particularly true for microfluidic methods of forming DIBs, since removing droplets from a microfluidic device for analysis is a nontrivial task. There is a need for new measurement techniques that allow the quantification of molecular transport on-chip (and off-chip) of a wider range of molecules. As we mentioned at the start of this article, the field has changed based on the types of analytical techniques available for detection in DIBs. Recent exciting work shows the integration of microfluidic platforms for the formation of DIBs with off-chip label-free analysis using liquid chromatography–mass spectrometry[112]. New detection methods can also be based on the development of libraries of molecular recognition agents or through the development of on-chip sensors.

Looking to the future, we believe that these advances will allow DIBs to be used for a host of new applications. By exploiting the electrical properties of engineered DIB networks, we might be able to assemble more complex structures such as logic gates that function as tuneable biosensors. Through advances in microfluidic technologies we could build interconnected, three dimensional networks of DIBs to create new biomaterials for application in the medicinal sciences. We can also imagine a future that includes automated synthesis and testing platforms for drug discovery (Figure B.3), where combinatorial synthesis of drugs occurs in droplets which are then brought together to form DIBs to test molecular uptake through bespoke artificial cell membranes containing different types of lipids and transporter proteins. We look forward to looking back next decade to see whether DIBs have achieved their full potential.

Appendix C

Supplementary information for Chapter 3

C.1 Supplementary information for Chapter 3

Table C.1: **Overview of the experimental conditions tested**. The naturally derived phospholipids and phospholipid formulations used for DIB formation. Their T_m values are given where available. "No data" is indicated for the phospholipid formulations as only the T_m values for individual lipids are reported in the literature. The temperatures given indicate the set points of the heating platform during DIB formation. Successful formation at each specific temperature is indicated by green text and unsuccessful by red text. In the bespoke formulations, the biological source of PC, PE and PI is liver, and that of PS is brain.

Phospholipid	**Outcome**	**T_m (°C)**	**Temperatures tested (°C)**
Liver PC	DIBs	55[171]	25, 42, 50, 55, 60, 68, 69
Egg PC	DIBs	41[171]	25, 42, 55, 65
Liver PE	DIBs	74[171]	55, 60, 65, 70, 75
Brain PS	DIBs	68[171]	25, 50, 60, 65, 69
Liver PI	No DIBs	40.9[267]	25, 35, 45, 60, 69
1:1 PC:PS	DIBs	No data	25, 35, 68, 69, 70, 75, 80, 85
1:1 PS:PE	(No DIBs)	No data	70, 75, 80, 85, 90
4:1 PC:PS	DIBs	No data	50, 60, 65, 70, 75
1:1 PC:PE	DIBs	No data	25, 35, 45, 50, 55
1:1:1 PC:PE:PS	DIBs	No data	25, 35, 45, 50, 55, 60, 65, 70
4:4:1 PC:PE:PS	DIBs	No data	25, 30, 35, 45, 50, 55, 60, 65, 75, 80, 85, 90
4:4:1:1 PC:PE:PS:PI	DIBs	No data	25, 37, 55, 70, 75, 80, 85

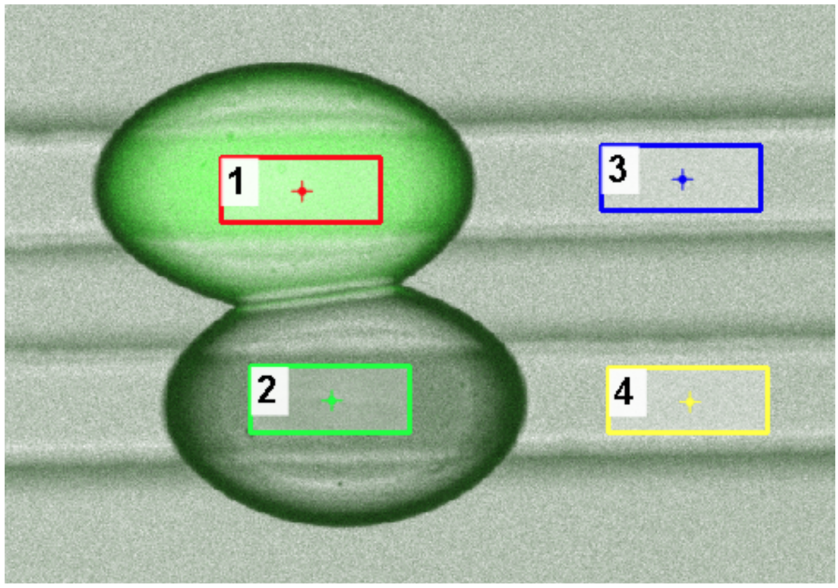

						Background Corrected Intensity	
Time [m:s]	A	B	A Background	B Background		A	B
00:00.5	585.69	169.4	148.41	148.01		437.28	21.39
00:05.6	579.82	173.04	148.28	147.73		431.54	25.31
00:10.6	578.59	176.08	148.59	147.6		430	28.48
00:15.6	576.82	179.55	148.49	147.72		428.33	31.83

Figure C.1: **Fluorescein intensity measurements.** Fluorescence intensity was measured over time using regions of interest (ROIs) in the centre of each droplet (shown as coloured squares in the image above). Background fluorescence intensity measurements were taken using ROIs in the channels near the droplets and were subtracted from the intensities measured inside the droplets. The table shows representative raw and treated data.

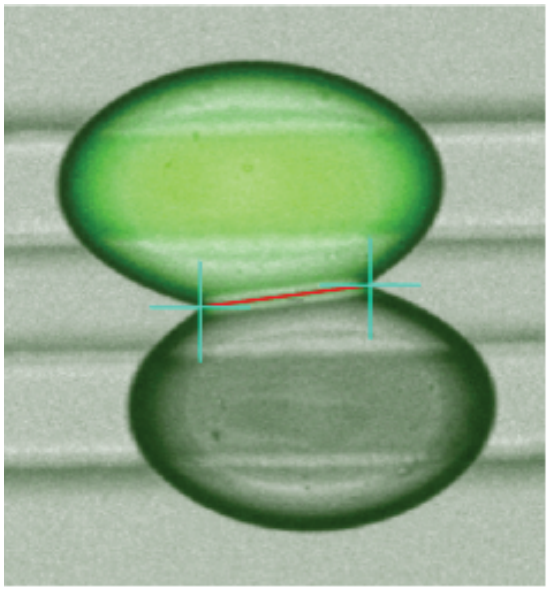

Time (s)	Diameter (µm)	Area (µm²)
0	87.75	3790.35
60	92.06	3976.73
120	99.47	4296.74
180	105.00	4535.49

Figure C.2: **Artificial cell membrane diameter measurements and surface area calculations.** DIBs were approximated as ellipses to allow for calculation of membrane surface area. DIB diameters were measured in NIS Elements AR as shown above (red line between droplets defined between blue crosses). This diameter and the depth of the channel (measured with a DekTak profilometer to be $(55 \pm 2)\,\mu m$) were used to calculate the artificial cell membrane surface area. The table shows representative raw and treated data.

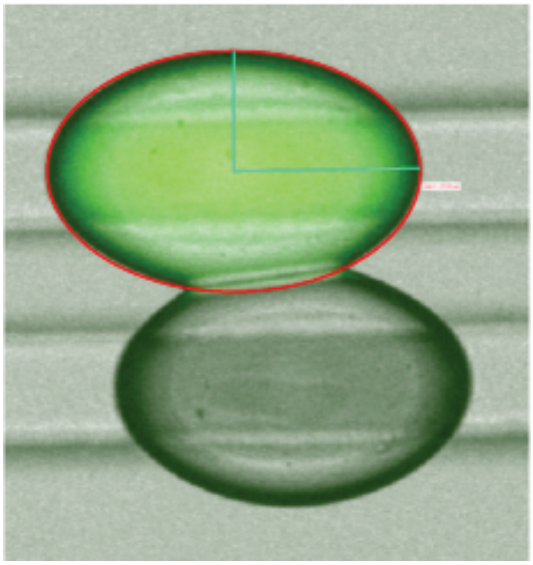

Time (s)	Axis A (µm)	Axis B (µm)	Volume (µm³)
0	73.96	60.48	0.52
60	73.72	60.40	0.51
120	74.56	60.40	0.52
180	74.43	60.33	0.52

Figure C.3: **Droplet circumference measurements and volume calculations.** Droplets were approximated as ellipsoids to enable calculation of droplet volume. The semiaxes of each droplet were measured in NIS Elements AR as shown above in the fluorescent droplet (blue lines from the centre of the droplet to the edges, red ellipse around the droplet). The semiaxes and the depth of the channel (measured with a DekTak profilometer to be $(55 \pm 2)\,\mu m$) were used to calculate the droplet volume as well as the droplet circumference. The table shows representative raw and treated data.

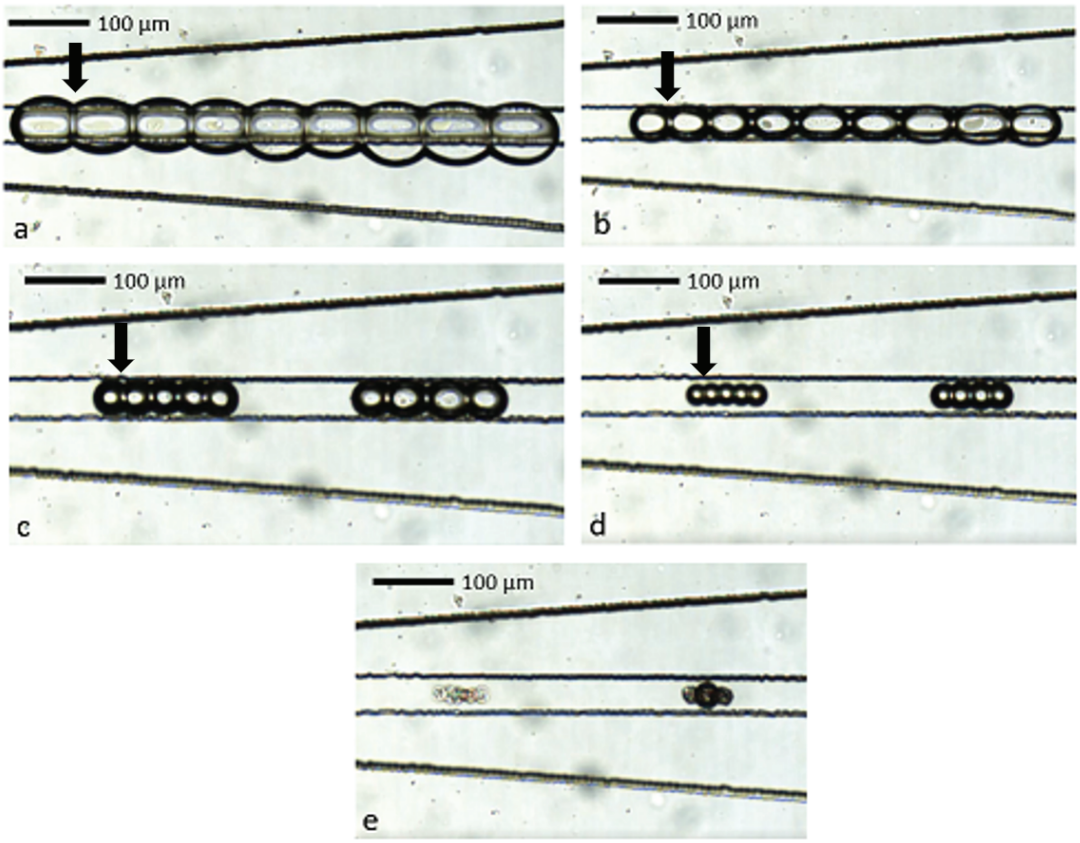

Figure C.4: **DIB stability over time.** DIBs formed using DPhPC (10 mg/mL, pH 7.59, HEPES buffer) at times a) 0 h, b) 1 h, c) 2 h, d) 3 h and e) 3.75 h. The continuous phase was squalene. Magnification: 2x/0.10. Arrows indicate example sites of DIB formation, showing the DIBS are extremely robust over time despite droplet evaporation.

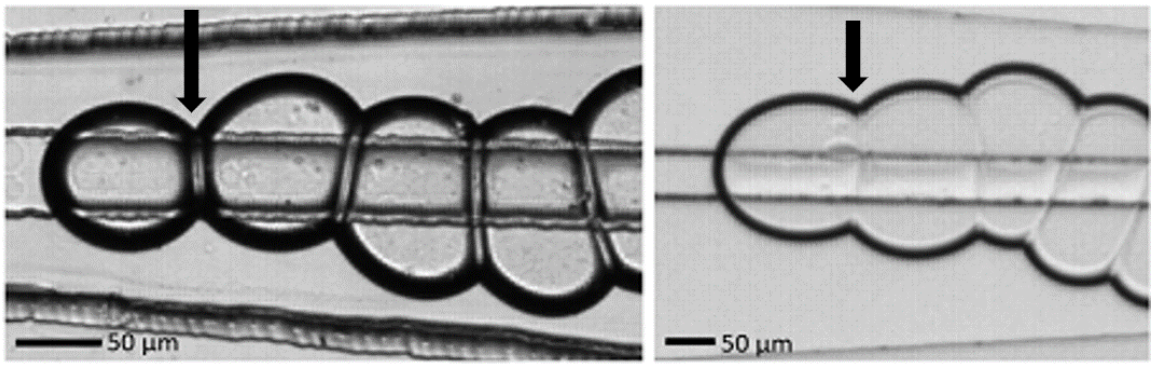

Figure C.5: **"Meltiness" of DIBs.** DIB formation using DPhPC (10 mg/mL, pH 7.59, HEPES buffer) in a squalene mobile phase. Magnification: 2x/0.10. The image on the left was taken at 22°C and the image on the right was taken at 40°C. Arrows indicate example sites of DIB formation. DPhPC forms DIBs at a range of temperatures, but they only "melt" above 40C. DPhPC has been observed in a liquid phase over a large temperature range (-120C to 120C)[268] and so is in a liquid phase in all of our experiments. This along with our other "meltiness" data indicates that a temperature above the melting point (T_m) is necessary to observe "meltiness," but that the lipid also has to be cylindrical.

Table C.2: **Measurements for membrane lateral pressure calculations.** Interfacial tension measurements, half contact angle measurements, and calculated membrane lateral pressures are given for 4:1 PC:PS, 4:4:1 PC:PE:PS, and 4:4:1:1 PC:PE:PS:PI.

Phospholipid Formulation	4:1 PC:PS	4:4:1 PC:PE:PS	4:4:1:1 PC:PE:PS:PI
Average Half Contact Angle (°)	37.00	48.62	51.73
Average Interfacial Tension (mN/m)	11.7	11.6	10.8
Membrane Lateral Pressure (mN/m)	2.35±0.05	3.92±0.86	4.13±0.23

Equation S1. Normalization of DIB formation rate data. The DIB diameter and droplet circumference were measured over time as shown in Figures S3 and S4. The ratio of the DIB diameter to the droplet circumference (X) was calculated and each dataset (i.e. the ratio over time for each DIB measured) was normalized to a percentage (X') using the equation shown below. This allowed for direct comparison between replicates by accounting for minor variations in droplet size.

$$X' = \frac{X - X_min}{X_max - X_min}$$

Video S1. DIB formation

DIB formation using 4:4:1:1 PC:PE:PS:PI (10 mg/mL, pH 7.59, HEPES buffer) in a squalene mobile phase.

Video S2. Controlled droplet stopping

DIB formation using 4:1 PC:PS (10 mg/mL, pH 7.59, HEPES buffer) in a squalene mobile phase at 69.9°C. The fast-response pressure pump allows for precise control over droplet location on the rail.

Video S3. DIB formation and "melting"

"Melty" DIB formation using 1:1 PC:PS (10 mg/mL, pH 7.59, HEPES buffer) in a squalene mobile phase at 70.0°C. DIBs form and melt in the video.

Video S4. Droplet merging in squalene

DIB formation using 4:4:1:1 PC:PE:PS:PI (10 mg/mL, pH 7.59, HEPES buffer) in a squalene mobile phase at room temperature. When not heated to the appropriate temperature, DIBs fail to form and aqueous droplets merge.

Video S5. DPhPC DIB formation, melting, and separation

DIB formation using DPhPC (10 mg/mL, pH 7.59, HEPES buffer) in a squalene mobile phase at 40.0°C. DIBs form, melt, and separate as the oil flow pushes the droplets toward the outlet of the microfluidic device.

Appendix D

Supplementary information for Chapter 4

D.1 Supplementary information for Chapter 4

D.1.1 Calibration Curves

Calibration curves were generated by first creating a dilution series of 100 µM, 50 µM, 25 µM, 10 µM, 5 µM, and 1 µM of fluorescein in all buffer solutions using a P1000 pipette. These buffers were pumped onto a chip, and the fluorescence of droplets in the main chamber were measured as with the experimental intensity measurements. Background was subtracted from all intensity measurements and linear fit generated in OriginPro 2019b.

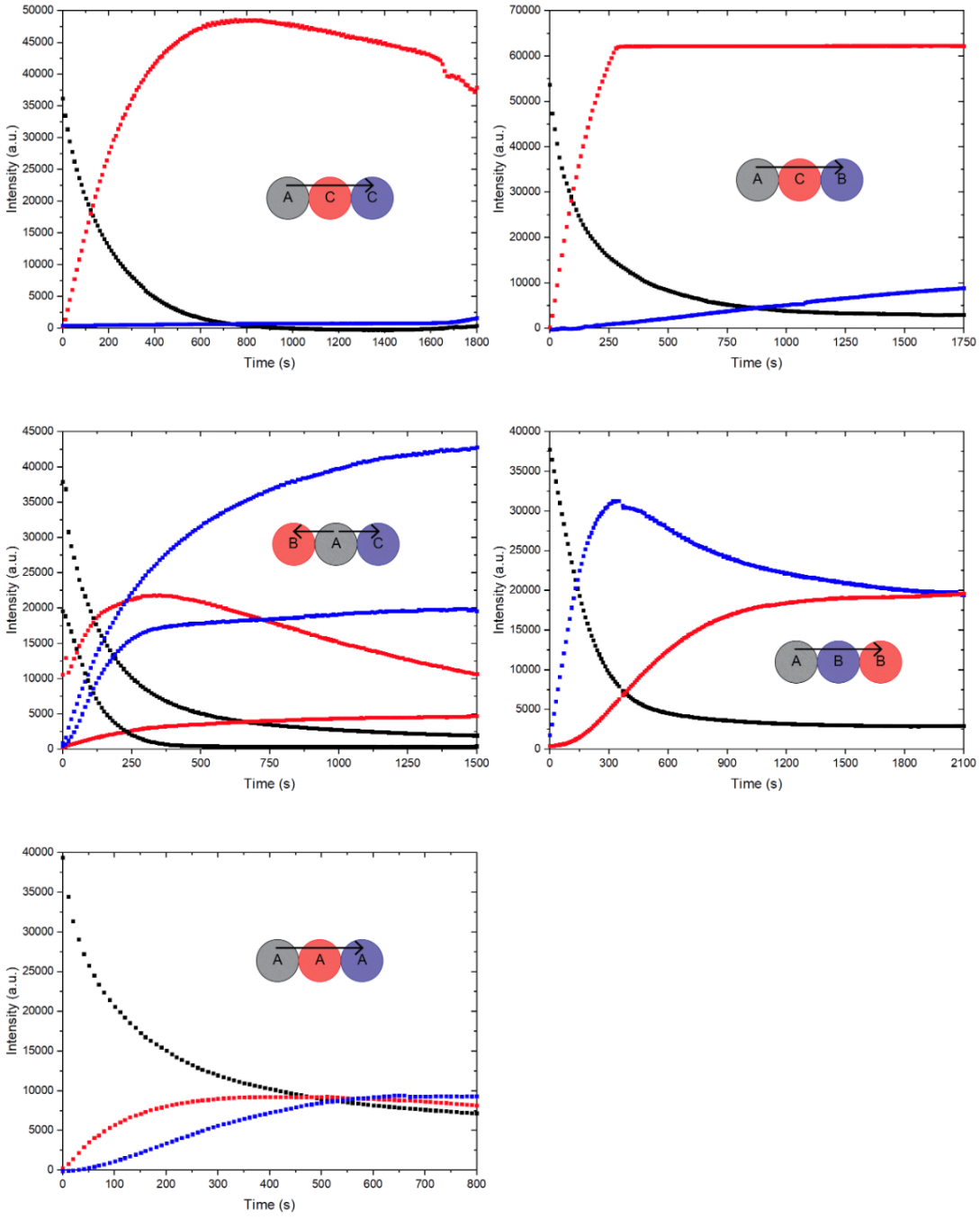

Figure D.1: **Control experiments.** Graphed data for each of the control experiments detailed in the paper. The configuration of the droplet triplets is shown as a diagram, where the colour corresponds to the data, and A corresponds to the intestinal space compartment, B corresponds to the enterocyte compartment and C corresponds to the blood compartment. The direction of fluorophore diffusion in each triplet is shown with arrows.

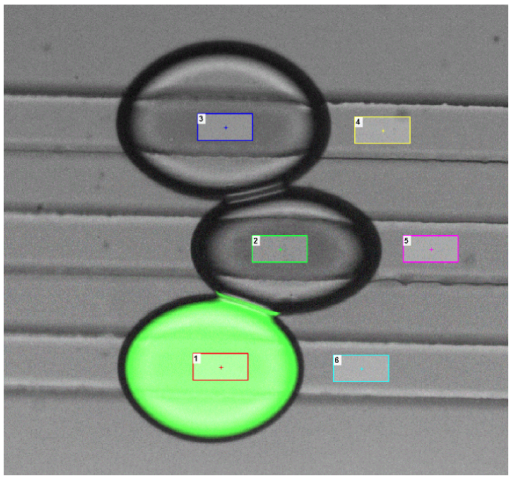

		Intensity (a.u.)					
Frame Number	Time (h:m.s)	Droplet A	Droplet B	Droplet C	A Background	B Background	C Background
1	00:00.4	49398.18	7157.96	6388.00	3346.52	3280.43	3244.00
2	00:10.5	47625.79	8969.97	6422.77	3340.18	3275.58	3229.18
3	00:20.5	45771.15	11060.22	6450.77	3345.15	3276.74	3227.89
4	00:30.5	43717.29	13354.58	6473.10	3349.04	3278.36	3227.09
5	00:40.5	41398.91	15870.70	6515.75	3358.16	3283.73	3234.70

	Background-Corrected Intensity (a.u.)		
Time (s)	Droplet A	Droplet B	Droplet C
0	46051.66	3877.53	3144.00
11	44285.61	5694.39	3193.59
21	42426.00	7783.48	3222.88
31	40368.25	10076.22	3246.01
41	38040.75	12586.97	3281.05

Figure D.2: **Fluorescence intensity measurements.** Regions of interest (ROIs) were drawn manually in the centre of each droplet (shown as coloured squares in the image above), allowing for the time-based measurement of fluorescence intensity by NIS Elements AR. Measurements based on ROIs were also taken in the channels near the droplets to determine the background intensity, which was subsequently subtracted from the sample intensities. Representative raw and treated data are shown in the table.

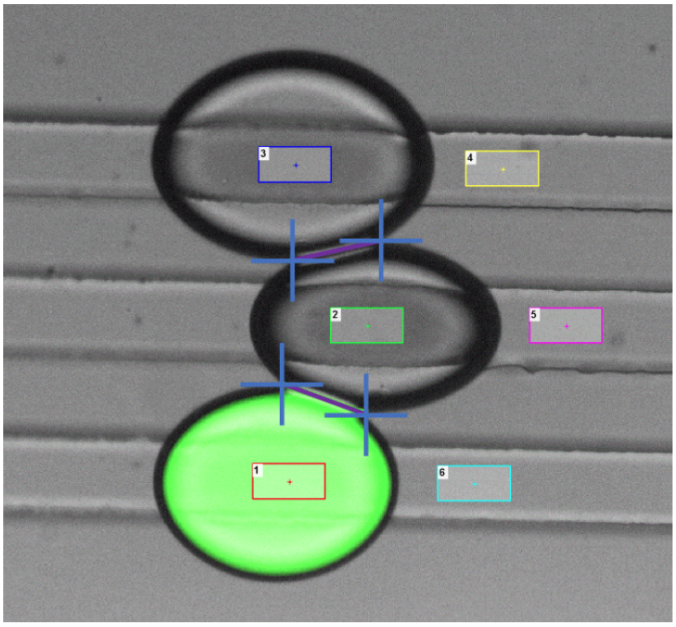

Time (s)	Frame Number	Diameter (µm)	Area (µm^2)
0	1	53.85	2277.48
10	2	65.50	2829.29
20	3	70.75	3056.31
30	4	78.03	3370.45
40	5	87.42	3776.31

Figure D.3: **Artificial cell membrane surface area calculations.** Artificial cell membrane surface area was calculated by approximating droplet interface bilayers (DIBs) as ellipses, the diameters of which were measured in NIS Elements AR as shown above (lines between droplets defined between crosses; enlarged to show detail). This diameter and the depth of the channel (measured with a DekTak profilometer to be (55 ± 2) µm were used to calculate the artificial cell membrane surface area. Representative raw and treated data are shown in the table.

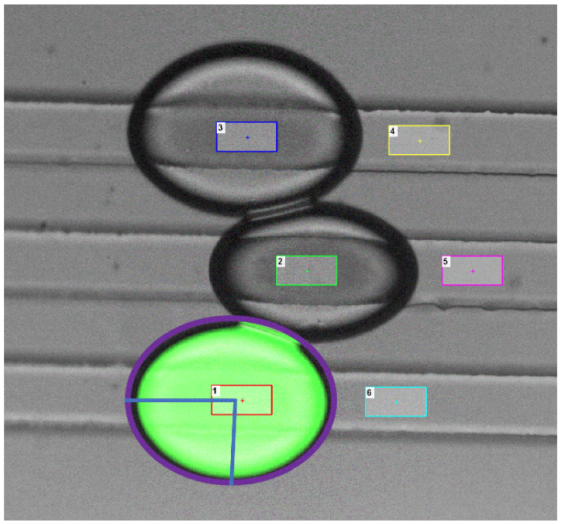

Time (s)	Axis A (µm)	Axis B (µm)	Volume (µm³)
0	88.05	64.97	658966.79
300	85.25	73.12	718045.35
600	80.97	71.80	669683.94
900	79.81	69.16	635819.14
1200	78.94	67.67	615339.23

Figure D.4: **Droplet volume calculations.** Droplet volume was calculated by approximating droplets as ellipsoids, the semiaxes of which were measured in NIS Elements AR as shown above in the fluorescent droplet (lines from the centre of the droplet to the edges. enlarged to show detail). The semiaxes and the depth of the channel (measured with a DekTak profilometer to be (55 ± 2) µm were used to calculate the droplet volume. Representative raw and treated data are shown in the table.

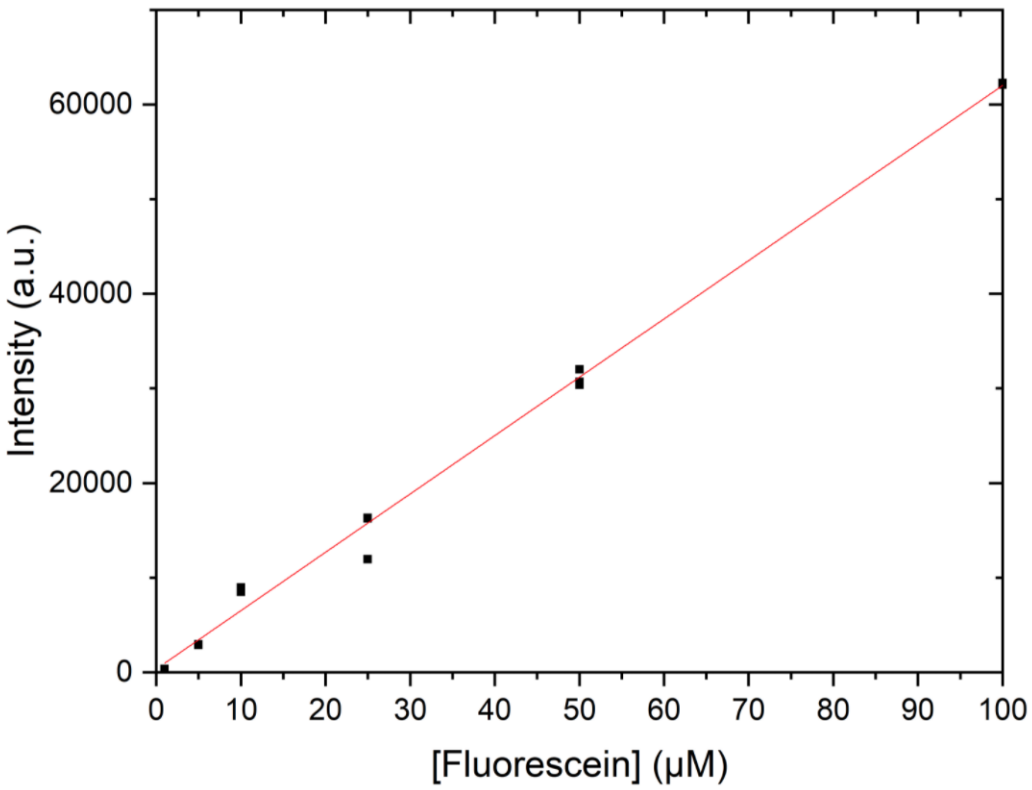

Figure D.5: **Calibration curve for fluorescein in intestinal compartment buffer** . Fit $y = a + bx$ where $a = 393.23729465.43736$ and $b = 616.271529.90404$. $R2 = 0.99588$.

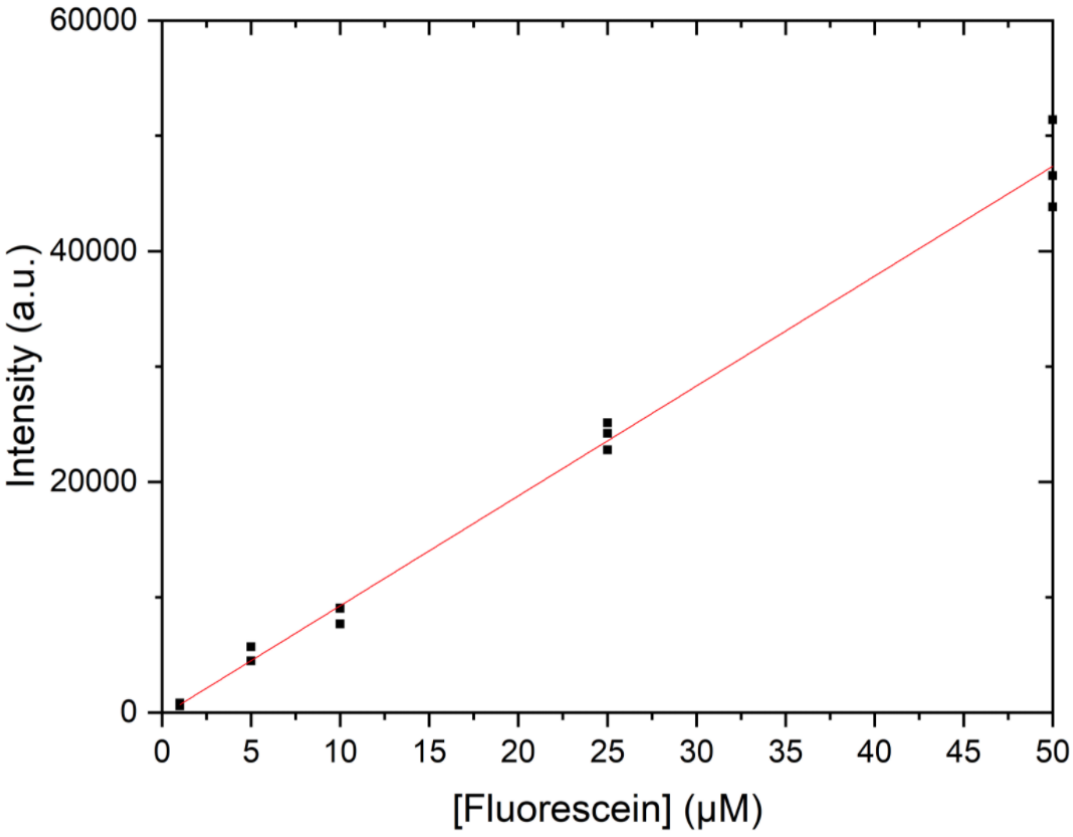

Figure D.6: **Calibration curve for fluorescein in enterocyte compartment buffer.** Fit $y = a + bx$ where $a = -229.04392 \pm 620.96026$ and $b = 952.02902 \pm 24.35232$.$R2 = 0.99157$. 100 µM replicates not included due to saturating the detector.

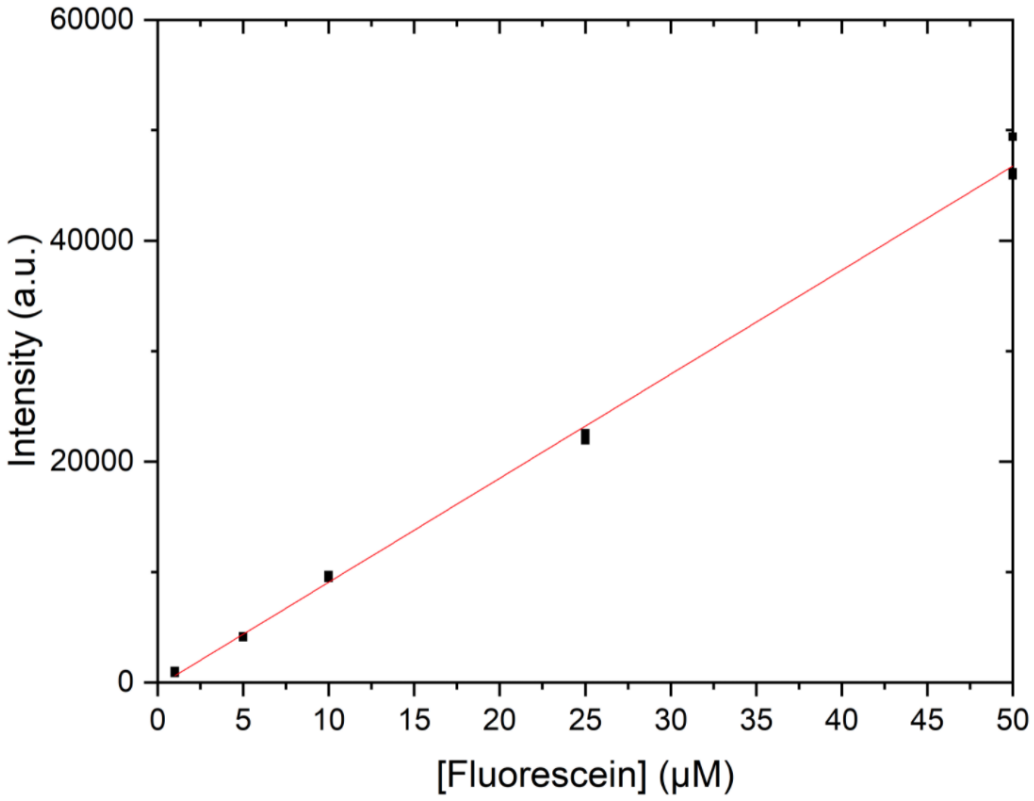

Figure D.7: **Calibration curve for fluorescein in blood compartment buffer.** Fit $y = a + bx$ where $a = -308.81683 \pm 360.559$ and $b = 941.38738 \pm 14.14011$.$R2 = 0.99708$. 100 µM replicates not included due to saturating the detector.

D.1.2 Heating platform

The heating platform used to maintain the on-chip assays at a physiological temperature of 37°C was designed to fit into the stage of Nikon Ti2-E and Ti2-U inverted microscopes, and was conceptually based on a platform previously used by Scheuble et al.[269]

The heating platform is made of brass and uses resistive heaters and a proportional-integral-derivative (PID) controller to maintain programmed temperatures. The brass platform base was machined to include a viewing aperture (25.4 mm by 12.7 mm), allowing for consistent heating and visualisation of the microfluidic devices. Brass was used since it is resistant to corrosion and has low thermal conductivity. A lid was constructed from acrylic glass after initial tests showed that temperature measurements of the heating platform were not stable due to overhead draft from the laboratory ventilation system. The lid has a viewing port with the same dimensions as the mantle viewing port. Figure S8 shows a scale three dimensional drawing.

The PID controller uses a PID control system to maintain a setpoint temperature on the mantle. The mantle uses 3 inch by 1 inch resistive heating foils that output 5W/sq. in. of heat (35475K442, 28 V AC, McMaster). The foils are connected to a step down transformer (Hammond Manufacturing) which is connected to the output of a PID controller (CSI32K-C24, Omega Engineering). A type K surface thermocouple is used by the PID controller to monitor the temperature (± 0.4°C accuracy, SA3-K Fast Response Self Adhesive Thermocouple, Omega Engineering). Fridge magnets were used to clamp the glass slide containing the microfluidic device to the surface of the heating platform.

Video of device operation

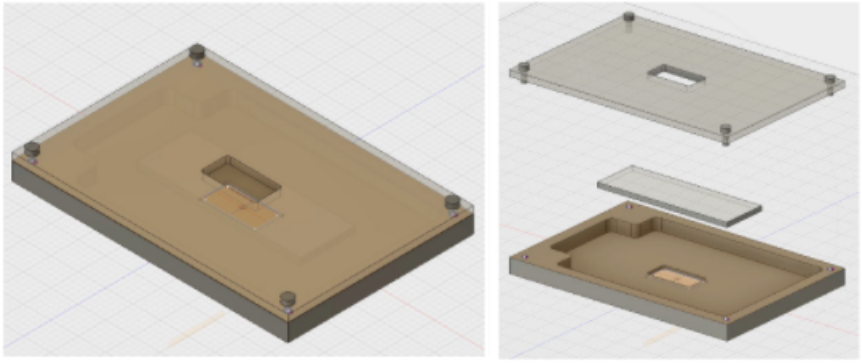

Figure D.8: **Three-dimensional constructed (left) and exploded (right) view of the heating platform.** The middle piece in the exploded view denotes a microfluidic device. The heating mantle itself is shown in brown and is constructed in brass. The lid is shown as clear since it is constructed in acrylic glass. The heating platform was calibrated using an ice water bath to determine whether the surface thermocouple was in good working condition. This was done by submerging the probe in ice water and leaving it for 10 min to stabilise. After 10 minutes the measured value of the ice water on the controller was 0°C for the surface thermocouple. Since the heating foils do not cover the entire surface of the mantle, the platform was also heated to 37°C and 50°C and observed with a thermal camera (FLIR) to determine the temperature variability on the surface of the heating platform. Figure D.9 shows that the temperature variability is low.

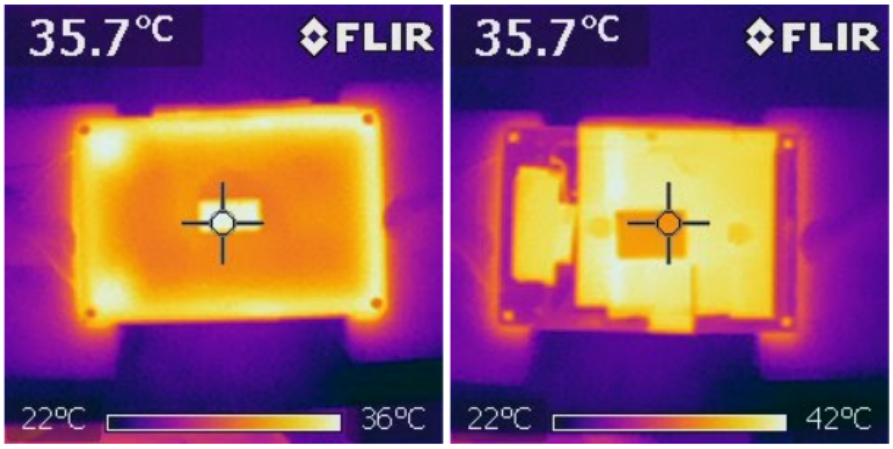

Figure D.9: **Thermal camera images of the heating platform containing a microfluidic device both when the platform is covered (left) and uncovered (right).** The heating platform was heated to 37°C and the images show relative temperature readings between 22°C and 36°C as a colour scale. The lack of colour variation indicates that there is consistent temperature on the heating platform and on the microfluidic device. The heating period of the mantle was determined by programming the mantle to heat and log the temperature readings over the course of 30 min at 5 s intervals. The mantle was set to heat up to 30°C, 37°C and 50°C and Figure D.10 shows the temperature readings we measured. The elapsed time before the readings stabilised (deviation of ± 0.1°C) was 900 s, or approximately 15 min of heating. All experiments in the paper were performed after temperature stabilisation of the heating platform.

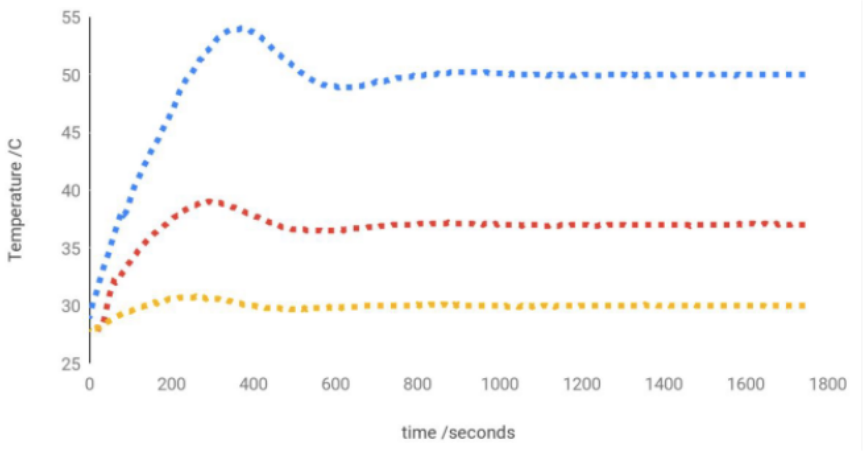

Figure D.10: **Heating platform temperature readings taken every** 5 s **over** 30 min **after setting the temperature to 30°C (yellow data), 37°C (red data), and 50°C (blue data).** PID control parameters are P = 10, I = 45, D = 0, cycle time = 2 s and damping factor = 2.

File name: Device in Operation.mp4

Example of flow stoppage and triplet selection using the OB1 pressure pump. Squalene is the carrier phase, and the content of the droplets is 10 mg/mL DPhPC in aqueous buffer (10 mM HEPES, pH = 7.6, 200 mM KCl). This video was collected at room temperature with 180 mbar of pressure on the oil inlet and 140 mbar of pressure on each of the aqueous inlets. The video was captured at 30 fps with a Phantom V710L camera on a Nikon Eclipse Ti2-U inverted microscope.

Bibliography

1. Institute of Medicine (US) Committee on Conflict of Interest in Medical Research, Education, and Practice. *Conflict of Interest in Medical Research, Education, and Practice* eng (eds Lo, B. & Field, M. J.) ISBN: 978-0-309-13188-9. http://www.ncbi.nlm.nih.gov/books/NBK22942/ (2020) (National Academies Press (US), Washington (DC), 2009).
2. DiMasi, J. A., Grabowski, H. G. & Hansen, R. W. Innovation in the pharmaceutical industry: New estimates of R&D costs. en. *Journal of Health Economics* **47,** 20–33. ISSN: 01676296. https://linkinghub.elsevier.com/retrieve/pii/S0167629616000291 (2020) (May 2016).
3. Brodniewicz, T. & Grynkiewicz, G. Preclinical drug development. eng. *Acta Poloniae Pharmaceutica* **67,** 578–585. ISSN: 0001-6837 (Dec. 2010).
4. Seyhan, A. A. Lost in translation: the valley of death across preclinical and clinical divide – identification of problems and overcoming obstacles. *Translational Medicine Communications* **4,** 18. ISSN: 2396-832X. https://doi.org/10.1186/s41231-019-0050-7 (2021) (Nov. 2019).
5. Avdeef, A. Physicochemical profiling (solubility, permeability and charge state). eng. *Current Topics in Medicinal Chemistry* **1,** 277–351. ISSN: 1568-0266 (Sept. 2001).

6. Ceccarelli, M., Wagner, B., Alvarez-Sánchez, R., Cruciani, G. & Goracci, L. Use of the Distribution Coefficient in Brain Polar Lipids for the Assessment of Drug-Induced Phospholipidosis Risk. *Chemical Research in Toxicology* **30.** Publisher: American Chemical Society, 1145–1156. ISSN: 0893-228X. https://doi.org/10.1021/acs.chemrestox.6b00459 (2021) (May 2017).

7. Hingorani, A. D. *et al.* Improving the odds of drug development success through human genomics: modelling study. en. *Scientific Reports* **9.** Number: 1 Publisher: Nature Publishing Group, 18911. ISSN: 2045-2322. https://www.nature.com/articles/s41598-019-54849-w (2021) (Dec. 2019).

8. Lin, L. & Wong, H. Predicting Oral Drug Absorption: Mini Review on Physiologically-Based Pharmacokinetic Models. *Pharmaceutics* **9,** 41. ISSN: 1999-4923. https://www.ncbi.nlm.nih.gov/pmc/articles/PMC5750647/ (2021) (Sept. 2017).

9. Waring, M. J. *et al.* An analysis of the attrition of drug candidates from four major pharmaceutical companies. en. *Nature Reviews Drug Discovery* **14.** Bandiera_abtest: a Cg_type: Nature Research Journals Number: 7 Primary_atype: Research Publisher: Nature Publishing Group Subject_term: Drug discovery;Drug discovery and development;Small molecules Subject_term_id: drug-discovery;drug-discovery-and-development;small-molecules, 475–486. ISSN: 1474-1784. https://www.nature.com/articles/nrd4609 (2021) (July 2015).

10. *Reducing Drug Attrition* en (eds Empfield, J. R. & P Clark, M.) ISBN: 978-3-662-43913-5 978-3-662-43914-2. http://link.springer.com/10.1007/978-3-662-43914-2 (2021) (Springer Berlin Heidelberg, Berlin, Heidelberg, 2014).

11. Di, L. *et al.* The Critical Role of Passive Permeability in Designing Successful Drugs. eng. *ChemMedChem* **15,** 1862–1874. ISSN: 1860-7187 (Oct. 2020).

12. Smith, D. *et al.* Passive lipoidal diffusion and carrier-mediated cell uptake are both important mechanisms of membrane permeation in drug disposition. eng. *Molecular Pharmaceutics* **11,** 1727–1738. ISSN: 1543-8392 (June 2014).

13. Kansy, M., Avdeef, A. & Fischer, H. Advances in screening for membrane permeability: high-resolution PAMPA for medicinal chemists. eng. *Drug Discovery Today. Technologies* **1,** 349–355. ISSN: 1740-6749 (Dec. 2004).

14. Mandagere, A. K., Thompson, T. N. & Hwang, K.-K. Graphical model for estimating oral bioavailability of drugs in humans and other species from their Caco-2 permeability and in vitro liver enzyme metabolic stability rates. eng. *Journal of Medicinal Chemistry* **45,** 304–311. ISSN: 0022-2623 (Jan. 2002).

15. Sun, H., Chow, E. C., Liu, S., Du, Y. & Pang, K. S. The Caco-2 cell monolayer: usefulness and limitations. eng. *Expert Opinion on Drug Metabolism & Toxicology* **4,** 395–411. ISSN: 1742-5255 (Apr. 2008).

16. Balimane, P. V. & Chong, S. Cell culture-based models for intestinal permeability: A critique. en. *Drug Discovery Today* **10,** 335–343. ISSN: 1359-6446. `http://www.sciencedirect.com/science/article/pii/S1359644604033549` (2019) (Mar. 2005).

17. Avdeef, A. *et al.* PAMPA—critical factors for better predictions of absorption. en. *Journal of Pharmaceutical Sciences* **96,** 2893–2909. ISSN: 0022-3549. `http://www.sciencedirect.com/science/article/pii/S0022354916324054` (2019) (Nov. 2007).

18. Alqahtani, S., Mohamed, L. A. & Kaddoumi, A. Experimental models for predicting drug absorption and metabolism. *Expert Opinion on Drug Metabolism & Toxicology* **9,** 1241–1254. ISSN: 1742-5255. `https://doi.org/10.1517/17425255.2013.802772` (2019) (Oct. 2013).

19. Nigsch, F., Klaffke, W. & Miret, S. In vitro models for processes involved in intestinal absorption. *Expert Opinion on Drug Metabolism & Toxicology* **3,** 545–556. ISSN: 1742-5255. https://doi.org/10.1517/17425255.3.4.545 (2019) (Aug. 2007).

20. Berben, P. *et al.* Drug permeability profiling using cell-free permeation tools: Overview and applications. en. *European Journal of Pharmaceutical Sciences* **119,** 219–233. ISSN: 0928-0987. https://www.sciencedirect.com/science/article/pii/S0928098718301751 (2021) (July 2018).

21. Cooper, G. M. Cell Membranes. en. *The Cell: A Molecular Approach. 2nd edition.* Publisher: Sinauer Associates. https://www.ncbi.nlm.nih.gov/books/NBK9928/ (2020) (2000).

22. Bretscher, M. S. & Raff, M. C. Mammalian plasma membranes. en. *Nature* **258,** 43–49. ISSN: 0028-0836, 1476-4687. http://www.nature.com/articles/258043a0 (2020) (Nov. 1975).

23. Van Meer, G., Voelker, D. R. & Feigenson, G. W. Membrane lipids: where they are and how they behave. *Nature reviews. Molecular cell biology* **9,** 112–124. ISSN: 1471-0072. https://www.ncbi.nlm.nih.gov/pmc/articles/PMC2642958/ (2021) (Feb. 2008).

24. Overton, C. E. *Ueber die osmotischen eigenschaften der lebenden pflanzen- und tierzelle,* German. OCLC: 67895032 (Fäsi & Beer, Zurich, 1895).

25. Katzung, B. G. & Katzung, B. G. *Basic & clinical pharmacology / by Betram G. Katzung.* en. OCLC: 1162211818. ISBN: 978-1-259-64115-2 (McGraw-Hill, New York, 2018).

26. Balon, K., Riebesehl, B. U. & Müller, B. W. Drug Liposome Partitioning as a Tool for the Prediction of Human Passive Intestinal Absorption. en. *Pharma-*

ceutical Research **16,** 882–888. ISSN: 1573-904X. https://doi.org/10.1023/A:1018882221008 (2019) (June 1999).

27. Lipinski, C. A., Lombardo, F., Dominy, B. W. & Feeney, P. J. Experimental and computational approaches to estimate solubility and permeability in drug discovery and development settings1PII of original article: S0169-409X(96)00423-1. The article was originally published in Advanced Drug Delivery Reviews 23 (1997) 3–25.1. en. *Advanced Drug Delivery Reviews. Special issue dedicated to Dr. Eric Tomlinson, Advanced Drug Delivery Reviews, A Selection of the Most Highly Cited Articles, 1991-1998* **46,** 3–26. ISSN: 0169-409X. https://www.sciencedirect.com/science/article/pii/S0169409X00001290 (2021) (Mar. 2001).

28. Refsgaard, H. H. F. *et al.* In silico prediction of membrane permeability from calculated molecular parameters. eng. *Journal of Medicinal Chemistry* **48,** 805–811. ISSN: 0022-2623 (Feb. 2005).

29. Winiwarter, S. *et al.* Correlation of human jejunal permeability (in vivo) of drugs with experimentally and theoretically derived parameters. A multivariate data analysis approach. eng. *Journal of Medicinal Chemistry* **41,** 4939–4949. ISSN: 0022-2623 (Dec. 1998).

30. Raevsky, O. A., Fetisov, V. I., Trepalina, E. P., McFarland, J. W. & Schaper, K.-J. Quantitative Estimation of Drug Absorption in Humans for Passively Transported Compounds on the Basis of Their Physico-chemical Parameters. en. *Quantitative Structure-Activity Relationships* **19,** 366–374. ISSN: 1521-3838. http://onlinelibrary.wiley.com/doi/abs/10.1002/1521-3838%28200010%2919%3A4%3C366%3A%3AAID-QSAR366%3E3.0.CO%3B2-E (2021) (2000).

31. Agatonovic-Kustrin, S., Beresford, R. & Yusof, A. P. Theoretically-derived molecular descriptors important in human intestinal absorption. eng. *Journal of Pharmaceutical and Biomedical Analysis* **25,** 227–237. ISSN: 0731-7085 (May 2001).

32. Faassen, F., Vogel, G., Spanings, H. & Vromans, H. Caco-2 permeability, P-glycoprotein transport ratios and brain penetration of heterocyclic drugs. eng. *International Journal of Pharmaceutics* **263,** 113–122. ISSN: 0378-5173 (Sept. 2003).

33. Palumbo, P. *et al.* A general approach to the apparent permeability index. eng. *Journal of Pharmacokinetics and Pharmacodynamics* **35,** 235–248. ISSN: 1567-567X (Apr. 2008).

34. Volpe, D. A. Application of method suitability for drug permeability classification. eng. *The AAPS journal* **12,** 670–678. ISSN: 1550-7416 (Dec. 2010).

35. Sforzi, J., Palagi, L. & Aime, S. Liposome-Based Bioassays. *Biology* **9.** ISSN: 2079-7737. `https://www.ncbi.nlm.nih.gov/pmc/articles/PMC7466007/` (2021) (Aug. 2020).

36. Pascoe, R. J., Masucci, J. A. & Foley, J. P. Investigation of vesicle electrokinetic chromatography as an in vitro assay for the estimation of intestinal permeability of pharmaceutical drug candidates. en. *ELECTROPHORESIS* **27.** _eprint: https://onlinelibrary.wiley.com/doi/pdf/10.1002/elps.200500647, 793–804. ISSN: 1522-2683. `http://analyticalsciencejournals.onlinelibrary.wiley.com/doi/abs/10.1002/elps.200500647` (2021) (2006).

37. Rodrigues, C., Gameiro, P., Reis, S., Lima, J. L. & de Castro, B. Derivative spectrophotometry as a tool for the determination of drug partition coefficients in water/dimyristoyl-L-alpha-phosphatidylglycerol (DMPG) liposomes. eng. *Biophysical Chemistry* **94,** 97–106. ISSN: 0301-4622 (Dec. 2001).

38. Osiecka, I., Porter, P. A., Borchardt, R. T., Fix, J. A. & Gardner, C. R. In Vitro Drug Absorption Models. I. Brush Border Membrane Vesicles, Isolated Mucosal Cells and Everted Intestinal Rings: Characterization and Salicylate Accumulation. en. *Pharmaceutical Research* **2,** 284–293. ISSN: 1573-904X. https://doi.org/10.1023/A:1016341601273 (2019) (Nov. 1985).

39. Eyer, K. *et al.* A liposomal fluorescence assay to study permeation kinetics of drug-like weak bases across the lipid bilayer. eng. *Journal of Controlled Release: Official Journal of the Controlled Release Society* **173,** 102–109. ISSN: 1873-4995 (Jan. 2014).

40. Saitoh, H., Kobayashi, Y., Miyazaki, K. & Arita, T. A highly sensitive HPLC method for the assay of propantheline used to measure its uptake by rat intestinal brush border membrane vesicles. eng. *The Journal of Pharmacy and Pharmacology* **39,** 9–12. ISSN: 0022-3573 (Jan. 1987).

41. Balon, K., Riebesehl, B. U. & Müller, B. W. Determination of liposome partitioning of ionizable drugs by titration. en. *Journal of Pharmaceutical Sciences* **88,** 802–806. ISSN: 0022-3549. https://www.sciencedirect.com/science/article/pii/S0022354915508526 (2021) (Aug. 1999).

42. Escher, B. I., Schwarzenbach, R. P. & Westall, J. C. Evaluation of Liposome-Water Partitioning of Organic Acids and Bases. 1. Development of a Sorption Model. *Environmental Science & Technology* **34.** Publisher: American Chemical Society, 3954–3961. ISSN: 0013-936X. https://doi.org/10.1021/es0010709 (2021) (Sept. 2000).

43. Beigi, F., Yang, Q. & Lundahl, P. Immobilized-liposome chromatographic analysis of drug partitioning into lipid bilayers. eng. *Journal of Chromatography. A* **704,** 315–321. ISSN: 0021-9673 (June 1995).

44. Liu, X.-Y., Nakamura, C., Yang, Q., Kamo, N. & Miyake, J. Immobilized liposome chromatography to study drug–membrane interactions: Correlation with drug absorption in humans. en. *Journal of Chromatography A. International Symposium on High Performance Liquid Phase Separations and Related Techniques* **961,** 113–118. ISSN: 0021-9673. https://www.sciencedirect.com/science/article/pii/S0021967302005058 (2021) (June 2002).

45. Lundahl, P. & Beigi, F. Immobilized liposome chromatography of drugs for model analysis of drug-membrane interactions. en. *Advanced Drug Delivery Reviews. In Vitro Models for Selection of Development Candidates* **23,** 221–227. ISSN: 0169-409X. https://www.sciencedirect.com/science/article/pii/S0169409X96004371 (2021) (Jan. 1997).

46. Flaten, G. E., Dhanikula, A. B., Luthman, K. & Brandl, M. Drug permeability across a phospholipid vesicle based barrier: A novel approach for studying passive diffusion. en. *European Journal of Pharmaceutical Sciences* **27,** 80–90. ISSN: 09280987. https://linkinghub.elsevier.com/retrieve/pii/S0928098705002538 (2021) (Jan. 2006).

47. Naderkhani, E., Isaksson, J., Ryzhakov, A. & Flaten, G. Development of a Biomimetic Phospholipid Vesicle-based Permeation Assay for the Estimation of Intestinal Drug Permeability. *Journal of pharmaceutical sciences* **103** (June 2014).

48. Naderkhani, E., Vasskog, T. & Flaten, G. E. Biomimetic PVPA in vitro model for estimation of the intestinal drug permeability using fasted and fed state simulated intestinal fluids. eng. *European Journal of Pharmaceutical Sciences: Official Journal of the European Federation for Pharmaceutical Sciences* **73,** 64–71. ISSN: 1879-0720 (June 2015).

49. Falavigna, M. *et al.* Mucus-PVPA (mucus Phospholipid Vesicle-based Permeation Assay): An artificial permeability tool for drug screening and formulation development. en. *International Journal of Pharmaceutics* **537,** 213–222. ISSN: 0378-5173. https://www.sciencedirect.com/science/article/pii/S0378517317311821 (2021) (Feb. 2018).

50. Di Cagno, M., Bibi, H. A. & Bauer-Brandl, A. New biomimetic barrier Permeapad™ for efficient investigation of passive permeability of drugs. en. *European Journal of Pharmaceutical Sciences* **73,** 29–34. ISSN: 0928-0987. https://www.sciencedirect.com/science/article/pii/S0928098715001190 (2021) (June 2015).

51. Bozzuto, G. & Molinari, A. Liposomes as nanomedical devices. *International Journal of Nanomedicine* **10,** 975–999. ISSN: 1176-9114. https://www.ncbi.nlm.nih.gov/pmc/articles/PMC4324542/ (2021) (Feb. 2015).

52. Arias, J. L. Liposomes in drug delivery: a patent review (2007 – present). *Expert Opinion on Therapeutic Patents* **23.** Publisher: Taylor & Francis, 1399–1414. ISSN: 1354-3776. https://doi.org/10.1517/13543776.2013.828035 (2021) (Nov. 2013).

53. Kansy, M., Senner, F. & Gubernator, K. Physicochemical high throughput screening: parallel artificial membrane permeation assay in the description of passive absorption processes. eng. *Journal of Medicinal Chemistry* **41,** 1007–1010. ISSN: 0022-2623 (Mar. 1998).

54. Yu, H. *et al.* A new PAMPA model proposed on the basis of a synthetic phospholipid membrane. eng. *PloS One* **10,** e0116502. ISSN: 1932-6203 (2015).

55. Warren, R. C. *Physics and the architecture of cell membranes* en. Google-Books-ID: DpxqAAAAMAAJ. ISBN: 978-0-85274-446-8 (Hilger, Jan. 1987).

56. Di, L., Kerns, E. H., Fan, K., McConnell, O. J. & Carter, G. T. High throughput artificial membrane permeability assay for blood–brain barrier. *European Journal of Medicinal Chemistry* **38,** 223–232. ISSN: 0223-5234. http://www.sciencedirect.com/science/article/pii/S0223523403000126 (2018) (Mar. 2003).

57. Di, L., Kerns, E. H., Bezar, I. F., Petusky, S. L. & Huang, Y. Comparison of blood-brain barrier permeability assays: in situ brain perfusion, MDR1-MDCKII and PAMPA-BBB. eng. *Journal of Pharmaceutical Sciences* **98,** 1980–1991. ISSN: 1520-6017 (June 2009).

58. Mensch, J. *et al.* Evaluation of various PAMPA models to identify the most discriminating method for the prediction of BBB permeability. en. *European Journal of Pharmaceutics and Biopharmaceutics* **74,** 495–502. ISSN: 0939-6411. https://www.sciencedirect.com/science/article/pii/S0939641110000056 (2021) (Mar. 2010).

59. Proulx, P. Structure-function relationships in intestinal brush border membranes. en. *Biochimica et Biophysica Acta (BBA) - Reviews on Biomembranes* **1071,** 255–271. ISSN: 0304-4157. http://www.sciencedirect.com/science/article/pii/030441579190016P (2020) (Nov. 1991).

60. Sugano, K. *et al.* Optimized conditions of bio-mimetic artificial membrane permeation assay. en. *International Journal of Pharmaceutics* **228,** 181–188. ISSN: 0378-5173. http://www.sciencedirect.com/science/article/pii/S0378517301008456 (2020) (Oct. 2001).

61. Kataoka, M. *et al.* A new in vitro system for evaluation of passive intestinal drug absorption: establishment of a double artificial membrane permeation assay. eng. *European Journal of Pharmaceutics and Biopharmaceutics:*

Official Journal of Arbeitsgemeinschaft Fur Pharmazeutische Verfahrenstechnik e.V **88,** 840–846. ISSN: 1873-3441 (Nov. 2014).

62. Hidalgo, I. J., Raub, T. J. & Borchardt, R. T. Characterization of the human colon carcinoma cell line (Caco-2) as a model system for intestinal epithelial permeability. en. *Gastroenterology* **96,** 736–749. ISSN: 0016-5085. http://www.sciencedirect.com/science/article/pii/0016508589908974 (2019) (Mar. 1989).
63. Van Breemen, R. B. & Li, Y. Caco-2 cell permeability assays to measure drug absorption. eng. *Expert Opinion on Drug Metabolism & Toxicology* **1,** 175–185. ISSN: 1742-5255 (Aug. 2005).
64. Li, Y. *et al.* Increasing the throughput and productivity of Caco-2 cell permeability assays using liquid chromatography-mass spectrometry: application to resveratrol absorption and metabolism. eng. *Combinatorial Chemistry & High Throughput Screening* **6,** 757–767. ISSN: 1386-2073 (Dec. 2003).
65. Roux, F. & Couraud, P.-O. Rat Brain Endothelial Cell Lines for the Study of Blood–Brain Barrier Permeability and Transport Functions. en. *Cellular and Molecular Neurobiology* **25,** 41–57. ISSN: 1573-6830. https://doi.org/10.1007/s10571-004-1376-9 (2021) (Feb. 2005).
66. Poller, B. *et al.* The human brain endothelial cell line hCMEC/D3 as a human blood-brain barrier model for drug transport studies. en. *Journal of Neurochemistry* **107,** 1358–1368. ISSN: 1471-4159. http://onlinelibrary.wiley.com/doi/abs/10.1111/j.1471-4159.2008.05730.x (2021) (2008).
67. Liu, Y. & Jiang, X. Why microfluidics? Merits and trends in chemical synthesis. en. *Lab on a Chip* **17.** Publisher: The Royal Society of Chemistry, 3960–3978. ISSN: 1473-0189. http://pubs.rsc.org/en/content/articlelanding/2017/lc/c7lc00627f (2021) (Nov. 2017).

68. Sibbitts, J., Sellens, K. A., Jia, S., Klasner, S. A. & Culbertson, C. T. Cellular Analysis Using Microfluidics. *Analytical Chemistry* **90.** Publisher: American Chemical Society, 65–85. ISSN: 0003-2700. https://doi.org/10.1021/acs.analchem.7b04519 (2021) (Jan. 2018).

69. Halldorsson, S., Lucumi, E., Gómez-Sjöberg, R. & Fleming, R. M. T. Advantages and challenges of microfluidic cell culture in polydimethylsiloxane devices. eng. *Biosensors & Bioelectronics* **63,** 218–231. ISSN: 1873-4235 (Jan. 2015).

70. Lee, C.-Y., Chang, C.-L., Wang, Y.-N. & Fu, L.-M. Microfluidic Mixing: A Review. *International Journal of Molecular Sciences* **12,** 3263–3287. ISSN: 1422-0067. https://www.ncbi.nlm.nih.gov/pmc/articles/PMC3116190/ (2021) (May 2011).

71. Cho, S. H., Godin, J. & Lo, Y.-H. Optofluidic Waveguides in Teflon AF-Coated PDMS Microfluidic Channels. *IEEE photonics technology letters : a publication of the IEEE Laser and Electro-optics Society* **21,** 1057–1059. ISSN: 1041-1135. https://www.ncbi.nlm.nih.gov/pmc/articles/PMC2923848/ (2018) (Aug. 2009).

72. Sinton, D. Energy: the microfluidic frontier. en. *Lab on a Chip* **14.** Publisher: The Royal Society of Chemistry, 3127–3134. ISSN: 1473-0189. http://pubs.rsc.org/en/content/articlelanding/2014/lc/c4lc00267a (2021) (July 2014).

73. Stone, H. A. en. in *CMOS Biotechnology* (eds Lee, H., Westervelt, R. M. & Ham, D.) 5–30 (Springer US, Boston, MA, 2007). ISBN: 978-0-387-68913-5. https://doi.org/10.1007/978-0-387-68913-5_2 (2021).

74. Whitesides, G. M. The origins and the future of microfluidics. en. *Nature* **442.** Number: 7101 Publisher: Nature Publishing Group, 368–373. ISSN: 1476-4687. https://www.nature.com/articles/nature05058 (2021) (July 2006).

75. Punnamaraju, S. & Steckl, A. J. Voltage Control of Droplet Interface Bilayer Lipid Membrane Dimensions. *Langmuir* **27.** Publisher: American Chemical Society, 618–626. ISSN: 0743-7463. https://doi.org/10.1021/la1036508 (2021) (Jan. 2011).

76. Elani, Y., J. deMello, A., Niu, X. & Ces, O. Novel technologies for the formation of 2-D and 3-D droplet interface bilayer networks. en. *Lab on a Chip* **12.** Publisher: Royal Society of Chemistry, 3514–3520. https://pubs.rsc.org/en/content/articlelanding/2012/lc/c2lc40287d (2020) (2012).

77. Nisisako, T., Portonovo, S. A. & Schmidt, J. J. Microfluidic passive permeability assay using nanoliter droplet interface lipid bilayers. eng. *The Analyst* **138,** 6793–6800. ISSN: 1364-5528 (Nov. 2013).

78. Hwang, W. L., Chen, M., Cronin, B., Holden, M. A. & Bayley, H. Asymmetric Droplet Interface Bilayers. *Journal of the American Chemical Society* **130,** 5878–5879. ISSN: 0002-7863. http://dx.doi.org/10.1021/ja802089s (2017) (May 2008).

79. Funakoshi, K., Suzuki, H. & Takeuchi, S. Lipid Bilayer Formation by Contacting Monolayers in a Microfluidic Device for Membrane Protein Analysis. *Analytical Chemistry* **78,** 8169–8174. ISSN: 0003-2700. https://doi.org/10.1021/ac0613479 (2018) (Dec. 2006).

80. Kara, S. *et al.* Diphytanoyl lipids as model systems for studying membrane-active peptides. en. *Biochimica et Biophysica Acta (BBA) - Biomembranes* **1859,** 1828–1837. ISSN: 0005-2736. http://www.sciencedirect.com/science/article/pii/S0005273617301840 (2020) (Oct. 2017).

81. Van Hoogevest, P. & Wendel, A. The use of natural and synthetic phospholipids as pharmaceutical excipients. *European Journal of Lipid Science and Technol-*

ogy **116,** 1088–1107. ISSN: 1438-7697. https://www.ncbi.nlm.nih.gov/pmc/articles/PMC4207189/ (2021) (Sept. 2014).

82. Barlow, N. E. *et al.* Engineering plant membranes using droplet interface bilayers. eng. *Biomicrofluidics* **11,** 024107. ISSN: 1932-1058 (Mar. 2017).

83. Taylor, G. J. & Sarles, S. A. Heating-Enabled Formation of Droplet Interface Bilayers Using Escherichia coli Total Lipid Extract. *Langmuir* **31,** 325–337. ISSN: 0743-7463. https://doi.org/10.1021/la503471m (2019) (Jan. 2015).

84. Taylor, G. J. *et al.* Capacitive Detection of Low-Enthalpy, Higher-Order Phase Transitions in Synthetic and Natural Composition Lipid Membranes. en. *Langmuir* **33,** 10016–10026. ISSN: 0743-7463, 1520-5827. https://pubs.acs.org/doi/10.1021/acs.langmuir.7b02022 (2020) (Sept. 2017).

85. Faugeras, V., Duclos, O., Bazile, D. & Thiam, A. R. Membrane determinants for the passive translocation of analytes through droplet interface bilayers. en. *Soft Matter.* Publisher: The Royal Society of Chemistry. ISSN: 1744-6848. http://pubs.rsc.org/en/content/articlelanding/2020/sm/d0sm00667j (2020) (June 2020).

86. Korner, J. L., Stephenson, E. B. & Elvira, K. S. A bespoke microfluidic pharmacokinetic compartment model for drug absorption using artificial cell membrane. en. *Lab on a Chip.* Publisher: The Royal Society of Chemistry. ISSN: 1473-0189. https://pubs.rsc.org/en/content/articlelanding/2020/lc/d0lc00263a (2020) (Apr. 2020).

87. Stephenson, E. B. & Elvira, K. S. Biomimetic artificial cells to model the effect of membrane asymmetry on chemoresistance. en. *Chemical Communications.* Publisher: The Royal Society of Chemistry. ISSN: 1364-548X. http://pubs.rsc.org/en/content/articlelanding/2021/cc/d1cc02043a (2021) (June 2021).

88. Michalak, Z., Muzzio, M., Milianta, P. J., Giacomini, R. & Lee, S. Effect of Monoglyceride Structure and Cholesterol Content on Water Permeability of the Droplet Bilayer. *Langmuir* **29.** Publisher: American Chemical Society, 15919–15925. ISSN: 0743-7463. https://doi.org/10.1021/la4040535 (2020) (Dec. 2013).

89. Lopez, M., Evangelista, S. E., Morales, M. & Lee, S. Enthalpic Effects of Chain Length and Unsaturation on Water Permeability across Droplet Bilayers of Homologous Monoglycerides. *Langmuir* **33.** Publisher: American Chemical Society, 900–912. ISSN: 0743-7463. https://doi.org/10.1021/acs.langmuir.6b03932 (2020) (Jan. 2017).

90. Lopez, M. *et al.* Effects of Acyl Chain Unsaturation on Activation Energy of Water Permeability across Droplet Bilayers of Homologous Monoglycerides: Role of Cholesterol. *Langmuir* **34.** Publisher: American Chemical Society, 2147–2157. ISSN: 0743-7463. https://doi.org/10.1021/acs.langmuir.7b03590 (2020) (Feb. 2018).

91. Tamaddoni, N., Taylor, G., Hepburn, T., Kilbey, S. M. & Sarles, S. A. Reversible, voltage-activated formation of biomimetic membranes between triblock copolymer-coated aqueous droplets in good solvents. en. *Soft Matter* **12.** Publisher: The Royal Society of Chemistry, 5096–5109. ISSN: 1744-6848. https://pubs.rsc.org/en/content/articlelanding/2016/sm/c6sm00400h (2020) (June 2016).

92. Bai, Y. *et al.* A double droplet trap system for studying mass transport across a droplet-droplet interface. en. *Lab on a Chip* **10.** Publisher: The Royal Society of Chemistry, 1281–1285. ISSN: 1473-0189. https://pubs.rsc.org/en/content/articlelanding/2010/lc/b925133b (2020) (May 2010).

93. Sarles, S. A. & Leo, D. J. Tailored Current—Voltage Relationships of Droplet-Interface Bilayers Using Biomolecules and External Feedback Control. *Journal of Intelligent Material Systems and Structures* **20.** Publisher: SAGE Publications Ltd STM, 1233–1247. ISSN: 1045-389X. https://doi.org/10.1177/1045389X09104390 (2020) (July 2009).

94. Gross, L. C. M., Heron, A. J., Baca, S. C. & Wallace, M. I. Determining Membrane Capacitance by Dynamic Control of Droplet Interface Bilayer Area. *Langmuir* **27.** Publisher: American Chemical Society, 14335–14342. ISSN: 0743-7463. https://doi.org/10.1021/la203081v (2020) (Dec. 2011).

95. Poulos, J. L., Nelson, W. C., Jeon, T.-J., Kim, C.-J. ". & Schmidt, J. J. Electrowetting on dielectric-based microfluidics for integrated lipid bilayer formation and measurement. en. *Applied Physics Letters* **95,** 013706. ISSN: 0003-6951, 1077-3118. http://aip.scitation.org/doi/10.1063/1.3167283 (2020) (July 2009).

96. Punnamaraju, S., You, H. & Steckl, A. J. Triggered Release of Molecules across Droplet Interface Bilayer Lipid Membranes Using Photopolymerizable Lipids. *Langmuir* **28.** Publisher: American Chemical Society, 7657–7664. ISSN: 0743-7463. https://doi.org/10.1021/la3011663 (2020) (May 2012).

97. Carreras, P. *et al.* A microfluidic platform for size-dependent generation of droplet interface bilayer networks on rails. eng. *Biomicrofluidics* **9,** 064121. ISSN: 1932-1058 (Nov. 2015).

98. Nguyen, M.-A., Srijanto, B., Collier, C. P., Retterer, S. T. & Sarles, S. A. Hydrodynamic trapping for rapid assembly and in situ electrical characterization of droplet interface bilayer arrays. eng. *Lab on a Chip* **16,** 3576–3588. ISSN: 1473-0189 (2016).

99. Czekalska, M. A. *et al.* A droplet microfluidic system for sequential generation of lipid bilayers and transmembrane electrical recordings. en. *Lab on a Chip* **15.** Publisher: The Royal Society of Chemistry, 541–548. ISSN: 1473-0189. https://pubs.rsc.org/en/content/articlelanding/2015/lc/c4lc00985a (2021) (Dec. 2014).

100. Maglia, G. *et al.* Droplet networks with incorporated protein diodes show collective properties. eng. *Nature Nanotechnology* **4,** 437–440. ISSN: 1748-3395 (July 2009).

101. Holden, M. A., Needham, D. & Bayley, H. Functional Bionetworks from Nanoliter Water Droplets. *Journal of the American Chemical Society* **129.** Publisher: American Chemical Society, 8650–8655. ISSN: 0002-7863. https://doi.org/10.1021/ja072292a (2020) (July 2007).

102. Huang, J., Lein, M., Gunderson, C. & Holden, M. A. Direct Quantitation of Peptide-Mediated Protein Transport across a Droplet–Interface Bilayer. *Journal of the American Chemical Society* **133.** Publisher: American Chemical Society, 15818–15821. ISSN: 0002-7863. https://doi.org/10.1021/ja2046342 (2020) (Oct. 2011).

103. Leptihn, S., Thompson, J. R., Ellory, J. C., Tucker, S. J. & Wallace, M. I. In Vitro Reconstitution of Eukaryotic Ion Channels Using Droplet Interface Bilayers. *Journal of the American Chemical Society* **133.** Publisher: American Chemical Society, 9370–9375. ISSN: 0002-7863. https://doi.org/10.1021/ja200128n (2020) (June 2011).

104. Barriga, H. M. G. *et al.* Droplet interface bilayer reconstitution and activity measurement of the mechanosensitive channel of large conductance from Escherichia coli. *Journal of The Royal Society Interface* **11.** Publisher: Royal

Society, 20140404. https://royalsocietypublishing.org/doi/full/10.1098/rsif.2014.0404 (2020) (Sept. 2014).

105. Zhang, Y., Bracken, H., Woolhead, C. & Zagnoni, M. Functionalisation of human chloride intracellular ion channels in microfluidic droplet-interface-bilayers. eng. *Biosensors & Bioelectronics* **150,** 111920. ISSN: 1873-4235 (Feb. 2020).

106. Findlay, H. E., Harris, N. J. & Booth, P. J. In vitro synthesis of a Major Facilitator Transporter for specific active transport across Droplet Interface Bilayers. en. *Scientific Reports* **6.** Number: 1 Publisher: Nature Publishing Group, 39349. ISSN: 2045-2322. https://www.nature.com/articles/srep39349 (2020) (Dec. 2016).

107. Syeda, R., Holden, M. A., Hwang, W. L. & Bayley, H. Screening Blockers Against a Potassium Channel with a Droplet Interface Bilayer Array. *Journal of the American Chemical Society* **130.** Publisher: American Chemical Society, 15543–15548. ISSN: 0002-7863. https://doi.org/10.1021/ja804968g (2020) (Nov. 2008).

108. Stanley, C. E. *et al.* A microfluidic approach for high-throughput droplet interface bilayer (DIB) formation. eng. *Chemical Communications (Cambridge, England)* **46,** 1620–1622. ISSN: 1364-548X (Mar. 2010).

109. Schlicht, B. & Zagnoni, M. Droplet-interface-bilayer assays in microfluidic passive networks. eng. *Scientific Reports* **5,** 9951. ISSN: 2045-2322 (Apr. 2015).

110. Barlow, N. E. *et al.* Rheological Droplet Interface Bilayers (rheo-DIBs): Probing the Unstirred Water Layer Effect on Membrane Permeability via Spinning Disk Induced Shear Stress. en. *Scientific Reports* **7.** Number: 1 Publisher: Nature Publishing Group, 1–12. ISSN: 2045-2322. https://www.nature.com/articles/s41598-017-17883-0 (2020) (Dec. 2017).

111. Valet, M., Pontani, L.-L., Voituriez, R., Wandersman, E. & Prevost, A. M. Diffusion through Nanopores in Connected Lipid Bilayer Networks. *Physical Review Letters* **123.** Publisher: American Physical Society, 088101. https://link.aps.org/doi/10.1103/PhysRevLett.123.088101 (2020) (Aug. 2019).

112. Bachler, S., Ort, M., Krämer, S. D. & Dittrich, P. S. Permeation Studies across Symmetric and Asymmetric Membranes in Microdroplet Arrays. eng. *Analytical Chemistry* **93,** 5137–5144. ISSN: 1520-6882 (Mar. 2021).

113. Elani, Y., I. Solvas, X. C., B. Edel, J., V. Law, R. & Ces, O. Microfluidic generation of encapsulated droplet interface bilayer networks (multisomes) and their use as cell-like reactors. en. *Chemical Communications* **52.** Publisher: Royal Society of Chemistry, 5961–5964. http://pubs.rsc.org/en/content/articlelanding/2016/cc/c6cc01434h (2021) (2016).

114. Milianta, P. J., Muzzio, M., Denver, J., Cawley, G. & Lee, S. Water Permeability across Symmetric and Asymmetric Droplet Interface Bilayers: Interaction of Cholesterol Sulfate with DPhPC. eng. *Langmuir: the ACS journal of surfaces and colloids* **31,** 12187–12196. ISSN: 1520-5827 (Nov. 2015).

115. Braziel, S., Sullivan, K. & Lee, S. Quantitative Raman microspectroscopy for water permeability parameters at a droplet interface bilayer. en. *Analyst* **143.** Publisher: The Royal Society of Chemistry, 747–755. ISSN: 1364-5528. http://pubs.rsc.org/en/content/articlelanding/2018/an/c7an01349c (2021) (Jan. 2018).

116. Livingston, J. N. *et al.* Binding and molecular weight properties of the insulin receptor from omental and subcutaneous adipocytes in human obesity. eng. *Diabetologia* **27,** 447–453. ISSN: 0012-186X (Oct. 1984).

117. Carreras, P. *et al.* A DROPLET TRAPPING MICROFLUIDIC DEVICE FOR THE STUDY OF MASS-TRANSPORT ACROSS DROPLET INTERFACE BILAYERS. en, 3.

118. Bayley, H. *et al.* Droplet interface bilayers. *Molecular bioSystems* **4,** 1191–1208. ISSN: 1742-206X. https://www.ncbi.nlm.nih.gov/pmc/articles/PMC2763081/ (2020) (Dec. 2008).

119. Malmstadt, N., Nash, M. A., Purnell, R. F. & Schmidt, J. J. Automated Formation of Lipid-Bilayer Membranes in a Microfluidic Device. en. *Nano Letters* **6,** 1961–1965. ISSN: 1530-6984, 1530-6992. https://pubs.acs.org/doi/10.1021/nl0611034 (2020) (Sept. 2006).

120. Carreras, P., Law, R. V., Brooks, N., Seddon, J. M. & Ces, O. Microfluidic generation of droplet interface bilayer networks incorporating real-time size sorting in linear and non-linear configurations. *Biomicrofluidics* **8.** ISSN: 1932-1058. https://www.ncbi.nlm.nih.gov/pmc/articles/PMC4222292/ (2020) (Oct. 2014).

121. Sui, G. *et al.* Solution-phase surface modification in intact poly(dimethylsiloxane) microfluidic channels. eng. *Analytical Chemistry* **78,** 5543–5551. ISSN: 0003-2700 (Aug. 2006).

122. Zhou, J., Ellis, A. V. & Voelcker, N. H. Recent developments in PDMS surface modification for microfluidic devices. en. *ELECTROPHORESIS* **31.** _eprint: https://onlinelibrary.wiley.com/doi/pdf/10.1002/elps.200900475, 2–16. ISSN: 1522-2683. http://analyticalsciencejournals.onlinelibrary.wiley.com/doi/abs/10.1002/elps.200900475 (2021) (2010).

123. Trantidou, T., S. Friddin, M., Salehi-Reyhani, A., Ces, O. & Elani, Y. Droplet microfluidics for the construction of compartmentalised model membranes. en. *Lab on a Chip* **18.** Publisher: Royal Society of Chemistry, 2488–2509. http:

//pubs.rsc.org/en/content/articlelanding/2018/lc/c8lc00028j (2021) (2018).

124. Shirtcliffe, N. J., Toon, R. & Roach, P. Surface treatments for microfluidic biocompatibility. eng. *Methods in Molecular Biology (Clifton, N.J.)* **949,** 241–268. ISSN: 1940-6029 (2013).

125. Hillborg, H. & Gedde, U. W. Hydrophobicity changes in silicone rubbers. *IEEE Transactions on Dielectrics and Electrical Insulation* **6.** Conference Name: IEEE Transactions on Dielectrics and Electrical Insulation, 703–717. ISSN: 1558-4135 (Dec. 1999).

126. Homma, H. *et al.* Diffusion of low molecular weight siloxane from bulk to surface. *IEEE Transactions on Dielectrics and Electrical Insulation* **6,** 370–375. ISSN: 1070-9878 (June 1999).

127. Larson, B. J. *et al.* Long-term reduction in poly(dimethylsiloxane) surface hydrophobicity via cold-plasma treatments. eng. *Langmuir: the ACS journal of surfaces and colloids* **29,** 12990–12996. ISSN: 1520-5827 (Oct. 2013).

128. Debon, A. P., Wootton, R. C. R. & Elvira, K. S. Droplet confinement and leakage: Causes, underlying effects, and amelioration strategies. *Biomicrofluidics* **9.** ISSN: 1932-1058. https://www.ncbi.nlm.nih.gov/pmc/articles/PMC4409622/ (2021) (Apr. 2015).

129. Bian, P., Wang, Y. & McCarthy, T. J. Rediscovering Silicones: The Anomalous Water Permeability of "Hydrophobic" PDMS Suggests Nanostructure and Applications in Water Purification and Anti-Icing. eng. *Macromolecular Rapid Communications* **42,** e2000682. ISSN: 1521-3927 (Mar. 2021).

130. Sarles, S. A. & Leo, D. J. Physical encapsulation of droplet interface bilayers for durable, portable biomolecular networks. eng. *Lab on a Chip* **10,** 710–717. ISSN: 1473-0197 (Mar. 2010).

131. Bjork, S. M., Sjostrom, S. L., Andersson-Svahn, H. & Joensson, H. N. Metabolite profiling of microfluidic cell culture conditions for droplet based screening. *Biomicrofluidics* **9.** ISSN: 1932-1058. https://www.ncbi.nlm.nih.gov/pmc/articles/PMC4560712/ (2021) (Aug. 2015).

132. Park, J. W., Na, S., Kang, M., Sim, S. J. & Jeon, N. L. PDMS microchannel surface modification with teflon for algal lipid research. en. *BioChip Journal* **11,** 180–186. ISSN: 2092-7843. https://doi.org/10.1007/s13206-017-1302-0 (2018) (Sept. 2017).

133. Shemesh, J. *et al.* Stationary nanoliter droplet array with a substrate of choice for single adherent/nonadherent cell incubation and analysis. en. *Proceedings of the National Academy of Sciences* **111.** Publisher: National Academy of Sciences Section: Biological Sciences, 11293–11298. ISSN: 0027-8424, 1091-6490. https://www.pnas.org/content/111/31/11293 (2021) (Aug. 2014).

134. Bhattacharya, S., Datta, A., Berg, J. & Gangopadhyay, S. Studies on Surface Wettability of Poly(Dimethyl) Siloxane (PDMS) and Glass Under Oxygen-Plasma Treatment and Correlation With Bond Strength. *Microelectromechanical Systems, Journal of* **14,** 590–597 (July 2005).

135. Eddington, D. T., Puccinelli, J. P. & Beebe, D. J. Thermal aging and reduced hydrophobic recovery of polydimethylsiloxane. *Sensors and Actuators B: Chemical* **114,** 170–172. ISSN: 0925-4005. http://www.sciencedirect.com/science/article/pii/S092540050500451X (2018) (Mar. 2006).

136. Zheng, F. *et al.* The surface structure and hydrophobic recovery of poly-dimethylsiloxane insulator after Ar plasma treatment. *JJAP Conference Proceedings* **2.** ISBN: 9784863484450. https://journals.jsap.jp (2021) (May 2014).

137. Bodas, D. & Khan-Malek, C. Hydrophilization and hydrophobic recovery of PDMS by oxygen plasma and chemical treatment—An SEM investigation.

Sensors and Actuators B: Chemical **123,** 368–373. ISSN: 0925-4005. http://www.sciencedirect.com/science/article/pii/S0925400506006113 (2018) (Apr. 2007).

138. Jokinen, V., Suvanto, P. & Franssila, S. Oxygen and nitrogen plasma hydrophilization and hydrophobic recovery of polymers. *Biomicrofluidics* **6,** 016501. http://aip.scitation.org/doi/abs/10.1063/1.3673251 (2018) (Jan. 2012).

139. Wong, I. & Ho, C.-M. Surface molecular property modifications for poly(dimethylsiloxane) (PDMS) based microfluidic devices. en. *Microfluidics and Nanofluidics* **7,** 291. ISSN: 1613-4982, 1613-4990. https://link.springer.com/article/10.1007/s10404-009-0443-4 (2017) (Sept. 2009).

140. Dalvi, V. H. & Rossky, P. J. Molecular origins of fluorocarbon hydrophobicity. eng. *Proceedings of the National Academy of Sciences of the United States of America* **107,** 13603–13607. ISSN: 1091-6490 (Aug. 2010).

141. Drummond, C. J., Georgaklis, G. & Chan, D. Y. C. Fluorocarbons: Surface Free Energies and van der Waals Interaction. *Langmuir* **12,** 2617–2621. ISSN: 0743-7463. http://dx.doi.org/10.1021/la951020v (2017) (Jan. 1996).

142. Arkles, B. Silane Coupling Agents. en, 76.

143. Zec, H. C. *et al.* Method for controlling water evaporation in PDMS-based microfluidic devices. en, 3.

144. De Givenchy, E. T. *et al.* Fabrication of Superhydrophobic PDMS Surfaces by Combining Acidic Treatment and Perfluorinated Monolayers. *Langmuir* **25,** 6448–6453. ISSN: 0743-7463. http://dx.doi.org/10.1021/la900064m (2017) (June 2009).

145. Dangla, R., Gallaire, F. & Baroud, C. N. Microchannel deformations due to solvent-induced PDMS swelling. eng. *Lab on a Chip* **10,** 2972–2978. ISSN: 1473-0197 (Nov. 2010).

146. Law, K.-Y. Definitions for Hydrophilicity, Hydrophobicity, and Superhydrophobicity: Getting the Basics Right. eng. *The Journal of Physical Chemistry Letters* **5,** 686–688. ISSN: 1948-7185 (Feb. 2014).

147. Mueller, P., Rudin, D. O., Ti Tien, H. & Wescott, W. C. Reconstitution of Cell Membrane Structure in vitro and its Transformation into an Excitable System. en. *Nature* **194.** Number: 4832 Publisher: Nature Publishing Group, 979–980. ISSN: 1476-4687. https://www.nature.com/articles/194979a0 (2020) (June 1962).

148. Bangham, A. D., Hill, M. W. & Miller, N. G. A. en. in *Methods in Membrane Biology: Volume 1* (ed Korn, E. D.) 1–68 (Springer US, Boston, MA, 1974). ISBN: 978-1-4615-7422-4. https://doi.org/10.1007/978-1-4615-7422-4_1 (2020).

149. Carugo, D., Bottaro, E., Owen, J., Stride, E. & Nastruzzi, C. Liposome production by microfluidics: potential and limiting factors. en. *Scientific Reports* **6.** Number: 1 Publisher: Nature Publishing Group, 25876. ISSN: 2045-2322. https://www.nature.com/articles/srep25876 (2020) (May 2016).

150. Robinson, T. en. in *Advances in Biomembranes and Lipid Self-Assembly* (ed Lipowsky, R.) 271–315 (Academic Press, Jan. 2019). http://www.sciencedirect.com/science/article/pii/S2451963419300275 (2020).

151. Deng, N.-N. & Huck, W. T. S. Microfluidic Formation of Monodisperse Coacervate Organelles in Liposomes. en. *Angewandte Chemie International Edition* **56.** _eprint: https://onlinelibrary.wiley.com/doi/pdf/10.1002/anie.201703145,

9736–9740. ISSN: 1521-3773. http://onlinelibrary.wiley.com/doi/abs/10.1002/anie.201703145 (2020) (2017).

152. Ugrinic, M. *et al.* Microfluidic formation of proteinosomes. en. *Chemical Communications* **54.** Publisher: The Royal Society of Chemistry, 287–290. ISSN: 1364-548X. http://pubs.rsc.org/en/content/articlelanding/2018/cc/c7cc08466h (2020) (Jan. 2018).

153. Hutter, I., Müller, E., Kristiansen, P. M., Kresak, S. & Tiefenauer, L. Polymer-based microfluidic device for measuring membrane protein activities. en. *Microfluidics and Nanofluidics* **14,** 421–429. ISSN: 1613-4990. https://doi.org/10.1007/s10404-012-1061-0 (2020) (Mar. 2013).

154. Dixit, S. S., Pincus, A., Guo, B. & Faris, G. W. Droplet Shape Analysis and Permeability Studies in Droplet Lipid Bilayers. *Langmuir : the ACS journal of surfaces and colloids* **28,** 7442–7451. ISSN: 0743-7463. https://www.ncbi.nlm.nih.gov/pmc/articles/PMC3502024/ (2020) (May 2012).

155. Hwang, W. L., Holden, M. A., White, S. & Bayley, H. Electrical Behavior of Droplet Interface Bilayer Networks: Experimental Analysis and Modeling. *Journal of the American Chemical Society* **129.** Publisher: American Chemical Society, 11854–11864. ISSN: 0002-7863. https://doi.org/10.1021/ja074071a (2020) (Sept. 2007).

156. Creasy, M. A. & Leo, D. J. Non-invasive measurement techniques for measuring properties of droplet interface bilayers. *Smart Material Structures* **19,** 094016. ISSN: 0964-1726. http://adsabs.harvard.edu/abs/2010SMaS...19i4016C (2021) (Sept. 2010).

157. Freeman, E. C., Najem, J. S., Sukharev, S., Philen, M. K. & Leo, D. J. The mechanoelectrical response of droplet interface bilayer membranes. en. *Soft Matter* **12.** Publisher: The Royal Society of Chemistry, 3021–3031. ISSN: 1744-

6848. http://pubs.rsc.org/en/content/articlelanding/2016/sm/c5sm02779a (2021) (Mar. 2016).

158. *Brain Extract Total* en-US. https://avantilipids.com/product/131101 (2021).

159. Najem, J. S. *et al.* Assembly and Characterization of Biomolecular Memristors Consisting of Ion Channel-doped Lipid Membranes. eng. *Journal of Visualized Experiments: JoVE.* ISSN: 1940-087X (Mar. 2019).

160. Najem, J. S. *et al.* Memristive Ion Channel-Doped Biomembranes as Synaptic Mimics. *ACS Nano* **12.** Publisher: American Chemical Society, 4702–4711. ISSN: 1936-0851. https://doi.org/10.1021/acsnano.8b01282 (2020) (May 2018).

161. Yanagisawa, M., Yoshida, T.-a., Furuta, M., Nakata, S. & Tokita, M. Adhesive force between paired microdroplets coated with lipid monolayers. en. *Soft Matter* **9.** Publisher: The Royal Society of Chemistry, 5891–5897. ISSN: 1744-6848. http://pubs.rsc.org/en/content/articlelanding/2013/sm/c3sm50938a (2021) (June 2013).

162. Ringley, J. D. & Sarles, S. A. Temperature-Controlled Assembly and Characterization of a Droplet Interface Bilayer. eng. *Journal of Visualized Experiments: JoVE.* ISSN: 1940-087X (Apr. 2021).

163. Lee, S., Kim, D. H. & Needham, D. Equilibrium and Dynamic Interfacial Tension Measurements at Microscopic Interfaces Using a Micropipet Technique. 1. A New Method for Determination of Interfacial Tension. *Langmuir* **17.** Publisher: American Chemical Society, 5537–5543. ISSN: 0743-7463. https://doi.org/10.1021/la0103259 (2021) (Sept. 2001).

164. Solvas, X. C. i. & deMello, A. Droplet microfluidics: recent developments and future applications. en. *Chemical Communications* **47.** Publisher: The Royal

Society of Chemistry, 1936–1942. ISSN: 1364-548X. http://pubs.rsc.org/en/content/articlelanding/2011/cc/c0cc02474k (2020) (Feb. 2011).

165. Venkatesan, G. A. *et al.* Adsorption Kinetics Dictate Monolayer Self-Assembly for Both Lipid-In and Lipid-Out Approaches to Droplet Interface Bilayer Formation. eng. *Langmuir: the ACS journal of surfaces and colloids* **31,** 12883–12893. ISSN: 1520-5827 (Dec. 2015).

166. Abbyad, P., Dangla, R., Alexandrou, A. & Baroud, C. N. Rails and anchors: guiding and trapping droplet microreactors in two dimensions. en. *Lab on a Chip* **11,** 813–821. ISSN: 1473-0189. https://pubs.rsc.org/en/content/articlelanding/2011/lc/c0lc00104j (2020) (Mar. 2011).

167. Niu, X., Gulati, S., Edel, J. B. & deMello, A. J. Pillar-induced droplet merging in microfluidic circuits. en. *Lab on a Chip* **8.** Publisher: The Royal Society of Chemistry, 1837–1841. ISSN: 1473-0189. http://pubs.rsc.org/en/content/articlelanding/2008/lc/b813325e (2021) (Nov. 2008).

168. Antonietti, M. & Förster, S. Vesicles and Liposomes: A Self-Assembly Principle Beyond Lipids. en. *Advanced Materials* **15,** 1323–1333. ISSN: 1521-4095. https://onlinelibrary.wiley.com/doi/abs/10.1002/adma.200300010 (2020) (2003).

169. Boggs, J. M. Lipid intermolecular hydrogen bonding: influence on structural organization and membrane function. eng. *Biochimica Et Biophysica Acta* **906,** 353–404. ISSN: 0006-3002 (Oct. 1987).

170. *Liver PC* en-US. Library Catalog: avantilipids.com. https://avantilipids.com/product/840055 (2020).

171. *Phase Transition Temperatures for Glycerophospholipids* en-US. Library Catalog: avantilipids.com. https://avantilipids.com/tech-support/physical-properties/phase-transition-temps (2020).

172. McMahon, H. T. & Boucrot, E. Membrane curvature at a glance. en. *J Cell Sci* **128,** 1065–1070. ISSN: 0021-9533, 1477-9137. http://jcs.biologists.org/content/128/6/1065 (2018) (Mar. 2015).

173. Furse, S. *et al.* Lipid membrane curvature induced by distearoyl phosphatidylinositol 4-phosphate. en. *Soft Matter* **8.** Publisher: The Royal Society of Chemistry, 3090–3093. ISSN: 1744-6848. https://pubs.rsc.org/en/content/articlelanding/2012/sm/c2sm07358g (2021) (Feb. 2012).

174. Shearman, G. C., Ces, O., Templer, R. H. & Seddon, J. M. Inverse lyotropic phases of lipids and membrane curvature. eng. *Journal of Physics. Condensed Matter: An Institute of Physics Journal* **18,** S1105–1124. ISSN: 0953-8984 (July 2006).

175. Janmey, P. A. & Kinnunen, P. K. J. Biophysical properties of lipids and dynamic membranes. English. *Trends in Cell Biology* **16.** Publisher: Elsevier, 538–546. ISSN: 0962-8924, 1879-3088. https://www.cell.com/trends/cell-biology/abstract/S0962-8924(06)00226-1 (2021) (Oct. 2006).

176. Beltramo, P. J., Scheidegger, L. & Vermant, J. Toward Realistic Large-Area Cell Membrane Mimics: Excluding Oil, Controlling Composition, and Including Ion Channels. *Langmuir* **34.** Publisher: American Chemical Society, 5880–5888. ISSN: 0743-7463. https://doi.org/10.1021/acs.langmuir.8b00837 (2021) (May 2018).

177. Huang, Y., Chandran Suja, V., Tajuelo, J. & Fuller, G. G. Surface energy and separation mechanics of droplet interface phospholipid bilayers. *Journal of The Royal Society Interface* **18.** Publisher: Royal Society, 20200860. https://royalsocietypublishing.org/doi/10.1098/rsif.2020.0860 (2021) (2021).

178. Boreyko, J. B., Polizos, G., Datskos, P. G., Sarles, S. A. & Collier, C. P. Air-stable droplet interface bilayers on oil-infused surfaces. en. *Proceedings of the National Academy of Sciences* **111.** Publisher: National Academy of Sciences Section: Biological Sciences, 7588–7593. ISSN: 0027-8424, 1091-6490. https://www.pnas.org/content/111/21/7588 (2021) (May 2014).

179. Baillie, T. A. Metabolism and Toxicity of Drugs. Two Decades of Progress in Industrial Drug Metabolism. *Chemical Research in Toxicology* **21,** 129–137. ISSN: 0893-228X. https://doi.org/10.1021/tx7002273 (2019) (Jan. 2008).

180. Chung, T. D. Y., Terry, D. B. & Smith, L. H. eng. in *Assay Guidance Manual* (eds Sittampalam, G. S. *et al.*) (Eli Lilly & Company and the National Center for Advancing Translational Sciences, Bethesda (MD), 2004). http://www.ncbi.nlm.nih.gov/books/NBK326710/ (2019).

181. Volpe, D. A. Drug-permeability and transporter assays in Caco-2 and MDCK cell lines. eng. *Future Medicinal Chemistry* **3,** 2063–2077. ISSN: 1756-8927 (Dec. 2011).

182. Irvine, J. D. *et al.* MDCK (Madin-Darby canine kidney) cells: A tool for membrane permeability screening. eng. *Journal of Pharmaceutical Sciences* **88,** 28–33. ISSN: 0022-3549 (Jan. 1999).

183. Purushothaman, S., Cama, J. & F. Keyser, U. Dependence of norfloxacin diffusion across bilayers on lipid composition. en. *Soft Matter* **12,** 2135–2144. https://pubs.rsc.org/en/content/articlelanding/2016/sm/c5sm02371h (2019) (2016).

184. Czekalska, M., Kaminski, T., Makuch, K. & Garstecki, P. Passive and parallel microfluidic formation of droplet interface bilayers (DIBs) for measurement of leakage of small molecules through artificial phospholipid membranes. *Sensors and Actuators B: Chemical* **286** (May 2019).

185. Tonooka, T., Sato, K., Osaki, T., Kawano, R. & Takeuchi, S. Lipid Bilayers on a Picoliter Microdroplet Array for Rapid Fluorescence Detection of Membrane Transport. en. *Small* **10,** 3275–3282. ISSN: 1613-6829. http://onlinelibrary.wiley.com/doi/abs/10.1002/smll.201303332 (2021) (2014).

186. Soga, N., Watanabe, R. & Noji, H. Attolitre-sized lipid bilayer chamber array for rapid detection of single transporters. en. *Scientific Reports* **5.** Number: 1 Publisher: Nature Publishing Group, 11025. ISSN: 2045-2322. https://www.nature.com/articles/srep11025 (2021) (June 2015).

187. Urban, M. *et al.* Highly Parallel Transport Recordings on a Membrane-on-Nanopore Chip at Single Molecule Resolution. *Nano Letters* **14.** Publisher: American Chemical Society, 1674–1680. ISSN: 1530-6984. https://doi.org/10.1021/nl5002873 (2021) (Mar. 2014).

188. Czekalska, M. A., Kaminski, T. S., Horka, M., Jakiela, S. & Garstecki, P. An Automated Microfluidic System for the Generation of Droplet Interface Bilayer Networks. *Micromachines* **8.** ISSN: 2072-666X. https://www.ncbi.nlm.nih.gov/pmc/articles/PMC6190347/ (2020) (Mar. 2017).

189. Jones, H. M. & Rowland-Yeo, K. Basic Concepts in Physiologically Based Pharmacokinetic Modeling in Drug Discovery and Development. en. *CPT: Pharmacometrics & Systems Pharmacology* **2,** 63. ISSN: 2163-8306. https://ascpt.onlinelibrary.wiley.com/doi/abs/10.1038/psp.2013.41 (2020) (2013).

190. Stippler, E., Kopp, S. & Dressman, J. B. Comparison of US Pharmacopeia Simulated Intestinal Fluid TS (without pancreatin) and Phosphate Standard Buffer pH 6.8, TS of the International Pharmacopoeia with Respect to Their Use in In Vitro Dissolution Testing. en. *Dissolution Technologies* **11,** 6–10. ISSN: 1521298X. http://www.dissolutiontech.com/DTresour/200405Articles/DT200405_A01.pdf (2019) (2004).

191. Lang, F. Mechanisms and significance of cell volume regulation. *Journal of the American College of Nutrition* **26,** 613S–623S (2006).

192. Gilbert, D. L. Buffering of Blood Plasma. *The Yale Journal of Biology and Medicine* **32,** 378–389. ISSN: 0044-0086. https://www.ncbi.nlm.nih.gov/pmc/articles/PMC2604138/ (2019) (Apr. 1960).

193. Forstner, G. G., Tanaka, K. & Isselbacher, K. J. Lipid composition of the isolated rat intestinal microvillus membrane. en. *Biochemical Journal* **109,** 51–59. ISSN: 0264-6021, 1470-8728. http://www.biochemj.org/content/109/1/51 (2018) (Aug. 1968).

194. Schwarz, S. M., Hostetler, B., Ling, S., Mone, M. & Watkins, J. B. Intestinal membrane lipid composition and fluidity during development in the rat. *American Journal of Physiology-Gastrointestinal and Liver Physiology* **248,** G200–G207. ISSN: 0193-1857. http://www.physiology.org/doi/abs/10.1152/ajpgi.1985.248.2.g200 (2018) (Feb. 1985).

195. Brasitus, T. A., Yeh, K.-Y., Holt, P. R. & Schachter, D. Lipid fluidity and composition of intestinal microvillus membranes isolated from rats of different ages. *Biochimica et Biophysica Acta (BBA) - Biomembranes* **778,** 341–348. ISSN: 0005-2736. http://www.sciencedirect.com/science/article/pii/000527368490378X (2018) (Dec. 1984).

196. Christiansen, K. & Carlsen, J. Microvillus membrane vesicles from pig small intestine Purity and lipid composition. *Biochimica et Biophysica Acta (BBA) - Biomembranes* **647,** 188–195. ISSN: 0005-2736. http://www.sciencedirect.com/science/article/pii/0005273681902455 (2018) (Oct. 1981).

197. Hauser, H., Howell, K., Dawson, R. M. C. & Bowyer, D. E. Rabbit small intestinal brush border membrane. Preparation and lipid composition. *Biochimica et Biophysica Acta (BBA) - Biomembranes* **602,** 567–577. ISSN: 0005-2736. http:

//www.sciencedirect.com/science/article/pii/0005273680903351 (2018) (Nov. 1980).

198. Brasitus, T. A., Davidson, N. O. & Schachter, D. Variations in dietary triacylglycerol saturation alter the lipid composition and fluidity of rat intestinal plasma membranes. *Biochimica et Biophysica Acta (BBA) - Biomembranes* **812,** 460–472. ISSN: 0005-2736. http://www.sciencedirect.com/science/article/pii/0005273685903219 (2018) (Jan. 1985).

199. Ginzberg, M. B., Kafri, R. & Kirschner, M. On being the right (cell) size. *Science (New York, N.Y.)* **348,** 1245075. ISSN: 0036-8075. https://www.ncbi.nlm.nih.gov/pmc/articles/PMC4533982/ (2021) (May 2015).

200. MacLeod, R. J. *et al.* Corticostatic peptides cause nifedipine-sensitive volume reduction in jejunal villus enterocytes. eng. *Proceedings of the National Academy of Sciences of the United States of America* **88,** 552–556. ISSN: 0027-8424 (Jan. 1991).

201. Buschmann, R. J. & Manke, D. J. Morphometric analysis of the membranes and organelles of small intestinal enterocytes. I. Fasted hamster. eng. *Journal of Ultrastructure Research* **76,** 1–14. ISSN: 0022-5320 (July 1981).

202. Crowe, P. T. & Marsh, M. N. Morphometric analysis of small intestinal mucosa. IV. Determining cell volumes. eng. *Virchows Archiv. A, Pathological Anatomy and Histopathology* **422,** 459–466. ISSN: 0174-7398 (1993).

203. Stein, S., Bogdahn, M., Rosenbaum, C., Weitschies, W. & Seidlitz, A. Distribution of fluorescein sodium and triamcinolone acetonide in the simulated liquefied and vitrectomized Vitreous Model with simulated eye movements. eng. *European Journal of Pharmaceutical Sciences: Official Journal of the European Federation for Pharmaceutical Sciences* **109,** 233–243. ISSN: 1879-0720 (Nov. 2017).

204. Khosroshahi, M. E. & Mahmoodi, M. Fabrication, Visualization and Analysis of Fluorescein Sodium Encapsulated PLGA@CS Nanoparticles as Model for Photothermomechanical Drug Delivery Using Pulsed 532 nm Laser. en. *Advances in Nanoparticles* **7,** 720–726. https://m.scirp.org/papers/abstract/87066 (2019) (Aug. 2018).

205. Liu, Y., Miyoshi, H. & Nakamura, M. Novel drug delivery system of hollow mesoporous silica nanocapsules with thin shells: Preparation and fluorescein isothiocyanate (FITC) release kinetics. en. *Colloids and Surfaces B: Biointerfaces* **58,** 180–187. ISSN: 0927-7765. http://www.sciencedirect.com/science/article/pii/S0927776507001191 (2019) (Aug. 2007).

206. Fisher, K. A., Huddersman, K. D. & Taylor, M. J. Comparison of Micro- and Mesoporous Inorganic Materials in the Uptake and Release of the Drug Model Fluorescein and Its Analogues. en. *Chemistry – A European Journal* **9,** 5873–5878. ISSN: 1521-3765. https://onlinelibrary.wiley.com/doi/abs/10.1002/chem.200304764 (2019) (2003).

207. Maurer, J. M. *et al.* Gastrointestinal pH and Transit Time Profiling in Healthy Volunteers Using the IntelliCap System Confirms Ileo-Colonic Release of ColoPulse Tablets. *PLoS ONE* **10.** ISSN: 1932-6203. https://www.ncbi.nlm.nih.gov/pmc/articles/PMC4503763/ (2019) (July 2015).

208. Kokubo, T. & Takadama, H. How useful is SBF in predicting in vivo bone bioactivity? en. *Biomaterials* **27,** 2907–2915. ISSN: 0142-9612. https://www.sciencedirect.com/science/article/pii/S0142961206000457 (2021) (May 2006).

209. Berginc, K., Zakelj, S., Levstik, L., Ursic, D. & Kristl, A. Fluorescein transport properties across artificial lipid membranes, Caco-2 cell monolayers and rat jejunum. eng. *European Journal of Pharmaceutics and Biopharmaceutics: Of-*

ficial Journal of Arbeitsgemeinschaft Fur Pharmazeutische Verfahrenstechnik e.V **66,** 281–285. ISSN: 0939-6411 (May 2007).

210. Sjöback, R., Nygren, J. & Kubista, M. Characterization of fluorescein-oligonucleotide conjugates and measurement of local electrostatic potential. eng. *Biopolymers* **46,** 445–453. ISSN: 0006-3525 (Dec. 1998).

211. Martin, M. M. & Lindqvist, L. The pH dependence of fluorescein fluorescence. en. *Journal of Luminescence* **10,** 381–390. ISSN: 0022-2313. http://www.sciencedirect.com/science/article/pii/0022231375900034 (2019) (July 1975).

212. Doughty, M. J. pH dependent spectral properties of sodium fluorescein ophthalmic solutions revisited. eng. *Ophthalmic & Physiological Optics: The Journal of the British College of Ophthalmic Opticians (Optometrists)* **30,** 167–174. ISSN: 1475-1313 (Mar. 2010).

213. Worthley, L. I. G., Guerin, M. & Pain, R. W. For Calculating Osmolality, the Simplest Formula is the Best. en. *Anaesthesia and Intensive Care* **15.** Publisher: SAGE Publications Ltd, 199–202. ISSN: 0310-057X. https://doi.org/10.1177/0310057X8701500214 (2020) (May 1987).

214. Soldin, O. P., Chung, S. H. & Mattison, D. R. *Sex Differences in Drug Disposition* en. Research article. 2011. https://www.hindawi.com/journals/bmri/2011/187103/ (2019).

215. Sugano, K., Takata, N., Machida, M., Saitoh, K. & Terada, K. Prediction of passive intestinal absorption using bio-mimetic artificial membrane permeation assay and the paracellular pathway model. eng. *International Journal of Pharmaceutics* **241,** 241–251. ISSN: 0378-5173 (July 2002).

216. Sugano, K., Nabuchi, Y., Machida, M. & Aso, Y. Prediction of human intestinal permeability using artificial membrane permeability. *International Journal of*

Pharmaceutics **257,** 245–251. ISSN: 0378-5173. http://www.sciencedirect.com/science/article/pii/S0378517303001613 (2018) (May 2003).

217. Schwartz, J. B. The Influence of Sex on Pharmacokinetics. en. *Clinical Pharmacokinetics* **42,** 107–121. ISSN: 1179-1926. https://doi.org/10.2165/00003088-200342020-00001 (2021) (Feb. 2003).

218. Soldin, O. & Mattison, D. Sex Differences in Pharmacokinetics and Pharmacodynamics. *Clinical pharmacokinetics* **48,** 143–157. ISSN: 0312-5963. https://www.ncbi.nlm.nih.gov/pmc/articles/PMC3644551/ (2019) (2009).

219. Zucker, I. & Prendergast, B. J. Sex differences in pharmacokinetics predict adverse drug reactions in women. *Biology of Sex Differences* **11,** 32. ISSN: 2042-6410. https://doi.org/10.1186/s13293-020-00308-5 (2021) (June 2020).

220. Whitley, H. P. & Lindsey, W. Sex-Based Differences in Drug Activity. *American Family Physician* **80,** 1254–1258. ISSN: 0002-838X, 1532-0650. https://www.aafp.org/afp/2009/1201/p1254.html (2021) (Dec. 2009).

221. Bigos, K. L., Pollock, B. G., Stankevich, B. A. & Bies, R. R. Sex differences in the pharmacokinetics and pharmacodynamics of antidepressants: An updated review. English (US). *Gender Medicine* **6.** Publisher: Excerpta Medica, 522–543. ISSN: 1550-8579. https://jhu.pure.elsevier.com/en/publications/sex-differences-in-the-pharmacokinetics-and-pharmacodynamics-of-a-3 (2021) (Dec. 2009).

222. Franconi, F., Brunelleschi, S., Steardo, L. & Cuomo, V. Gender differences in drug responses. eng. *Pharmacological Research* **55,** 81–95. ISSN: 1043-6618 (Feb. 2007).

223. Grant, R., Lees, S., Legg, G. & Burdge, G. Gender differences in the PUFA-fatty acid composition of membrane phospholipids in rats. en. *Proceedings of the Nutrition Society* **67.** Publisher: Cambridge University Press. ISSN: 1475-2719,

0029-6651. https://www.cambridge.org/core/journals/proceedings-of-the-nutrition-society/article/gender-differences-in-the-pufafatty-acid-composition-of-membrane-phospholipids-in-rats/8F5EE3F284262B4B68A081ED03833C7F (2021) (May 2008).

224. Lohner, S., Fekete, K., Marosvölgyi, T. & Decsi, T. Gender differences in the long-chain polyunsaturated fatty acid status: systematic review of 51 publications. eng. *Annals of Nutrition & Metabolism* **62,** 98–112. ISSN: 1421-9697 (2013).

225. Fallingborg, J. Intraluminal pH of the human gastrointestinal tract. eng. *Danish Medical Bulletin* **46,** 183–196. ISSN: 0907-8916 (June 1999).

226. Peisajovich, S. G. & Shai, Y. Liposomes in identification and characterization of viral fusogenic peptides. eng. *Methods in Enzymology* **372,** 361–373. ISSN: 0076-6879 (2003).

227. Pardridge, W. M. The blood-brain barrier: Bottleneck in brain drug development. en. *NeuroRX* **2,** 3–14. ISSN: 1545-5343. https://doi.org/10.1602/neurorx.2.1.3 (2021) (Jan. 2005).

228. Campbell, S. D., Regina, K. J. & Kharasch, E. D. Significance of Lipid Composition in a Blood Brain Barrier-Mimetic PAMPA Assay. *Journal of biomolecular screening* **19,** 437–444. ISSN: 1087-0571. https://www.ncbi.nlm.nih.gov/pmc/articles/PMC4078735/ (2018) (Mar. 2014).

229. Tsinman, O., Tsinman, K., Sun, N. & Avdeef, A. Physicochemical Selectivity of the BBB Microenvironment Governing Passive Diffusion—Matching with a Porcine Brain Lipid Extract Artificial Membrane Permeability Model. *Pharmaceutical research* **28,** 337–363. ISSN: 0724-8741. https://www.ncbi.nlm.nih.gov/pmc/articles/PMC3034772/ (2021) (Feb. 2011).

230. Avdeef, A., Deli, M. A. & Neuhaus, W. en. in *Blood-Brain Barrier in Drug Discovery* 188–237 (John Wiley & Sons, Ltd, Jan. 2015). ISBN: 978-1-118-78852-3. http://onlinelibrary.wiley.com/doi/10.1002/9781118788523.ch10 (2021).

231. Müller, J., Esső, K., Dargó, G., Könczöl, Á. & Balogh, G. T. Tuning the predictive capacity of the PAMPA-BBB model. eng. *European Journal of Pharmaceutical Sciences: Official Journal of the European Federation for Pharmaceutical Sciences* **79,** 53–60. ISSN: 1879-0720 (Nov. 2015).

232. Natarajan, R., Northrop, N. & Yamamoto, B. Fluorescein Isothiocyanate (FITC)-Dextran Extravasation as a Measure of Blood-Brain Barrier Permeability. eng. *Current Protocols in Neuroscience* **79,** 9.58.1–9.58.15. ISSN: 1934-8576 (Apr. 2017).

233. Najem, J. S. *et al.* Activation of bacterial channel MscL in mechanically stimulated droplet interface bilayers. eng. *Scientific Reports* **5,** 13726. ISSN: 2045-2322 (Sept. 2015).

234. Müller, C. P. *et al.* Brain membrane lipids in major depression and anxiety disorders. eng. *Biochimica Et Biophysica Acta* **1851,** 1052–1065. ISSN: 0006-3002 (Aug. 2015).

235. Parekh, A., Smeeth, D., Milner, Y. & Thuret, S. The Role of Lipid Biomarkers in Major Depression. *Healthcare* **5.** ISSN: 2227-9032. https://www.ncbi.nlm.nih.gov/pmc/articles/PMC5371911/ (2021) (Feb. 2017).

236. Alves, A. C., Ribeiro, D., Nunes, C. & Reis, S. Biophysics in cancer: The relevance of drug-membrane interaction studies. eng. *Biochimica Et Biophysica Acta* **1858,** 2231–2244. ISSN: 0006-3002 (Sept. 2016).

237. Ran, S. & Thorpe, P. E. Phosphatidylserine is a marker of tumor vasculature and a potential target for cancer imaging and therapy. eng. *International Jour-*

nal of Radiation Oncology, Biology, Physics **54,** 1479–1484. ISSN: 0360-3016 (Dec. 2002).

238. Bogorad, M. I. & Searson, P. C. Real-time imaging and quantitative analysis of doxorubicin transport in a perfusable microvessel platform. eng. *Integrative Biology: Quantitative Biosciences from Nano to Macro* **8,** 976–984. ISSN: 1757-9708 (Sept. 2016).

239. Kauffman, M. K., Kauffman, M. E., Zhu, H., Jia, Z. & Li, Y. R. Fluorescence-Based Assays for Measuring Doxorubicin in Biological Systems. *Reactive oxygen species (Apex, N.C.)* **2,** 432–439. ISSN: 2380-2367. https://www.ncbi.nlm.nih.gov/pmc/articles/PMC5921830/ (2021) (2016).

240. Pautke, C. *et al.* Characterization of eight different tetracyclines: advances in fluorescence bone labeling. *Journal of Anatomy* **217,** 76–82. ISSN: 0021-8782. https://www.ncbi.nlm.nih.gov/pmc/articles/PMC2913014/ (2021) (July 2010).

241. Lingwood, D. & Simons, K. Lipid rafts as a membrane-organizing principle. eng. *Science (New York, N.Y.)* **327,** 46–50. ISSN: 1095-9203 (Jan. 2010).

242. Zachowski, A. Phospholipids in animal eukaryotic membranes: transverse asymmetry and movement. *Biochemical Journal* **294,** 1–14. ISSN: 0264-6021. https://www.ncbi.nlm.nih.gov/pmc/articles/PMC1134557/ (2021) (Aug. 1993).

243. *Brain Extract Polar* en-US. https://avantilipids.com/product/141101 (2021).

244. Chesler, M. Regulation and Modulation of pH in the Brain. *Physiological Reviews* **83.** Publisher: American Physiological Society, 1183–1221. ISSN: 0031-9333. https://journals.physiology.org/doi/full/10.1152/physrev.00010.2003 (2021) (Oct. 2003).

245. Hawkins, B. T., Ocheltree, S. M., Norwood, K. M. & Egleton, R. D. Decreased blood-brain barrier permeability to fluorescein in streptozotocin-treated rats. *Neuroscience letters* **411,** 1–5. ISSN: 0304-3940. https://www.ncbi.nlm.nih.gov/pmc/articles/PMC1785293/ (2021) (Jan. 2007).

246. Kaya, M. & Ahishali, B. en. in *Permeability Barrier: Methods and Protocols* (ed Turksen, K.) 369–382 (Humana Press, Totowa, NJ, 2011). ISBN: 978-1-61779-191-8. https://doi.org/10.1007/978-1-61779-191-8_25 (2021).

247. Barlow, N. E. *et al.* Measuring bilayer surface energy and curvature in asymmetric droplet interface bilayers. *Journal of The Royal Society Interface* **15.** Publisher: Royal Society, 20180610. https://royalsocietypublishing.org/doi/10.1098/rsif.2018.0610 (2020) (Nov. 2018).

248. Taylor, G. *et al.* Electrophysiological interrogation of asymmetric droplet interface bilayers reveals surface-bound alamethicin induces lipid flip-flop. eng. *Biochimica Et Biophysica Acta. Biomembranes* **1861,** 335–343. ISSN: 1879-2642 (2019).

249. F. Mohammed, F., El-Din, K. M. B. & Derayea, S. M. Switch on fluorescence probe for the selective determination of lisinopril in pharmaceutical formulations: application to content uniformity testing. en. *RSC Advances* **8.** Publisher: Royal Society of Chemistry, 16269–16277. http://pubs.rsc.org/en/content/articlelanding/2018/ra/c8ra01617h (2021) (2018).

250. Beatty, M. A., Selinger, A. J., Li, Y. & Hof, F. Parallel Synthesis and Screening of Supramolecular Chemosensors That Achieve Fluorescent Turn-on Detection of Drugs in Saliva. *Journal of the American Chemical Society* **141.** Publisher: American Chemical Society, 16763–16771. ISSN: 0002-7863. https://doi.org/10.1021/jacs.9b07073 (2021) (Oct. 2019).

251. Sugano, K., Nabuchi, Y., Machida, M. & Asoh, Y. Permeation characteristics of a hydrophilic basic compound across a bio-mimetic artificial membrane. eng. *International Journal of Pharmaceutics* **275,** 271–278. ISSN: 0378-5173 (May 2004).

252. Taylor, P. Ostwald ripening in emulsions. en. *Colloids and Surfaces A: Physicochemical and Engineering Aspects* **99.** Publisher: Elsevier, 175–185. ISSN: 0927-7757. http://www.sciencedirect.com/science/article/pii/0927775795031616 (2021) (June 1995).

253. Ziemecka, I., Steijn, V. v., M. Koper, G. J., T. Kreutzer, M. & Esch, J. H. v. All-aqueous core-shell droplets produced in a microfluidic device. en. *Soft Matter* **7.** Publisher: Royal Society of Chemistry, 9878–9880. http://pubs.rsc.org/en/content/articlelanding/2011/sm/c1sm06517c (2021) (2011).

254. Winterhalter, M. Black lipid membranes. en. *Current Opinion in Colloid & Interface Science* **5,** 250–255. ISSN: 1359-0294. https://www.sciencedirect.com/science/article/pii/S1359029400000637 (2021) (July 2000).

255. Oiki, S. en. in *Patch Clamp Techniques: From Beginning to Advanced Protocols* (ed Okada, Y.) 229–275 (Springer Japan, Tokyo, 2012). ISBN: 978-4-431-53993-3. https://doi.org/10.1007/978-4-431-53993-3_16 (2021).

256. Peetla, C., Stine, A. & Labhasetwar, V. Biophysical interactions with model lipid membranes: applications in drug discovery and drug delivery. eng. *Molecular Pharmaceutics* **6,** 1264–1276. ISSN: 1543-8384 (Oct. 2009).

257. Carreras, P. *et al.* A droplet trapping microfluidic device for the study of mass-transport across droplet interface bilayers. *18th International Conference on Miniaturized Systems for Chemistry and Life Sciences, MicroTAS 2014,* 1620–1622 (Jan. 2014).

258. Allen-Benton, M., Findlay, H. E. & Booth, P. J. Probing membrane protein properties using droplet interface bilayers. en. *Experimental Biology and Medicine* **244.** Publisher: SAGE Publications, 709–720. ISSN: 1535-3702. https://doi.org/10.1177/1535370219847939 (2020) (May 2019).

259. Booth, M. J., Cazimoglu, I. & Bayley, H. Controlled deprotection and release of a small molecule from a compartmented synthetic tissue module. en. *Communications Chemistry* **2.** Number: 1 Publisher: Nature Publishing Group, 1–8. ISSN: 2399-3669. https://www.nature.com/articles/s42004-019-0244-y (2020) (Dec. 2019).

260. Smith, S. M. Strategies for the purification of membrane proteins. eng. *Methods in Molecular Biology (Clifton, N.J.)* **681,** 485–496. ISSN: 1940-6029 (2011).

261. Giacomini, K. M. *et al.* Membrane transporters in drug development. eng. *Nature Reviews. Drug Discovery* **9,** 215–236. ISSN: 1474-1784 (Mar. 2010).

262. Makhoul-Mansour, M. M. & Freeman, E. C. Droplet-Based Membranous Soft Materials. eng. *Langmuir: the ACS journal of surfaces and colloids* **37,** 3231–3247. ISSN: 1520-5827 (Mar. 2021).

263. Sarles, S. A., Madden, J. D. W. & Leo, D. J. Hair cell inspired mechanotransduction with a gel-supported, artificial lipid membrane. en. *Soft Matter* **7,** 4644. ISSN: 1744-683X, 1744-6848. http://xlink.rsc.org/?DOI=c1sm05120b (2020) (2011).

264. Tamaddoni, N., Freeman, E. C. & Sarles, S. A. Sensitivity and directionality of lipid bilayer mechanotransduction studied using a revised, highly durable membrane-based hair cell sensor. en. *Smart Materials and Structures* **24.** Publisher: IOP Publishing, 065014. ISSN: 0964-1726. https://doi.org/10.1088%2F0964-1726%2F24%2F6%2F065014 (2020) (May 2015).

265. Venkatesan, G. A. *et al.* Evaporation-induced monolayer compression improves droplet interface bilayer formation using unsaturated lipids. *Biomicrofluidics* **12.** ISSN: 1932-1058. https://www.ncbi.nlm.nih.gov/pmc/articles/PMC5832467/ (2020) (Mar. 2018).

266. Barlow, N. *et al.* Multiplexed droplet Interface bilayer formation. en. *Lab on a Chip* **16.** Publisher: Royal Society of Chemistry, 4653–4657. https://pubs.rsc.org/en/content/articlelanding/2016/lc/c6lc01011c (2020) (2016).

267. Redfern, D. A. & Gericke, A. Domain Formation in Phosphatidylinositol Monophosphate/Phosphatidylcholine Mixed Vesicles. en. *Biophysical Journal* **86,** 2980–2992. ISSN: 0006-3495. http://www.sciencedirect.com/science/article/pii/S0006349504743489 (2020) (May 2004).

268. Lindsey, H., Petersen, N. O. & Chan, S. I. Physicochemical characterization of 1,2-diphytanoyl-sn-glycero-3-phosphocholine in model membrane systems. eng. *Biochimica Et Biophysica Acta* **555,** 147–167. ISSN: 0006-3002 (July 1979).

269. Scheuble, N. *et al.* Microfluidic Technique for the Simultaneous Quantification of Emulsion Instabilities and Lipid Digestion Kinetics. *Analytical Chemistry* **89,** 9116–9123. ISSN: 0003-2700. https://doi.org/10.1021/acs.analchem.7b01853 (2019) (Sept. 2017).